

M.T. Klein and P.S. Virk
Department of Chemical Engineering
Massachusetts Institute of Technology
Cambridge, MA 02139

We hypothesize that during pyrolysis of lignites, the primary evolution of gas occurs from lignin-related residues in the coal. Likely pathways for this primary gas release have been theoretically modelled by a set of thermally-allowed pericyclic reactions that respectively lead to each of methane, carbon monoxide, carbon dioxide, and water products from substrates containing lignoid moieties. The model pathways for methane formation can be experimentally examined by pyrolysis of a series of methoxy-benzenes, e.g.,

anisole COc1ccccc1, guaiacol COc1ccc(O)cc1, and iso-eugenol COc1ccc(C=C)cc1.

Experiments over the temperature range 200-500 C in batch tubing-bomb reactors equipped for gas and liquid product analyses showed that guaiacol was appreciably more reactive than anisole, fractional conversions of these substrates at 420 C and 120 s being respectively 0.083 and 0.0022. The former pyrolysis was essentially first order both in guaiacol disappearance as well as in methane gas appearance and yielded Arrhenius parameters ($\log_{10} A \text{ s}^{-1}$, $E^* \text{ kcal/mol}$) = (11.5, 45.8). These data accord with the hypothesis that methane release from guaiacyl moieties occurs by a concerted molecular group-transfer reaction.

EFFECTS OF COAL STRUCTURE
AND PROCESSING CONDITIONS ON ORGANIC EFFLUENTS
FROM SLAGGING FIXED-BED GASIFICATION

Jacquelyn K. Olson and Harold H. Schobert

Grand Forks Energy Technology Center
U.S. Department of Energy
Grand Forks, ND 58202

INTRODUCTION

Slagging fixed-bed gasification of low-rank coals is being investigated at the Grand Forks Energy Technology Center. In support of environmental and waste treatment studies, research is underway to determine the effect of process parameters on effluent production and composition.

The GFETC gasifier is a 1 ton/hour, pilot plant unit. The coal feed moves slowly down a shaft and is reacted with an oxygen-steam mixture injected through four tuyeres into the hearth. The product gas exits the gasifier at the top of the shaft. Operating parameters that may vary from test to test are pressure, 100 to 400 psig; oxygen/ steam molar ratio, 0.9 to 1.1; and oxygen feed rate, 4000 to 6000 scfh. Detailed information on the GFETC pilot plant studies has been published previously (1-3).

Tar, oils, water vapor and coal particles are removed from the exiting raw gas stream in a spray washer. The liquids that accumulate in the spray washer are sampled periodically. A recent publication (4) describes spray washer sampling procedures. Samples considered in this report were collected at the end of the test.

An inherent problem in the analysis of effluents from coal conversion processes is the complexity of the mixtures. Several schemes have been suggested for the analysis and environmental assessment of coal gasification effluents. The methodology defined by the EPA-IERL/RTP Procedure Manual: Level 1 Environmental Assessment (5) was applied to the analysis of spraywasher samples. Effluent samples produced by gasification of three coals at a range of conditions were used for this study.

EXPERIMENTAL

Figure 1 is the flow diagram of the separations and analyses performed on the tar and liquor samples.

Simulated distillation was obtained by FID gas chromatography using 3% OV-17, 1/8" x 4' ss columns. The temperature was programmed from 50 to 300°C at 10°/min. ASTM standard D2887 was used to establish boiling point ranges. The extracted organics were separated using gradient elution liquid chromatography. Silica gel adsorbent was used. Table 1 shows the solvent sequence for the procedure.

FIGURE 1. Analytical Flow Diagram for Spraywasher Tar and Liquor

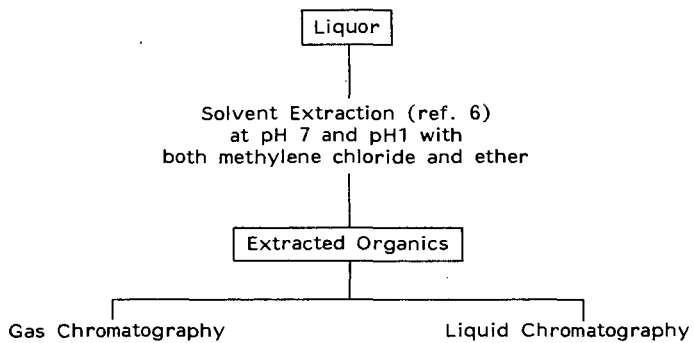
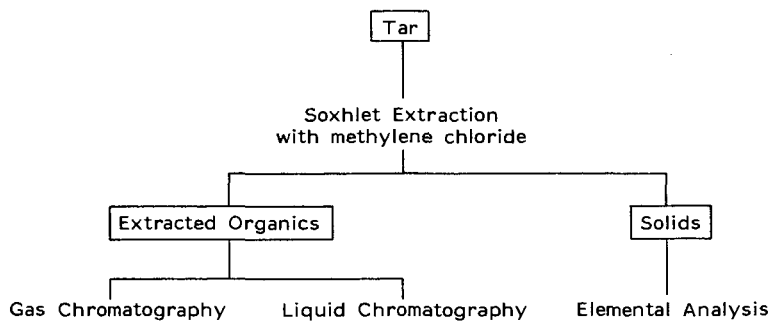


TABLE 1. Solvent Series for LC Separations

<u>Fraction</u>	<u>Solvent Composition</u>
1	Pentane
2	20% methylene chloride in pentane
3	50% methylene chloride in pentane
4	Methylene chloride
5	5% methanol in methylene chloride
6	20% methanol in methylene chloride
7	50% methanol in methylene chloride
8	Methanol

Instruments used in this study were an AEI MS-30* mass spectrometer, Perkin-Elmer 240 elemental analyzer, Leco sulfur analyzer, Varian 2400 gas chromatograph, and Perkin-Elmer 283 infrared spectrophotometer.

RESULTS

End-of-run tar and liquor samples produced from five gasification tests were obtained for this study. The summary of coals and operating parameters for these tests is shown in Table 2.

TABLE 2. Summary of Coals and Operating Parameters

<u>Run No.</u>	<u>Coal/Rank</u>	<u>Operating Pressure (psig)</u>	<u>Oxygen Feed Rate (scfh)</u>	<u>Oxygen-Steam Molar Ratio</u>
RA-40	Indian Head Lignite	200	4000	1.0
RA-52	Indian Head Lignite	300	6000	1.0
RA-37	Indian Head Lignite	400	6000	1.0
RA-45	Rosebud Subbituminous	200	4000	1.1
RA-58	Gascoyne Lignite	300	6000	1.1

Tar

The as-received tar contained 28 to 35% extractable organic material, 0.4 to 2.0% solids (entrained coal particles) and 63 to 71% water. The gas chromatographic analysis of the organic extracts is shown in Table 3.

TABLE 3. GC Analysis of Organics Extracted from Tar

<u>Range</u>	<u>BP(°C)</u>	<u>% of Extract</u>				
		<u>RA-40</u>	<u>RA-52</u>	<u>RA-37</u>	<u>RA-45</u>	<u>RA-58</u>
C ₇	90 to 110	0.4	0.1	0	0	1.5
C ₈	110 to 140	0.8	0.2	0.1	0	2.4
C ₉	140 to 160	0.1	0.6	0.2	0.2	3.3
C ₁₀	160 to 180	1.1	0.6	0.3	0.8	6.8
C ₁₁	180 to 200	2.5	0.8	0.6	1.4	5.0
C ₁₂	200 to 220	10.0	11.6	11.8	7.3	20.0
>C ₁₂	> 220	85.1	86.1	87.0	90.3	61.0

* Identification of specific brands or models is done to facilitate understanding and does not constitute or imply endorsement by the Department of Energy.

The distribution of compound classes in the liquid chromatography separations was determined by low voltage mass spectrometry and confirmed by infrared spectroscopy. Fraction 1 consists of paraffins and olefins, mostly branched. Fractions 2 and 3 consist primarily of naphthalene, C₁ and C₂ naphthalenes, and C₁ biphenyl or C₁ acenaphthene. Fractions 4 and 5 consist primarily of C₁ acenaphthylene or C₁ fluorene, phenanthrene, anthracene, C₁ and C₂ phenanthrene, C₁ and C₂ anthracene, fluoranthene, pyrene, and C₁ pyrene. Fractions 6 and 7 consist primarily of C₁ and C₃ indoles, naphthol, C₁ and C₂ naphthols, carbazole, C₂, C₃, and C₄ pyridines, phenol, and C₁, C₂, and C₃ phenols. No specific assignments were made to the compounds in fraction 8. The results of the liquid chromatography separations of the organics extracted from the tar are shown in Table 4.

TABLE 4. LC Analysis of Organics Extracted from Tar

Fraction(s)	% of Extract				
	RA-40	RA-52	RA-37	RA-45	RA-58
1	10.3	11.4	9.0	12.0	13.0
2,3,4	32.3	29.9	27.8	33.9	41.0
5,6,7	51.8	57.4	61.7	48.6	45.3
8	5.6	1.3	1.5	5.5	0.7

Liquor

Runs RA-40, RA-45, and RA-58 liquor yielded from 1200 to 2050 ppm solvent extractable organics. It is unlikely that the majority of organics were extracted since the total organic carbon for these liquors ranges from 6550 to 7800 ppm. The gas chromatography analysis of the extracted organics is shown in Table 5.

TABLE 5. GC Analysis of Organics Extracted from Liquor

Range	BP(°C)	% of Extract		
		RA-40	RA-45	RA-58
C ₇	90 to 110	0	0	0.4
C ₈	110 to 140	0	0	0.7
C ₉	140 to 160	0	0	1.3
C ₁₀	160 to 180	0	0	2.5
C ₁₁	180 to 200	0.1	0	3.2
C ₁₂	200 to 220	16.1	11.5	7.8
>C ₁₂	> 220	83.9	88.5	84.0

The liquid chromatography separations of the organic extract were not useful in defining specific classes of compounds. There was a considerable amount of overlap in the compounds found in fractions 5 through 8. These fractions consist primarily of C₄ and C₅ benzenes, C₁ and C₂ pyridines, C₂ and C₃ phenols, quinolines, naphthols, phenanthrene, anthracene, binaphthyl, and thiophenes. These assignments were made by mass spectrometry and infrared spectroscopy. The liquid chromatography analysis of the extracted organics is shown in Table 6.

TABLE 6. LC Analysis of Organics Extracted from Liquor

Fraction(s)	% of Extract		
	RA-40	RA-45	RA-58
1	0	0	1.6
2,3,4	0.4	0.4	8.3
5,6,7	80.8	89.2	83.0
8	18.8	10.2	7.1

Tar Solids

The solids were found to contain a higher percentage of mineral matter than the original coal feed. The relative proportion of nitrogen and sulfur was also higher in the solids. For RA-45, the coal feed contained 0.85% nitrogen and 1.81% sulfur; the solids contained 3.32% nitrogen and 2.42% sulfur. Table 7 shows the ultimate analyses of the tar solids and the feed coals.

TABLE 7. Comparison of Tar Solids with Feed Coal

	RA-40		RA-45		RA-58	
	feed coal	tar solids	feed coal	tar solids	feed coal	tar solids
Ultimate Analysis*, pct						
C	64.42	65.34	64.23	58.99	62.14	63.05
H	4.35	4.11	4.31	1.49	4.39	3.05
N	0.85	3.32	1.01	1.46	0.84	1.21
S	1.81	2.42	2.05	3.59	1.42	1.74
O(by diff)	18.23	13.77	13.06	0.66	18.06	10.22
Ash	10.34	11.04	15.34	33.81	13.15	20.73

*moisture-free basis

DISCUSSION

Tar Characterization

The variation observed in the amount of organic material extracted from the tar phase is consistent with experimental error in sampling. The procedure for obtaining tar samples has been described previously (4). The phase separation of tar from liquor depends on operator judgement in observing the interface between two darkly colored phases. Tar extraction data for runs 40, 45, and 58 shows a relative standard deviation of 6.01% for the amount of water. Three other runs made with Indian Head lignite at 200 psi and 4000 scfh oxygen rate showed a relative standard deviation of 6.47% for water content. Thus the variation between samples of different coals tested at different gasification conditions is nearly identical to that for replicate runs with the same coal.

The boiling point distribution of the tar extract shows distinct differences when comparing tars obtained from different coals gasified under same conditions. For example, a comparison of Rosebud and Indian Head gasified at 200 psi shows the tar from Indian Head to be comprised of more lower boiling materials. The cumulative boiling point distribution shows that 46% of Indian Head tar has distilled by 254°C and 87% by 343°, while the comparable figures for Rosebud tar are 34% and 76%. Of these two coals, Indian Head contains the greater amount of volatile

matter on an maf basis. A similar effect was observed for tars from gasification of Gascoyne and Indian Head lignites at 300 psi: Gascoyne contains a greater amount of volatile matter and produces more low boiling compounds in the tar.

A comparison of the boiling point distributions of tars produced from gasification of Indian Head lignite at different pressures shows that the effect of increasing gasification pressure is to shift the boiling point distribution downward. For example, the temperatures at which 75% of the tar has distilled drop from 316°C for tar produced at 200 psi, to 287° for 300 psi, and to 271° for tar produced at 400 psi. The fraction corresponding to phenol (180-200°C) decreases with increasing gasification pressure, as shown previously (7) for a high-pressure, low-temperature carbonization process in the SFBG.

The amounts of the fractions obtained in the liquid chromatographic separations of the tar were correlated with gasification conditions and coal composition. The treatment used followed the fractional factorial analysis procedures given by Lipson and Sheth (8). Since the absolute numerical values of the factors vary over several orders of magnitude -from thousands of scfm for oxygen feed rates to one or two percentage units for coal nitrogen and sulfur - comparisons were made on the basis of percentage changes in each factor.

The amounts of fractions 1 (paraffins and olefins), 2-4 (aromatics), and 5-7 (polar compounds) depend most heavily on the maf carbon content of the coals. Both the paraffins and olefins and the aromatics show a direct correlation with maf carbon, while the polar compounds vary inversely. These results demonstrate that as more carbon is added to the molecular framework of the coal proportionately fewer oxygen or nitrogen functional groups will be present; hence as the coal undergoes pyrolysis or hydrocracking in the carbonization zone of the SFBG (9) relatively fewer polar species will be formed. Correlation of the amounts of one LC fraction vs. another show that the paraffins and olefins are directly proportional to the aromatics, but that both the paraffin-olefin and the aromatic fractions vary inversely with the polar fraction.

When the effect of maf carbon content in the coal is removed statistically (8), no other factors were found to influence the amount of the paraffin-olefin fraction. The amount of the aromatic fraction, corrected for the effect of carbon, shows a direct correlation with the amount of hydrogen in the product gas. A recent publication (10) describing the detailed mass spectroscopic analysis of SFBG tars also demonstrated such a correlation for the concentrations of many of the aromatic compounds. The amount of the polar fraction showed no other correlations above the 80% confidence limit.

With respect to the amount of the very polar fraction (fraction 8) no factors were found to display both a large slope and greater than 80% confidence correlation.

Liquor Characterization

The amount of organic material extractable from the liquor accounted for only 18 to 28% of the total organic carbon content of the samples. The amount of extractable material shows an inverse correlation with the maf oxygen content of the coal. As the oxygen content of the coal increases, more compounds with polar functional groups should appear in the organic effluents; these compounds should dissolve in the liquor and in turn be resistant to extraction into relatively non-polar solvents. The amount of extractable organic material when added to the "phenols" as determined by gas chromatographic analysis of filtered liquor (11) agrees well with the total organic carbon content. For example, in the liquor produced during gasification of Rosebud coal, phenols accounted for 75.9% of the TOC and the extractable organics, 28.3%.

The boiling point distributions of liquor organic extracts from gasification of Indian Head (RA-40), Rosebud, and Gascoyne are similar. The most appreciable difference is that the extract from liquor produced in gasification of Gascoyne lignite is the only one of the three samples containing material boiling below 196°C. The liquid chromatographic separation of the extract from Gascoyne liquor was the only one showing material in the paraffin-olefin and aromatic fractions.

A correlation of the amounts of fractions in the liquid chromatographic separations with gasification conditions and coal composition was performed in the same manner as for the tar extracts. Only the polar and polar fractions were considered, and only the three samples from runs 40, 45, and 58 were used.

The major factor affecting the amount of both fractions is the maf carbon content of the coal. The polar fraction correlates directly with maf carbon; the very polar fraction thus shows an inverse correlation, since these two fractions account for 90 to 99% of the total material in the liquor or organic extract.

Solids Characterization

A comparison of the ultimate analysis of solids recovered from the tar samples with that of the respective coals shows that in all cases the tar solids contain greater amounts of nitrogen and sulfur than the coals. Since these solids are coal particles which did not descend through the entire SFBG shaft to the gasification/combustion zone this finding suggests that compounds of carbon, hydrogen, and oxygen are more easily formed in the carbonization zone whereas nitrogen and sulfur linkages are more resistant to cleavage or reaction.

The ash in the solids recovered from tar from Indian Head gasification shows an enrichment on sodium, magnesium, sulfur, and iron when compared with the ash of the feed coal. As-yet unpublished work on the volatilization of ash components in the SFBG gasification/combustion zone has shown that sodium, magnesium, and sulfur are the most volatile of the ash components.

In the case of both lignites, the mole fractions of the principal basic oxides essentially balance those of the silica and sulfur trioxide. The inorganic solids are therefore a mixture of alkali and alkaline earth silicates and sulfates. The ash from the solids recovered from Rosebud tar does not display such a balance. A petrographic classification by the Niggli method (12) shows that free quartz should be present, suggesting that the inorganic solids in this case are a mixture of alkali and alkaline earth sulfates with quartz particles.

CONCLUSIONS

The carbon content of the coal plays the most predominant role in determining the relative amounts of compound types in the organic extracts from tar and liquor. An increase in maf carbon will increase the percentage of paraffins and olefins and aromatics in the tar and will increase the percentage of polar compounds in the liquor extract. The polar fraction in the tar extract decreases as maf carbon in the coal increases. The oxygen content of the coal correlates inversely with the amount of organic material extractable from the liquor. Since the carbon content of the coal is of great importance in determining the molecular framework, and since the oxygen is the major contributor to heteroatomic functional groups, these results show that the effluent composition is dependent upon the molecular structure of the coal. Other coal-specific characteristics of the SFBG effluents include the volatility of the tar and the nature of the inorganic materials exiting the gasifier in the raw gas.

Research on the development of detailed relationships between coal composition or structure and effluent composition is continuing. The results of this study indicate the desirability of testing a wide variety of coals in the SFBG to augment the data base on effluent characteristics.

References

1. Gronhovd, G. H., Harak, A. E., Fegley, M. M. and D. E. Severson. Slagging Fixed-Bed Gasification of North Dakota Lignite at Pressures to 400 Psig. U.S. Bureau of Mines Report of Investigations 7408 (1970).
2. Ellman, R. C., Johnson, B. C., and M. M. Fegley. Studies in Slagging Fixed-Bed Gasification at the Grand Forks Energy Technology Center. Tenth Synthetic Pipeline Gas Symposium, Chicago (1978).
3. Ellman, R. C., and E. A. Sondreal. Environmental Control Activities on Slagging Fixed-Bed Gasification at the Grand Forks Energy Technology Center. U.S. Department of Energy Environmental Control Symposium, Washington, D.C. (1978).
4. Paulson, L. E., Schobert, H. H., and R. C. Ellman. Sampling, Analysis, and Characterization of Effluents from the Grand Forks Energy Research Center Slagging Fixed-Bed Gasifier. Division of Fuel Chemistry Preprints, 23(2):107 (1978).
5. Hamersma, J. W., Reynolds, S. L., and R. F. Maddalone. IERL-RTP Procedures Manual: Level 1 Environmental Assessment. EPA-600/2-76-160a (1976).
6. Bombaugh, K. J. Analysis of Grab Samples from Fixed-Bed Coal Gasification Processes. EPA-600/7-77-141 (1977).
7. Schobert, H. H., Johnson, B. C., and M. M. Fegley. Carbonization Reactions in the Grand Forks Fixed-Bed Slagging Gasifier. Div. Fuel Chemistry Preprints 23 (3), 136 (1978).
8. Lipson, C., and N. J. Sheth. Statistical Design and Analysis of Engineering Experiments. McGraw-Hill Book Co., New York (1973).
9. Johnson, B. C., Schobert, H. H., and M. M. Fegley. The Grand Forks Slagging Gasifier. Coal Processing Technology, vol. IV. American Institute of Chemical Engineers, New York (1978).
10. Miller, D. J., Olson, J. K., and H. H. Schobert. Mass Spectroscopic Characterization of Tars from the Gasification of Low Rank Coals. Div. Fuel Chemistry Preprints, in press (1979).
11. ASTM. Annual Book of ASTM Standards - Part 31 - Water. American Society for Testing and Materials, Philadelphia (1978).
12. Barth, T. F. W. Theoretical Petrology. John Wiley and Sons, New York (1962).

CATALYSIS OF LIGNITE CHAR GASIFICATION BY VARIOUS
EXCHANGED CATIONS -- DEPENDENCE OF ACTIVITY ON REACTIVE ATMOSPHERE

P. L. Walker, Jr., O. P. Mahajan* and M. Komatsu

Department of Materials Science and Engineering
The Pennsylvania State University
University Park, PA 16802

INTRODUCTION

We have previously reported reactivities of a vast spectrum of coal-derived chars in air (1), CO₂ (2), steam (3) and H₂ (4). In oxidizing atmospheres, char reactivity decreases with increase in the rank of the parent coal. In contrast, char reactivity in H₂ shows little dependence on rank of the coal precursor.

Because of the large reserves of lignites and subbituminous coals in the United States, they are potentially of importance in coal conversion processes. These coals contain significant amounts of carboxylic acid groups, where a fraction of the H⁺ ions have been exchanged by different cations such as Na⁺, K⁺, and Ca⁺⁺, as a result of extended contact with ground water containing different salts. The higher reactivity of lignite and sub-bituminous coal chars in oxidizing atmospheres is thought to be due, at least in part, to the presence of exchangeable metal cations. Therefore, it is desirable to study the possible catalytic effect of different exchangeable cations present on the surfaces of these coals on subsequent char reactivity in different atmospheres. This paper describes the results of such a study.

EXPERIMENTAL

Char Preparation. A Darco (Texas) lignite (28x48 mesh) was demineralized by boiling with 10% HCl and subsequently with a 50-50 mixture of 50% HF-10% HCl. The carboxyl content of the demineralized coal was 2.4 mmoles/g. Schafer's method was used to effect cation-exchange (5). Demineralized (Dem) lignite was contacted with 0.10 molar solutions of sodium acetate, potassium acetate, calcium acetate, magnesium acetate and ferric nitrate. Approximately 0.3 mmoles of cation per gram of coal were exchanged from the various solutions in 24 hr. Ten levels of exchangeable calcium ions in the range 0.10 to 2.14 mmoles/g of coal were introduced by contacting the Dem coal with calcium acetate solutions varying in concentration from 0.04 to 2.0 molar for 24 hr.

Raw, Dem and cation-exchanged samples were carbonized in N₂ in a fluidized bed. In each case, the sample was heated up to 800°C at a rate of 10°C/min. Soak time at 800°C was 2 hr.

Reactivity Measurements

Reactivities of various char samples were measured in air (1 atm, 390°C), CO₂ (1 atm, 760°C), steam (1 atm, 650°C), H₂ (1 atm, 790°C), 50% CO-50% H₂ mixture (total pressure 1 atm, 790°C), N₂-H₂O mixture (790°C), H₂-H₂O mixture (790°C), H₂-N₂-H₂O mixture (790°C) and CO-H₂-H₂O mixture (790°C). The partial pressure of water vapor in the last four mixtures (total pressure 1 atm) was 12.8 torr. This pressure was generated by bubbling the gas through deaerated distilled water thermostated at 15°C.

* Present Address: Standard Oil Co. (Indiana), Amoco Research Center,
P. O. Box 400, Naperville, IL 60540

Reactivity measurements in 1 atm steam were carried out in a fluid bed reactor. Weight losses occurring during gasification in the other atmospheres studied were monitored using a DuPont 951 TGA system in conjunction with a 990 Thermal Analyzer. Details of the experimental procedures for reactivity measurements have been described elsewhere (6).

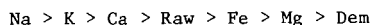
In the text, reactivity parameter, R, has been defined as:

$$R = \frac{1}{W_0} \cdot \frac{dW}{dt}$$

where W_0 is the initial char weight (daf) and dW/dt is the maximum rectilinear weight loss rate.

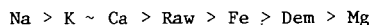
RESULTS AND DISCUSSION

Burn-off versus time plots for various char samples reacted in air are shown in Figure 1. The Dem char is significantly less reactive than the raw char. This has previously been attributed to the loss of catalytic inorganic matter upon demineralization (6). The following order of reactivities is observed for chars produced from raw, Dem and cation-exchanged samples:

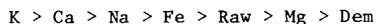


These results clearly show that the replacement of surface H^+ ions of carboxylic acid groups present on the surface of Dem lignite by metal cations increases the reactivity of the chars produced, but the extent of the increase is markedly dependent upon the nature of the cation. The higher reactivity of the char produced from the raw lignite compared to the iron and magnesium containing chars is thought to be due to the presence of catalytically active calcium ions in the raw lignite.

The following order of reactivities for various char samples was observed for the reaction in CO_2 :



and in steam:



Even though the C-O_2 , C-CO_2 and $\text{C-H}_2\text{O}$ reactions all involve an intermediate oxygen transfer step followed by a gasification step, the order of reactivities of chars produced from different cation-exchanged samples is not the same in the three atmospheres. This shows the high specificity of different catalytic species.

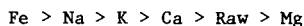
For the various calcium containing chars, the reactivity parameter in air, CO_2 and steam increased linearly with increase in the amount of calcium present in the char. Furthermore, normalized reactivities of these chars in the three oxidizing atmospheres were essentially the same.

Burn-off plots for various char samples in H_2 are shown in Figure 2. The order of reactivities of various samples in H_2 is markedly different from that observed in the three oxidizing atmospheres. Below 45% burn-off, sodium is the most effective hydrogasification catalyst; whereas at higher burn-offs iron is a better catalyst. It is noteworthy that even though calcium and potassium are excellent oxidation catalysts, chars containing these species are much less reactive in H_2 than the raw char. In fact, for the various calcium-containing

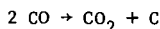
samples reactivity in H_2 decreased monotonically with increase in calcium loading.

Two extreme cases of the effect of H_2 addition to steam on char reactivity are illustrated by the plots in Figures 3 and 4. At one extreme, for the raw char (Figure 3), which has calcium as the major inorganic impurity, gasification is more rapid in wet N_2 than in wet H_2 . At the other extreme, the char produced from the iron exchanged sample has a higher reactivity in wet H_2 than in wet N_2 (Figure 4). It is known that in the elemental form iron is a good oxidation catalyst but in the oxide form it is a poor catalyst (7). In the present study, when the iron-containing char is reacted with wet H_2 , the percentage of H_2 in the mixture is sufficient to keep iron in the reduced state.

In the $CO-H_2$ mixture, chars produced from raw and Na, K, Ca and Mg exchanged samples showed little or no weight loss. However, in the $CO-H_2-H_2O$ mixture small but finite gasification rates were observed and the order of reactivity for various samples was:



Results for the iron-containing char were unique (Figure 5). In the $CO-H_2-H_2O$ mixture, the gasification rate is significantly lower than in N_2-H_2O or $N_2-H_2-H_2O$ mixtures. Further, in the dry $CO-H_2$ mixture, after a slight initial weight loss, there is a rapid continuous increase in weight. This increase is attributed to the disproportionation of CO:



For this reaction, iron is an excellent catalyst but is gradually deactivated due to the formation of cementite (8). In this study, the amount of H_2 in the $CO-H_2$ mixture is sufficient to keep iron in the catalytically active form, that is as elemental iron. Even though iron is an excellent catalyst for the $C-H_2$ reaction (7), it appears that in the presence of CO the weight increase due to disproportionation of CO offsets any weight loss due to hydrogasification.

ACKNOWLEDGEMENTS

This research was supported by DOE on Contract EX-76-C-01-2030. Professor W. Spackman, Jr. supplied the lignite used in this study. We appreciate the assistance of A. Linares-Solano on preliminary portions of this study.

REFERENCES

1. Jenkins, R. G., Nandi, S. P. and Walker, P. L., Jr., Fuel, 52, 288 (1973).
2. Hippo, E. and Walker, P. L., Jr., Fuel, 54, 245 (1975).
3. Linares-Solano, A., Mahajan, O. P. and Walker, P. L., Jr., "Reactivity of Heat Treated Coals in Steam " Fuel, in press.
4. Tomita, A., Mahajan, O. P. and Walker, P. L., Jr., Fuel, 56, 137 (1977).
5. Schafer, H. N. S., Fuel, 49, 197 (1970).
6. Mahajan, O. P. and Walker, P. L., Jr., in "Analytical Methods for Coal and Coal Products " (Ed. C. Karr, Jr.), Vol. 2, Academic Press, 1978, pp. 465-494.

7. Walker, P. L., Jr., Shelef, M. and Anderson, R. A. in "Chemistry and Physics of Carbon " (Ed. P. L. Walker, Jr.), Vol. 4, Marcel Dekker, New York, 1968, pp. 287-380.
8. Walker, P. L., Jr., Rakszawski, J. F. and Imperial, G. R., J. Phys. Chem., 63, 140 (1959).

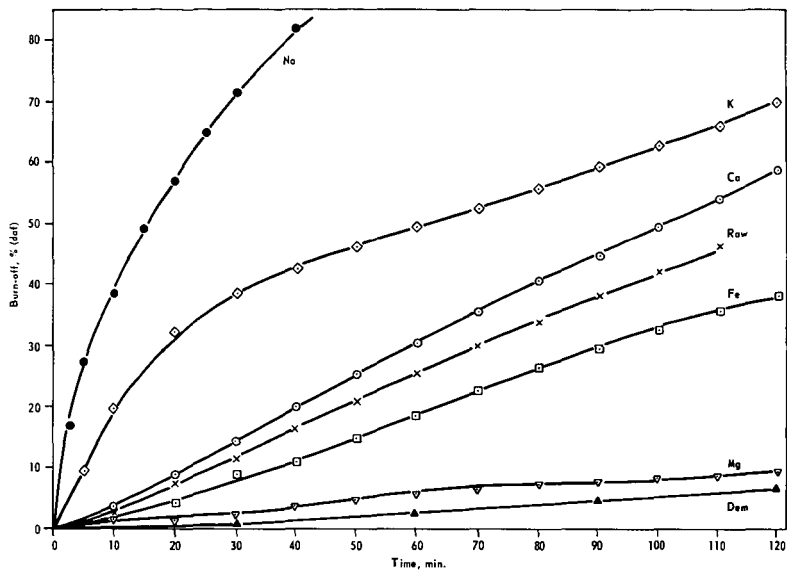


Figure 1. GASIFICATION OF LIGNITE CHARS IN AIR AT 390°C

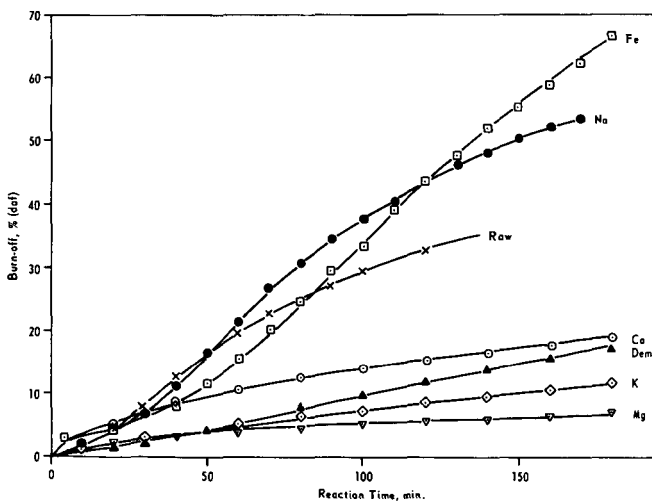


Figure 2. GASIFICATION OF LIGNITE CHARS IN 1 ATM H₂ AT 790°C

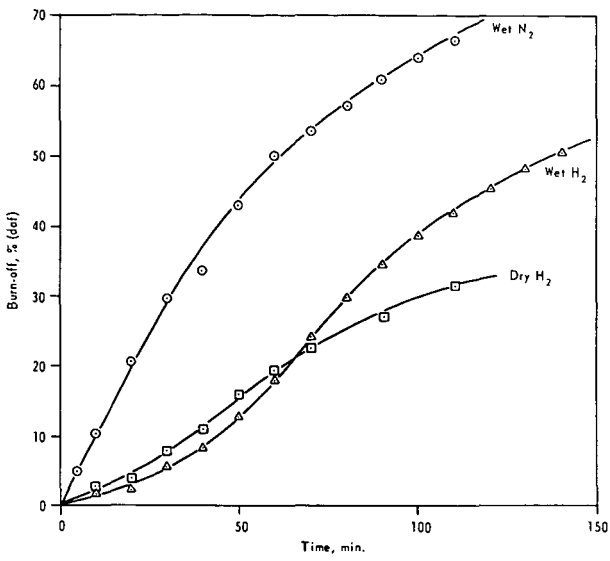


Figure 3. GASIFICATION AT 790°C OF CHAR PRODUCED FROM RAW LIGNITE IN VARIOUS ATMOSPHERES

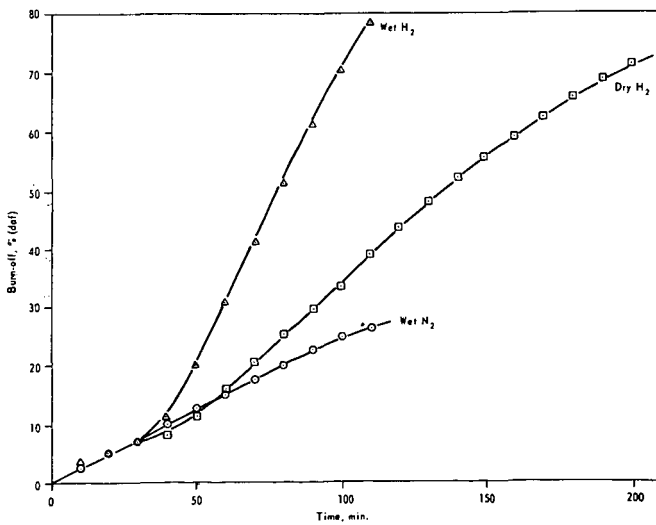


Figure 4. GASIFICATION AT 790°C OF IRON - CONTAINING CHAR IN VARIOUS ATMOSPHERES

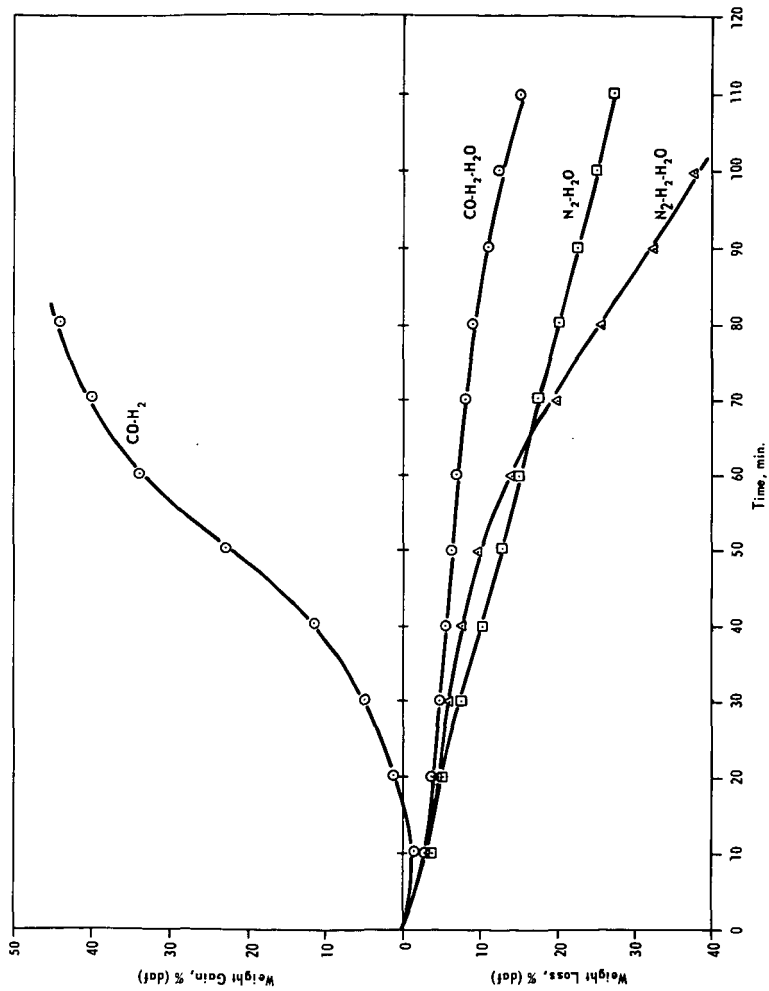


Figure 5. WEIGHT CHANGES FOR IRON-CONTAINING CHARS AT 790°C IN THE PRESENCE OF VARIOUS ATMOSPHERES

CATALYTIC GASIFICATION OF LIGNITE CHARs

S.P. Nandi and J.L. Johnson

Institute of Gas Technology
3424 S. State St.
Chicago, Illinois 60616

INTRODUCTION

In a previous study (1), the kinetics of the gasification of chars derived from coals ranging from anthracite to lignite were determined in different gasification media. The relative reactivity factor decreased systematically with increasing carbon content in the parent coal. The overall decrease is caused both by decreasing surface areas and by decreasing specific surface reactivities of the chars. The correlations developed, however, do not generally apply to the lignite chars because of catalytic effects of exchangeable cations, particularly sodium and calcium, which are associated with the carboxyl groups of the lignites. Therefore, a systematic investigation was conducted to obtain detailed data describing the gasification characteristics of Montana and North Dakota lignite chars with particular emphasis given to determining the effect of sodium and calcium inherent or added by base exchange on the gasification rate. Calcium and sodium were chosen because these are the predominant exchangeable cations present in Montana and North Dakota lignites.

APPARATUS AND EXPERIMENTAL PROCEDURE

A high-pressure thermobalance was used in this work to obtain reaction rates. The main feature of this apparatus is that the weight of a small fixed-bed sample of char (approximately 0.5 gram) contained in a wire mesh basket can be continuously measured as it undergoes gasification in a desired environment at constant temperature and pressure. In all of the tests conducted, chars in -20+40 USS sieve size particles were used, and gas flow rates in the reactor were maintained at sufficiently high values to result in negligible gas conversion. The weight loss versus time characteristics obtained during individual tests were used to calculate the base carbon conversion fraction (1).

The proximate and ultimate analyses of the lignite samples are shown in Table 1. The acid-washed lignites were prepared from the original lignites by treatment with 1N HCl at room temperature followed by washing with distilled water until the effluents were chloride free. The wet samples were dried at 60°C under vacuum. The acid-washed lignites were treated, in turn, with solutions of sodium or calcium acetate, and a number of lignite samples of varying concentrations of base exchanged sodium and calcium were prepared. The nomenclature of the original and treated lignites, together with the concentration of sodium and calcium, is given in Table 2. Chars were prepared from samples by devolatilization in nitrogen (1 atmosphere) for 30 minutes at temperatures from 1400° to 1700°F. For these samples, devolatilization was essentially complete at the lowest temperature used, and the concentration of sodium and/or calcium for chars from the same starting lignite was assumed to be the same at different char preparation temperatures.

Gasification of the chars was conducted at the char preparation temperatures with hydrogen and equimolar steam-hydrogen mixtures at pressures ranging from 14.6 to 69.0 atmospheres. With one sample (G), gasification was conducted in synthesis gas mixtures. The compositions of the synthesis gas mixtures are shown in Table 3.

Table 1. ANALYSES OF LIGNITES

Sample	Proximate Analysis			Ultimate Analysis					
	VM	FC	Ash	C	H	O	N	S	Ash
	wt % dry			wt % dry					
Montana, Raw	43.6	51.3	5.1	65.13	4.13	24.20	0.89	0.57	5.08
Montana, Acid Washed	46.9	52.1	1.0	68.60	4.42	24.57	0.90	0.58	1.00
North Dakota, Raw	43.7	49.6	6.7	62.90	4.27	24.09	0.97	1.10	6.67
North Dakota, Acid Washed	45.8	52.5	1.7	67.70	4.33	24.38	1.00	0.90	1.69

Table 2. NOMENCLATURE OF THE SAMPLES AND THEIR SODIUM AND CALCIUM CONTENT

No.	Sample	Name	Concentration, g-atoms/g-atom base carbon		
			Na	Ca	Na + Ca
1.	Montana, Acid Washed	A	0.00000	0.00000	0.00000
2.	Montana, Ca-Ex. 1	B	0.00000	0.00139	0.00139
3.	Montana, Ca-Ex. 2	C	0.00000	0.00972	0.00972
4.	Montana, Raw	D	0.00164	0.01364	0.01528
5.	Montana, Na+Ca-Ex	E	0.01098	0.00505	0.01603
6.	Montana, Na-Ex. 1	F	0.00274	0.00000	0.00274
7.	Montana, Na-Ex. 2	G	0.01955	0.00000	0.01955
8.	North Dakota, Raw	N	0.00329	0.00758	0.01087
9.	North Dakota, Acid Washed	O	0.00000	0.00000	0.00000
10.	North Dakota, Ca-Ex	P	0.00000	0.01326	0.01326

Table 3. COMPOSITION OF SYNTHESIS GAS MIXTURES

	$\frac{H_2}{2}$	$\frac{H_2O}{2}$	CO	$\frac{CO_2}{2}$	$\frac{CH_4}{4}$
	vol %				
Syn-Gas 1	47.5	40.4	6.0	3.6	2.5
Syn-Gas 2	43.6	35.3	11.8	8.2	1.1
Syn-Gas 3	36.8	29.3	19.3	11.3	3.3

RESULTS AND DISCUSSION

Gasification in Hydrogen

Initial gasification tests in hydrogen were conducted with Montana and North Dakota chars obtained from acid-treated lignites to provide a basis for determining gasification kinetics in the absence of exchangeable cations. Typical results are shown in Figures 1 and 2. The results show that, at a given temperature, gasification rates increased significantly with increasing hydrogen pressure. Similarly, at a constant hydrogen pressure, gasification rates increase significantly with increasing temperature. For Montana char, a carbon conversion of approximately 0.09, which tends to be independent of temperature and pressure, occurred during the heat-up period of char (which takes about 1 to 2 minutes after lowering the sample to the reaction zone). It was hypothesized that Montana chars contain two types of carbon - Type I, which gasifies very rapidly during the heat-up period, and Type II, which is subsequently gasified. For North Dakota chars, only Type II carbon was indicated.

In previous studies (2) with bituminous coal chars, gasification kinetics in hydrogen was described by the expression --

$$\frac{dX}{dt} = f_L K_H (1-X) \quad 1)$$

where --

X = base carbon fraction

t = time, min

K_H = rate constant for reference char ($f_L = 1$), min^{-1} .

The rate constant was determined by the equation --

$$K_H = \frac{P_{H_2}^2 \exp(2.674 - 24,609/T)}{1 + P_{H_2} \exp(-10.452 + 19.976/T)} \quad 2)$$

where --

f_L = relative reactivity factor

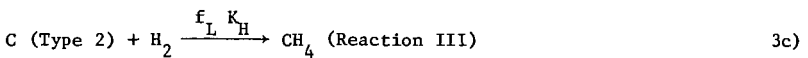
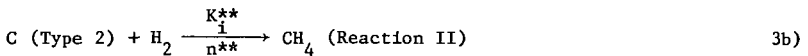
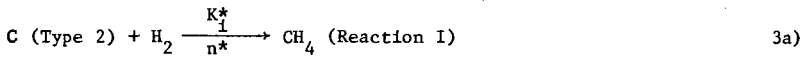
T = temperature, °R

P_{H_2} = hydrogen partial pressure, atm.

Figure 3 shows the $-\ln(1-X)$ versus reaction time plots for the experimental results of gasification in hydrogen for Montana lignite chars. Also included in the figure is the calculated base carbon conversion fraction for the reference bituminous coal char (char from preoxidized Pittsburg No. 8 seam coal). The experimental base carbon conversion data for Montana lignite are nonlinear when plotted according to Equation 1. The curve for the char from Raw Montana starts with a high initial slope; however, the value of the slope decreases with the increase of X and, at high value of X, becomes lower than that for the reference bituminous char. Upon removal of exchangeable cations, the reactivity of char decreases and the extent of nonlinearity is diminished but not entirely removed.

To take into account the characteristics of lignite char gasification mentioned above, it has been assumed that there are two transient reactions in addition to the low-rate gasification reactions that determine the rate of lignite char gasification. The first transient reaction is assumed to be catalyzed by some structural component present in lignite char, and the second transient reaction is assumed to be catalyzed by the exchangeable cations present in lignite. It is also assumed that the low-rate gasification of lignite char is kinetically similar to the low-rate gasification occurring in bituminous coal char.

The following reaction model was proposed: The Montana lignite char is composed of two types of carbon. In the presence of hydrogen, a fraction of carbon (Type 1) is gasified very rapidly to methane during the heat-up period (1 to 2 minutes in thermobalance tests). The remaining carbon (Type 2) gasifies by three possible paths, as indicated below:



Reaction III is assumed to be similar to the reaction path followed by bituminous coal char (low-rate gasification). The parameters f_L and K_H have been defined (2). Reaction I corresponds to a path in which some entity, n^* , catalyzes gasification. The entity n^* is assumed to be a structural component present in char. It is also assumed that n^* deactivates by a first-order process. For Reaction II, n^{**} is a metal, catalyst-containing complex that catalyzes this reaction. Similar to Reaction I, it was assumed that n^{**} also deactivates by a first-order process.

With the above assumptions, the following rate expression results -

$$-\ln(1-X) = -\ln(1-X^*) + \frac{K^*_1 C^*_O}{K^*_O} (1 - e^{-\frac{K^*_1 t}{n^*}}) + \frac{K^{**}_1 C^*_O}{K^{**}_O} (1 - e^{-\frac{K^{**}_1 t}{n^{**}}}) + f_L K_H t \quad 4)$$

The different parameters of Equation 4 were evaluated from experimental data. For chars from both lignites -

$$K^*_O = K^{**}_O = 5.74 \exp(-9770/T) \quad 5)$$

Particular evaluations for chars from Montana lignite are the following:

$$f_L = 0.70$$

$$X^* = 0.086$$

$$\frac{K^*_1 C^*_O}{K^*_O} = 0.026 P_{\text{H}_2}^{1/2}$$

$$K^{**}_1 C^*_O / n^{**} = (380C_{\text{Na}} + 32C_{\text{Ca}}) f_L K_H \quad 6)$$

where C_{Na} and C_{Ca} are concentrations of sodium and calcium, g-atom/g-atom base carbon.

Equation 4 was used with the evaluation given above to calculate the base carbon conversion for the chars from Raw Montana lignite. In Figure 4, the solid line represents the calculated values of X. The experimental points shown follow the line closely except for the first 5 minutes of reaction time. A similar match was obtained for the other char samples.

Particular evaluations for chars from North Dakota lignite are the following:

$$f_L = 0.85$$

$$X^* = 0.0$$

$$\frac{K^*C_o^o}{K_o^*} = 0.045 P_{H_2}^{1/2}$$

$$K_{i n^{**}}^{**o} = (500C_{Na} + 75C_{Ca}) f_L K_H \quad 7)$$

The evaluation of the term $K_{i n^{**}}^{**o}$, in terms of catalyst concentration show that, for both lignites, sodium was a better catalyst than calcium for hydrogasification. This observation can also be verified by choosing the time for 50% ($T_{0.5}$) carbon conversion as a rate parameter. The time to reach a certain fraction of carbon conversion is a measure of reaction rate even for a reaction which is not first-order (3). The $T_{0.5}$ values are presented in Table 4 for different chars obtained from Montana lignite. The $1/T_{0.5}$ values of the chars containing only sodium or only calcium are shown in Figure 5, plotted against the concentration of Na or Ca. The values for the acid-washed lignite chars are also shown. It is clear that calcium is a poor catalyst for hydrogasification.

Table 4. TIME FOR 50% BASE CARBON CONVERSION OF MONTANA CHARS

Sample	Reaction Temperature, °F	Hydrogen Pressure, atm	$T_{0.5}$, min (time for X=0.5)	$\frac{1}{T_{0.5}}$, min ⁻¹
A	1600	35	100.0	0.0100
A	1700	35	39.0	0.0256
A	1600	69	44.0	0.0227
A	1700	69	18.5	0.0540
B	1600	35	105.0	0.0095
B	1700	35	34.0	0.0294
C	1600	35	100.0	0.0100
C	1700	35	31.0	0.0322
D	1600	35	78.0	0.0128
D	1700	35	26.5	0.0377
E	1600	35	48.5	0.0206
E	1700	35	19.0	0.0526
E	1600	69	11.8	0.0847
E	1700	69	4.5	0.2222
F	1600	35	68.0	0.0147
F	1700	35	23.5	0.0425
G	1600	35	20.5	0.0488
G	1700	35	9.0	0.1111

Gasification in Equimolar Steam-Hydrogen Mixtures:

Gasification in equimolar steam-hydrogen mixtures was conducted with different char samples at temperatures of 1500° to 1700°F and at pressures of 14.6 to 69.0 atmospheres. The effect of total pressure on gasification for char, obtained from acid-washed North Dakota lignite is shown in Figure 6. The rate of gasification increased with the increase of total pressure. These results were anticipated because at higher total pressure, the partial pressure of hydrogen will be higher; that alone could enhance the rate of gasification, even if the rate was independent of steam partial pressure. In contrast, it was observed that, for samples containing Na or Ca, the gasification rate in this medium was independent of total pressure. Typical results indicating this behavior are presented in Figure 7. In this context, Vadovic and Eakman (4) have shown that for steam gasification of chars catalyzed by potassium, the rate was independent of steam partial pressure. The results of the current investigation indicate that, for chars containing Na or Ca as catalyst, the gasification rate is controlled by the steam-carbon reaction, even though the gasification medium contains 50% hydrogen. For all of the char samples, the rate of gasification in equimolar steam-hydrogen mixtures increased with temperature. Typical gasification data for chars containing different amounts of catalyst are shown in Figure 8.

It has been shown (2) that, with bituminous coal chars, gasification in steam-hydrogen mixtures could be correlated by the expression -

$$\frac{dX}{dt} = f_L K_T (1-X)^{2/3} \exp(-\alpha X^2) \quad 8)$$

Integrating Equation 8, we obtain -

$$M(X) = \int_0^X \frac{\exp(\alpha X^2)}{(1-X)^{2/3}} = f_L K_T + I \quad 9)$$

where -

K_T = overall rate constant

f_L = relative reactivity factor

α = kinetic parameter dependent on gas composition

I = integration constant.

For bituminous coal chars, which were devolatilized at temperatures of 1400°F or higher, I = 0.0, and α , for equimolar steam-hydrogen mixtures, is equal to 1.67. The char gasification data of this study was analyzed by Equation 9 assuming α to be equal to 1.67. Typical plots of M(X) versus time for three char samples are shown in Figure 9. Linear plots of up to a value of X=0.86 were obtained, but all the lines do not pass through the origin. The acid-washed lignite chars tend to have an intercept of about 0.1. The slope and intercept values of all the chars tested are shown in Table 5. In Figure 10, the values of the overall rate constant ($f_L K_T$) for steam-hydrogen gasification of Montana chars are plotted against the total concentration of sodium and/or calcium present in the char. All of the experimental points, whether the char contained only sodium, only calcium, or their mixture, tended to fall on the same line at a particular temperature, indicating that, in steam-hydrogen mixtures, calcium is as effective a catalyst as sodium. For Montana chars, the increase of rate with the increase of catalyst concentration and temperature can be correlated by the following experimental equation:

$$\text{Overall rate} = f_{L,T} K_T = [C_{(Na+Ca)} + 0.0032] \exp(19.80 - 38000/T) \quad 10)$$

Table 5. KINETIC PARAMETERS FOR GASIFICATION OF CHARs FROM MONTANA AND NORTH DAKOTA LIGNITES IN EQUIMOLAR STEAM-HYDROGEN MIXTURES

Char Source	Temperature, °F	$f_{L,T} K_T$ (Slope)	I (Intercept)
A	1500	0.0030	0.10
A	1600	0.0082	0.10
A	1700	0.0262	0.08
B	1500	0.0050	0.10
B	1600	0.0240	0.08
B	1700	0.0473	0.10
C	1600	0.0546	0.05
C	1700	0.1175	0.00
D	1500	0.0235	0.06
D	1600	0.0796	0.00
D	1700	0.1640	0.00
F	1600	0.0340	0.05
F	1700	0.1000	0.00
G	1500	0.0332	0.08
G	1600	0.0954	0.00
G	1700	0.1892	0.00
O	1500	0.0046	0.05
O	1600	0.0136	0.09
O	1700	0.0249	0.08
N	1500	0.0410	0.00
N	1600	0.0972	0.00
N	1700	0.1680	0.00
P	1500	0.0502	0.00
P	1600	0.1050	0.00
P	1700	0.2205	0.00

For North Dakota chars, the following correlations satisfy the experimental results:

$$\text{Overall rate} = f_{L,T} K_T = [C_{(Ca+Na)} + 0.0015] \exp(16.58 - 30000/T) \quad 11)$$

The gasification characteristics of chars from two lignites having similar elemental compositions are qualitatively similar, but, the numerical magnitude of the rate parameters differ. That is, enhancement of rate by a catalyst is dependent upon the nature of the char on which the catalyst is distributed.

Gasification in Synthesis Gas Mixtures

Gasification of one sample of char from Montana lignite was conducted in synthesis gas (syn-gas) mixtures. Tests were done with Syn-Gas 2 at 35 and 69 atmospheres at a temperature of 1700°F, and it was noted that the rate of base carbon conversion was the same at both pressures. The effect of pressure on rate of gasification in synthesis gas mixtures seems to be the same as was observed for gasifi-

cation in steam-hydrogen mixtures. The results of gasification with different syn-gas mixtures are shown in Figure 11. The gasification data in equimolar steam-hydrogen mixtures are also shown in this figure. The (P_{H_2}/P_{H_2O}) ratio for the syn-gas mixtures are 1.18, 1.23, and 1.25 for the three mixtures shown in Table 3. The (P_{CO}/P_{H_2O}) ratios are 0.15, 0.33, and 0.66. Therefore, the main compositional variable between the three synthesis gas mixtures is the CO/H₂O ratio. The effect of CO₂ and CH₄ in the mixture was considered to be minor. It is seen from Figure 11 that at the same temperature and pressure, the rate of carbon conversion decreases with the increase of the CO/H₂O ratio. The overall rate constants ($f_L K_T$) for the gasification in syn-gas was calculated with Equation 9. The values are 0.100, 0.076, and 0.039 respectively, for the three mixtures. It is seen that, for char from Sample G the rate of gasification in equimolar steam-hydrogen mixtures was approximately five times higher compared with that for Syn-Gas 3.

CONCLUSIONS

For gasification of lignite chars in hydrogen, sodium was more efficient as a catalyst than calcium. The gasification rate of lignite chars containing sodium or calcium remains essentially constant with the increase of total pressure in steam-hydrogen and synthesis gas mixtures. Both calcium and sodium enhance the rate of gasification of lignite chars in steam-hydrogen mixtures, and the effect is proportional to the concentration (g-atom/g-atom carbon) of sodium and/or calcium present. The catalytic effect of sodium or calcium depends on the nature of char on which the catalyst is dispersed; that is, the same concentration of sodium does not produce the same quantitative effect on rate for chars obtained from lignites having similar elemental composition. The catalysts tend to selectively enhance the rate of the steam-carbon reaction, preferring the carbon-hydrogen reaction when gasification is conducted in steam-hydrogen mixtures.

LITERATURE CITED

1. Johnson, J.L., "Relation Between the Gasification Reactivity of Coal Chars and the Physical and Chemical Properties of Coals," ACS Div. Fuel Chem. Prepr. 20, No. 4, 85 (1975).
2. Johnson, J.L., "Kinetics of Bituminous Coal Char Gasification With Gases Containing Steam and Hydrogen," Advances in Chemistry Series 131, 145 (1974).
3. Mahajan, Om.P., Yarzab, R. and Walker, P.L., Jr., "Unification of Coal Char Gasification Mechanism," Fuel 57, 643 (1978).
4. Vadovic, C.J. and Eakman, J.M., "Kinetics of Potassium Catalyzed Gasification," ACS Div. Fuel Chem. Prepr. 23, No. 8, 89 (1978).

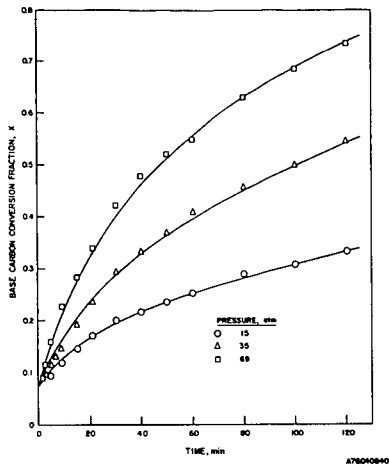


Figure 1. CONVERSION OF ACID-TREATED MONTANA LIGNITE CHAR IN HYDROGEN AT 1600°F

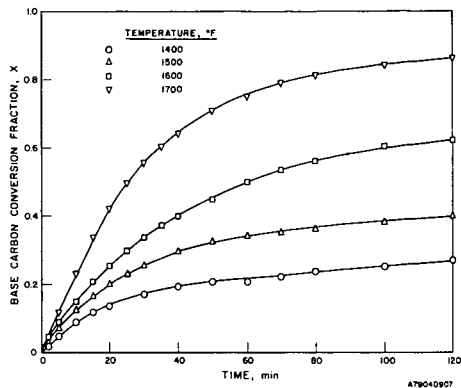


Figure 2. GASIFICATION OF ACID-WASHED NORTH DAKOTA CHARS IN HYDROGEN AT 35 atm

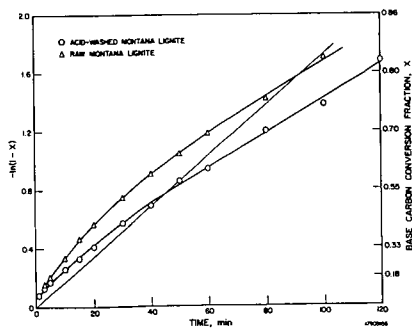


Figure 3. GASIFICATION OF RAW AND ACID-WASHED MONTANA LIGNITE CHARS IN HYDROGEN AT 1700°F AND 35 atm

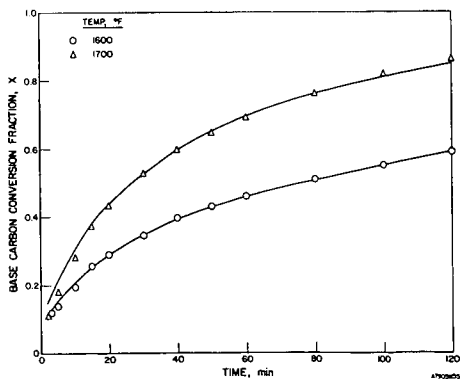


Figure 4. GASIFICATION OF RAW MONTANA CHARS IN HYDROGEN AT 35 atm

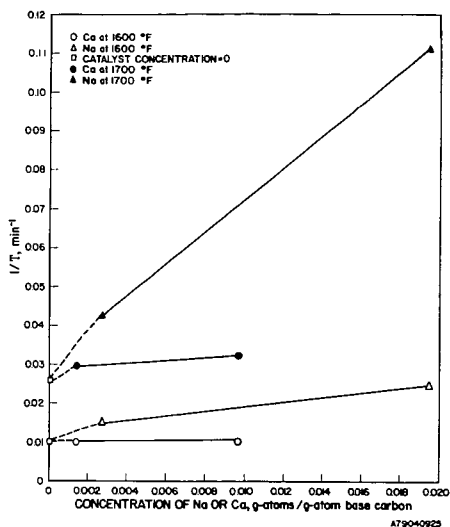


Figure 5. EFFECT OF CATALYST CONCENTRATION ON THE RECIPROCAL TIME FOR 50% BASE CARBON CONVERSION

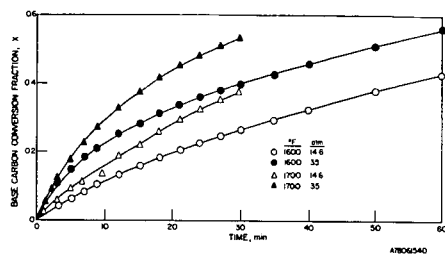


Figure 6. GASIFICATION OF ACID-WASHED NORTH DAKOTA CHARS IN STEAM-HYDROGEN MIXTURES ($H_2O/H_2 = 1$)

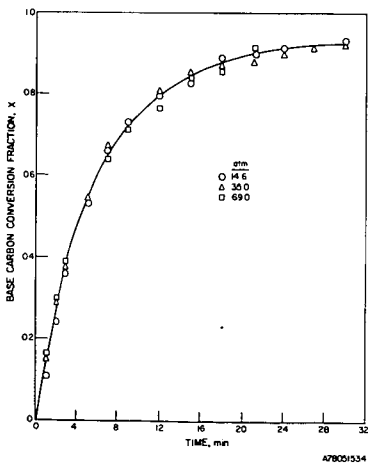


Figure 7. EFFECT OF PRESSURE ON THE GASIFICATION OF NORTH DAKOTA RAW CHAR IN STEAM-HYDROGEN MIXTURES ($H_2O/H_2=1$) AT 1700 °F

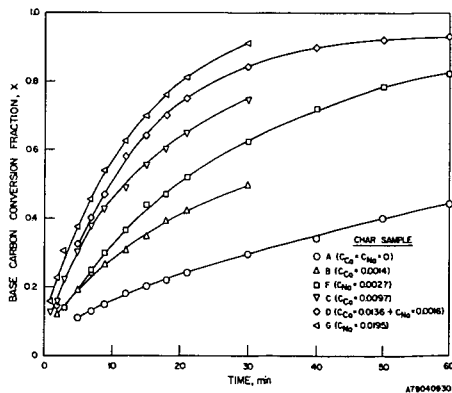


Figure 8. GASIFICATION OF MONTANA CHARS IN EQUIMOLAR STEAM-HYDROGEN MIXTURES AT 1600 °F AND 35 atm

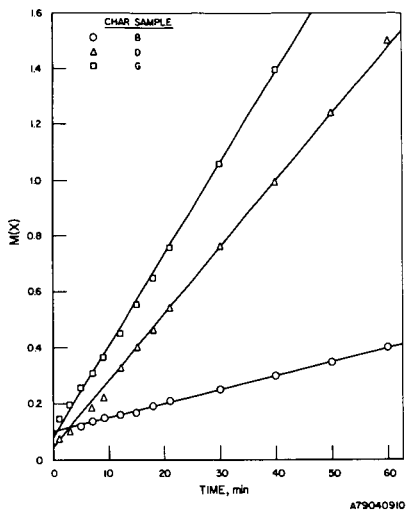


Figure 9. BASE CARBON CONVERSION FUNCTION VS. TIME PLOTS FOR THE GASIFICATION OF MONTANA LIGNITE CHARS IN EQUIMOLAR STEAM-HYDROGEN MIXTURES AT 1500°F AND 35 atm

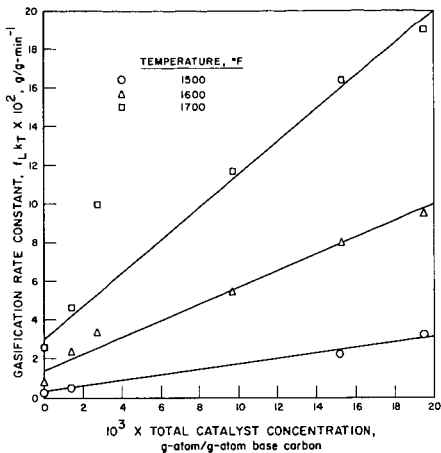


Figure 10. EFFECT OF CATALYST CONCENTRATION ON THE OVERALL RATE OF GASIFICATION OF MONTANA LIGNITE CHARS IN EQUIMOLAR STEAM-HYDROGEN MIXTURES AT A TOTAL PRESSURE OF 35 atm

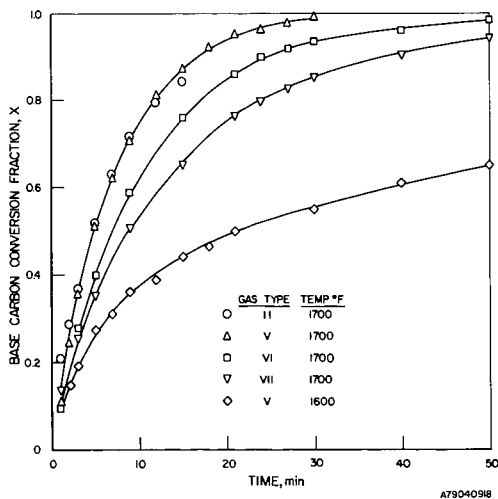


Figure 11. GASIFICATION OF CHARS FROM SAMPLE G IN SYNTHESIS GAS MIXTURES AT 35 atm

CHEMISTRY OF GASIFICATION AND ASH AGGLOMERATION IN THE U-GAS^R PROCESS.
J. G. Patel, D. M. Mason, 3424 South State Street, Chicago, IL 60616

A single-stage, fluidized-bed, ash-agglomerating process for generation of industrial fuel gas or synthesis gas from coal has been tested in a pilot plant with coke, char, and coal as feed. Pilot plant and laboratory data on gasification reactivities have been obtained and incorporated into a mathematical model. The chemistry of agglomeration of ash was investigated by methods including optical and electron microscopy, chemical analyses, and fusibility tests. Agglomeration of ash into rounded beads occurred with relative ease in runs on coke; the agglutinating agent is an iron-rich, relatively low-melting silicate in which other ash is embedded. Agglomeration of ash from coal was more difficult, because most of the iron was present in the form of sulfide and thus unavailable for reaction with aluminosilicates (clay minerals). The gas composition in the reactor bed is thermodynamically favorable for oxidation of the ferrous sulfide at regions near the oxygen inlet only. Oxidation of the ferrous sulfide and agglomeration of ash from coal were achieved by changing the mode of oxygen feed to the reactor.

REACTIVITY OF TRI-GAS CHAR IN A FLUIDIZED-BED REACTOR

Mario A. Colaluca, Kanwal Mahajan, Mark A. Paisley

Bituminous Coal Research, Inc.
350 Hochberg Road, Monroeville, Pennsylvania 15146

INTRODUCTION

The evolution and the development of the BCR TRI-GAS fluidized-bed gasification process to produce low- to medium-Btu fuel gas has been described in two earlier papers.^{1,2} TRI-GAS is a multiple fluidized-bed coal gasification process. The overall objective of TRI-GAS is the gasification of a range of coals, with the only product being a clean, low-Btu fuel gas. No liquids, tar, or char are produced as a waste or by-product. The process consists of three fluidized-bed reactors connected in series. Each reactor has its own specific function. Stage 2 is the main gasification stage. In this stage, devolatilized coal (char) and the volatile products from Stage 1 are gasified with air and steam, producing a low-Btu (about 150 Btu/cu ft) fuel gas.

The objective of the current study is to establish a model for the overall gasification reaction in a fluidized bed and to use this model to predict conversion in the TRI-GAS Stage 2 reactor during PEDU tests. The model assumes that the overall reaction rate is determined by the separate rates of two processes in series; first, mass transfer, where steam must be transported out of the bubble to the particulate phase, and second, the chemical reaction. The chemical reaction process has been isolated from mass-transfer effects and studied independently in the thermogravimetric analysis (TGA) unit where a chemical reaction rate is established, describing the resistance of the chemical process. Similarly, the tests in the bench-scale fluidized-bed reactor establish a parameter characterizing the mass transfer process from the bubble to the particulate phase.

APPARATUS AND PROCEDURE

Char Preparation

Char (+100 mesh) from the Rosebud seam coal pretreated during a typical PEDU test was used for reactivity studies in the TGA apparatus and the bench-scale fluidized-bed batch reactor. This char was produced by pretreating the Rosebud seam coal in a fluidized bed at 900 F to remove volatile matter and tars from the coal prior to feeding to the gasification reactor.

TGA Reactivity

An American Instrument Company basic thermogravimetric analysis unit was used for the reactivity measurements. About 100 mg of char contained in a ceramic pan was heated in nitrogen to the chosen reaction temperature. Since some devolatilization occurred during this process, heating continued until the char weight became constant. The nitrogen was then bubbled through water held at a specified temperature and this reactant passed over the char. Char weight loss was recorded continuously as a function of time.

The measure of reactivity chosen in this study was the same as Jenkins' "reactivity parameter".³ The definition is (symbols defined in Appendix A):

$$R_5 = \frac{1}{W_0} \frac{dW}{dt}$$

The maximum rate of weight loss ($\frac{dW}{dt}$) was determined experimentally from the slope of the weight loss data recorded on an X-Y plotter. The maximum rate could be defined without difficulty since, in all cases, the initial rate was constant.

The reactivity parameter was assumed to depend on reacting gas concentration, C_p , in the following manner:

$$R_5 = k C_p^n \quad (1)$$

where

$$k = \alpha \exp - \frac{E}{RT}$$

Taking the natural logarithm of both sides of Equation (1) results in

$$\ln R_5 = \ln k + n \ln C_p \quad (2)$$

A multiple linear regression analysis was performed using reaction rate (R_5) data taken at constant temperature for various values of C_p , resulting in values of n . The values of n , taken for several temperatures, were then averaged.

With n thus defined, Equation (1) can be used to determine the apparent activation energy and frequency factor for each reaction. Solving for k in Equation (1) results in

$$k = \frac{R_5}{C_p^n} \quad (3)$$

The right-hand side of this expression can be calculated from the data, the previously determined values of n , and the experimental conditions. Again, taking the logarithm of both sides results in

$$\ln k = \ln \frac{R_5}{C_p^n} = \ln \alpha - \frac{E}{RT} \quad (4)$$

A multiple regression analysis was performed using data at several temperatures resulting in the "apparent" activation energy E and the frequency factor α for each reaction. These results are reported in Table 1.

TABLE 1. TGA REACTIVITIES AND KINETIC PARAMETERS OF CHAR USED IN LABORATORY STUDIES

Test No.	Sample Temp, °K	Volatile Matter, mg	Steam Concentration, moles/cu cm	Reactivity, (hr) ⁻¹
1	1193	12.8	0.89×10^{-6}	2.21
2	1193	13.3	1.35×10^{-6}	3.11
3	1193	13.5	2.01×10^{-6}	3.76
4	1136	11.5	0.93×10^{-6}	1.67
5	1136	12.0	1.42×10^{-6}	2.12
6	1136	11.5	2.11×10^{-6}	2.67

$$R_5 = C_p^n \alpha \exp^{-E/RT}$$

$$n = 0.61$$

$$\alpha = 1.94 \times 10^7$$

$$E = 17,662 \text{ cal}$$

Fluidized-bed Reactor

A schematic of the bench-scale fluidized-bed pressurized batch reactor system is shown in Figure 1. This system can be used for reactivity analysis with steam, carbon dioxide, and air. The reactor is made of 5.08 cm diameter by 91 cm long Incoloy 800 pipe. The reactor furnace consists of two 1450 watt, 61 cm long, furnace half-sections. The steam is generated by bubbling the inert gas through a 10.16 cm diameter by 51 cm long 316SS water-filled vessel heated by 2KW immersion heater. This steam generator is capable of producing saturated steam at 150 psi pressure. The reactor is followed by a water-cooled vessel where condensibles can be collected. The precise metering of the reacting gases is accomplished through Brooks Instrument Model 1110 rotameters. Foxboro pressure and DP cell transmitters are used for pressure control in the system and differential pressure measurements in the bed. For efficient distribution of the reacting gases in the reactor, the grid system consists of a 5-cm fixed bed of Steatite packing, packed between two screens. The system is also equipped with necessary auxiliary equipment for indicating actual pressures and temperatures in the reactor and the boiler. The system can be used to generate the reactivity data at 2200 F temperature and 150 psi pressure.

A 200-gm sample of the char was heated to the chosen reaction temperature and pressure with nitrogen flowing through the bed. Then the water-vapor reactant was generated by bubbling the nitrogen through hot water at a specified temperature and passed through the reactor. After a specified period of time, the reaction was quenched when the bed was purged with nitrogen. Conversion was determined by weighing the sample after cooling.

In a fluidized-bed reactor, the experimental value of the percent unreacted char is given by:

$$Y_{\text{exp}} = \frac{W}{W_0} \times 100$$

THEORETICAL MODEL

The model assumes that the overall reaction rate is determined by the separate rates of two processes in series; first, mass transfer, where steam must be transported out of the bubble to the particulate phase, and second, the chemical reaction. The chemical reaction process has been isolated from mass-transfer effects and studied independently in the thermogravimetric analysis (TGA) unit where a chemical reaction rate constant describing the resistance of the chemical process was established.

The following development is essentially that presented by Orcutt.⁴ Only the detailed form of the reactant conversion term (R_c) differs. The form used in this study was developed empirically from differential reactor (TGA) data. The fluid bed is assumed to be divided into two distinct phases called the bubble and particulate phase. The reactant flow above that required to just fluidize the bed forms the bubble phase. No solids exist in this phase so no chemical reactions can occur. It is assumed that the bubble size is uniform. The particulate phase consists of the remainder of the flow and the solid char. The char-steam chemical reaction occurs in the particulate phase. Furthermore, the turbulent action in the bed allows the assumption that the steam concentration and temperature are constant throughout the particulate phase.

A material balance on a single rising bubble gives:

$$U_B V \frac{dC_B}{dy} = Q (C_P - C_B) \quad (1)$$

Since C_P is assumed to be a constant, Equation (1) can be integrated directly to obtain:

$$\int_{C_0}^{C_B} \frac{dC_B}{C_P - C_B} = \frac{Q}{U_B V} \int_0^y dy$$

$$C_B = C_P + (C_0 - C_P) \exp^{-X(y)} \quad (2)$$

where
$$X(y) = \frac{Qy}{U_B V}$$

The particulate phase material balance is:

$$R_1 + R_2 = R_3 + R_4 + R_5 \quad (3)$$

The amount of reactant transferred from the bubble, R_1 , is determined by integrating the flow from the individual bubbles to the particulate phase over the entire reactor:

$$R_1 = A_T NQ \int_0^L C_B dy$$

Using Equation (2) for C_B results in:

$$R_1 = A_T NQ \left[C_P L - (C_0 - C_P) \frac{U_B V}{Q} \exp^{-X(L)} + (C_0 - C_P) \frac{U_B V}{Q} \right] \quad (4)$$

The amount of reactant fed directly to the particulate phase is:

$$R_2 = A_T U_{mf} C_0 \quad (5)$$

and leaving the particulate phase is:

$$R_4 = A_T U_{mf} C_P \quad (6)$$

The amount of reactant transported from the particulate to the bubble phase is given by:

$$R_3 = A_T NQ L C_P \quad (7)$$

Finally, the reactant consumed by the gasification reaction in the particulate phase is given by:

$$R_5 = A_T L_{mf} \left(\frac{1}{V_{TMF}} \frac{dN_R}{dt} \right) \quad (8)$$

The TGA data are used to evaluate the right-hand side of Equation (8). The TGA reaction rate is given by:

$$\frac{1}{W_o} \frac{dW}{dt} = -k C_P^n \frac{W}{W_o} \quad (9)$$

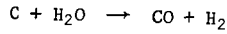
But,

$$dW = M_C dN_C$$

Thus,

$$\frac{dN_C}{dt} = - \frac{W_o}{M_C} k C_P^n Y$$

For the reaction:



$$\frac{dN_C}{dt} = \frac{dN_R}{dt}$$

so that,

$$\frac{1}{V_{TMF}} \frac{dN_R}{dt} = - \frac{W_o}{M_C V_{TMF}} k C_P^n Y \quad (10)$$

Substituting this expression into Equation (8) gives:

$$R_5 = \frac{A_T L_{mf}}{V_{TMF}} \left(\frac{W_o}{M_C} \right) k C_P^n Y \quad (11)$$

Substituting Equations (4), (5), (6), (7), and (11) into Equation (3) gives:

$$(VNU_B) (C_O - C_P) (1 - \exp^{-X(L)}) + U_{mf} (C_O - C_P) = \frac{1}{A_T} \frac{W_o}{M_C} k C_P^n Y$$

From Reference 6

$$VNU_B = U_o - U_{mf}$$

and defining:

$$\beta = 1 - \frac{U_{mf}}{U_o}$$

$$\xi_P = \frac{C_P}{C_O}$$

and

$$\lambda = \frac{W_o}{M_C} \frac{k C_o}{A_T U_o}^{n-1}$$

the nondimensional form for the particulate phase balance becomes,

$$(1 - \xi_p) [B (1 - \exp^{-X(L)}) + (1 - \beta)] = \lambda Y \xi_p^n \quad (12)$$

In nondimensional form, Equation (9), describing the char conversion, becomes:

$$\frac{dY}{d\tau} = - Y \xi_p^n \quad (13)$$

where

$$\tau = \frac{t}{t_R}$$

$$Y = k C_o^n t_R$$

To compare this model with data from the batch laboratory tests, Equation (13) is integrated numerically to determine char weight for various run times. For each integration step, Equation (12) is solved for ξ_p .

RESULTS AND DISCUSSION

The results of the char conversion experiments at atmospheric pressure are shown in Figure 2. Also shown on this figure are the theoretical conversions predicted using transfer parameters (X) calculated from the Kunii and Levenspiel (K&L)⁵ and the Davidson and Harrison (D&H)⁶ models. Reactivities determined from TGA tests (Table 1) were used in the theoretical conversion calculation. In both models, average bubble size was calculated from Mori and Wen⁷ and the self-diffusion coefficient calculated as in Reference 8. Both theories overpredict the char conversion. Actual conversion corresponds to a mass-transfer parameter $X = 0.75$ as opposed to $X = 1.79$ predicted by K&L and $X = 4.73$ predicted by D&H, Table 2.

TABLE 2. MASS TRANSFER PARAMETER, X, FOR CHAR
USED IN LABORATORY TESTS

Reactor Pressure, psia	U_o/U_{mf}	Kunii & Levenspiel	Davidson & Harrison	Experimental	Gas Diffusivity D_g (adjusted) cm ² /sec
14.7	9.34	1.79	4.73	0.75	0.52
70.0	3.78	1.99	5.78	0.08	0.0008

Examination of the expressions used to calculate X from both models reveals two parameters that can be adjusted to allow agreement between the experiment and the theory. These are the bubble diameter (D_B) and the gas self-diffusion coefficient (D_g). The bubble diameter would have to be adjusted to about 10 cm to allow $X = 0.75$. Since this is considerably larger than the reactor ($D_T = 5.08$ cm), it is necessary to adjust D_g . Adjusting D_g from a theoretical value of $D_g = 3.33$ cm²/sec down to $D_g = 0.52$ cm²/sec and using the Kunii and Levenspiel model results in $X = 0.75$ and agreement with the experimental data. The conversion results at 70 psia are shown in Figure 3. The experimentally determined X and D_g adjusted to achieve this X at 70 psia are shown in Table 2.

It is interesting to note that to achieve these low transfer parameters, models must be employed with more than one transfer resistance in series. One of the resistances must depend on gaseous diffusion. Figure 4 shows the comparison of mass-transfer parameters calculated using a simple resistance theory (D&H) and a three-resistance theory (K&L). In the D&H model, it is assumed that two transfer mechanisms are occurring in parallel. There is a macroscopic movement of gas from the bubble along with a microscopic diffusive transfer. As D_g goes to zero, the D&H model predicts that X approaches a finite value ($X \approx 0.5$)⁸ dependent only on the macroscopic transfer between the bubble and particulate phase. Calculation as D_g goes to zero at the elevated pressures results in about the same value for X. Since this is substantially greater than the experimental X, a theory incorporating a totally diffusive resistance in series must be used.

The K&L theory assumes the same transfer mechanisms as D&H out of the bubble, but places a third resistance, namely the cloud, between the bubble and the particulate. The transfer through the cloud is only due to gaseous diffusion. Thus, for the K&L case, the diffusive transfer between the cloud and the particulate phase can choke off the flow and the overall coefficient between bubble and particulate can be adjusted as low as needed to agree with experiment.

SUMMARY OF RESULTS

1. A two-phase fluidized-bed model can be used to predict the conversion observed in the char-steam gasification reaction in a 5.08-cm fluidized-bed reactor.

2. The best fit of the experimental data was obtained using the K&L model to calculate the mass exchange between the bubble and particulate phases.

ACKNOWLEDGMENT

The work described in this paper was conducted under the sponsorship of the U.S. Department of Energy under Contract No. DE-AC21-78MCO2798.

REFERENCES

1. Stewart, J. T. and Diehl, E. K., "Fluidized bed coal gasification - process and equipment development," Third International Conference on Fluidized Bed Combustion, Hueston Woods, Ohio, 1972. 19 pp.
2. Colaluca, M. A., Paisley, M. A., and Mahajan, K., "Development of the TRI-GAS gasification process," AIChE 71st Annual Meeting, Miami Beach, Florida, 1978. 27 pp.
3. Jenkins, R. G., Nandi, S. P. and Walker, P. L., Jr., "Reactivity of heat-treated coals in air at 500°C," Fuel 52, 288 (1973).
4. Orcutt, J. C., Davidson, J. F., and Pigford, R. L., "Reaction time distribution in fluidized catalytic reactors," AIChE Symposium Series 38, 58, 1 (1962).
5. Kunii, D. and Levenspiel, U., "Fluidization Engineering," New York: John Wiley & Sons, 1969. page 227.
6. Davidson, J. F. and Harrison, D., "Fluidized Particles," Cambridge: Cambridge University Press, 1963. page 98.
7. Mori, S. and Wen, C. Y., "Estimation of bubble diameter in gaseous fluidized beds," Fluidization Theories and Applications, AIChE Symposium Series 161, 73, 121 (1977).
8. Perry, R. M. and Chilton, C. H., "Chemical Engineers' Handbook," Fifth Edition, McGraw-Hill Book Co., 1973. page 3-230.

APPENDIX A

NOMENCLATURE

- A_T = Reactor cross-sectional area, sq cm
- C_O, C_P, C_B = Steam concentration in reactor inlet, particulate phase and bubble phase, moles/cu cm
- D_g = Gas Diffusivity, sq cm/sec
- D_T = Reactor diameter, cm
- k = Reaction rate constant
- L, L_{mf} = Fluid bed height, height at minimum fluidization, cm
- M_C = Char molecular weight, gm/gm mole
- n = Exponent for char reactivity
- N = Number of bubbles per unit volume, 1/cu cm
- N_C, N_R = Number of reacting moles of char and steam
- Q = Effective volumetric flow rate from the bubble phase to the particulate phase, cu cm/sec
- R_1, R_2, R_3, R_4, R_5 = Reactant transported from the bubble to particulate phase, fed to particulate phase, transported from the particulate to bubble phase, left the particulate phase and disappeared due to chemical reaction in particulate phase, moles/sec
- S = Surface area of the rising bubble, sq cm
- t, t_R = Time, solids residence time, sec
- U_O, U_B, U_{mf} = Superficial velocity, bubble velocity, minimum fluidization velocity, cm/sec
- V, V_P, V_{TMF} = Bubble volume, particulate phase gas volume, total fluid bed volume at minimum fluidization conditions, cu cm
- W, W_O = Instantaneous char weight, weight at the instant the reacting gas is introduced (on ash-free basis), mg
- X = Mass transfer parameter
- y = Axial distance from the reactor inlet, cm
- Y = W/W_O
- α = Frequency factor

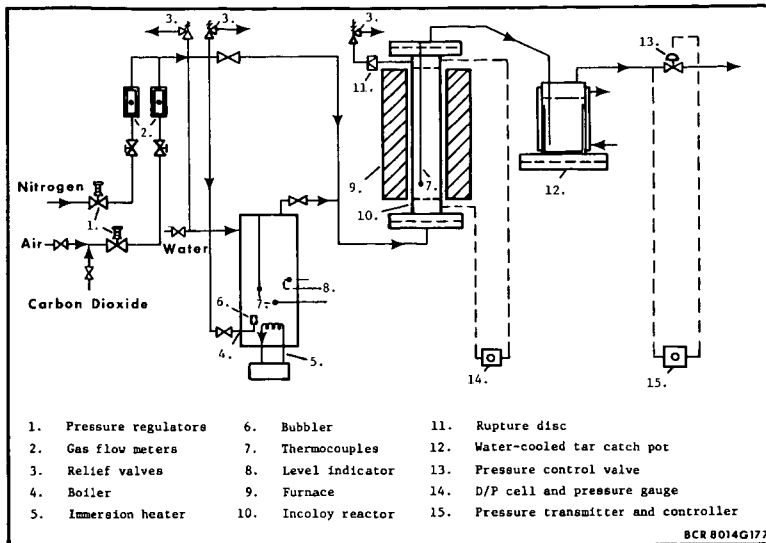


Figure 1. Flow Diagram of Laboratory Fluidized-bed Test Unit

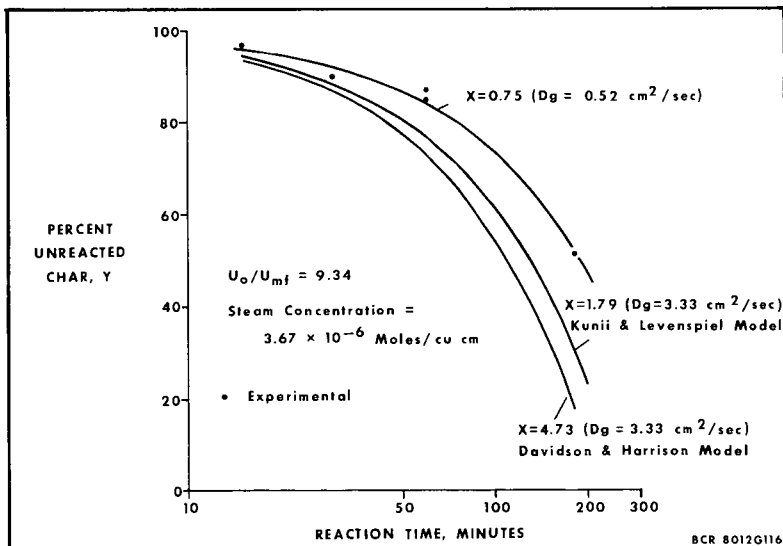


Figure 2. Char Conversion at Atmospheric Pressure and 1800°F Temperature

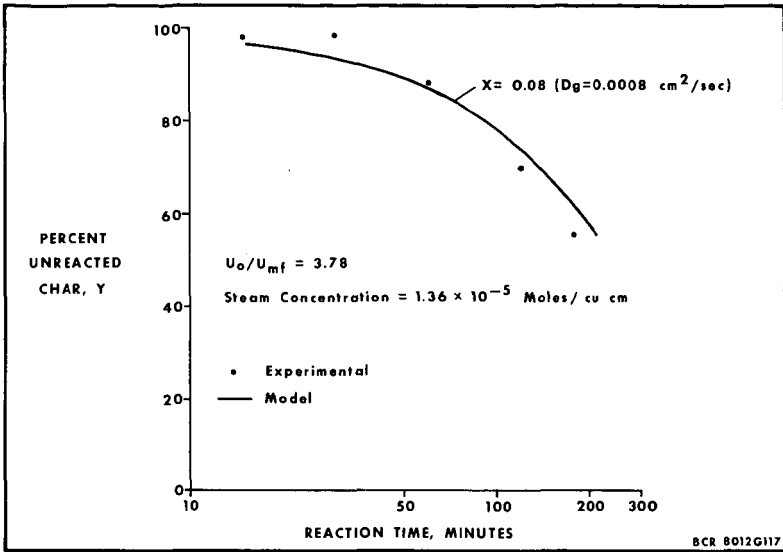


Figure 3. Char Conversion at 70 psia Pressure and 1800°F Temperature

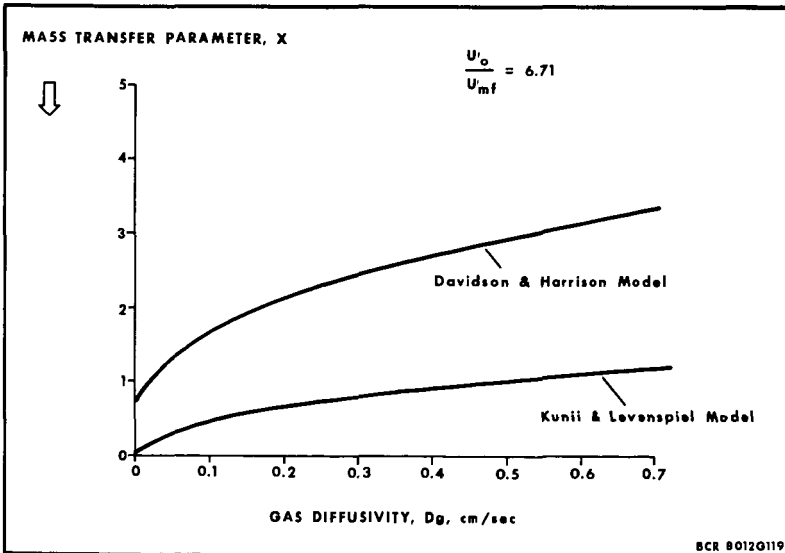


Figure 4. Diffusivity Effect on the Mass Transfer Parameter in a Fluidized-bed

ELECTROCHEMICAL ROUTE TO COAL GASIFICATION

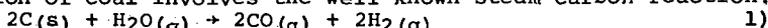
AND ITS TECHNOLOGICAL IMPLICATIONS

Robert W. Coughlin and M. Farooque

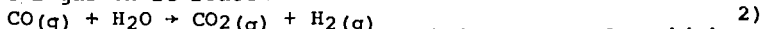
Department of Chemical Engineering
University of Connecticut
Storrs, CT 06268

Introduction

The production of synthetic natural gas or synthetic oil from coal consumes copious quantities of hydrogen that can be generated in large amounts only by processes which split the water molecule. Here we report on a new method for producing such hydrogen from coal, water and electric energy at mild temperatures. Conventional hydrothermal gasification of coal involves the well known steam-carbon reaction;

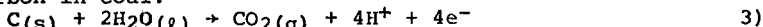


and the water gas shift reaction:

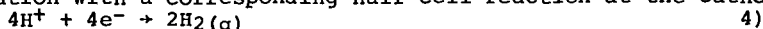


To ensure favorable equilibrium reaction 1) is conducted at high temperatures. The chemistry and technology of such coal gasification are complex and a detailed discussion of such matters, including hardware and gasification equipment, has been published by Squires [1] and others [2-3].

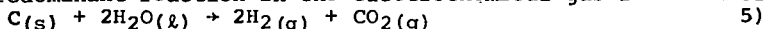
We have reported [4] a newly developed electrochemical process which converts coal and water into two separate gaseous products, the one comprising essentially gaseous oxides of carbon and the other essentially pure hydrogen. The process chemistry takes place at mild temperatures (even room temperature) and the gaseous products are essentially free of impurities such as ash, tar and sulfur compounds. This new electrochemical gasification process involves the anodic oxidation of coal at an electrode for which we postulate the half-cell reaction of the carbon in coal:



in combination with a corresponding half-cell reaction at the cathode:



The net sum of these half-cell reactions 3) and 4) is just the equation for the predominant reaction in the electrochemical gasification of coal:



The application of an electrical potential and the input of electrical energy overcomes the free-energy barrier for reaction 5) at low temperatures and permits it to be accomplished even at room temperatures and actual practical potentials of about 0.85V - 1.0V. The thermodynamic reversible potential ($|\Delta G|/nF$) for equation 5) at room temperature is only 0.21V. A notable advantage of electrochemical gasification of coal over conventional methods of coal gasification is the production of gaseous oxides of carbon at the anode and the simultaneous production of essentially pure hydrogen separately at the cathode. Because each gaseous product is produced separately and essentially free of impurities such as sulfur, tar and ash, subsequent cleaning, separation and purification steps are minimized. Other manuscripts [4,5,6] have introduced the process of electrochemical coal gasification and reported initial data as to the reactivities of various coals, the effect of different operating conditions and variables, and distinguished the process from conventional water electrolysis. Its relationship to conventional methods of coal gasification and the well known steam carbon reaction was also discussed. In the present paper we present results obtained in galvanostatic and potentiostatic studies, and we also consider the

technological implication of this process in the field of H₂ production, and electrowinning of metals from aqueous electrolytes.

Experimental

All experiments were conducted with stirred slurries of coal in aqueous electrolyte within the anode compartment of a cell (details of the experimental apparatus are given in references [4,5]). The external emf was applied by a potentiostat (both Model PAR 371 and PAR 179A were used) and the electrodes (both anode and cathode) were Pt mesh, gauge 52 (0.004" diameter wire) supplied by Mathey Bishop, Inc.

Potentiostatic Studies: Effect of Potential and Course of the Reaction

The higher the potential the greater the oxidation current. As the coal is consumed by oxidation at a given potential the current diminishes very slowly. This behavior is shown in Figure 1 where current is plotted vs. potential for various extents of coal consumption* as a parameter. Similar behavior is evident in Figure 2, where observed reaction rates of three different coal samples and one activated charcoal at 1.0V, using a coal slurry concentration of 0.069 gm/cm³ are plotted against cumulative coulombs passed. The results indicate that the rate of oxidation falls gradually as the reaction proceeds for all the samples studied. Only a portion (up to about 18% for NDL) of the coal can be consumed* before the rate of oxidation begins to fall steeply.

Previous workers [7-9] have reported that controlled oxidation of purer carbons, whether by electrochemical or chemical means results in the formation of several surface oxides. Of these oxides, the carboxylic group usually predominates. We believe, such oxides also form during the anodic oxidation of coal and they increase in concentration on the surface of the coal particles as the reaction advances, rendering electron abstraction more and more difficult, with consequent lowering of the oxidation current. Preliminary results obtained by analyzing the residual carbon values after partial electrochemical gasification of Pittsburgh coal also supports this view. Based on the known decomposition temperatures reported [10] for such surface oxygen compounds on carbon it should be possible to maintain a higher and steady oxidation rate at 200° - 600°C. It seems reasonable to consider surface oxides as intermediates in the pathway from coal and water as reactants to gaseous oxides of carbon and hydrogen as reaction products.

The decrease in oxidation current may also result in part from the accumulation on the coal particles of a tar-like coating that is formed during electrochemical coal gasification. Such a coating may be additional reaction products in the form of small aliphatic fragments which break away from larger coal molecules during anodic oxidation.

From Figure 2 it can be seen that the rate of oxidation of the Pittsburgh coal has dropped by a factor of about 7 when about 16% of the coal is electrochemically consumed. After it had been consumed to this extent, the coal was subjected to several treatments, to investigate the nature of the deactivation and explore the possibility of regeneration. The results disclose that the following treatments restore the original activity of the coal to a great extent: (A) washing with acetone which was also observed to remove tar-like material from the coal with the formation of a dark, perhaps colloidal, extract solution, and (B) heating in air to 250°C, which presumably removes accumulated

*Throughout this paper the extent of coal consumption is computed as the mass of carbon equivalent to total electrical charge passed during the experiment.

oxygen-containing surface functional groups [7]. In another experiment, North Dakota lignite was anodically oxidized at 1.0V and at 114°C with consumption of 26% of the coal, the remaining coal was filtered from the electrolyte, washed with acetone, and then heated in air to 250°C for 2 hours. This reactivated coal was then returned to the anolyte, and was further consumed an additional 20%. With the regenerated coal the oxidation current was almost equal to that observed with virgin coal and curve 2 of Figure 2 was essentially reproduced under the same conditions and with similar product formation. These experiments suggest that it would be possible to consume coal to a much larger extent at a meaningful rate by conducting the electrochemical gasification reaction at temperatures of about 200°C and above. Experiments at higher temperatures are planned and will be reported in another paper.

Galvanostatic Studies: Effect on the Cell Potential

North Dakota lignite was electrochemically gasified under galvanostatic conditions. Initially, the fresh coal samples were oxidized at a constant oxidation current of 150 mA until 9.82% of the coal was consumed, then the oxidation rate was lowered to 100 mA. The corresponding change of cell potential is plotted against the percentage of the total coal consumed in the process in Figure 3. The results clearly indicate that to maintain the desired rate of the reaction, the cell potential gradually rises because, as explained above, the coal particles become more and more unreactive as the reaction progresses (there may also be some effect due to decreasing coal concentration as well.) The potential required to maintain a constant current of 150 mA continues to rise in Figure 3 to about 1.2V (attained at first after about 97 hr) whereupon the required potential rises abruptly to about 1.7V, thereby suggesting the onset of a different reaction mechanism. As evident in Figure 3 this discontinuity at 1.2V was reproducible at two different currents (150mA and 100mA) and two corresponding different stages of coal consumption. It should be noted that analysis of the anode gas revealed only CO₂ and CO and no trace of O₂ until the potential reached 1.98V. It appears, therefore, that the discontinuity at 1.2V may correspond to the onset of a different mechanism of electrochemical coal gasification; it cannot be explained as the onset of simple water electrolysis.

Temperature Effects

It is suggested above that it would be possible to consume coal to a much larger extent at a meaningful rate by conducting the electrochemical gasification reaction at temperatures of about 200°C and above. Higher temperature operations may also provide other benefits:

- (i) polarization potentials (overvoltages) would be lowered and
- (ii) the reversible (thermodynamic) cell potential would also be lowered as explained below.

Figure 4 shows the effect of temperature on the reversible cell potential as computed from the thermodynamic ΔG and ΔH values of the electrochemical coal gasification reaction 5). Referring to this figure, the electrochemical coal gasification cannot occur below the reversible thermodynamic potential that corresponds to the Gibbs free energy of reaction (ΔG); this voltage decreases with increasing temperature. It is possible in principle for electrolysis to occur at any potential above the reversible thermodynamic value, if TAS is supplied as heat from the surroundings, but in practice polarization effects and other irreversibilities require larger potentials in order to operate at reasonable rates of reaction.

If the cell is operated at or above the thermoneutral voltage

($= \frac{|\Delta H|}{nF}$) both ΔG and $T\Delta S$ are supplied as electrical energy and no additional energy is required because the entire endothermic heat of reaction is supplied as electrical energy. Above the thermoneutral voltage there would be net heat generation and heat removal would be necessary.

Gases Produced and the Current Efficiency

During the oxidation of NDL, Pittsburgh coal, activated carbon and Montana Rosebud char at potentials between 0.8V to 1.2V the gas produced at the cathode was essentially pure H_2 and in each case the current efficiency of H_2 production was around 100% based on measured current integrated over time. The gas produced within the anode compartment was almost pure CO_2 with small amounts of CO. The composition of the anode gas, however, varies somewhat over the course of the gasification reaction; this may be attributed to corresponding changes in population of surface oxides on the coal. It is also observed that the volume ratio of the gases collected at the cathode to those at the anode ranged from about 9.1 to 3.7; the higher ratios were obtained at the beginning of the experiment but then decreased. According to the stoichiometry of reaction 5) this gas ratio should be about 2. Cathode-to-anode gas ratios greater than about 2.0 can be attributed mainly to accumulation of oxygen on the coal particles in the form of functional groups such as $-COOH$, $-CHO$, CH_2OH and the like. Moreover, higher relative amounts of H_2 may also be attributed in part as arising from the hydrogen content of the coal. Preliminary proximate analysis of the residual carbon after NDL gasification reveals preferential consumption of volatile components which are expected to be rich in hydrogen. The production of anode gas is probably strongly related to the concentration of the surface oxides of coal. Binder et al reported [7] that a surface layer forms first on graphite and only then does CO_2 evolution begin. As the oxidation process advances, surface oxides may build up to steady-state concentrations on the coal, whereupon the anode compartment gas generation rate becomes constant. A qualitative but sensitive mass spectrometric analysis was made of the gases produced at both anode and cathode. It is noteworthy that no lines were observed for molecular weights corresponding to SO_2 or H_2S --even though the parent coals contain significant sulfur.

Implications for Hydrogen Production

The more common approaches to splitting the water molecule to recover hydrogen have utilized either electrical energy alone or fossil fuel in combination with thermal energy. It appears that the production of hydrogen by the combined use of fossil fuel and electrical energy as we report has not previously been investigated or applied. In the following the efficiency of H_2 production by our new process ("Coal-Consuming Water Electrolysis") is compared with ordinary water electrolysis. In water electrolysis the energy required to split the water molecule is supplied solely by electricity, whereas in our new process the required energy is supplied only in part by electricity with the balance arising by way of the concomitant anodic oxidation of coal. The following quantitative development gives a first order approximation of how much energy comes from each such source and thereby provides a rough feeling for efficiency. The energy consumed by conventional water electrolysis conducted at a potential of E_2 to produce N_{H_2} moles of H_2 is $2N_{H_2} F E_2$ whereas the energy required by the present process under investigation operating at a potential of E is:

$$E \int_0^t i dt + N_c (-\Delta H) \quad (6)$$

where E is the potential applied across the cell, i is the current and

t is time. N_C is the number of moles of carbon consumed and ΔH is the enthalpy of combustion of carbon to CO_2 .

The foregoing expression can be simplified by assuming a constant operating potential E , and noting that:

$$N_{H_2} = \int i dt / 2F \quad 7)$$

$$\text{and } N_C = 1/2 N_{H_2} \quad 8)$$

where F , the Faraday constant, is 96,500 coulombs/equivalent.

Eliminating $\int i dt$ and N_C the expression for total energy consumption by our process becomes:

$$2FN_{H_2}E + 1/2 N_{H_2}(-\Delta H) \quad 9)$$

The relative energy usage (REU) is accordingly:

$$\text{REU} \left(\frac{\text{Ordinary Electrolysis}}{\text{Coal Assisted Electrolysis}} \right) = \frac{2N_{H_2}F E_2}{2F N_{H_2}E + 1/2 N_{H_2}|\Delta H|} \quad 10)$$

$$= E_2 / (E + |\Delta H|/4F)$$

Inserting $|\Delta H| = 94,100 \times 4.18$ joules/mole and the value of F gives:

$$\text{REU} = E_2 / (E + 1.02) \quad 11)$$

Practical values of E_2 for conventional electrolysis are about 1.8-2.0V whereas values of E observed in the present work have ranged from about 0.8 to about 1.0 volt at room temperature. This means that, per unit of hydrogen produced, the total energy consumption is about the same ($\text{REU} \approx 1$) for ordinary water electrolysis and for coal-assisted water electrolysis conducted in the experiments near room temperature reported here. In the case of electrochemical gasification to hydrogen, however, about half the required energy comes directly from coal and half from electricity. We expect that the total energy requirement for coal-assisted water electrolysis can be lowered further by conducting it at higher temperatures thereby permitting operation at lower potentials (E) than 0.8 - 1.0 volt. A detailed economic analysis reported elsewhere [5] shows that coal-assisted electrolysis has its most favorable effect when electricity costs are high because cheaper coal energy is substituted for more costly electrical energy. The greatest effect (a 27% reduction in hydrogen cost) is evident for application with SPE technology at "normal" power costs of \$0.027/kw.hr.: the corresponding cost reduction for conventional electrolysis is 18%. For off-peak power at \$0.01/kw.hr. it is seen that direct incorporation of coal into the electrolysis process seems to offer no particular advantage.

Implications for Electrowinning of Metals

Electrochemical coal gasification can be extended to the electro-winning of metals by substituting the half cell reaction 3) (which consumes coal) for the half-cell reaction of oxygen evolution which ordinarily takes place during conventional electrowinning of metals from aqueous solutions of their salts. By this coal-based innovation the total overall cell potential of the resulting metal electrowinning process is lowered by about 1.10V with a corresponding significant reduction in the consumption of electrical energy. As a test case Cu was deposited on a platinum mesh cathode (separated from the anode by a fritted glass barrier) from aqueous electrolyte (0.125 M $CuSO_4$ in 0.5 M H_2SO_4) at 60°C, at two different galvanostatic rates; 5.9 mA and 12 mA. The corresponding change in cell potential is plotted in Figure 5. It is evident that the conventional copper electrowinning

reactions took place at cell potentials of about 1.65V and 1.73V respectively. Also plotted in Figure 5 are the results obtained in parallel experiments conducted in identical fashion except that the coal was simultaneously oxidized at the anode according to equation 3) while Cu cations were reduced at the cathode. In these latter experiments, North Dakota lignite (NDL) coal slurry (0.15 gm/cm^3) was introduced into the anode compartment of the cell and was anodically oxidized while copper deposited on the cathode under identical galvanostatic experimental conditions. As a result of the oxidation or gasification of the coal at the anode, the overall cell potential was lowered by about 1.1V, compared to the conventional process. This is evident from the comparative data plotted in Figure 5.

Concluding Remarks

It has been shown in this study that

- (i) different coals have different reactivities for electrochemical gasification and in each case the reactivity of the particular coal falls gradually as the reaction advances.
- (ii) the original reactivity of the coal samples can be restored by acetone washing and heating at temperatures between $200^\circ - 600^\circ\text{C}$.
- (iii) high temperature operation promises several advantages.
- (iv) two different coal oxidation mechanisms appear to occur in two correspondingly different potential regions of oxidation.
- (v) hydrogen production and electrowinning of metals from aqueous electrolytes are the processes where electrochemical coal gasification may find application.

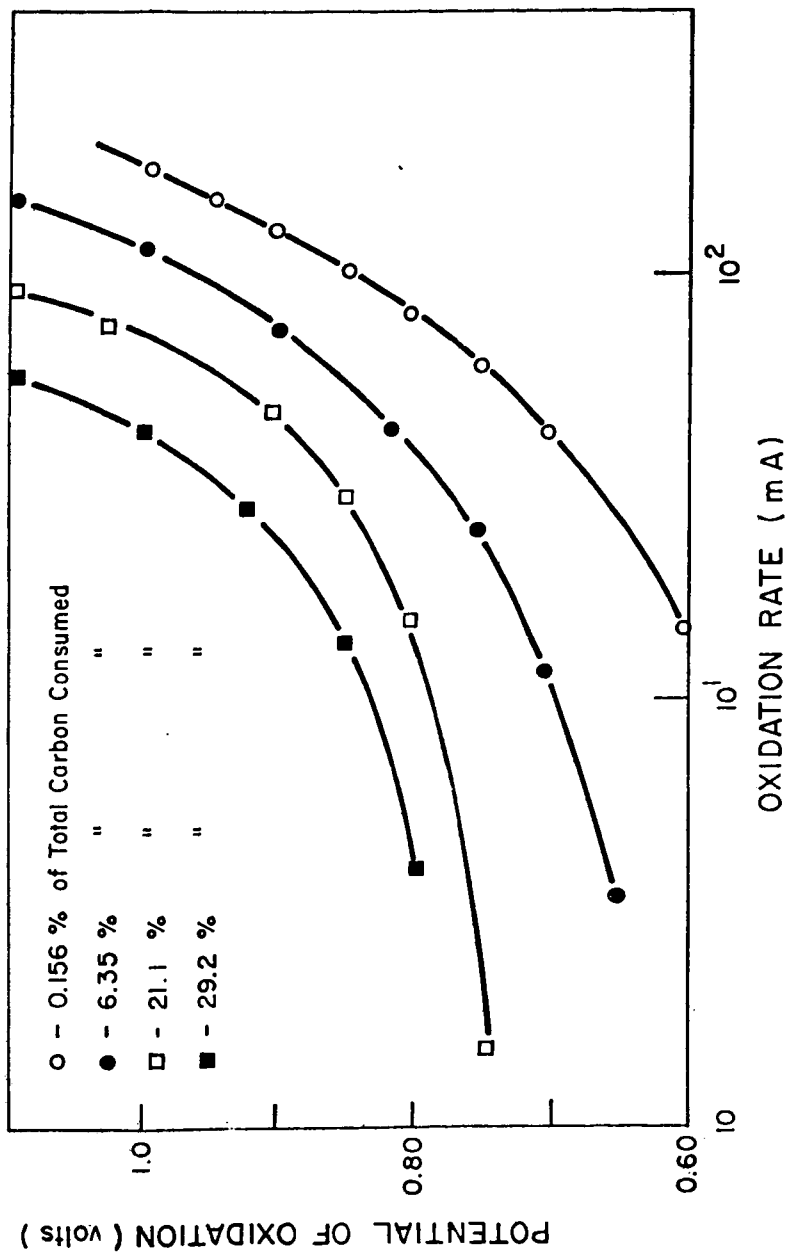
Mass balance calculations, high temperature reaction and use of anodes other than platinum are currently in progress.

Acknowledgement

We are grateful for the financial support of this research by the University of Connecticut Research Foundation and the U.S. Department of Energy. Valuable experimental assistance was provided by Larry Veneziano.

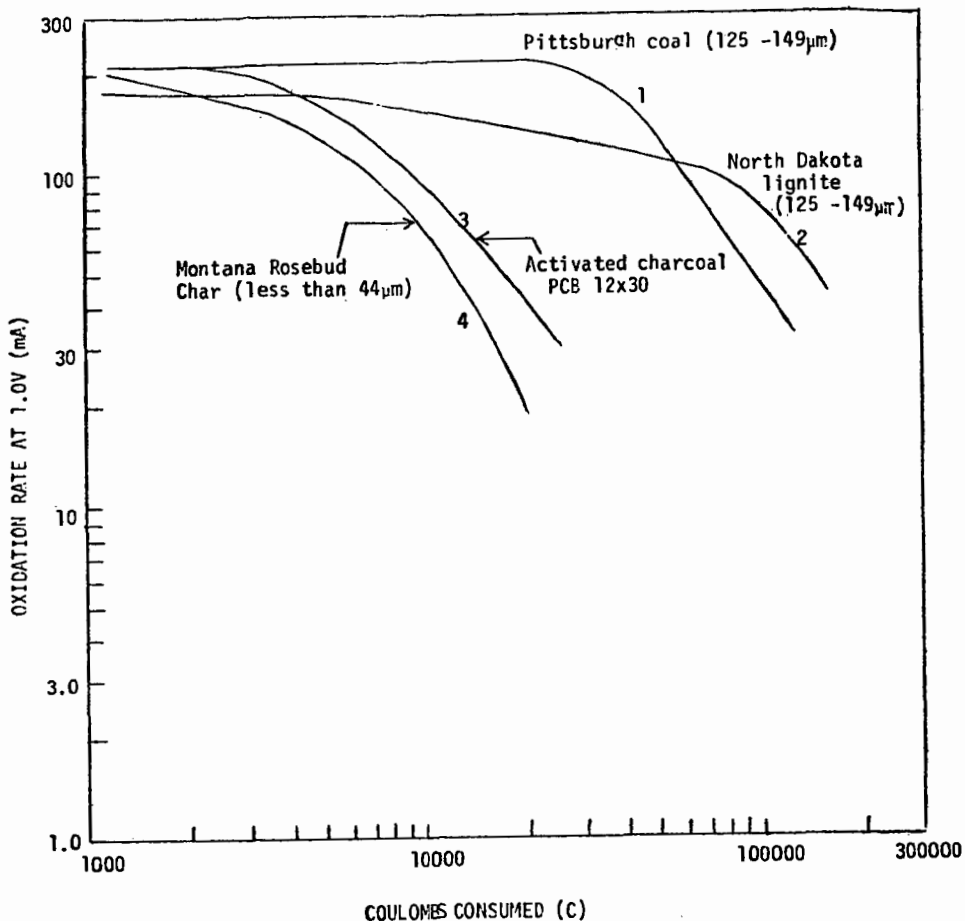
References

1. A. M. Squires, *Science* 184, 340-46 (1974).
2. G. E. Klingman and R. P. Schaaf, *Hydrocarbon processing*, pp. 97-101 (April 1972).
3. A. Verma, *Chem. Tech*; 372-81, June (1978).
4. R. W. Coughlin and M. Farooque, *Nature* (accepted for publication).
5. R. W. Coughlin and M. Farooque, *IC & E* (submitted).
6. M. Farooque and R. W. Coughlin, *Fuels* (submitted).
7. H. Binder, A. Köhling, K. Richter and G. Sundstede, *Electrochimica Acta*, 1964, Vol. 9, 255 (1964).
8. R. E. Panzer and P. J. Elving, *Electrochimica Acta*, Vol. 20, 635 (1975).
9. R. W. Coughlin, *Ind. Eng. Chem. Prod. R & D* 8, 12 (1969).
10. Y. A. Zarifyanz, V. F. Kiselev, N. N. Lezhnev and D. V. Nikitina, *Carbon* 5, 127 (1967).



1. Effect of Potential on the Oxidation Rate as the Reaction Proceeds.

(North Dakota Lignite; Coal Slurry Conc.: 0.069 gm/cm³; Supporting Electrolyte: 5.60 M H₂SO₄; Particle Size: 125 - 149μm, Temp. 114°C; Anode area: 96.5 cm² (geometrical)).



2. Oxidation Rate of Different Samples At 1.0V as the Reaction Proceeds •

(Slurry Conc.: 0.069 gm/cm³; Particle Size: 44 μ m and below;
 Electrolyte: 5.6M H₂SO₄; Potential: 1.0V; Anode area:
 96.5 cm² (geometrical); Temp. 114°C.

Electrolysis discontinued after:

- Curve 1: 343 hours and 16.36% consumed
- Curve 2: 353 hours and 29.2% consumed
- Curve 3: 110 hours and about 2.56% consumed
- Curve 4: 78 hours and 3.2% consumed

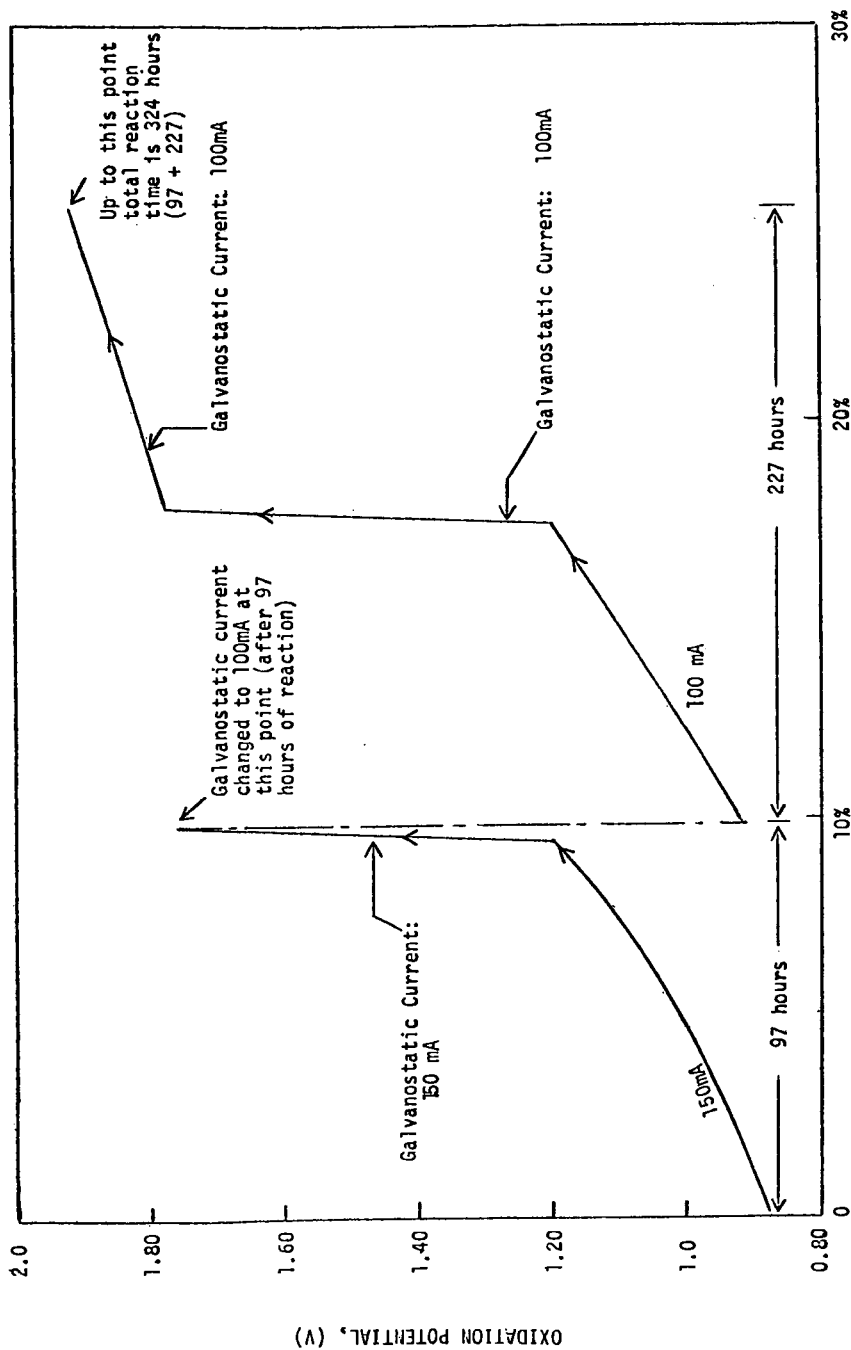


Figure 3. Change of Cell Potential During Galvanostatic Study.

(Coal sample: Fresh ND1; Slurry Conc.: 0.069 gm/cm³;
 Electrolyte: 5.6M H₂SO₄; Particle size: 105-125µm;
 Anode area: 96.5 cm² (geometrical).)

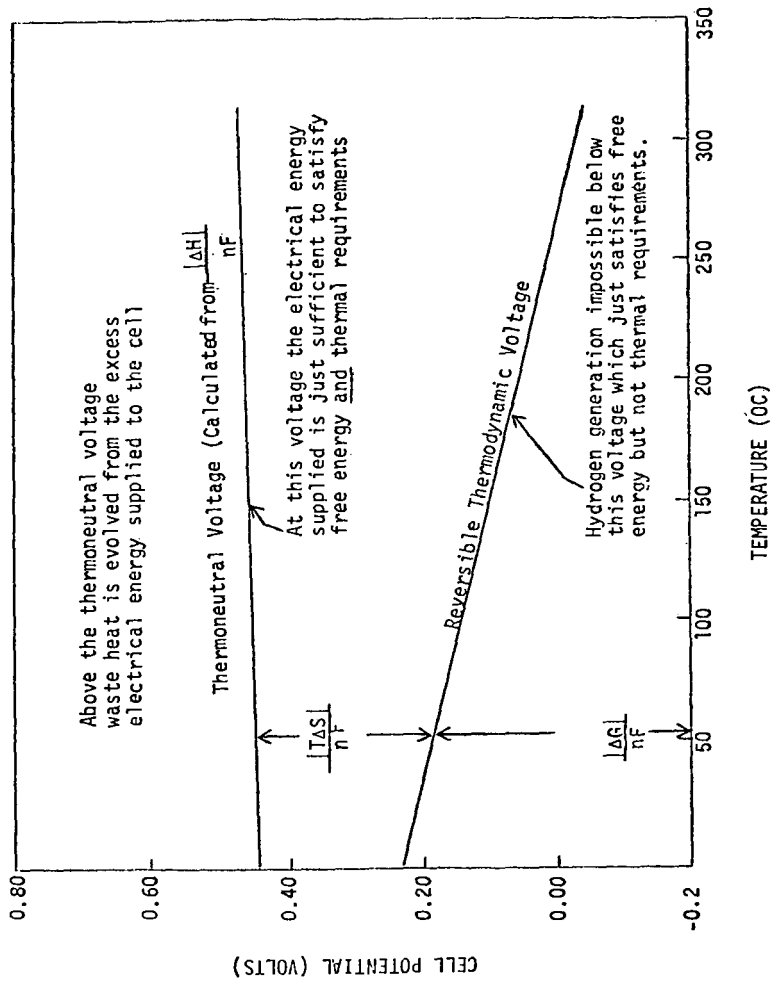


Figure 4. Effect of Operating Temperature on Cell Voltage.

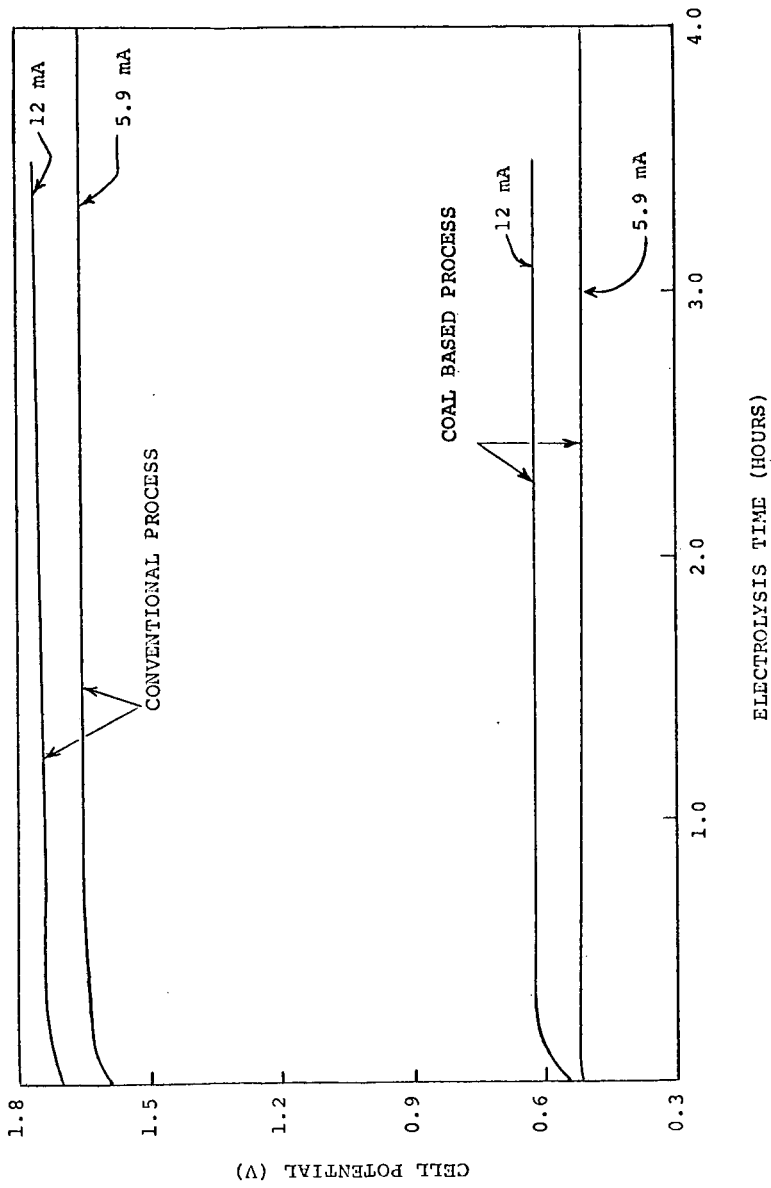


Figure 5. Comparison of the Cell Potentials of the Conventional and Coal Based Copper Electro-winning Processes .
 (Electrolyte: 0.125M CuSO₄ and 0.5M H₂SO₄; Coal Sample N. Dakota Lignite; Slurry Conc.: 0.15gm/cm³; Particle size: 74-88µm; Temp.: 60°C; Anode area: 5.3 cm² (geometrical).

THE FLASH HYDROPYROLYSIS OF LIGNITE AND SUB-BITUMINOUS COALS TO BOTH LIQUID AND GASEOUS HYDROCARBON PRODUCTS

P. T. Fallon, B. Bhatt, and M. Steinberg

Brookhaven National Laboratory, Upton, New York 11973

May 1979

Introduction

Flash Hydropyrolysis (FHP) is a short residence time (1 to 10 sec) gas phase non-catalytic coal hydrogenation process in which coal is converted directly to liquid and gaseous hydrocarbon products. Pulverized coal is contacted with hydrogen at elevated pressure and heated at average rates of 20,000 to 30,000°C/sec causing thermally-induced fractures in the polycyclic structure of the coal molecule. The free radicals formed readily add on hydrogen thus increasing the hydrogen to carbon ratio of 0.8 in the feed coal to approximately 1 to 4 depending upon whether liquid or gaseous hydrocarbons are formed. The products are then rapidly quenched to terminate the reaction and to prevent any decomposition or recombination. The purpose of this work is to provide data on the process chemistry of the reaction by studying the liquid and gaseous products formed as they vary with such operating parameters as temperature, pressure, and residence time. These results are also applied to a kinetic model and an economic evaluation of a large scale integrated coal conversion processing plant. Experiments using catalysts and much lower heating rates were conducted by Hitsche et al (1) in the late 1950's. Small-scale non-catalytic, direct hydrogenation experiments were conducted by Graff et al (2) as further background information for the work reported here.

Experimental Equipment and Procedure

A schematic of the experimental equipment is shown in Figure 1 and a detailed description is reported elsewhere.(3,4) The system utilizes a 1-in. I.D. entrained down-flow tubular reactor with coal fed by gravity from above. Preheated hydrogen enters just above the 8 ft heated reaction zone and a 3 ft cooling section and char trap are below. The products formed in the reactor are kept in the gas phase at approximately 250°C and reactor pressure until reaching the two liquid product condensers, one water cooled and the other cooled by a refrigerant. The gaseous products and excess hydrogen are then reduced to atmospheric pressure and passed through a positive displacement integrating gas meter before being vented. The maximum operating conditions of the system (4000 psi and 800°C or 2500 psi and 900°C) are limited by the 10,000 hr rupture life of the Inconel 617 reactor. Problems unrelated to the mechanics of the system, mainly reactor plugging at high hydrogen pressures, even when using non-caking coal, has limited most experiments to a maximum of 2500 psi.

At the beginning of each experiment, the coal feeder is charged with approximately three pounds of coal ground to minus 100 mesh (< 150 μ). The experiments are generally of about two hour duration and coal and hydrogen are fed at approximately 1 lb/hr each. Product samples are taken every 8 minutes from one of four sample taps located every 2 ft along the length of the reactor. An on-line programmable gas chromatograph is used for determination of CO, CO₂, CH₄, C₂H₆, BTX (benzene, toluene, xylene) and H₂O. The heavier liquid hydrocarbon products (ΣC_9) are collected and measured at the end of the experiment. The use of the reactor sample taps provide information on both the yields and distribution of products as a function of gas and coal particle residence time. There is also another sample tap located down stream of the product condenser which provides information as to their efficiency.

Experimental Results

Product Yields and Distribution

The process chemistry of two coals are presently being studied, a North Dakota lignite and a New Mexico sub-bituminous. The ultimate analyses of these coals are given in Table 1. Since the detailed study of the sub-bituminous coal is not yet completed, more experimental data is available using the lignite. Figure 2 shows a summary of the BTX yields from the lignite at hydrogen pressures of 500 to 2000 psi and reactor temperatures of 700° to 800°C. The experimental points were not included because of their great number (≈ 50). The yield is expressed as fraction of carbon in feed coal converted to the hydrocarbon product. Maximum yields were generally observed between 775° and 800°C except at the highest pressure (2500 psi) studied in detail where the yield was approximately constant at 9% at temperatures between 725° and 775°C. A significant increase in yield is seen as the pressure is increased from 500 to 1000 psi. The yield increases from 4.5 to 7%. Further increases in pressure above 1000 psi show less significant increases in yield, the increase maximum yield going from 7 to 9% as the pressure is increased to 2000 psi. As the pressure is further increased to 2500 psi, no appreciable increase in yield above 9% is observed; only a reduction in temperature at which the maximum occurs. Although at 2500 psi the maximum yield was essentially constant over a broad range of temperatures, the coal residence time at which this maximum was observed decreased from a maximum of approximately 9 sec at 725°C to a minimum of 2 sec at 850°C as shown in Figure 3. At residence times greater than required to produce the maximum yield, significant decomposition of the BTX was observed. For example, in Figure 4, the results of an experiment conducted at 2500 psi and 825°C, the BTX is seen to decrease from the maximum observed of 8% at 2.5 sec to approximately 0 at 9.5 sec.

Since presently the minimum residence that can be measured is approximately 2 sec, it is possible that slightly higher BTX may exist at shorter residence time. This looks to be the case when considering the initial steep gradient of the BTX curve in Figure 4. The liquid hydrocarbon products of molecular weight greater than xylene cannot be measured with the on-line gas chromatograph because they tend to condense in the sample lines. For this reason, they are not included in the correlations given in Figure 4 which exhibit the effect of residence time on the product distribution. These liquids are collected in the condenser traps and measured and analyzed via gas chromatography at the end of each experiment. Generally, these heavier liquids have been found to be exclusively polynuclear aromatic hydrocarbons (PNA), approximately 40% of which is naphthalene. A typical composition of this liquid is given in Table 2. Only on very rare occasions has any phenols been found and then only in trace amounts. The maximum yield of these heavier liquids is generally of the same order as that of the BTX though obtained at a lower temperature. For example, in Figure 5 which shows the total yield of liquid hydrocarbon products from lignite at a hydrogen pressure of 2,000 psi, the liquids of $> C_9$ are seen to maximize at approximately 9% yield at a temperature of 750°C while the BTX maximum of approximately 10% occurs at 800°C. These heavier liquids are also seen to decompose very rapidly as the temperature is increased above 750°C to the extent that at 850°C only approximately 0.5% yield remains. Since the yield of BTX with temperature is shown to be much more uniform than the heavier liquids within the temperature range shown, the total yield of liquids is seen to peak at 18% and occurs at the same temperature at which the heavier liquids peak (750°C).

Although the yields obtained from sub-bituminous coal is still being investigated, a significant amount of information has been accumulated. In Figure 6, the maximum yield of BTX is shown to be as high as approximately 15% at 2000 to 2500 psi and decreases only to approximately 12% as the pressure is reduced to 1000 psi. Also, the temperatures at which the maximum yields are obtained decrease with increased pressure, going from 825°C at 1000 psi to 775°C at 2500 psi. When these yields plus the gaseous hydrocarbons formed ($CH_4 + C_2H_6$) are compared to the same products from lignite as shown in Figure 7,

a constant incremental yield of approximately 5% for both the BTX and gaseous hydrocarbons is observed for the sub-bituminous coal. This results in an overall 10% increase in yield of hydrocarbon products for the sub-bituminous coal compared to the lignite. The yield of heavier liquid products ($\geq C_9$) from the sub-bituminous, although not completely investigated, appears to be much lower than that obtained from lignite, ranging from 4.5 to 1.5% or less. When this is added to the maximum yields of BTX, however, the total liquid yield is on the average equal to or greater than that from lignite.

At temperatures of 850°C and greater, the liquid hydrocarbons are seen to decompose almost entirely to produce gaseous hydrocarbons, principally methane and ethane. This plus the additional gaseous products formed directly from the coal result in maximum gaseous yields ($CH_4 + C_2H_6$) shown in Figure 8. The formation of these products appear to be a direct function of the hydrogen pressure, increasing at the rate of 18% conversion for each 500 psi increase in pressure. These yields were all produced at a hydrogen to coal feed ratio of approximately 1 lb/lb and at coal residence times between 2.4 and 7 seconds. It was found that at shorter residence times the reaction has not reached completion and at longer residence times, decomposition of the methane reduced total yields. Also, since higher temperatures accelerate the decomposition, the competing reactions of formation and decomposition at 2000 to 2500 psi result in the maximum yield occurring at temperatures lower than the maximum studied (900°C). A total conversion of 88% to CH_4 and C_2H_6 was obtained at 875°C and 2500 psi pressure.

When the hydrogen to coal feed ratio is reduced by approximately 4 to a ratio of 0.25, some reduction in gaseous products is observed (Figure 9). Some or all of this reduction could be attributed to a reduction in hydrogen partial pressure caused by higher concentrations of product in the process stream.

The study of the New Mexico sub-bituminous coal is still in progress. The information to date indicates it behaves similarly to lignite in gasification except that greater yields are obtained at lower pressure, as shown in Figure 10. At 1000 psi the lignite yields approximately 35% gaseous products and the sub-bituminous 55%, an almost 60% increase over the lignite. The temperatures and residence times necessary to produce maximum gaseous products were approximately the same.

Sulfur and Nitrogen

To date, most of the detailed determinations of sulfur distributions in the products and effluents have been made on experiments using lignite. The distribution of the sulfur among the various forms in lignite is given in Table 3 and a summary of the disposition of this sulfur after hydrolysis is given in Table 4. In comparing these tables, it should be noted that in most experiments greater than 50% of the sulfur in the feed lignite is retained in the spent char. Approximately 64% of the sulfur in the lignite is in the organic form while 90% of the sulfur in the char was found to be in the organic form. Also, the liquid hydrocarbon products contained much less than the 0.3% sulfur considered to be the maximum allowable for further hydrotreating. The sulfur dissolved in the water produced is probably limited by the solubility of H_2S which is approximately 0.66 wt% at the temperatures ($\sim 0^\circ C$) at which the water is collected.

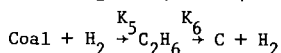
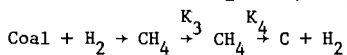
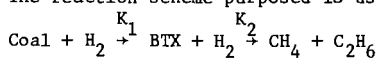
The nitrogen balance shown in Table 5 follows very closely the same distribution as the sulfur, again the largest single portion remaining in the char. In this case, the nitrogen dissolved in the water produced is not solubility limited since it is assumed to be in the form of ammonia which can be as high as 47 wt% at $0^\circ C$.

Reaction Scheme and Kinetic Model

In order to develop a reaction scheme and a kinetic model, the following assumptions were made:

- 1) Isothermal conditions exist along the length of the reactor.
- 2) Chemical reactions are the rate determining steps.
- 3) Only hydrocarbons and not oxides of carbon considered.
- 4) Methane and ethane from decomposition of BTX are small compared to that produced from coal.
- 5) Free carbon formed from decomposition of products has negligible reactivity.
- 6) Liquids heavier than BTX are intermediate species.

The reaction scheme purposed is as follows:



Realizing this scheme to be a first approximation of the true reaction mechanism, a kinetic model was developed and the appropriate rate constants calculated. Only those results from experiments using lignite and in which sufficient residence time data was available were used. The results are shown in Table 6. As can be seen from the calculated activation energies, all reactions are chemical reaction rate limiting rather than diffusion limiting except possibly for the decomposition of methane (K_4).

Economic Evaluation

A summary of the results from the more recent economic evaluation for utilization of FHP in an integrated coal conversion process (5) is given in Table 7. The feed coal was assumed to be lignite since at the initiation of the study little experimental data was available using sub-bituminous coal. Three product slates were assumed, liquids only (motor gasoline and liquified petroleum gas-LPG), pipeline gas only, and co-products of liquids and pipeline gas. The plant capacity is assumed to be 25,000 to 30,000 tons per day of lignite, producing 47,700 bbl/day of motor gasoline in the liquid process or 395 MM SCFD of pipeline gas for the gas process. The net thermal efficiencies which include internal plant energy needs were calculated to vary from 61% for the all gas slate to 72% for the combined product slate to a low of 50% for the all liquids slate. The reason for the low efficiency of the all liquids slate is that the methane produced must be performed with steam to produce hydrogen. The capital costs, based on 1978 dollars, ranged from a low of \$839 million for the all liquids plant to a high of \$936 million for the all gases plant. In all cases, the two most costly items in the plants were the product separation from the recycle gas and the production of hydrogen. Combined, these represented approximately 50% of the capital investment. The flash hydropropyrolzyer only amounted to approximately 5% of the investment. The last entry in Table 8 shows the fuel oil equivalent cost of production for the three product slates. The most expensive at \$32.34/bbl is the all liquids, mostly due to the low net thermal efficiency and the most attractive or cheapest at \$23/bbl is for the mixed products.

Conclusions

The following conclusions can be drawn from this work so far.

- The maximum yield of BTX observed from the FHP of sub-bituminous coal is at least 50% greater than that from lignite (10% for lignite and 15% for sub-bituminous).
- The total liquids yields (BTX + \geq C₉) are approximately the same for both coals (~18-20%).
- Both coals can be hydrogasified to methane and ethane up to approximately 85% of the total carbon in the fuel at 2500 psi and 875° to 900°C.
- The sub-bituminous coal yields 60% more gaseous hydrocarbons at 1000 psi and 875° to 900°C than the lignite.
- The gaseous yields from both coals is directly proportional to the hydrogen pressure in the range of 500 to 2500 psi.

-Negligible quantities of the sulfur or nitrogen in the coal are found in the liquid hydrocarbon products.

-The FHP reactions are basically chemical rate and not diffusion rate controlled.

-In the commercial application of FHP, a mixed product slate of liquids and gases is the most economical.

References

1. Hiteschue, R. W., Anderson, R. B., and Schlesinger, M. D., Hydrogenation of Coal at 800°C, Ind. Engrg. Chem., 49, 2008 (1957).
2. Graff, R. A., Dobner, S., and Squires, A. M., Flash Hydrogenation of Coal. 1. Experimental Methods and Preliminary Results, Fuel, 55, 109 (1976).
3. Steinberg, M., Fallon, P. T., Doering, R., Farber, G., Smith, J., and Woodson, G., Safety Analysis Report on the Brookhaven Coal Flash Hydropyrolysis Experiment, BNL 21919 (October 1976).
4. Fallon, P. and Steinberg, M., Flash Hydropyrolysis of Coal, The Design, Construction, Operation, and Initial Results of a Flash Hydropyrolysis Experimental Unit, BNL 22519 (January 1977), presented at 173rd National American Chemical Society Meeting, New Orleans, La. (March 20-25, 1977).
5. Steinberg, M., Fallon, P., Dang, V., Bhatt, B., Ziegler, E., and Lee, Q., Reaction, Process, and Cost Engineering for the Flash Hydropyrolysis (FHP) of Coal, BNL 25232 (November 1978), presented at 71st Annual Meeting of the American Institute of Chemical Engineers, Miami Beach, Florida (November 12-16, 1978).

Table 1

ULTIMATE ANALYSIS (WT PCT DRY) OF LIGNITE AND SUB-BITUMINOUS COALS

	North Dakota Lignite	New Mexico Sub-Bituminous
Carbon	59.0	59.3
Hydrogen	4.0	4.2
Oxygen*	25.5	16.8
Nitrogen	0.9	1.2
Sulfur	0.6	0.8
Ash	10.0	17.7

*By difference.

Table 2

TYPICAL COMPOSITION OF OILS AND HEAVIER LIQUID HYDROCARBON PRODUCT ($\geq C_9$) FROM THE FLASH HYDROPYROLYSIS OF LIGNITE

	Wt %
Naphthalene	38.1
Other 2 ring aromatics (methyl naphthalene fluorene, etc.)	19.5
Three ring aromatics (phenanthrene, etc.)	11.1
Four ring aromatics (pyrene, etc.)	5.1
Five ring aromatics (chrysene, etc.)	3.1
High boiling fraction (asphaltenes)	23.1

Table 3

SULFUR DISTRIBUTION IN NORTH DAKOTA LIGNITE

Sulfur Form	% in Lignite	% of Total
SO ₄ (soluble)	0.089	14.8
FeS ₂ (pyritic)	0.129	21.6
Organic	0.382	63.6

Table 4

FLASH HYDROLYSIS OF LIGNITE
Sulfur Balance
 Sulfur Conc. in Lignite Feed - 0.6%

	% Distribution in product	Concentration in Product Stream (wt%)
Contained in liquid HC product	1	0.09
Contained in char	48-77	0.85-1.7
Dissolved in water produced	12-22	0.54-0.73
Vented to atmosphere	15-25*	0.1-0.15

*By difference.

Table 5

FLASH HYDROLYSIS OF LIGNITE
Nitrogen Balance
 Nitrogen Conc. in Lignite Feed - 0.9% N

	% Distribution in Product	Concentration in Product Stream (wt%)
Contained in liquid HC product	4	0.16
Contained in char	30-55	0.6-1.1
Dissolved in water produced	15-40	2.7-5.0
Vented to atmosphere	21-26*	0.19-0.23

*By difference.

Table 6

CALCULATED RATE CONSTANTS
 Pressure (P_{H_2}) 1500-2500 psi
 Temperature (T) 973-1173°K

$$k_1 = 3.16 \times 10^{12} P_{H_2}^{0.137} e^{-68700/RT}$$

$$k_2 = 1.33 \times 10^{14} P_{H_2}^{.004} e^{-71700/RT}$$

$$k_3 = 3.93 \times 10^4 P_{H_2}^{0.07} e^{-29700/RT}$$

$$k_4 = 97.5 P_{H_2}^{-0.043} e^{-15100/RT}$$

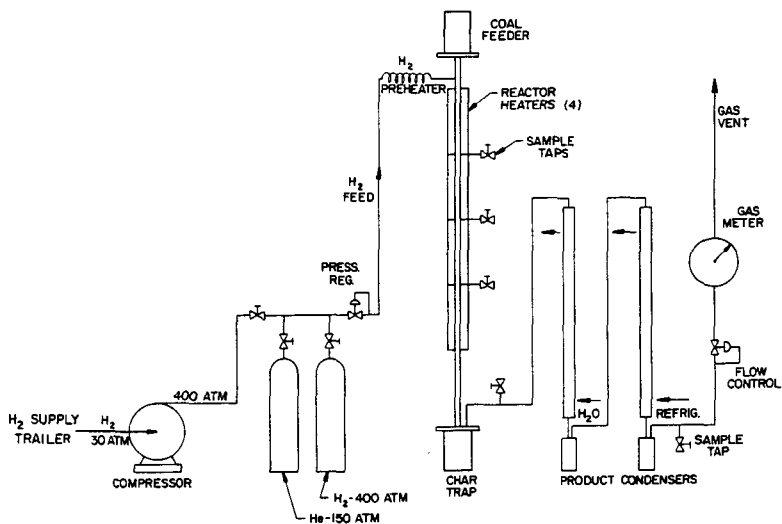
$$k_5 = 1.03 \times 10^8 P_{H_2}^{-0.12} e^{-44000/RT}$$

$$k_6 = 3.30 \times 10^{14} P_{H_2}^{1.17} e^{-85700/RT}$$

Table 7

FLASH HYDROLYSIS OF COAL
Manufacturing Cost of Product Fuel

<u>Main Fuel Product Made</u>	<u>Liquids</u>	<u>Liquids and Gases</u>	<u>Gases</u>
<u>Reactor Operating Conditions</u>			
Pressure, psi	2000 (136 ATM)	2000 (136 ATM)	2500 (170 ATM)
Temperature, °C	750°C (1382°F)	750°C (1382°F)	825°C (1517°F)
<u>Product Values</u>			
Pipeline gas	-0-	159 MM SCFD	395 MM SCFD
Motor gasoline	47,700 BB/D	47,700 BB/D	-0-
LPG	134 tons/D	134 tons/D	134 tons/D
<u>Operating Cost</u>			
	<u>\$ MM/yr</u>	<u>\$ MM/yr</u>	<u>\$ MM/yr</u>
Lignite @ \$20/ton	204.4	212.7	212.5
Catalyst and chemicals	5.5	5.5	5.0
Power @15 mills/kwh	1.1	6.8	8.3
Ash disposal	2.6	2.8	2.7
Ins. Maint. GA (8% of capital)	57.2	71.4	74.9
Operating labor	8.0	8.0	8.0
Total operating cost	278.8	307.2	311.4
Mortgage 10%	93.4	104.8	109.9
Depreciation @5% (20 yrs)	41.9	44.6	44.8
10% ROI and income tax	167.8	178.4	187.1
Total	\$581.9	\$635.0	\$653.2
Selling Price (Total FOE)	\$5.13/MM BTU	\$3.83/MM BTU	\$4.53/MM BTU
Pipeline gas, \$/MSCF)	\$5.13/MM BTU	\$3.83/MM BTU	\$4.53/MM BTU
Motor gasoline, (90 RON)	\$0.77/gal	\$0.54/gal	-0-
Fuel oil equivalent (FOE)	\$32.34/bbl	\$23.00/bbl	\$30.17/bbl



SCHMATIC FLOWSHEET OF ENTRAINED TUBULAR REACTOR EXPERIMENT

Figure 1

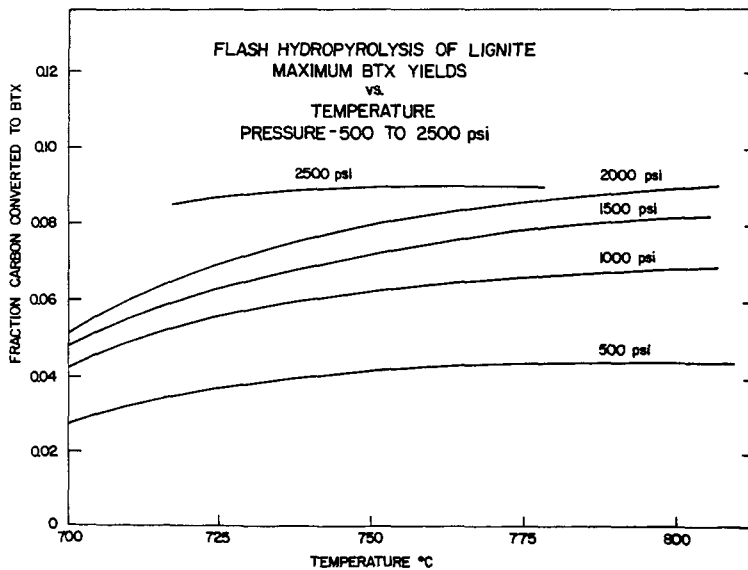


Figure 2

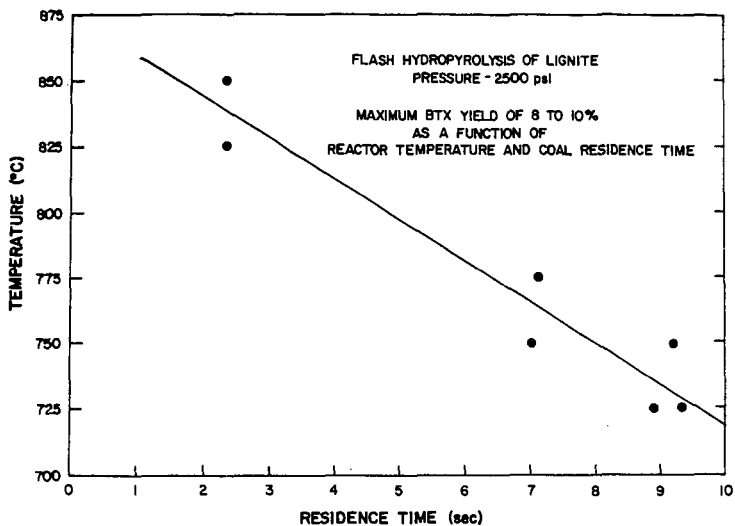


Figure 3

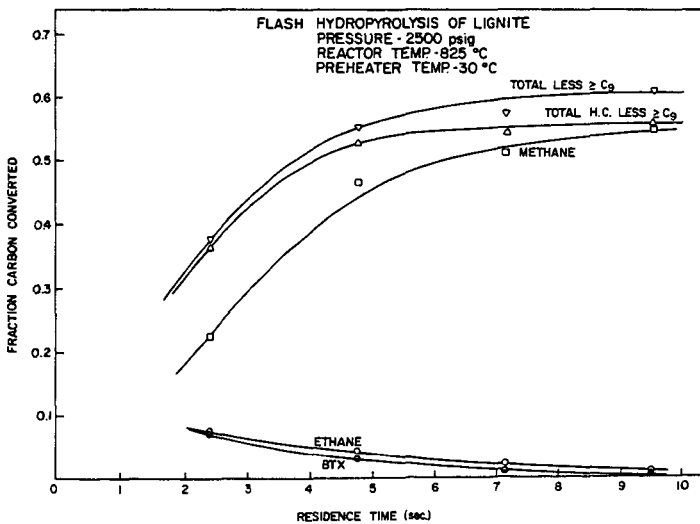


Figure 4

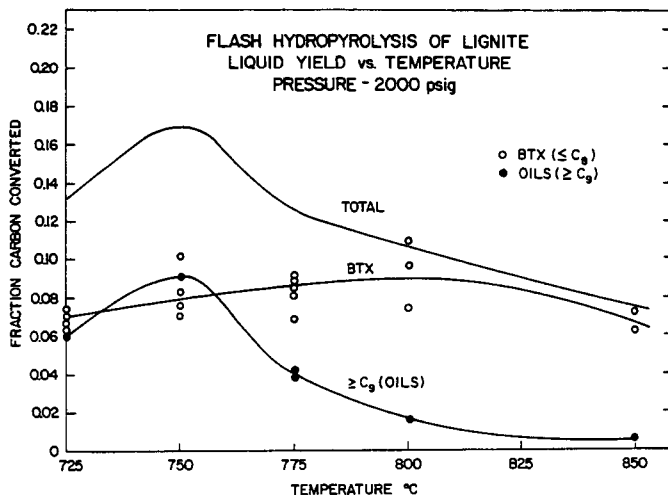


Figure 5

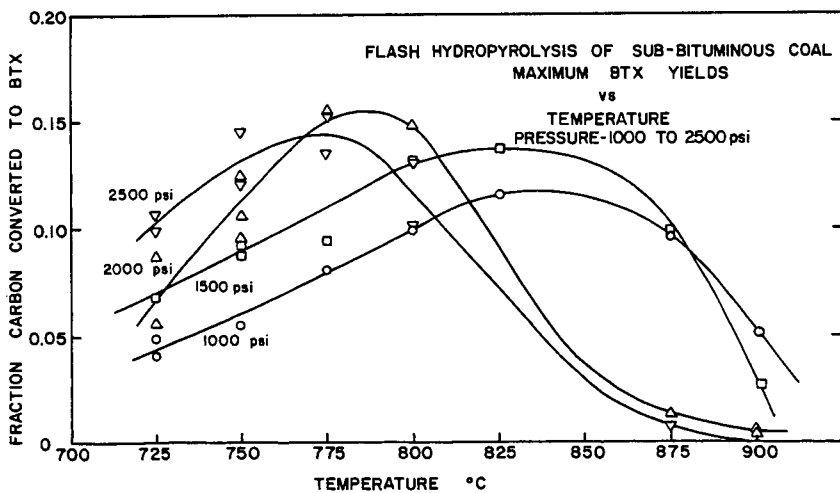


Figure 6

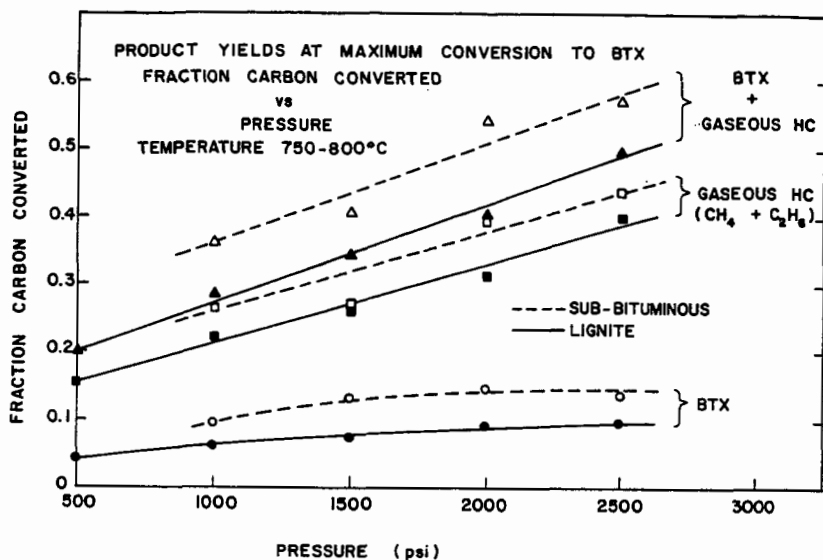


Figure 7

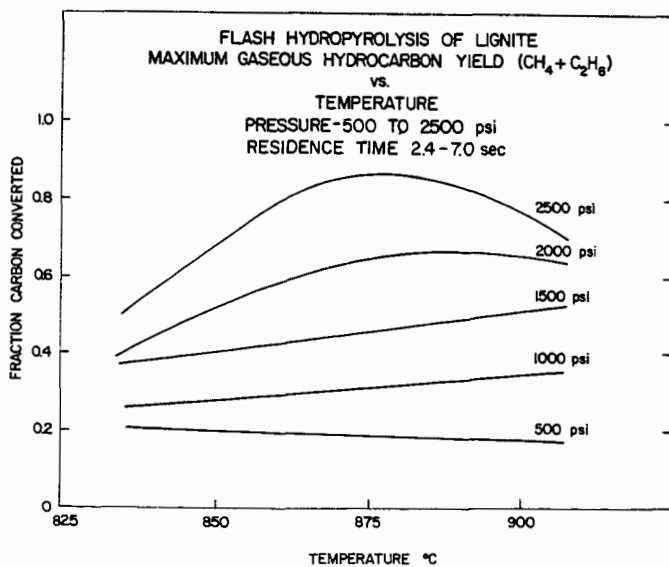


Figure 8

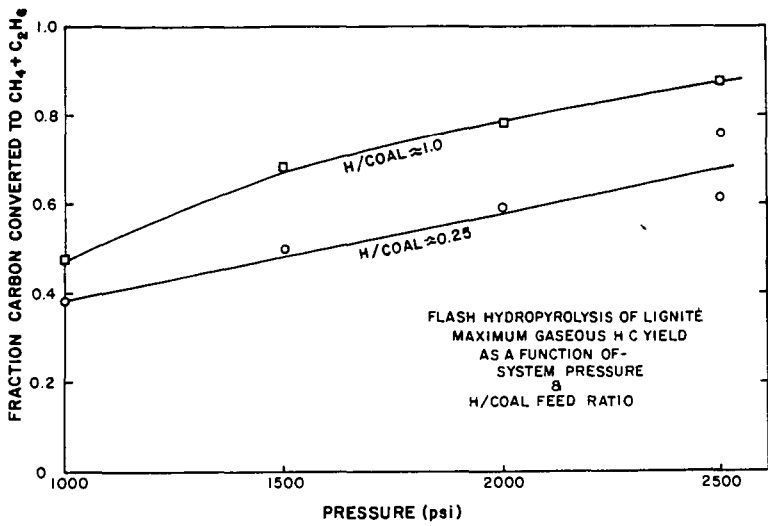


Figure 9

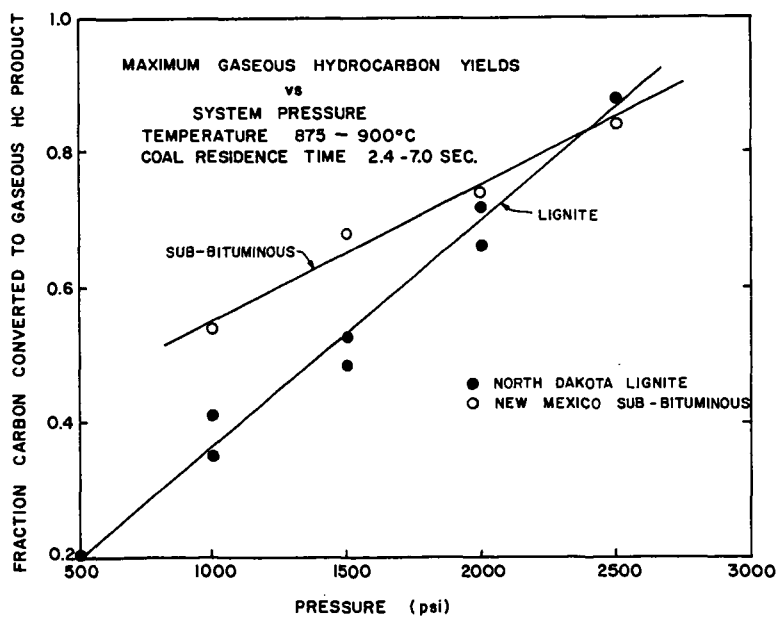


Figure 10

EXPERIMENTAL INVESTIGATION OF PEAT HYDROGASIFICATION

F. D. Raniere, L. P. Combs, and A. Y. Falk

Energy Systems Group
Rockwell International
8900 De Soto Avenue
Canoga Park, California 91304

INTRODUCTION

The availability and accessibility of peat as a domestic fossil resource have been well publicized by Minnesota Gas (Minnegasco) and the Institute of Gas Technology (IGT) (References 1 and 2). It has been established that peat, with an estimated 1440 quads (10^{15} Btu) of available energy, is second only to coal as the most abundant fossil energy resource in the United States. Also, hydrogasification tests at IGT (Reference 1) have shown that, due to peat's unique properties of high volatility and hydrogen-to-carbon ratio, peat is highly reactive yielding good conversion to methane.

Based on these studies and the concurrent DOE-sponsored* development of a short residence time coal hydrogasifier at Rockwell International, with the Cities Service Research and Development Company as a subcontractor, an additional task to the existing DOE contract was established to furnish a preliminary performance profile for peat in the Rockwell hydrogasifier. Rockwell and Cities Service have entered into an agreement to develop jointly short-residence-time, flash hydro-pyrolysis process technology. Acknowledgement is given to both Louis Jablansky and Melvyn-Kopstein of DOE for their administration of this add-on effort.

The background technology and details of development for the Rockwell hydrogasifier reactor have been previously reported over the last few years (References 3, 4, and 5). However, a brief review is necessary to establish the conditions under which the peat hydrogasification tests were made.

The Rockwell reactor is based on the application of rocket engine techniques to achieve rapid mixing-reaction at optimum temperature and residence time. Adjustment of reactor conditions, principally temperature and residence time, allows a range of product distribution from predominantly liquids to complete gasification to substitute natural gas (SNG). Intermediate conditions permit maximized yields of byproduct BTX (benzene, toluene, and xylene).

Successful operation has been demonstrated at engineering scales from 1/4- to 1-ton/h (tph) feedrates. This success was achieved by feeding dry, pulverized carbonaceous solids (coal or peat) into the reactor with a minimum of carrier gas (dense-phase flow) and there, achieving almost instantaneous mixing and concurrent heating with a preheated gaseous hydrogen stream. Reactor conditions were controlled to produce the desired products (liquids or gas). The current reactor development program (DOE Contract ET-78-C-01-3125) will optimize the injector-reactor configuration at 4 tph and be a full-scale element for straightforward, multi-element scaling to commercial-size reactors.

REACTOR SYSTEM

A description of the dense-phase, dry-solids feed system has been presented in previous papers and reports (References 3 and 4). Without modification, this

*Hydrogasifier Development for the Hydrane Process, Contract EX-77-C-01-2518, Louis Jablansky, Department of Energy (DOE) Program Manager.

system was used to feed dry, ground reed sedge Minnesota peat (<10% moisture and 78% through 200 mesh) with no problems at the 1/4-tph test level. Sieve analyses for a typical sample of peat and the resulting char are shown in Figure 1.

The reactor system (see Figure 2), as also described in References 3 and 4, uses a stream of hot hydrogen as the working fluid for the reaction. Hydrogen is preheated to 1100°F in an electrical heater, then to 2000 to 2100°F by combusting a small amount of hydrogen with oxygen in a preburner assembly. After rapid, injector-induced mixing (and heating) of the dry solids (coal or peat) with the hot hydrogen, the resulting reaction products are cooled at the appropriate residence time to achieve the desired product distribution. Cooling is accomplished with a water spray, which reduces the product gas temperature to 600 to 1000°F. The vapor phase products are separated from the char, and subsequently directed through a high-pressure, water-cooled condenser to remove water and any oils which may have been produced. The vapors are then sampled and regulated down to the appropriate venting pressure (<100 psig). Before venting, an activated-carbon, packed-bed adsorber is used to recover the vapor-phase BTX from the product stream.

Char is collected in a spherical receiver (located just under the water spray quench as shown in Figure 2) until completion of the test. Vapor-phase condensate is decanted (if necessary) to separate oil product for analysis. The char, gas, oil, condensed aqueous phase, and the activated carbon are analyzed to permit material balance calculations. It is important to mention that no modifications of the reactor system (as used for coal hydrogasification) are necessary to conduct the peat test.

PEAT TEST RESULTS

Ultimate and proximate analyses for the dried and ground peat, as received, are presented in Table 1. Eleven hydrogasification tests were conducted as shown in Table 2 at the 1/4-tph test level. Due to limited feed tank volume, test durations were ~6 to 10 min. The data are quite consistent, with high overall carbon conversions up to 84.2%, with the principal products being methane (CH₄) and carbon monoxide (CO). Small amounts (1 to 2%) of carbon dioxide were obtained. Except for the very low temperature Run 54, all of the liquids produced were essentially pure benzene.

TABLE 1
CHARACTERISTICS OF PEAT TESTED

	Minnesota Peat	
	As Received	Dry
Proximate Analysis (%)		
Moisture	9.40	—
Ash	16.87	18.62
Volatiles	53.76	59.34
Fixed Carbon	19.97	22.04
Ultimate Analysis (%)		
Moisture	9.40	—
Carbon	42.44	46.84
Hydrogen	4.50	4.97
Nitrogen	1.60	1.77
Chlorine	0.03	0.03
Sulfur	0.18	0.20
Ash	16.87	18.62
Oxygen (by diff.)	24.98	27.57
Heating Value (Btu/lb)	7,596	8,328

Figure 3 shows the effect of reactor residence time on overall carbon conversion and specific conversion to liquids (the difference is the conversion to gas). Liquid byproduct can be eliminated by high temperature (>1800°F) and longer residence time (>2.8 s). Data points are segregated into two reactor exhaust temperature groups. This graph shows that conversion is a function of residence time and temperature predominantly and essentially independent of pressure within the range of 500 to 1500 psig. The mild effect of reactor temperature is shown in Figure 4. The total carbon conversion increases slightly as reactor temperature is increased from 1550 to 1850°F. The apparent effect of pressure in Figure 4 is caused by the concurrent increase in residence time as pressure is increased in a given reactor configuration. Two different size reactor tubes were used to isolate the effect of pressure

from residence time. The low overall conversion and low conversion to gases of Run 54, which had a reactor temperature of only $\sim 1000^{\circ}\text{F}$, are dramatically shown in Figure 4.

Conversion to benzene as a function of reactor temperature is magnified in Figure 5. Conversion ranged from 0.0 to 11.7 wt % benzene as an inverse function of temperature and residence time. This graph (Figure 5) is useful for defining reactor conditions required for elimination of liquid product. One hundred percent selectivity to gases with an overall carbon conversion of 84% is attainable in a 3-s residence reactor at reactor temperatures above $\sim 1850^{\circ}\text{F}$. As shown in Table 2, analyses of the product gas composition for peat indicate that, in general, the carbon is converted primarily to CH_4 and CO at a mole ratio of $\sim 2:1$ (CH_4 to CO). Almost all of the carbon monoxide results from the relatively high oxygen content of the peat.

DISCUSSION

Using a computerized analytical model of the fluid dynamics and specific hydrogenation reactions, previously developed for coal conversion (Reference 6), peat results show consistent agreement with coal data (see Figure 6). The model assumes steady-state, one-dimensional (plug) flow, which is typical of the uniform flow patterns of rocket-type injectors at short distances from the injector face.

In order to compare these peat results for the Rockwell hydrogasifier with other peat hydrogenation investigations, the test data were plotted on a published IGT graph of hydrocarbon gas yield vs reactor temperature (Reference 1) for similar peat hydrogasification tests. Figure 7 shows this comparison. The Rockwell data are seen to be consistent with extrapolation of the IGT data to high reactor temperatures, and therefore to higher conversion levels. Together with the relative ease of processing peat in the unmodified Rockwell coal hydrogasifier, these high conversion levels provide encouraging support to the concept of peat hydrogasification to produce SNG. A commercial peat SNG plant might differ from one based on coal mainly in the more stringent requirements for drying the peat and for methanating the greater quantity of carbon monoxide.

CONCLUSIONS

The results of this experimental investigation clearly demonstrate that the Rockwell Flash Hydrogasifier is one of the most effective reactors for converting peat to SNG. Overall carbon conversions up to 84% with benzene byproduct yield ranging from 0 to nearly 12% were achieved. Both overall carbon conversion and conversion to benzene were found to be functions of reactor temperature and residence time, but not to depend upon reactor operating pressure. Rapid hydrogasification should be considered as a prime candidate for converting our abundant peat reserves to SNG.

REFERENCES

- 1) D. V. Punwani, and A. M. Rader, "Peat Gasification for SNG Production," a paper presented at the Ninth Synthetic Pipeline Gas Symposium, Chicago, Illinois, October 1977
- 2) D. V. Punwani, W. W. Bogle, A. M. Rader, and P. B. Tarman, "SNG Production From Peat," a paper presented at the International Conference on Alternative Energy Sources, Miami, Florida, December 1977
- 3) L. P. Combs, J. Silverman, J. Friedman, and M. I. Green, "Rockwell International Gasifier - Flash Hydropyrolysis," a paper presented at the Fifth Annual International Conference on Coal Gasification, Liquefaction, and Conversion to Electricity, University of Pittsburgh, Pittsburgh, Pennsylvania, August 1978

- 4) C. L. Oberg, A. Y. Falk, and J. Silverman, "Flash Hydropryolysis of Coal Using Rockwell Short-Residence-Time Reactors," a paper presented at the 71st Annual AIChE Meeting, Miami Beach, Florida, November 1978
- 5) S. K. Ubhayakar, C. L. Oberg, L. P. Combs, and J. Friedman, "Rocket Reactor Technology Applied to Coal Conversion," a paper presented at the IGT Symposium on Advances In Coal Utilization Technology, Louisville, Kentucky, May 1979
- 6) K. M. Sprouse, "Theory of Pulverized Coal Conversion In Entrained Flows, Part I: Hydrogasification," Rockwell International Technical Memorandum, NTIS FE-2518-14, December 1977

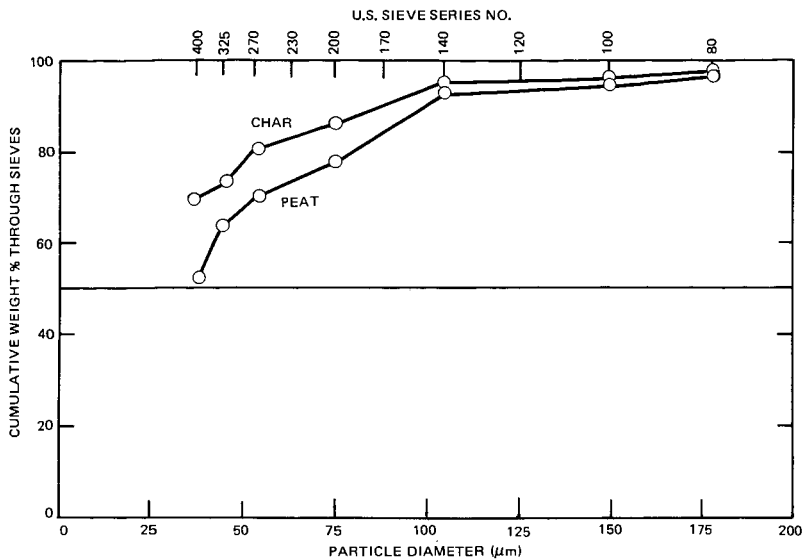
Energy Systems Group
8900 DeSoto Avenue
Canoga Park, California 91304



Rockwell
International

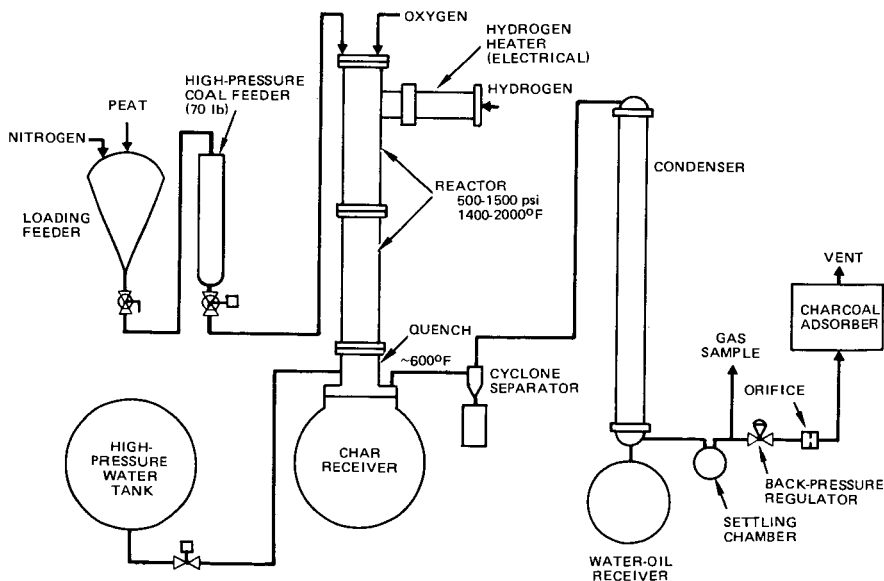
NOTICE

This report contains information of a preliminary nature prepared in the course of work for the United States Government. Since it is transmitted in advance of patent clearance, it is made available in confidence ~~solely for the performance of work under contracts with the U.S. Government.~~
This document is not to be published nor its contents otherwise disseminated or used for purposes other than specified above before patent approval for such release or use has been secured, ~~upon request~~ from the cognizant Government Patent Counsel.



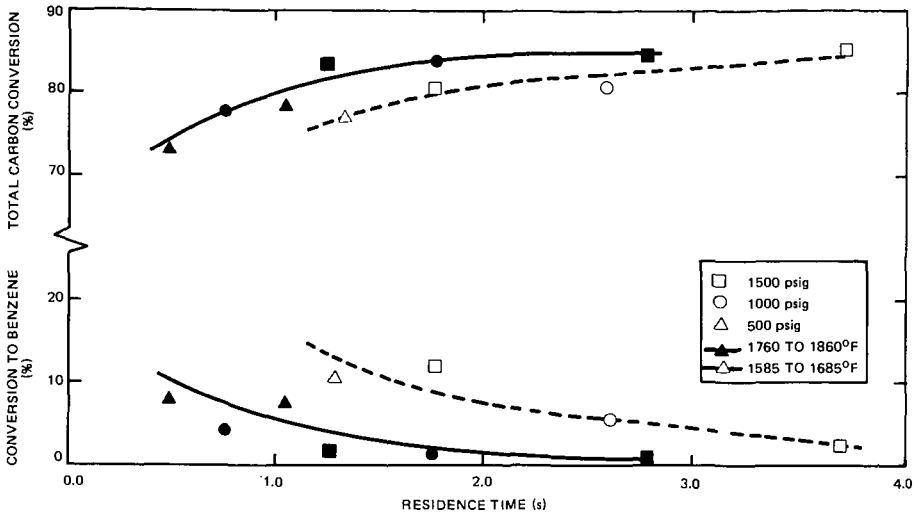
9317-100

Figure 1. Peat and Char Sieve Analyses



9317-101

Figure 2. Simplified Flow Diagram of Rockwell 1/4-TPH Hydrogasifier System



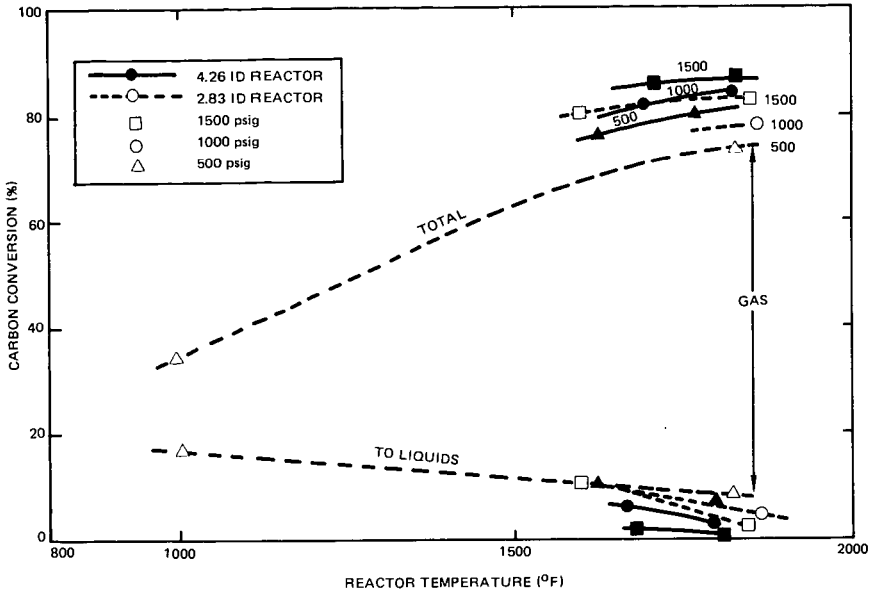
9317-102

Figure 3. Carbon Conversion as a Function of Reactor Residence Time

TABLE 2
TEST RESULTS

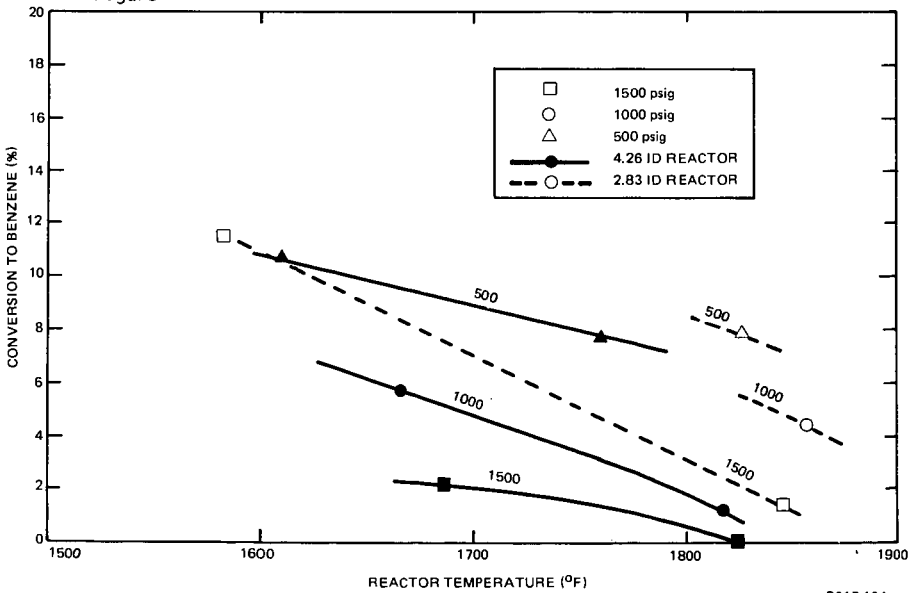
Run No.	Reactor Conditions					Carbon Conversion (%)				Heating Value (H ₂ -Free Basis) (Btu/scf)
	Diameter (in.)	P (psig)	T (°F)	τ _R (s)	H ₂ /Peat	Total	CH ₄	CO	Benzene*	
44	4.26	1500	1685	3.7	0.66	84.9	58.7	23.3	2.1	808
45	4.26	1000	1667	2.6	0.61	80.8	49.9	24.0	5.8	778
46	4.26	1000	1815	1.8	0.93	83.3	52.7	28.3	1.2	761
47	4.26	500	1610	1.3	0.53	76.6	39.8	24.8	10.5	731
48	4.26	500	1760	1.1	0.84	79.0	42.7	27.1	7.9	732
49	4.26	1500	1825	2.8	0.90	84.2	59.3	24.0	0.0	788
50	2.83	1500	1847	1.2	0.85	83.8	56.4	25.0	1.5	792
51	2.83	1500	1584	1.7	0.60	80.1	43.0	24.4	11.7	752
52	2.83	535	1825	0.5	0.57	73.4	38.9	25.3	7.9	726
53	2.83	1000	1857	0.8	0.91	77.4	46.7	25.3	4.4	760
54	2.83	500	998	0.8	0.59	34.2	1.6	7.2	16.2	330

*Liquids are vapor phase benzene for all tests except No. 54



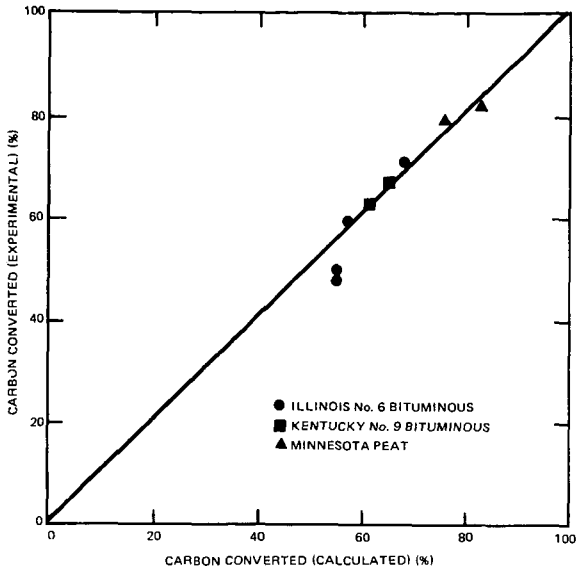
9317-103

Figure 4. Carbon Conversion as a Function of Reactor Temperature



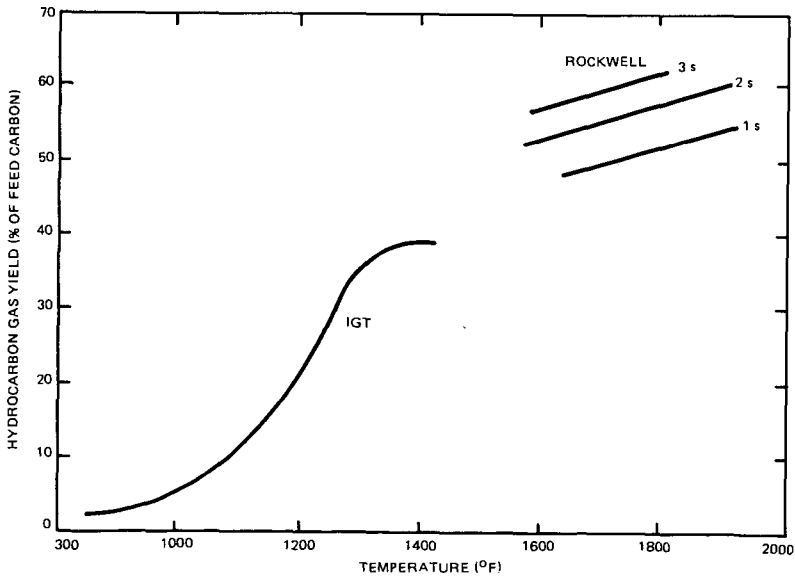
9317-104

Figure 5. Carbon Conversion to Benzene as a Function of Reactor Temperature



9317-105

Figure 6. Comparison of Reactor Model With Experimental Data



9317-106

Figure 7. Comparison of Hydrocarbon Gas Yields for Peat

FLASH HYDROGENATION OF LIGNITE AND BITUMINOUS COAL
IN AN ENTRAINED FLOW REACTOR

J. L. Beeson
D. A. Duncan
R. D. Oberle

Institute of Gas Technology
3424 S. State Street
Chicago, Illinois 60616

Introduction

This paper is a report of some recent developments in an on-going investigation of short residence time hydrogenolysis of lignite and coal to produce fuel gases, ethane, gasoline blending stock constituents, fuel oil and spent char. The program has been underway for three years, and in addition to the bench-scale unit described here will include the construction and operation of a process development unit. In results obtained to date, both lignite and bituminous coal have been successfully processed in the bench-scale unit. In a typical run, approximately 50% of the feed carbon is converted to liquid and gaseous products; as much as 15% of the feed carbon has been found to report to the hydrocarbon liquid products, and 35% to carbon oxides, methane, ethane and minor amounts of propane and propylene. Heavy tars are not produced, allowing the spent char to be collected as a dry, free-flowing material. Approximately 50% of the feed carbon remaining in the spent char would be utilized in hydrogen production, and would be sufficient for a "balanced plant" operation.

Hiteshue, *et al.* (1) observed that when coal is heated rapidly in the presence of hydrogen at high pressure, high yields of gaseous and liquid products are obtained. Over the past several years, several development programs (2,3,4,5,6) have been implemented to explore the various aspects of rapid or "flash" hydrolysis in the light of eventual commercialization. The work described here is intended, in general, to complement the work of other investigators, and also elucidate the behavior of reactants and products during the course of the pyrolysis. The exploration of processing conditions appropriate for the recovery of maximum possible yields of liquids suitable for use as motor fuels is an important additional aspect of the IGT program. Johnson (4) postulated that the hydrocarbon liquids are released early in the pyrolysis, and are hydrogenated to methane and ethane in subsequent reaction steps.

In the work described here, our data show that in addition to relatively slow hydrogasification to methane and ethane, there is considerable vapor phase dehydroxylation of oxygenated monoaromatics (phenols + cresols) and dealkylation of substituted benzenes which results in significant changes in the distribution of BTX and oxygenated aromatics in the gasoline boiling range fraction of the hydrocarbon liquid products. The dehydroxylation and dealkylation reactions appear to be dependent upon both hydrogen partial pressure and temperature in a manner analogous to the vapor phase dealkylation of toluene in the presence of hydrogen described by Silsby and Sawyer (7).

Equipment

A flow diagram showing the major equipment in the bench-scale unit used in the work described here is shown in Figure 1. In operation, solids charged to the feed hopper are metered into a carrier stream of hydrogen; the hydrogen and entrained solids are then heated concurrently in a 1/8-in I.D. helical tube reactor which is 70 feet in length. A predetermined "temperature profile" is imposed over the length of the reactor by means of 12 independently controlled radiant heaters. The effluent from

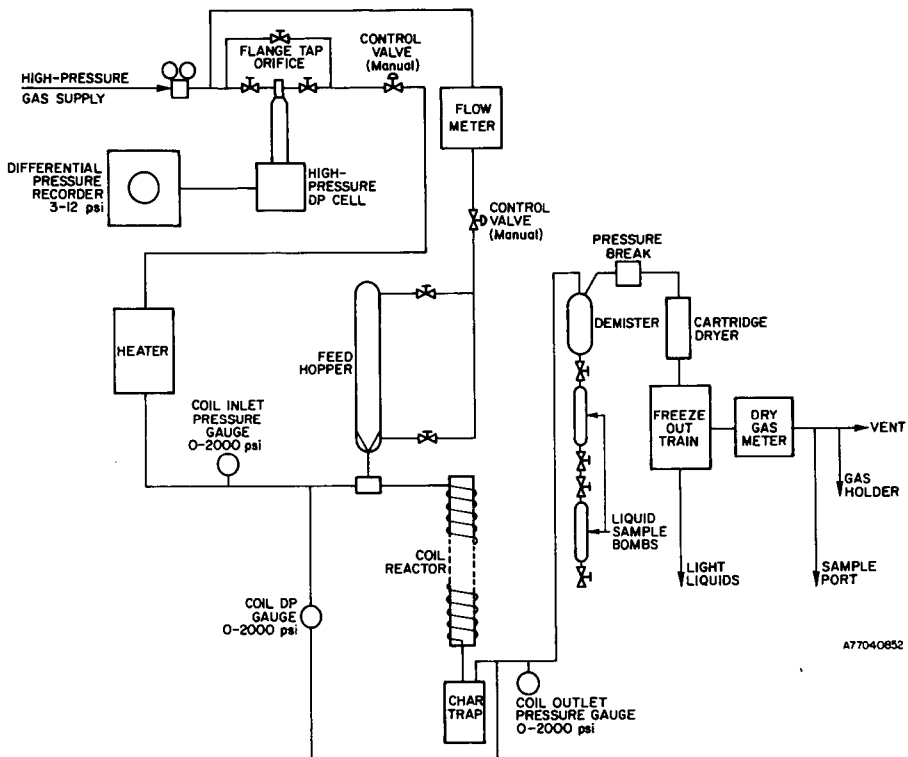


Figure 1. BENCH-SCALE UNIT

the reactor passes into the char trap where the spent char is disentrained and collected; the char-free gases are further cooled to ambient temperature to condense liquid products which are collected in sample bombs. The cooled gases are then reduced to essentially ambient pressure, and passed through a dryer and methanol/dry ice freeze-out train to strip benzene and other condensable materials from the make gas. The stripped gases are then metered, sampled, and vented.

A power plant grind (75% minus 200 mesh) of North Dakota lignite was used as solids feed in the work described here. Although feed gases can be preheated prior to mixing with feed solids, both the feed hydrogen and feed lignite were introduced into the reactor at ambient temperature. Runs using preheated hydrogen have been made, but analysis of data has not been completed at this writing; the results of these runs will be reported at a future time.

Experimental

In the experimental program described here, the objective was to explore the effect of heating rate on the distribution of feed carbon among products. Two kinds of temperature profile (Figure 2) were used in operating the equipment. In the first type, a linear heating rate was imposed on the lower end of the coil reactor. Due to a "chimney" effect, the upper end of the coil was heated by convection from the lower section, and idled at approximately 700°F. Using this first type of temperature profile, the feed was heated to a maximum temperature of 1500°F and quenched, with no appreciable residence time at 1500°F. In the second type of temperature profile, the lower section of the reactor was operated isothermally at 1500°F, and a linear heating rate imposed on the upper section of the coiled tube reactor, so that the reactants were held at 1500°F for times which were dependent upon the gas velocity chosen for a particular run.

Experimental Results

The operating conditions and results of the heating rate study are summarized in Table 1 which shows the distribution of carbon among products, the weight percent gasoline boiling range liquids obtained from the recovered liquids, and the weight percent of phenols + cresols and naphthalenes present in the gasoline boiling range liquids. Comparing Runs HR-1 and HR-3, it is apparent that with appreciable residence time at the maximum temperature (1500°F), feed carbon conversion actually decreased with increase in heating rate; a similar result was described by Johnson (4). At the higher heating rate, the liquid products were also more highly oxygenated, as measured by the amounts of phenols + cresols present in the gasoline boiling range liquids.

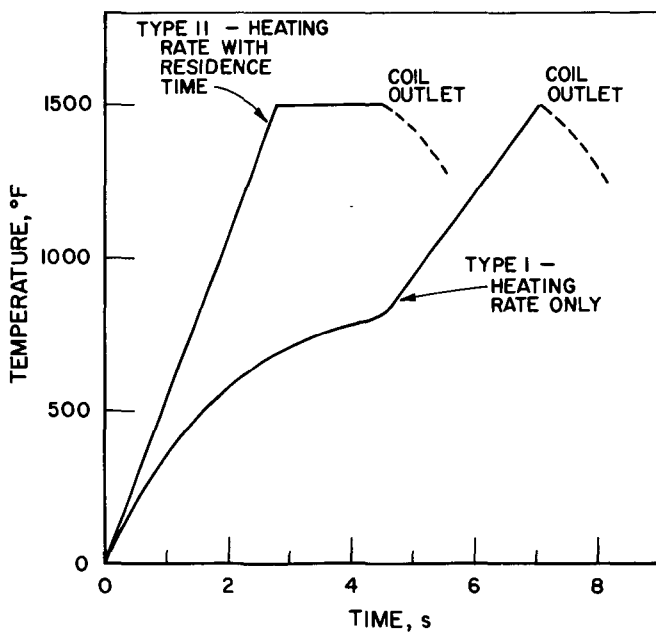
When a residence time at 1500°F was allowed, as in Runs HR-4 through HR-7, the methane yields improved considerably, and the degree of oxygenation of the liquid products as measured by the phenols + cresols in the gasoline boiling range liquids decreased. By inspection, however, there does not appear to be any effect that can be attributed to heating rate alone.

The intensity or severity of a time-temperature history can be measured by the magnitude of a severity function defined as -

$$\text{Severity Function} = \int_0^t k t \quad 1)$$

where k is a reaction rate constant and t is time. Using published data for the hydrogasification of anthracene (8), the rate constant can be calculated from -

$$k = k_0 e^{-E/RT} \quad 2)$$



A79061323

Figure 2. TEMPERATURE PROFILES USED IN HEATING RATE STUDIES

where k is 9.0×10^5 and E is 30,700 Kcals per gram mole. For the non-isothermal time-temperature histories used here, the value of the severity function was obtained by dividing the length of the coil into increments and calculating an incremental severity at the average temperature of the section. The value of the severity function was then obtained from -

$$\text{Severity Function} = \sum_{i=1}^n k \Delta t_n \quad 3)$$

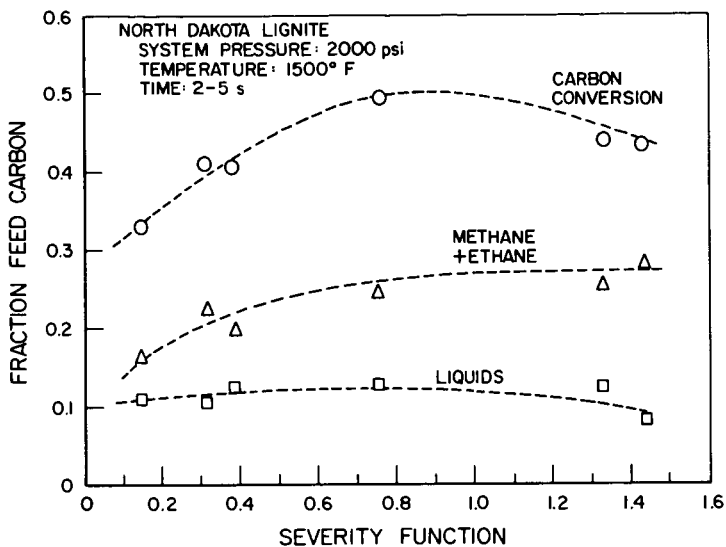
This severity function, based on anthracene hydrogasification kinetics is thus an arbitrary measure that can be used to characterize the thermal treatment under a given set of operating conditions. The data from the heating rate runs are plotted against severity function in Figure 3. From the figure, methane + ethane yield can be seen to increase with increase in severity function; while total carbon conversion passes through a maximum, suggesting that in a prolonged treatment, products are lost through thermal degradation. A similar result has been described by Steinberg, et al. (6). The total liquids yield also appears to decrease at high severity.

Table 1. OPERATING CONDITIONS AND SUMMARY OF RESULTS OBTAINED IN HEATING RATE STUDIES WITH NORTH DAKOTA LIGNITE

Run No.	HR-2	HR-1	HR-3	HR-4	HR-5	HR-7	HR-6
Coil Outlet Pressure	2000	2000	2000	2000	2000	2000	2000
Coil Outlet Temperature	1500	1500	1500	1500	1500	1500	1500
Severity Function	0.383	0.315	9.148	0.767	1.346	1.434	1.954
Heating Rate, °F/s	125	152	348	412	155	1275	780
H ₂ /MAF Feed Weight Ratio	0.44	0.26	0.48	0.43	0.30	0.55	0.45
Carbon Distribution, %							
Liquids	12.25	11.03	11.71	13.19	12.44	8.59	7.30
Carbon Oxides	9.47	9.05	8.18	11.27	9.72	10.35	8.47
Methane	12.40	10.90	10.59	16.34	17.35	19.47	19.69
Ethane + Light Gas	7.37	11.36	6.26	8.43	8.33	8.63	8.61
Char	52.20	51.23	58.87	52.51	52.52	54.55	52.69
Gasoline Boiling Range Liquid, wt % total liquids	51.8	55.2	49.5	54.1	54.5	67.5	58.5
Phenols + Cresols in C ₅ -400°F Liquid	22.7	18.0	31.2	7.1	1.6	0.2	Tr
Naphthalene in C ₅ -400°F Liquid	12.6	15.2	10.8	6.7	5.3	15.2	7.8
	No Residence Time at 1500°F			Variable Residence Time at 1500°F			

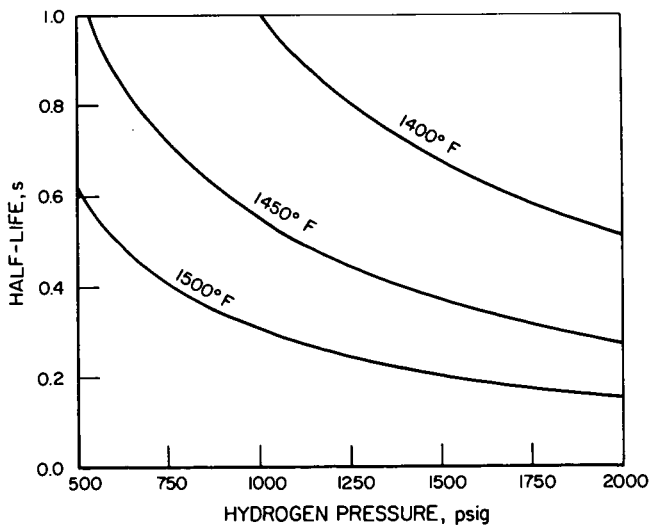
Discussion

Using kinetics published by Silsby and Sawyer (7), the change in the half-life of toluene with temperature and pressure was evaluated, and the results of these calculations are summarized in Figure 4. From the figure it can be seen that the dealkylation of toluene is accelerated by both an increase in temperature and hydrogen partial pressure. The observed changes in the composition of the gasoline boiling range liquids obtained from North Dakota lignite also appear to follow an analogous rule in which the dehydroxylation is accelerated by increase in hydrogen partial pressure (Figure 5). In a prior portion of the investigation, runs were made in the bench-scale unit at system pressures of 500, 1000, 1500, and 2000 psig, holding other parameters essentially constant. The fraction of phenols + cresols in the gasoline boiling range liquids was observed to decrease with increase in operating (essentially hydrogen) pressure while the fraction of BTX + ethylbenzene was observed to increase.



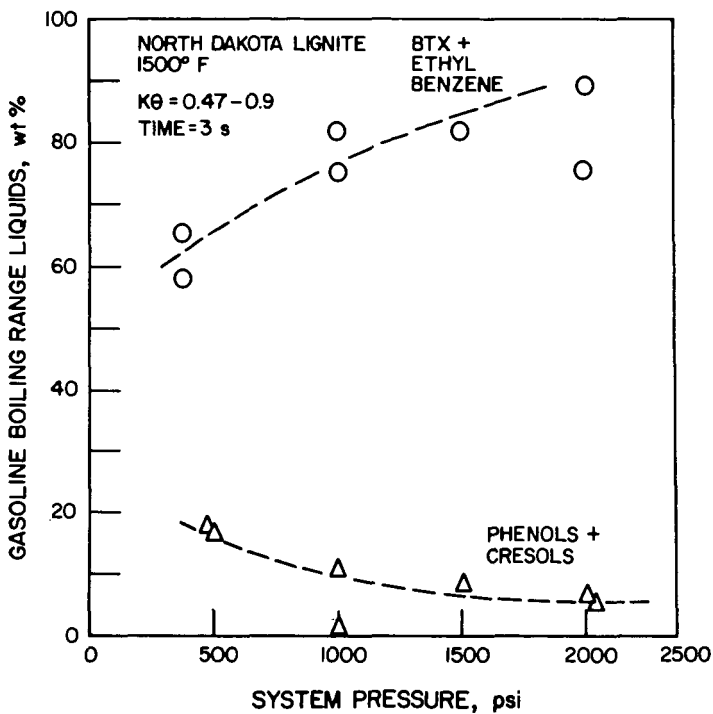
A79061322

Figure 3. CARBON CONVERSION, METHANE + ETHANE, AND LIQUIDS YIELDS IN HEATING RATE STUDIES



A79061326

Figure 4. CHANGE IN THE HALF-LIFE OF TOLUENE WITH TEMPERATURE AND HYDROGEN PARTIAL PRESSURE (6)



A79061325

Figure 5. CHANGE IN GASOLINE BOILING RANGE LIQUIDS COMPOSITION WITH PRESSURE

In the heating rate runs, the phenols + cresols fraction of the gasoline boiling range liquids was found to decrease with increase in severity function, as shown in Figure 6 with an attendant increase in BTX. The distribution of benzene, toluene, and xylene was observed to change as shown in Figure 7 which shows maxima for both toluene and xylene early in the pyrolysis with subsequent dealkylation to benzene. Finally, liquids, as they are devolved from the lignite at 1200° to 1300°F, are highly oxygenated, as shown in Table 2 which summarizes data from some runs with North Dakota lignite.

Table 2. OPERATING CONDITIONS AND SUMMARY OF RESULTS
OBTAINED AT 1200° AND 1300°F WITH NORTH DAKOTA LIGNITE

Run Number	PS-3	PS-5
Coil Outlet Pressure, psig	1500	1500
Coil Outlet Temperature, °F	1300	1200
Severity Function	0.334	0.217
H ₂ /MAF Feed Weight Ratio	0.31	0.53
Carbon Distribution, %		
Liquids	14.61	11.58
Carbon Oxides	9.46	9.23
Methane	9.62	5.88
Ethane + Light Gas	6.23	5.07
Char	64.51	68.33
Analysis of Gasoline Boiling Range Liquids		
BTX + Ethylbenzene	22.9	8.3
C ₉ Aromatics	5.4	4.0
Indenes + Indans	5.1	4.0
Phenols + Cresols	52.3	76.1
Naphthalenes	5.4	3.3
Not Identified	<u>8.9</u>	<u>4.3</u>
Total	100.0	100.0

Conclusions

From the foregoing it appears that the hydrocarbon liquids obtained from North Dakota lignite are highly oxygenated as they are devolved from the lignite, and are converted to BTX in the vapor phase by reaction with hydrogen. The conversion of oxygenated compounds to BTX exhibits a pressure and temperature dependency very similar to the dealkylation of toluene in the presence of hydrogen described by Silsby and Sawyer (7). The distribution of feed carbon among products and the composition of the gasoline boiling range liquids is a function of severity of thermal treatment, and appears to be independent of heating rate when heating rates of 150°F/s or higher are used.

The pressure dependency of the dehydroxylation reactions would affect reactor operations, particularly at low hydrogen-to-coal feed ratios where the hydrogen partial pressure would be substantially reduced with the release of methane, steam, and other reaction products. At this writing, the experimental work is being extended to the study of the effects of using preheated hydrogen. Analysis of data has not been completed, however, and the results of these runs will be reported at a future time.

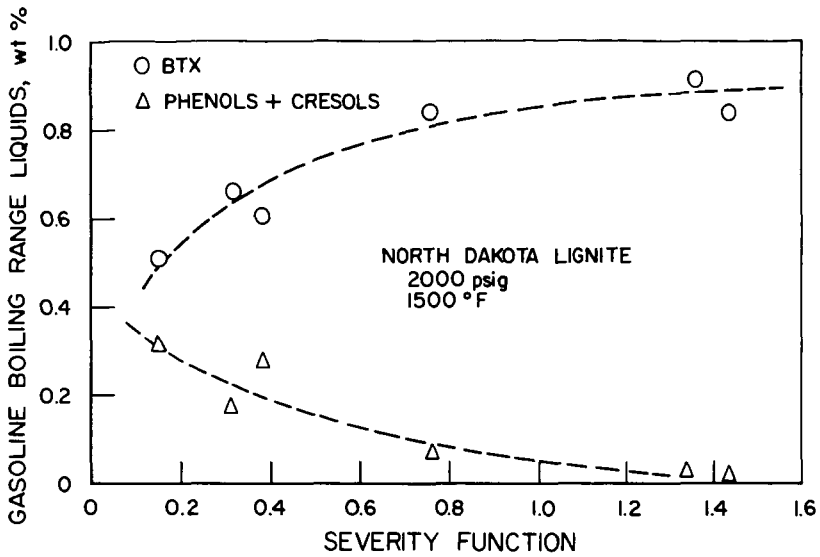


Figure 6. DISTRIBUTION OF BTX AND PHENOLS + CRESOLS WITH INCREASE IN SEVERITY A79061327

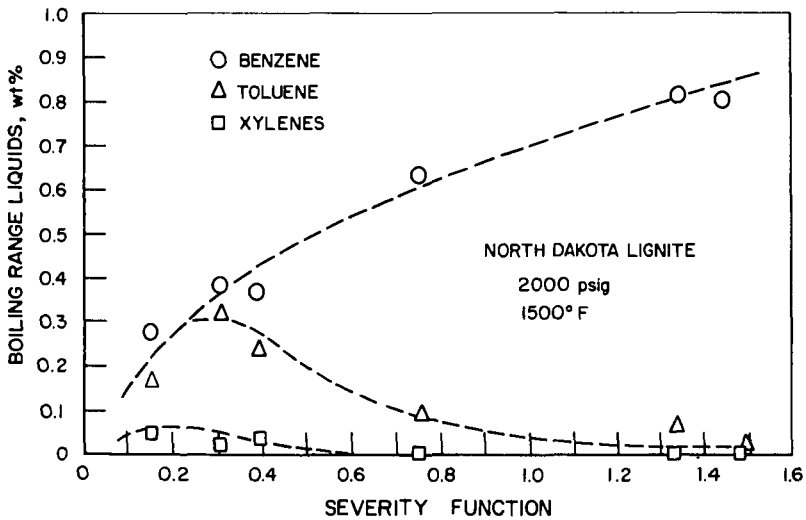


Figure 7. DISTRIBUTION OF BENZENE, TOLUENE, AND XYLENES IN THE BTX FRACTION OF GASOLINE BOILING RANGE LIQUIDS A79061324

Acknowledgements

This research was performed for the United States Department of Energy under Contract No. EX-76-C-01-2307; this support is gratefully acknowledged.

References

1. Hiteshue, R. W., Friedman, S., and Madden, R., "Hydrogasification of High-Volatile A Bituminous Coal," U.S. Bureau of Mines Report of Investigation 6376, Washington, D.C., 1964.
2. Chambers, H. F., Jr. and Yavorsky, P. M., "Production of SNG by Free-Fall Dilute-Phase Hydrogasification of Coal." Paper presented at the 174th National Meeting of the American Chemical Society, Miami Beach, September 1978.
3. Greene, M. I., "Engineering Development of a Short Residence Time, Coal Hydro-pyrolysis Process," Fuel Processing Technology 1, (1977/1978), 169-185, 1978.
4. Johnson, J. L., "Kinetics of Initial Coal Hydrogasification Stages." Paper presented at the 173rd National Meeting of the American Chemical Society, New Orleans, March 1977.
5. Oberg, C. L., Falk, A. Y., Hood, G. A., and Gray, J. A., "Coal Liquefaction Under High Mass Flux and Short-Residence Time Conditions." Paper presented at the 173rd National Meeting of the American Chemical Society, New Orleans, March 1977.
6. Steinberg, M., Fallon, P., Bhatt, V-B., Zeigler, E., and Lee, Q., "Reaction, Process, and Cost Engineering for the Flash Hydro-pyrolysis (FHP) of Coal." Paper presented at the 71st Annual Meeting of the American Institute of Chemical Engineers, Miami Beach, November 1978.
7. Silsby, R. J. and Sawyer, E. W., "The Dealkylation of Alkyl Aromatic Hydrocarbons I. The Kinetics and Mechanism of Toluene Decomposition in the Presence of Hydrogen," J. Appl. Chem. 6, No. 8, 347-355, 1956.
8. Virk, P. S., Chambers, L. E., and Woebecke, H. N., "Thermal Hydrogasification of Aromatic Compounds." Paper presented at the 165th National Meeting of the American Chemical Society, Dallas, April 1973.

MECHANISM OF SHORT RESIDENCE TIME HYDROLYSIS
REACTION FOR MONTANA ROSEBUD SUBBITUMINOUS COAL

by

U. M. Oko, J. A. Hamshar, G. Cuneo and S. Kim

A. Introduction

Research into short residence time hydrolysis of coal has been in progress at Cities Service Research and Development Company since 1974. More than 150 individual coal runs were performed in this time period using a bench-scale reactor recently described (1). Cost estimates for SWG and benzene production were also published (2)(3).

Some 50 runs were performed on Montana Rosebud Subbituminous coal at various reactor conditions. The results of these runs were reported elsewhere (1)(4)(5). In this report, a kinetic model originally proposed by Feldmann (6) is used to calculate reaction rate constants for carbon conversion for these 50 runs, at four distinct temperature zones. Also, the effect of reactor conditions are statistically correlated with gas and liquid hydrocarbons and the results of this analysis is reported.

B. Kinetics of Carbon Conversion

High heat up rates of finely divided coal particles and short residence time of less than 2 seconds at 500-1500°C under hydrogen atmosphere (7) were shown to promote carbon conversion into gas and liquids. Several reaction models were proposed to explain the kinetics of this phenomenon. Recently, Russel et al (8) illustrated that the role of mass transfer by bulk flow and diffusion including kinetics of devolatilization in single particles of coal can be explained by assuming a first order devolatilization reaction with instantaneous heatup to isothermal state and relatively long reaction time. Their model consists of three sets of reactions: primary devolatilization, secondary deposition and hydrogenation. This model was shown to fit data generated by Anthony and Howard (9) from hydrolysis of single discrete coal particles in a batch reactor.

For continuously operating reactors a simpler model has been used by several investigators including Wen, Feldmann, et al (6)(10). In this model the rate of gasification is proportional to the hydrogen partial pressure and to the rapid-rate carbon material remaining in the coal. For coal gasification into methane this simple model can be used by assigning the carbon in the coal into three categories (6). Type 1 carbon is a highly reactive specie which is almost instantaneously flashed off during the rapid heatup step. Type 2 is the solid carbon which readily hydrogasifies and type 3 is the low reactivity char carbon which will react upon long duration exposure (in order of minutes) to the hot hydrogen atmosphere. Type 1 and 2 carbon are classified "rapid rate carbon" and in this report are considered as a single specie.

For hydrogasification reaction the "rapid rate carbon" and hydrogen interaction follows the rate reaction (6):

$$\frac{dX}{dt} = k P_{H_2} (\alpha - X) \quad (1)$$

where X is the fractional carbon conversion, P_{H_2} the hydrogen partial pressure, α the fraction of carbon available for reaction in the regime of consideration and k the reaction rate constant. Best fit for conversion data were found by Feldmann (6)(12) when $\alpha = 1$. Hence, at any given constant temperature:

$$\int_0^X \frac{dX}{1-X} = \int_0^t k P_{H_2} dt \quad (2)$$

$$\ln(1-X) = -k P_{H_2} t \quad (3)$$

where t is the coal/hydrogen contact time in the reactor. From equation 3, the reaction rate constant k , can be calculated.

C. Particle Residence Time in the Reactors

The Cities Service R & D Co. short residence time bench-scale reactor system shown in Figure 1 was previously described (4). It can accept interchangeable reactors to investigate the effect of wide spans of residence time on the extent of carbon conversion into gas hydrocarbons and liquid hydrocarbon products. When short residence times are desired, straight vertical reactors of different diameters are fitted inside the electric furnace cavity. For longer residence times, helical reactors can be fitted.

The problem of estimating particle residence time in vertical entrained straight reactors can be solved by estimating the terminal velocity of a single char particle, and then correcting this value for entrained flow. This method was used by Gray et al (11) who used the equation:

$$U_T = \left[\frac{3.1g (\rho_s - \rho_g) \bar{d}_p}{\rho_g} \right]^{1/2} \quad (4)$$

to estimate the terminal settling velocity (14). Correction factors which were applied following Wen and Huebler (10) increased the final particle velocity by a factor of about 3. For helical reactors, the problem of estimating particle residence time is further aggravated by the almost total lack of experimental or theoretical data. In our work, we met these shortcomings with glass cold-flow models of straight and helical reactors and measured average particle velocities in these models. The same flow regimes that were experienced in the bench-scale apparatus were used in the model studies. The average average particle velocities were found by feeding coal-char at controlled rate from feed hoppers located above the glass model. Coal char was used because in most of these tests particle residence time exceeded 0.5 seconds. Coal is converted into char-like material within 0.200 seconds at the temperature regimes of 825-1000°C.

Holdup of particles in the model, at constant flow conditions, was measured by simultaneously closing plug valves at the inlet and exit. The velocities were calculated from the weight of the solids trapped in the section and the feed rate to the model. This work was done by Ming-Tsai Shu and C. B. Weinberger of Drexel University (15).

With the glass model for the vertical straight reactor of length L , (4) we found that the average average particle velocity is very close to that of the superficial gas velocity. This greatly simplified the task of calculating particle residence times t :

$$t = L/\bar{V}_p(dp) \quad (5)$$

where $\bar{V}_p(dp)$ is the average average particle velocity in m/sec. For helical reactors, at gas velocity in the excess of 6.3 m/sec. the following semi empirical equation was derived by Shu (15) to estimate the average average particle velocity:

$$\frac{\bar{v}_g - \bar{v}_p(dp)}{\bar{v}_g} = k_o \text{Re}^a R^b \left(\frac{D_H}{D_T}\right)^c \cdot \left(\frac{dp}{d\bar{p}}\right)^d \quad (6)$$

where for char of Montana Rosebud subbituminous coal:

$$\begin{aligned} k_o &= 0.323 \\ a &= 0.139 \\ b &= 0.185 \\ c &= -.102 \end{aligned}$$

When calculating the average average flow velocity of char:

$$dp/\bar{d}p = 1 \quad (7)$$

and t , residence time, is calculated from equation 5. A plot of the average variable size particle velocity for a constant gas velocity of 6.3 m/sec is shown in Figure 2. The plot indicates that selective classification occurs in the helical reactor. This was also observed visually. The large particles tend to settle at the glass model wall and because of wall friction move slower than the fine particles. Also, when the feeding rate of particles into the model is increased, the average average particle velocity in it decreases. This is because the particles are not uniformly dispersed and tend to concentrate at the outer periphery of the helix.

When the superficial gas velocity is below 6.3 m/sec, equation 6 becomes increasingly unreliable and velocity of the particles must be interpolated from specific flow measurements generated by Shu (15). However, even at somewhat lower velocity the equation may be used to predict average average particle residence times. For example, workers at the University of Utah (17) using iron filings as tracer in coal which was treated in a helical reactor in hydrogen at 122 atm. and 482°C reported residence time of 9 seconds. The reactor was a tube of 0.48 cm internal diameter, 14.5 meters long which was coiled into a 12.7 cm diameter helix. The gas velocity in their tests was only 5.6 m/sec. Yet even with this low velocity, equation 6 predicts residence time of 10 sec.

D. Hydrogasification Kinetics of Montana Rosebud Subbituminous Coal

Fifty subbituminous coal runs were performed (4) over a range of conditions summarized in Table 1. The data was further divided into four temperature ranges from 827°C to 1000°C. Plot of $-\ln(1-x)$ versus $P_{H_2} t$ in sec. atm is displayed in Figure 3. Table 2 summarizes the equations of each of the lines indicating the quality of fit of each as obtained by regression analysis.

A plot of $\ln k$ vs. $1/T$ on Figure 4 for Montana Rosebud Subbituminous coal is compared with results for Pittsburgh Seam bituminous coal (11). The Arrhenius activation energies for both coals are relatively high: about 15 kcal/mole for the Pittsburgh seam coal and 27 kcal/mole for Montana Rosebud Subbituminous coal. This indicates that both reactions are chemically controlled.

E. Statistical Correlation of Factors Affecting The Formation of Products

Statistical treatment of the data from the fifty runs is used to determine which of the reactor variables: temperature, pressure, vapor residence time, coal to hydrogen ratio, solids residence time or particle diameter are most likely to affect the degree of carbon conversion. The treatment can be extended to the effects of conditions on the yield of the various product

FIGURE 1

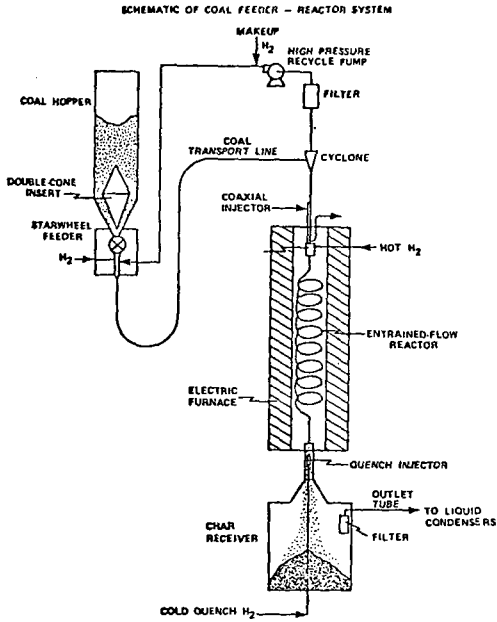


FIGURE 2

CHAR PARTICLES VELOCITY IN THE HELICAL REACTOR AS PREDICTED BY EQUATION

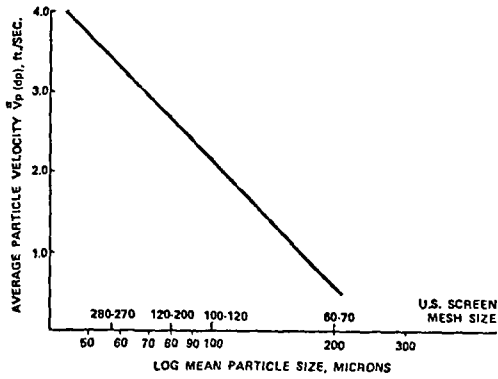


TABLE 1

RANGE OF OPERATING CONDITIONS FOR HYDROGASIFICATION
OF MONTANA ROSEBUD SUBBITUMINOUS COAL

	<u>Range</u>
Temperature - °C	825-1000
Pressure - atmospheres	34-160
Particle Residence Time - sec.	0.4-14.0
Superficial Gas Residence Time - sec.	0.3-4.0
Superficial Gas Velocity m/sec.	5.0-8.0
Hydrogen to Coal Weight Ratio	0.7-1.2

TABLE 2

DATA SUMMARY FOR EACH TEMPERATURE RANGE

<u>Temperature</u> °C	<u>No. of</u> <u>Data</u> <u>Points</u>	<u>Equation of line of best fit</u>	<u>r</u>	<u>$\frac{k}{\text{atm}^{-1} \text{hr}^{-1}}$</u>	<u>Equation</u> <u>No.</u>
827 ± 10°	15	$\ln(1-x) = 1.483 \times 10^{-4} P_{\text{H}_2} t + .3974$.861	.53	(8)
877 ± 10°	19	$\ln(1-x) = 2.36 \times 10^{-4} P_{\text{H}_2} t + .4036$.915	.85	(9)
902 ± 10°	8	$\ln(1-x) = 4.108 \times 10^{-4} P_{\text{H}_2} t + .3668$.892	1.48	(10)
927 ± 10°	8	$\ln(1-x) = 3.88 \times 10^{-4} P_{\text{H}_2} t + .3859$.972	1.40	(11)

FIGURE 3

PLOT OF $-\ln(1-X)$ vs. $P_{H_2} t$ - The slope of each of the lines is the reaction rate constant for Montana Rosebud Subbituminous Coal at the designated temperature

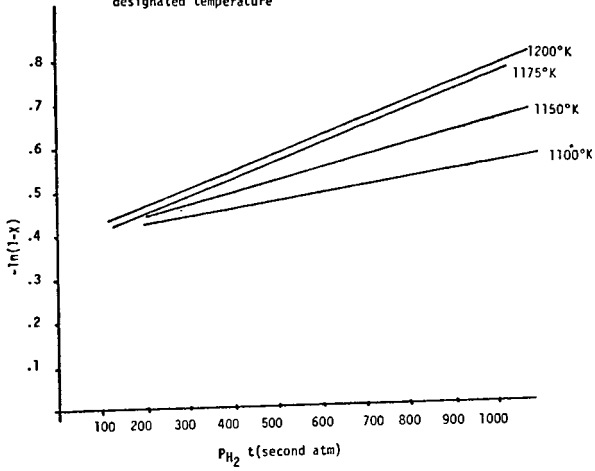
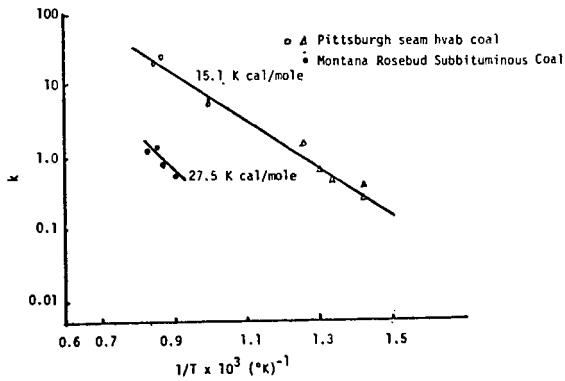


FIGURE 4

TEMPERATURE DEPENDENCE OF THE HYDROGASIFICATION REACTION RATE CONSTANTS FOR PITTSBURGH SEAM COAL (6) AND MONTANA ROSEBUD SUBBITUMINOUS COAL



fractions: gas, liquids, BTX and methane plus ethane. The computer program used for the analysis is available from IBM (16). It is capable of performing a stepwise linear regression followed by a polynomial fitting with orthogonal polynomials. With it, it is possible to analyze the effect of up to 40 variables. The results of the regression is expressed in a form of a linear equation:

$$y = b_0 + b_1x_1 + b_2x_2 + \dots b_nx_n \quad (12)$$

where x_1, x_2, \dots, x_n can be entered as independent transformation functions. The program selects the most effective functions to be fitted into the polynomial equation (12). In addition, it presents each dependent variable in order of importance and re-calculates the curve fitting correlation coefficient with each variable introduced. The forty functions shown in Table 3 were selected for each of the six independent variables:

T - temperature in degrees Kelvin
 P_{H_2} - hydrogen partial pressure - atmospheres
 t - residence time of solids in the reactor - gaseous
 X_g - gas residence time in the reactor - msec.
 $X_{H/C}$ - hydrogen to coal ratio - gm/gm
 dp - mean particle size - microns

and regressed against each of the dependent variables:

x - total fraction of carbon converted
 y_g - fraction of carbon converted to methane plus ethane
 y_e - fraction of carbon converted to liquid hydrocarbons
 y_b - fraction of carbon converted to BTX.

The following equations and correlation coefficients were obtained:

For total fraction of carbon converted:

$$X = \exp \left[\frac{-3276}{T} + .1282 \ln t + 1.761 \right] \quad r = 0.91 \quad (13)$$

For fraction of the carbon conversion into methane plus ethane:

$$y_g = \exp \left[\frac{-9428}{T} + .4457 \ln P_{H_2} + \ln t + 4.63 \right] \quad r = 0.93 \quad (14)$$

For fraction of the conversion into liquid hydrocarbons:

$$y_e = \exp \left[0.273 \ln P_{H_2} + 0.96 \ln t - 4.373 \right] \quad r = 0.67 \quad (15)$$

For fraction of carbon conversion to BTX:

$$y_b = \exp \left[\frac{-6814}{T} + .265 \ln t + 2.899 \right] \quad r = 0.87 \quad (16)$$

These results indicate that within limits of experimental conditions, and for the transformation functions selected gas residence time, hydrogen-to-coal ratio and mean particle diameter have no apparent effect on the degree of carbon conversion into any of the four products x , y_g , y_e , and y_b . The two most important variables seem to be temperature and solids residence time followed by the effects of pressure. Future work with other transformation functions and better modelling may however show that gas residence time may have effect on y_e .

Figure 5 illustrates the effects of temperatures and solids residence times on the total fraction of carbon converted. As expected, the effects of solids residence time are marginal compared to that of temperature. For example, in order to achieve $x = 0.3$, solids residence time of 15 seconds is required at 827°C but only 0.5 seconds if the temperature were to increase by 150°C.

Figure 6 illustrates the effect of temperature and pressure on conversion of carbon to methane and ethane. At constant pressure, the conversion rises steeply with the temperature but the effects of solids residence time are somewhat less pronounced than in Figure 5. At 880°C, $x = 0.3$ and only 60°C rise in temperature is required to drop the required solids residence time from 15 seconds to 0.5 seconds. The effect of pressure on conversion may even be smaller than that of solids residence time. When the pressure is reduced by about 34 atmospheres, the average reduction in conversion is less than 10% even at the high range of temperature. This is within the overall accuracy of gas analysis that can be claimed for this data.

Figure 7 illustrates the dependence of liquid yields on the partial pressure of hydrogen and on residence time. Because of poor correlation ($X = .67$), which indicates scatter in data and poor modelling, it is hard to draw more definitive conclusions. But when viewed with Figure 6 which has steeper slopes of carbon conversion to gas, it seems that optimum yield of liquid may be obtained at moderate temperatures, say 900°C and at hydrogen partial pressures which are as high as practicable.

Figure 8 suggests that conversion of carbon to BTX depends on the fraction of liquid hydrocarbons cracked to methane and ethane. Given long solids residence time with increasing temperature, most of the carbon will eventually be converted to gas probably undergoing intermediate liquefaction. BTX could be a product of liquid hydrocarbons which crack to produce methane and ethane. This may explain the positive slope of the yield curves and the relatively large effect of solids residence time on conversion.

TABLE 3

TRANSFORMATION EQUATIONS FOR REGRESSION ANALYSIS

X(1)	- Dependent Variable
X(2)	- Temperature
X(3)	- Total Reactor Pressure
X(4)	- Hydrogen Partial Pressure
X(5)	- Particle Residence Time
X(6)	- Gas Residence Time
X(7)	- Hydrogen/Coal Ratio
X(8)	- Mean Coal Feed Particle Size
X(11)	= $\text{ALOG}(X(1))$
X(12)	= $-1/X(2)$
X(13)	= $-\text{ALOG}(X(3))$
X(14)	= $\text{ALOG}(X(4))$
X(15)	= $\text{ALOG}(X(5))$
X(16)	= $-\text{ALOG}(X(6))$
X(17)	= $\text{ALOG}(X(7))$
X(18)	= $\text{ALOG}(X(8))$
X(19)	= $X(2)/X(3)$
X(20)	= $X(2)/X(4)$
X(21)	= $X(2)/X(5)$
X(22)	= $X(2)/X(6)$
X(23)	= $X(2)/X(7)$
X(24)	= $X(2)/X(8)$
X(25)	= $X(3)/X(4)$
X(26)	= $X(3)/X(5)$
X(27)	= $X(3)/X(6)$
X(28)	= $X(3)/X(7)$
X(29)	= $X(3)/X(8)$
X(30)	= $X(4)/X(5)$
X(31)	= $X(4)/X(6)$
X(32)	= $X(4)/X(7)$
X(33)	= $X(4)/X(8)$
X(34)	= $X(5)/X(6)$
X(35)	= $X(5)/X(7)$
X(36)	= $X(5)/X(8)$
X(37)	= $X(6)/X(7)$
X(38)	= $X(6)/X(8)$
X(39)	= $X(7)/X(8)$
X(40)	= $X(2) \times X(2)$
X(41)	= $\text{ALOG}(X(1))$
X(42)	= $\text{ALOG}(X(1))$
X(43)	= $\text{ALOG}(X(1))$
X(44)	= $\text{ALOG}(X(1))$
X(45)	= $1/X(2)$
X(46)	= $1/X(6)$
X(47)	= $1/X(7)$

FIGURE 5

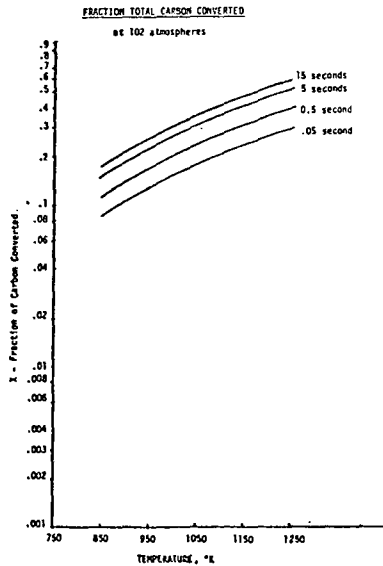


FIGURE 6

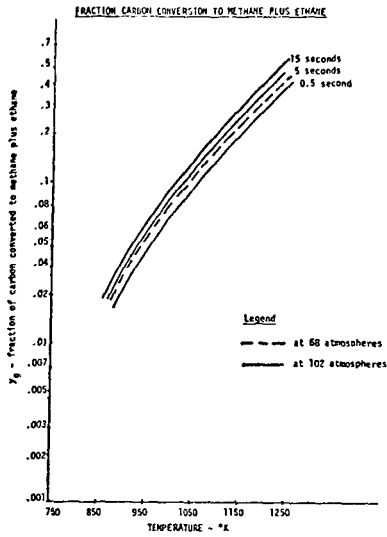


FIGURE 7

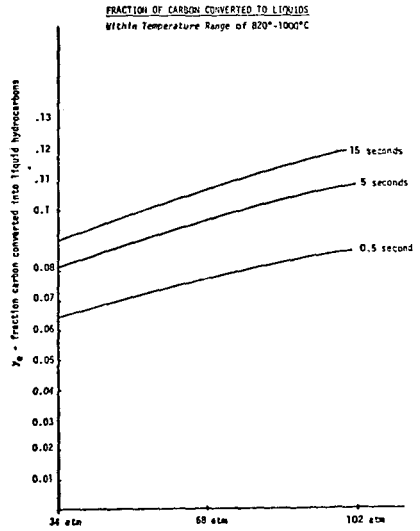
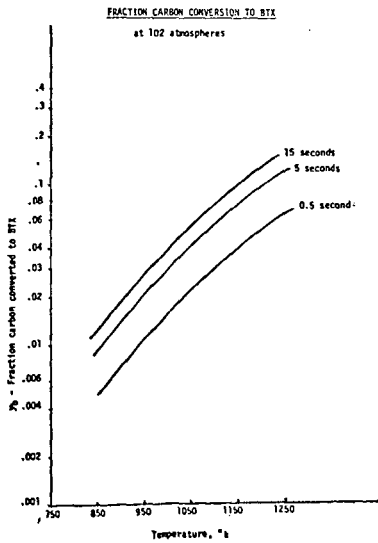


FIGURE 8



F. Bibliography

- (1) Hamshar J. A., S. J. Bivacca and M. I. Greene "Reaction Engineering of the CS/R Flash Hydropyrolysis Technique for Coal Gasification" AIChE 71st Annual Meeting, Miami Beach, Fla., Nov. 1978.
- (2) LaDelfa C. J., M. I. Greene "Economic Evaluation of Synthetic Natural Gas Production by Short Residence Time Hydropyrolysis of Coal" Fuel Processing Technology, 1 (1978) 187-208.
- (3) Greene M. I., C. J. LaDelfa, S. J. Bivacca "Benzene-Ethylene-SNG From Coal Via Short Residence Hydropyrolysis" AIChE 175th National Meeting Anaheim, Ca. March, 1978.
- (4) Data Appearing in the Appendix of Cities Service Report to U. S. DOE "Studies of Coal Liquefaction by Short Residence Time Hydropyrolysis Using Promoters", DOE Contract No. EF-76-C-01-2574, March, 1979.
- (5) Epstein M., T. P. Chen, M. A. Ghaly "An Analysis of Coal Hydrogasification Processes" Report by Bechtel Corporation to U. S. DOE Contract No. EF-77-A-01-2565 NTIS Publications FE-2565-14, UC90C (1978).
- (6) Feldmann H. F., W. H. Simons, J. A. Mima and R. W. Hiteshue, Fuel Div. ACS Vol. 14 No. 4 pt. 2 Sept., 1970.
- (7) Rosen B. H., A. H. Pelofsky, M. I. Greene, "Coal Hydrogenation to Produce Liquids", U. S. Patent 3,960,700, June 1, 1976.
- (8) Russel W. B., D. A. Seville and M. I. Greene "A Model For Short Residence Time Hydropyrolysis of Single Coal Particles", AIChE Journal Vol. 25, No. 1 p65-80, 1979.
- (9) Anthony D. B. and J. B. Howard, "Coal Devolatilization and Hydrogasification", AIChE Journal 22, 625 (1976).
- (10) Wen, C. Y. and J. Huebler, "Kinetic Study of Coal Char Hydrogasification", Ind. Eng. Chem. Process Design Development, 4, 142 (1965).
- (11) Gray, J. A., P. T. Donatelli and P. M. Yavorski, Reprints ACS Div. of Fuel Chemistry Vol. 20, No. 4, August, 1975.
- (12) Feldmann, H. F. and P. M. Yavorski, "The Hydrane Process", presented at the 5th AGA/OCR Synthetic Pipeline Gas Symposium, Chicago, Ill., Oct. 1973.
- (13) LaDelfa, C. J. and M. I. Greene "Comparative Economics of SNG Production by the Cities Service CS-SRT Process and Lurgi Process", AIChE 174th National Meeting, Chicago, Ill. 1977.
- (14) Kunii, D. and O. Levenspiel, Fluidization Engineering, John Wiley and Sons, Inc., p.76 New York 1969.
- (15) Ming-Tsai Shu "Concurrent Two-Phase Flow of Gas and Coal Particle Mixtures" A thesis submitted to the faculty of Drexel University, June, 1978. C. B. Weinberger, Director of Research.
- (16) International Business Machines Corporation, White Plains, N. Y. Program No. 1130-CA-06X, Applications Program GH20-0333-21.
- (17) Lytle, J. M., R. E. Wood, W. H. Wiser and M. G. Mladejovsky "Residence Time Measurements in a Coal Hydrogenation Process", Fuel Processing Technology 1, 95-102 (1978).

G. Nomenclature

- BTX - benzene, toluene and xylene
- \bar{d}_p - average particle diameter - m^3
- D_H - helix diameter - microns
- D_T - helix tube internal diameter - m
- g - gravity constant - m/sec^2
- k - reaction rate constant - $atm^{-1} hr^{-1}$
- L - reactor length - m
- LHC - liquid hydrocarbons produced, including the BTX fraction as analyzed in the gas
- P_{H_2} - partial pressure of hydrogen
- r - correlation coefficient of regression of the line of best fit by the root mean square through the experimental data points
- Re - Reynold's number
- R - char to gas weight ratio
- t - time - sec.
- U_T - terminal settling velocity - $m/sec.$
- \bar{V}_g - average gas velocity - $m/sec.$
- $\bar{V}_p(dp)$ - average average particle velocity - $m/sec.$
- X - fraction of carbon converted
- X_g - gas residence time - msec.
- $X_{H/C}$ - hydrogen to coal ratio gm/gm
- y_p - fraction carbon converted to methane plus ethane
- y_e - fraction carbon converted to LHC
- y_b - fraction carbon converted to BTX
- ρ_s - particle density - kg/m^3
- ρ_g - gas density - kg/m^3
- α - fraction of carbon available for reaction

CORRELATION OF FLASH HYDROGENATION YIELDS
WITH PETROGRAPHIC PROPERTIES

By W. Chen, A. LaCava and R.A. Graff
Clean Fuels Institute, Department of Chemical Engineering, The City
College of The City University of New York, New York, N.Y. 10031

INTRODUCTION

Recent studies (1,2) indicated that the rank (as measured by the carbon content) alone is not sufficient to predict the yield of volatiles from a coal during flash hydrogenation. The reason is that the rank provides only a gross means of chemical characterization. It is an average of different heterogeneous properties of coal, and does not adequately characterize the chemical structure.

As a consequence, two coals of the same rank may exhibit markedly different chemical properties, give different yields of volatiles and present different product distribution when subjected to flash hydrogenation (2).

On the other hand, a given maceral type occurring in different coals, has been reported to exhibit similar reactivity (3,4) in different processes.

Early work by the Bureau of Mines (5) established the clear dependence of the liquefaction behavior of a coal on its petrographic composition. Also, experimental results showed that vitrinites and exinites are the most readily liquefied (6), while fusinite is almost completely resistant to liquefaction (7).

After the new method of classification of maceral types by the reflected light was introduced (8), considerable information has been reported on the effect of petrographic composition on liquefaction (9-13).

The objective of the present paper is to show that it is possible to correlate flash hydrogenation yields with petrographic composition of the coal. The same type of correlation will be used to predict product distribution at fixed reaction conditions. Correlations based on the petrographic analysis of coal, can be used consequently, to build kinetic models of coal flash hydrogenation that would be applied to a large variety of coals.

EXPERIMENTAL

The experimental arrangements used in this study were similar to those described in previous papers (14). The analysis of products was performed by on-line mass spectrometry or by gas chromatography. Experiments were carried on at 100 atm. of hydrogen, a heating rate of 650°C/s., 10 s. of solids contact time, 0.6 s. of vapor residence time and temperatures from 600 to 1000°C.

A suite of eight U.S. coals from the Pennsylvania State University collection, from lignite to HVA, was used for this study. Their chemical properties and rank are tabulated in figure 1.

CORRELATION PROCEDURE

The fundamental assumption used for correlation purposes is that the total volatiles yield obtained during flash hydrogenation depends linearly on the maceral composition:

$$y = \sum_{i=1}^n r_i x_i \quad (1)$$

In a similar form, and since each one of the macerals can give a different product distribution, the yield of each one of the products can be assumed to depend linearly on the maceral composition:

$$y_j = \sum_{i=1}^n r_{ij} x_i \quad (2)$$

From equations (1) and (2) and in order to have a consistent set of definitions; we can deduce the following properties:

$$0 < \sum_{i=1}^n r_i \leq 1 ; 0 < r_i \leq 1 ; r_i = \sum_j r_{ij} \quad (3)$$

Also, the following correlation was used to transform the units of carbon conversion (% of original carbon) and weight loss (% of original dmmf. coal) (15):

$$y = 1.14w - 13.7 \quad (4)$$

A computer program on multiple linear regression was used to find the values of r_i in equation (1). After several tests with combinations of different macerals, it was found that the total yield was a function of the percentage of vitrinite and pseudo-vitrinite only. Consequently, the concentration of these two macerals were used as variables in all the correlations.

RESULTS

For comparison purposes, the data on total yields was correlated with the rank of the coal (carbon percent d.m.m.f.). The correlation was very poor, presenting a correlation coefficient $\rho = 0.579$.

When vitrinite and pseudo-vitrinite content are used as variables, the correlation improves considerably. The correlation coefficient of

the regression now is $\rho = 0.99$. Note that the number of free parameters in the new correlation is the same as in the rank case.

The correlation defined by equation (2) was applied to the yield of individual components during flash hydrogenation of different coals at fixed conditions. Figure 2 shows the results of the correlations.

DISCUSSION AND CONCLUSIONS

In view of the success of the attempts of correlating yields and products distribution with the petrographic composition of different coals, it is possible to conclude that the maceral content of a coal provides more information with respect to its reactivity (at least with respect to flash hydrogenation) than its rank. This conclusion, however, is based on a small group of different coals (8 coals only) and should be verified further with a larger sample of coals.

The fact that the yield of individual components can be correlated with the maceral composition, offers excellent possibilities for the use of maceral content-based correlations in the analysis of kinetic data from flash hydrogenation, and possibly for similar processes. It should be kept in mind that different macerals can present different selectivities towards individual components. Also, secondary reactions of the individual components (e.g., in the gas phase) could introduce deviations in the correlations.

As a final conclusion, correlations based on the petrographic composition of coals are a promising tool that could allow prediction of reactivities, total volatile yields and product distribution for any coal in flash hydrogenation given only its maceral content.

NOMENCLATURE

- r_i : reactivity of the i^{th} maceral (dimensionless)
 r_{ij} : reactivity of the i^{th} maceral to give the j^{th} product (dimensionless)
 x_i : the maceral content of the coal (5) (weight % on dmmf coal)
 y : total volatile yield (% of the initial carbon converted)
 y_i : yield of i^{th} component (% of initial carbon converted)
 σ : standard deviation of the regression defined from

$$\sigma^2 = \sum_{-i=1}^n \frac{(y_i, \text{experim.} - y_i, \text{calc})^2}{(n-2)}$$

REFERENCES

1. Chen, W.Y., R.A. Graff and A.I. LaCava, ACS, Div. of Petro. Chem. Preprints, 23, 4, 1316 (1978).
2. Chen, W.Y., S.J. Shen, A.I. LaCava and R.A. Graff, paper presented to the 13th MARM, ACS, West Long Branch, N.J., Mar. 23, 1979.
3. Berry, W.F., A.R. Cameron and B.N. Nandi, Centennial Review Paper #1, Canadian Inst. of Mining and Metallurgy, Ottawa, Mar. 29, 1967.
4. Dormans, H.N.M., F.J. Huntjens and D.W. vanKrevelen, Fuel, 36, 321 (1957).
5. Fisher, C.H., G.C. Sprunk, A. Eisner, H.J. O'Donnell, L. Clarke and H.H. Storch, Bureau of Mines Tech. Paper 642 (1942).
6. Parks, B.C. and H.J. O'Donnell, U.S. Bureau of Mines Bull. No. 550 (1956), p. 193.
7. Fisher, C.H., G.C. Sprunk, A. Eisner, L. Clarke and H.H. Storch, Ind. Eng. Chem., 31, 190 (1939).
8. Hacquebard, P.A., Proc. of 1st Conference on Origin and Constitution of Coal, Crystal Cliffs, Nova Scotia, pp. 8-48 (1950).
9. Ergun, S., H.J. O'Donnell and B.C. Parks, Fuel, 38, 205 (1959).
10. Davis, A., paper presented at Coal Chem. Workshop, Stanford Research Inst., Menlo Park, Calif., Aug. 26-27, 1976.
11. Gray, D., G. Barrass and J. Jezko, ACS, Div. Fuel Chem. Preprints, 24, 2, 2 (1979).
12. Durie, R.A., ACS, Div. Fuel Chem. Preprints, 24, 2, 12 (1979).
13. Mori, K., M. Taninchi, A. Kawashima, O. Okuma and T. Takahashi, ACS, Div. Fuel Chem. Preprints, 24, 2, 28 (1979).
14. Graff, R.A., S. Dobner and A.M. Squires, Fuel, 55, 109 (1976).
15. Anthony, D.B. and J.B. Howard, A.I.Ch.E. J., 22, 625 (1976).

Sample No.	Rank	Province	Age	State	Moist	M.M. direct	C dmmf	O dmmf	S Dry	DAF
PSOC 326	HVA	Eastern	Carb.	PA	2.21	21.18	84.49	5.56	4.36	5.28
PSOC 270	HVA	Eastern	Carb.	AL	1.27	17.72	85.15	4.85	2.34	2.77
PSOC 284	HVA	Interior	Carb.	IL	3.11	25.08	83.71	7.12	5.23	6.70
PSOC 314	HVA	RockyM.	Cret.	UT	4.08	11.55	81.47	10.13	0.76	0.84
PSOC 280	HVC	Interior	Carb.	IN	11.32	18.31	81.58	9.51	3.78	4.50
PSOC 248	S.8it. A	RockyM.	Cret.	WY	19.17	3.34	75.44	17.04	0.64	0.66
PSOC 240	S.8it. B	Pacific	Tert.	WA	19.73	16.47	73.96	18.98	0.50	0.60
PSOC 246	Lignite	NorthGr. Plains	Tert.	ND	34.12	10.99	71.85	21.22	0.65	0.72

Figure 1. Selected coals for flash hydrogenation studies

<u>Component</u>	<u>Corr. variable</u>	<u>Corr. coefficient</u>	<u>σ</u>
Methane	$0.17V + 0.58(PV+E+R)$	0.9811	0.67%
Ethane	$0.08V + 0.05(PV+E+R)$	0.7661	0.52%
BTX	$0.08V + 0.127(PV+E+R)$	0.427	0.92%

Figure 2: Correlations applied to individual components

THE FORMATION OF BTX BY THE HYDROPYROLYSIS OF COALS

M.J. Finn, G. Fynes, W.R. Ladner and J.O.H. Newman

National Coal Board, Coal Research Establishment
Stoke Orchard, Cheltenham, Glos. GL52 4RZ

ABSTRACT

The pyrolysis of British coals has been studied at hydrogen pressures of 50 to 150 bar in single- and two-stage, tube reactors at heating rates of up to 30 K s^{-1} . In the single stage reactor, hydrolypyrolysis of a high-volatile coal gave up to 4.5% single-ring aromatics; the results suggested that the evolution of volatiles and their cracking to benzene were sequential reactions. This was confirmed using a two-stage reactor in which the coal was heated at a controlled rate and the volatiles cracked in a separate zone at constant temperature. Yields of up to 12% benzene were obtained from a high volatile coal in hydrogen (similar to the yields obtained by various workers from American coals by flash pyrolysis) without very rapid heating of the coal. Hydrolypyrolysis of model compounds showed that benzene was a major product of the cracking of polynuclear aromatics under hydrogen pressure.

1. INTRODUCTION

The carbonisation of coal under hydrogen pressure is known as 'hydro-pyrolysis'. A review of published work¹ showed that flash hydrolypyrolysis of coal, which involves heating rates of hundreds of K s^{-1} , can give appreciable yields of light aromatic hydrocarbons such as benzene, toluene and xylenes (BTX). The present paper is concerned with studies of both single-stage and two-stage hydrolypyrolysis of coals aimed at producing single-ring aromatics, especially benzene, from coal. In the single-stage reactor the carbonisation and cracking zones are heated by the same source, while in the two-stage reactor there is independent control of the carbonisation and cracking zones.

2. MATERIALS

2.1. Coals

The analyses of the coals used for hydrolypyrolysis are given in Table 1. The coals were ground, sized +251 -500 μm and dried at 373 K in vacuum.

2.2. Model Compounds

Hydrolypyrolysis experiments were also carried out on six aromatic hydrocarbons: benzene, toluene, p-xylene, naphthalene, anthracene and phenanthrene. Where possible, 'ANALAR' grade chemicals were used without further purification. As the hydrolypyrolysis reactor was only suitable for solids, 1g of compound was either absorbed on or mixed with 9g of active carbon (NCB Anthrasorb).

3. SINGLE-STAGE HYDROPYROLYSIS

3.1. Experimental

The design of the reactor is based on that used by Hiteshue and co-workers at the USBM². A 1830 mm long x 8 mm ID stainless steel, pressure tube in which about 10g of coal were secured between degreased wire wool plugs was heated by passing a large current (up to 1600A) through its wall. The heating rate was controlled by switching tappings on a transformer. The pyrolysis

vapours were swept out of the reaction zone by pressurised hydrogen at up to 150 bar, some of the liquid products collecting in the ice-cooled trap. The remaining liquid products and gases were reduced to atmospheric pressure through a needle valve, which was also used to control the flow rate, before being collected for analysis. The products in the trap were weighed and then washed from the trap and adjoining tubing with chloroform. The residual char in the reactor was weighed and analysed.

3.2. Product Analysis

Both gaseous and liquid products were analysed by chromatography. The hydrocarbon gases were measured on an alumina column with a flame ionisation detector, and the permanent gases on a molecular sieve 5A column with a katharometer detector. The liquids were measured using a silicone SCOT column with a flame ionisation detector. Water was estimated by titration with Karl Fisher reagent. Proximate and ultimate analyses were carried out on selected char samples.

3.3. Results

The effect of variations in the final heat-treatment temperature and in the vapour residence time on the yields of single-ring aromatics formed by hydrolysis of high-volatile Linby coal was investigated using heating rates in the range 7 to 30 K s⁻¹, a pressure of 150 bar and zero solids residence time at maximum temperature.

3.3.1 The effect of final heat-treatment temperature

The effect of the final carbonisation temperature on the yields of benzene, toluene and xylenes (BTX) and phenol, cresols and xylenols (PCX) is shown in Figure 1, where it can be seen that for a vapour residence time of approximately 10 s the yields of both BTX and PCX passed through a maximum at a temperature of about 1000 K. The maximum yield of single-ring aromatics was approximately 4.5%, being composed of about equivalent amounts of BTX and phenolics.

3.3.2 The effect of vapour residence time

The effect of vapour residence on the yields of BTX and PCX at heating rates of 10, 20 and 30 K s⁻¹ to a final heat-treatment temperature of 1000 K is shown in Figures 2a and b. The yield of BTX increased steadily over the range of residence times investigated and was little affected by the heating rate. In contrast, the yield of PCX passed through a maximum at a residence time of 3 s and was markedly affected by the heating rate, at the two higher heating rates the PCX being almost completely destroyed after 8 s. Dehydroxylation of the PCX to BTX at the longer residence times only partly explains the fate of the PCX since the decrease in PCX is considerably greater than the increase in BTX.

4. TWO-STAGE HYDROLYSIS

4.1 Modification to Apparatus

The modification to the hydrolysis apparatus to enable the carbonisation and cracking zones to be separated is shown in Figure 3. The upper portion of the stainless steel tube reactor, which served as the cracking zone, was thermostatically controlled at temperatures up to 1273 K using two muffle furnaces; the lower portion which contained the coal was electrically heated as previously.

4.2 Experimental

The samples (coals, coking coals plus coke and model compounds on active carbon) to be pyrolysed were placed, as before, in the lower section of the tube. The flow of hydrogen through the reactor was established to give the required vapour residence time with the upper section maintained at the cracking temperature. Current was then passed through the lower section to heat it and the sample to the carbonisation temperature. The products were collected and analysed in the same way as with the single-stage reactor.

4.3. Results

4.3.1 Effect of carbonisation time, temperature and heating rate

The effect of varying the carbonisation time is shown in Figure 4. The methane increases monotonically with time and the benzene yield reaches a limit of about 11% w/w on d.a.f. coal at 9 minutes. Thus, to achieve optimum benzene yield with minimum methane formation, the residence time of the coal should be controlled.

Varying the final carbonisation temperature from 848 to 973 K (at a carbonisation time of 9 minutes) while cracking the products at 1123 K gave the results plotted in Figure 5. Methane increases monotonically with increase in final carbonisation temperature whereas ethane and benzene pass through broad maxima at about 923 K, the benzene yield peaking at 12% w/w on d.a.f. coal (13.4% C on C). The lower benzene yield at 973 K suggests that, at this temperature, some of the benzene is destroyed during the carbonisation stage. The volatile matter content of the char decreased from about 16% at a carbonisation temperature of 750 K to 5.5% at 923 K.

The results of tests on the effect of heating rate show that, at a carbonisation temperature of 750 K, increasing the heating rate of the coal from 1 to 25 K s⁻¹ has no significant effect on benzene yields, although the methane and ethane yields are reduced by the higher heating rate.

4.3.2 Effect of cracking temperature and residence time

The yields of gases and liquids were determined after cracking at temperatures from 773 to 1223 K using the relatively low carbonisation temperature of 750 K and a carbonisation time of 15 minutes.

The yields of methane, ethane, benzene and tar are given in Figure 6. Above 900 K, increasingly severe cracking of the carbonisation vapours gives continuously increasing yields of methane, whereas the ethane and benzene pass through broad maxima. The yield of tar decreases with increasing temperature, suggesting that tar vapours are the precursors of much of the ethane and benzene, themselves being hydrogenated to methane under more extreme conditions.

The effect of varying the hydrogen flow rate and hence the gaseous residence time was also investigated. The carbonisation temperature was 873 K and the pressure was 150 bar. The results are summarised in Figure 7 and show that, as the hydrogen flow was increased, the yields of ethane and benzene increased and the benzene passed through a broad maximum. At the lower hydrogen rates, the volatiles were overcracked to give high methane yields. The lowest hydrogen rate of 0.85g min⁻¹ (equivalent to a flow of 0.01 m³ min⁻¹ at room temperature and pressure) gave a gaseous residence time of about 7 s in the cracking zone at 150 bar and 1123 K.

4.3.3 Effect of pressure

Tests at 50, 100 and 150 bar in which the vapour residence time was maintained constant by using a constant linear hydrogen velocity gave the results shown in Figure 8. Methane and ethane yields increased linearly with pressure but the benzene yield increased less than proportionally to pressure.

4.3.4 Effect of coal-rank

The results on the effect of coal-rank are summarised as yields versus carbon content of coal in Figure 9 and suggest that the maximum ethane and benzene yields are obtained from the CRC 800 coals. Anthracite, as expected, gave less volatile hydrocarbons, and the coking coals tended to cake in the carboniser and would therefore be difficult to process continuously. The high volatile brown coal contained 24.8% oxygen and the oxygen appeared mainly as water rather than carbon oxides. The Lady Victoria coal gave comparatively low benzene and high methane yields, probably reflecting the high aliphatic content of this coal.

4.3.5 Model compounds

Table 2 gives the results of the hydrolysis of the aromatic compounds listed in Section 2.2.; only the aromatic products are listed. The cracking temperature was varied from 823 to 1173 K at a constant vapour residence time of about 5 s. As might be expected, the extent of decomposition increased with increasing temperature, and the percentage remaining undecomposed at 973 K was taken as a measure of thermal stability. The stability sequence in order of decreasing stability was as follows: benzene = naphthalene > phenanthrene > p-xylene > anthracene. It should however be stressed that the order depends on the temperature. Thus, at 1073 K toluene and p-xylene are less stable than anthracene.

The yield of benzene at three temperatures (973, 1073, 1173 K) from the model compounds is shown as a bar chart in Figure 10. Benzene survives both as a feedstock and as a product of the cracking of toluene, p-xylene and polynuclear hydrocarbons. It is interesting that naphthalene, anthracene and phenanthrene give benzene as a major product at the two higher cracking temperatures.

5. DISCUSSION

In line with the various groups of American workers²⁻⁵ who have studied hydrolysis, the carbonisation of coal under hydrogen pressure has been shown to give much higher yields of light aromatics, in particular benzene, than are obtained by conventional carbonisation, i.e. at atmospheric pressure in an inert atmosphere.

The results of the experiments carried out in a single-stage reactor similar to that used by Hiteshue, Anderson and Schlesinger² are in good agreement with their published data. With this apparatus which employs relatively slow heating rates (up to 30 K s^{-1}) a maximum yield of 4.5% single-ring aromatics can be expected from a low-rank coal.

In these single-stage reactors the temperature cycle of the reactor together with the hydrogen flow rate through it determine the conditions for both the pyrolysis of coal and the hydrocracking of the volatiles produced. Thus, it is impossible to optimise simultaneously both the carbonising and cracking conditions. However, in the two-stage hydrolysis reactor, the carbonisation and cracking processes have to a large extent been separated and it is therefore possible to optimise separately the conditions for each.

The present work with the two-stage reactor shows that yields of over 10% benzene can be obtained from a low-rank coal without the need for heating at very high rates (up to 1000 K s^{-1}). From the point of view of the design of a hydrolysis plant, a process employing a moderate heating rate should be preferable since it is likely to be difficult to achieve very fast heating on an industrial scale.

6. CONCLUSIONS

The present study has:

- (i) confirmed that hydrolysis of coal produces appreciable yields of single-ring aromatics, especially benzene, and has shown that a benzene yield in excess of 10% can be obtained without heating the coal very rapidly;
- (ii) shown that the benzene yield depends on the temperature of the cracking zone and the residence times of the volatiles in this zone;
- (iii) demonstrated the potential of a two-stage reactor whereby the pyrolysis and cracking stages can be independently controlled, and which should make it simpler to optimise the yields of desired products.

7. ACKNOWLEDGMENTS

We thank the National Coal Board for permission to publish this paper and the European Coal and Steel Community for financial support. The views expressed are those of the authors and not necessarily those of the National Coal Board.

8. REFERENCES

1. Fynes, G., Ladner, W.R., and Newman, J.O.H. to be published in "Progress in Energy and Combustion Science", Pergamon Press.
2. Hiteshue, R.W., Anderson, R.B., and Schlesinger, M.D., Ind. Eng. Chem., 49, 2008 (1957).
3. Graff, R.A., Dobner, S., and Squires, A.M., Fuel, 55, 109 and 113 (1976).
4. Steinberg, M., and Fallon, P., ACS Div. Petr. Chem., 20, (2), 542 (1975).
5. Pelofsky, A.H., Greene, M.I., and LaDelfa, C.J., ACS Div. Fuel. Chem. Prepr., 21, (5), 154 (1976).

Table 1: Analyses of Coals

Colliery or Coal Type	NCB CRC No.	Grade	Proximate analysis		Ultimate analysis					Maceral analysis			Coking Test			
			Moisture a.f.	Ash d.b.	V.H. d.a.f.	C	H	N	O	Total Cl S	Vitrinite	Exinite	Inertinite	Grey King Coke Type	Swelling No.	
																d.m.m.f.
Coed Bach	101	Washed duff	2.5	5.6	5.7	93.9	3.1	1.25	0.9	0.8	0.08	62	0	38	A	0
Garw	203	Washed smalls	0.8	10.1	17.9	91.6	4.7	1.55	1.6	0.8	0.01	71	Tr.	29	F	7
Detwent-haugh	301b	Washed smalls	0.5	5.3	29.7	87.6	5.5	1.75	4.3	0.8	0.04	N.D.	N.D.	N.D.	C ₉	8½
Bersham	402	Washed + 2 in.	1.9	2.0	38.3	85.9	5.6	1.75	6.8	1.0	0.39	87	3	10	G ₉	8½
Annesley	602	Washed doubles	4.5	2.4	38.6	84.3	5.5	1.9	7.2	0.8	0.49	73	9	18	G ₄	6½
Linby	802	Washed doubles	8.3	5.8	39.1	82.4	5.3	1.95	9.0	1.0	0.46	79	6	15	C	1
Daw Hill	802	Smalls	9.3	11.7	39.7	80.6	4.9	1.4	11.9	1.65	0.23	63	11	26	C	1
Cotgrave	902	Blend A	8.5	14.2	41.5	82.5	5.7	1.85	9.2	0.65	0.26	N.D.	N.D.	N.D.	A	1
Lady Victoria	-	Cannel	2.0	2.9	52.2	84.4	6.8	1.5	5.8	1.3	0.19	26	21	53	E	1
German brown	-	-	13.5	7.6	52.8	69.7	4.6	0.9	24.8	0.25	0.03	N.D.	N.D.	N.D.	A	0

N.D. = Not determined.

Table 2: Yields of Aromatics from Two-stage Hydropyrolysis of Aromatics

Feedstock	Cracking Temperature, K	Calc. vapour residence time, s	Yield % w/w on feed					
			Benzene	Toluene	Xylenes	Naphthalene	Anthracene	Phenanthrene
Benzene	973	5.2	92					
	1023	4.9	101					
	1073	4.6	95					
	1123	4.4	71					
	1173	4.3	18					
Toluene	823	6.1	20	66				
	873	5.7	21	42				
	973	5.2	59	32				
	1023	4.9	54	1				
	1073	4.6	73	0				
	1123	4.4	61	0				
p-xylene	773	6.5	4	21	97			
	873	5.7	4	6	76			
	973	5.2	14	23	21			
	1023	4.9	56	7	8			
	1073	4.6	67	0	0			
Naphthalene	773	6.5	1	0.2	0	99		
	973	5.2	4	0.8	0	93		
	1023	4.9	5	2	0	80		
	1073	4.6	24	1	0	52		
	1123	4.4	41	0.4	0	8		
	1173	4.3	23	0.3	0	0.2		
Anthracene	773	6.5	0.5	0.4	0	3	16	
	873	5.5	0.5	0.4	0	2	14	
	973	5.2	2	0.7	0	8	9	
	1073	4.6	15	0.4	0	20	7	
	1173	4.3	16	0.1	0	0.6	2	
Phenanthrene	773	6.5	0.4	0	0	0	0	37
	873	5.7	0.5	0	0	0	0	36
	973	5.2	0.9	0	0	0.9	0	42
	1073	4.6	4	0.1	0	2	0	18
	1173	4.3	21	0	0	0.1	0	0.7

Condition: 1g of feedstock with 9g of active carbon
 Carbonised at 750K with 15 min. solids residence time
 Heating rate 1 K s^{-1}
 8 mm ID carboniser and cracker
 Hydrogen 0.85 g min^{-1} at 100 bar.

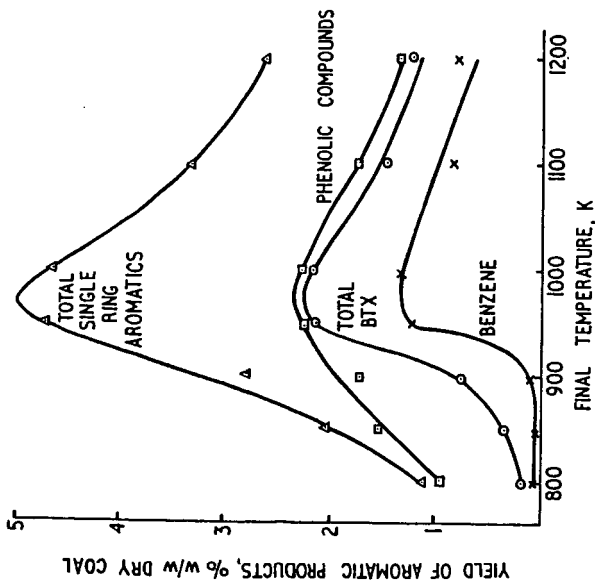


FIGURE 1. EFFECT OF FINAL TEMPERATURE ON YIELD OF PRODUCTS

HEATING RATE 7Ks⁻¹, PRESSURE 150 BAR, SOLIDS RESIDENCE TIME 0s, VAPOUR RESIDENCE TIME 11s, 10g OF 251 TO 500µm LINBY COAL, 8mm ID SINGLE-STAGE REACTOR.

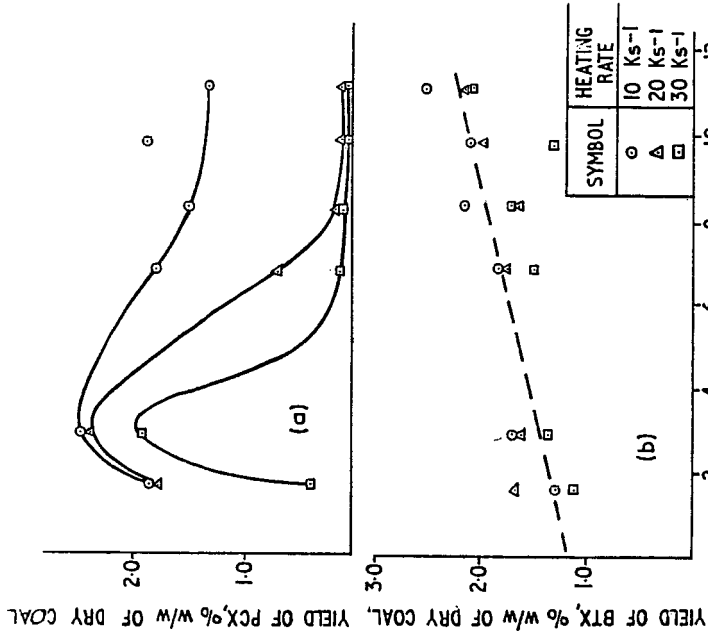


FIGURE 2. EFFECT OF VAPOUR RESIDENCE TIME AND HEATING RATE

ON YIELDS OF (a) PHENOL, CRESOLS AND XYLENOLS (PCX) AND (b) BENZENE, TOLUENE AND XYLENES (BTX)
 FINAL TEMPERATURE 1000K, HEATING RATE 7Ks⁻¹, PRESSURE 150BAR, SOLIDS RESIDENCE TIME 0s, 10g 251 TO 500µm LINBY COAL, 8mm ID SINGLE-STAGE REACTOR.

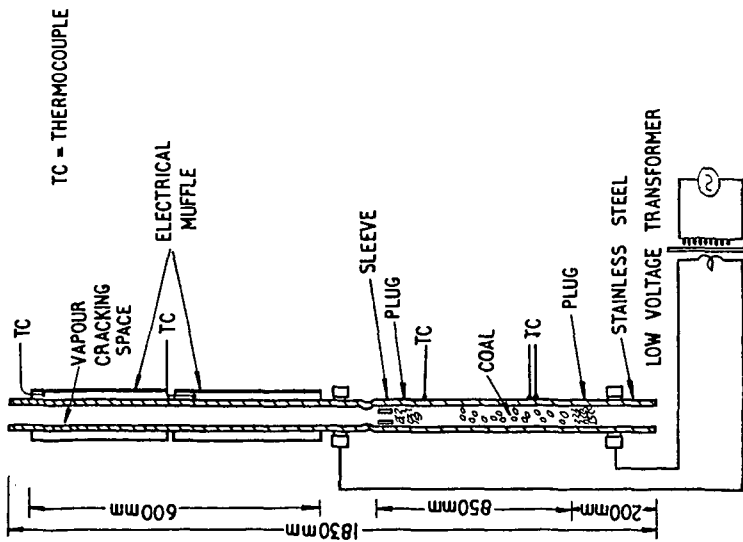


FIGURE 3. DETAILS OF C.R.E. TWO-STAGE REACTOR WITH TEMPERATURE CONTROL OF VAPOUR SPACE

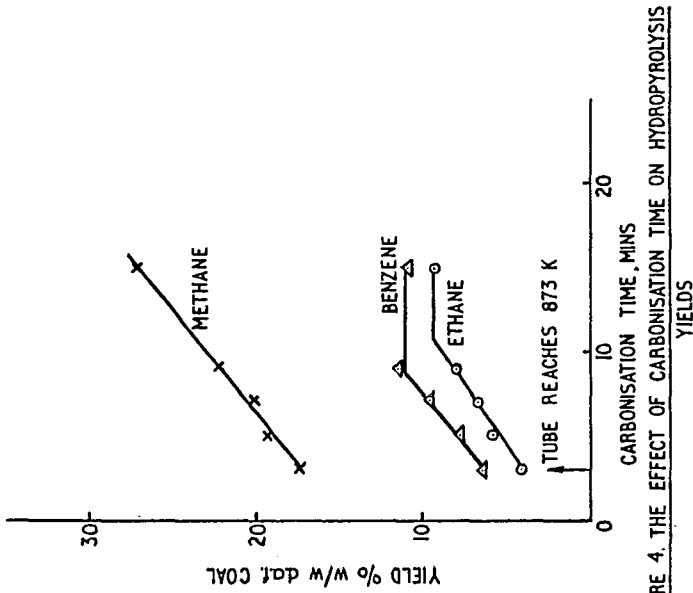


FIGURE 4. THE EFFECT OF CARBONISATION TIME ON HYDROLYSIS

CONDITIONS: HEATING RATE 5Ks^{-1} , CARBONISATION TEMPERATURE 873K , CRACKING TEMPERATURE 1123K , HYDROGEN 1.44g min^{-1} , PRESSURE 150 BAR , $10\text{g LINBY COAL } 251$ TO $500\mu\text{m}$, 8mm ID CARBONISER AND CRACKER.

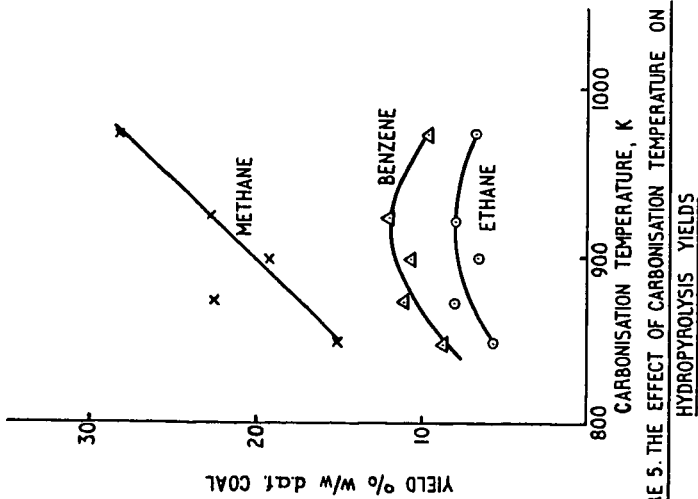


FIGURE 5. THE EFFECT OF CARBONISATION TEMPERATURE ON HYDROPYROLYSIS YIELDS
 CONDITIONS: HEATING RATE 5Ks^{-1} , CARBONISATION TIME 9 min, CRACKING TEMPERATURE 1123K , HYDROGEN 1.44g min^{-1} , PRESSURE 150BAR , 10g LINBY COAL 8mm ID CARBONISER AND CRACKER.

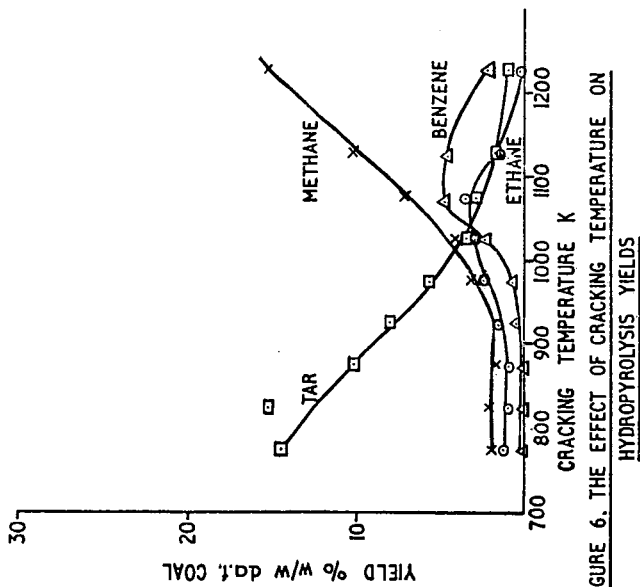


FIGURE 6. THE EFFECT OF CRACKING TEMPERATURE ON HYDROPYROLYSIS YIELDS
 CONDITIONS: HEATING RATE 1Ks^{-1} , FINAL CARBONISATION TEMPERATURE 750K , CARBONISATION TIME 15 min, HYDROGEN RATE 0.85g min^{-1} , PRESSURE 100BAR , 10g OF 251 TO $500\mu\text{m}$ LINBY COAL, 8mm ID CARBONISER AND CRACKER.

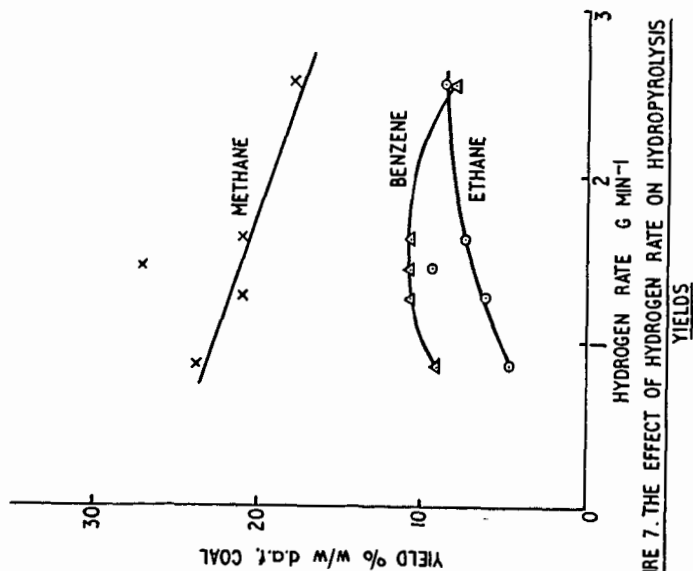


FIGURE 7. THE EFFECT OF HYDROGEN RATE ON HYDROLYSIS YIELDS

CONDITIONS: HEATING RATE 5Ks^{-1} ; FINAL CARBONISATION TEMPERATURE 873K , 873K , CARBONISATION TIME 15min , CRACKING TEMPERATURE 1123K , PRESSURE 150BAR , 10g OF 251 TO $500\mu\text{m}$ LINBY COAL, 8mm ID CARBONISER AND CRACKER.

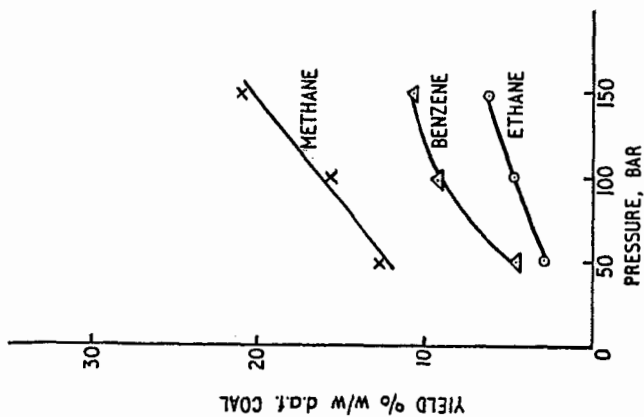


FIGURE 8. THE EFFECT OF PRESSURE ON HYDROLYSIS YIELDS

CONDITIONS: HEATING RATE 5Ks^{-1} , CARBONISATION TEMPERATURE 873K , CARBONISATION TIME 15min , CRACKING TEMPERATURE 1123K , 10g OF 251 TO $500\mu\text{m}$ LINBY COAL, 8mm ID CARBONISER AND CRACKER.

FIGURE 10. YIELDS OF BENZENE AT VARIOUS TEMPERATURES - FROM MODEL COMPOUNDS

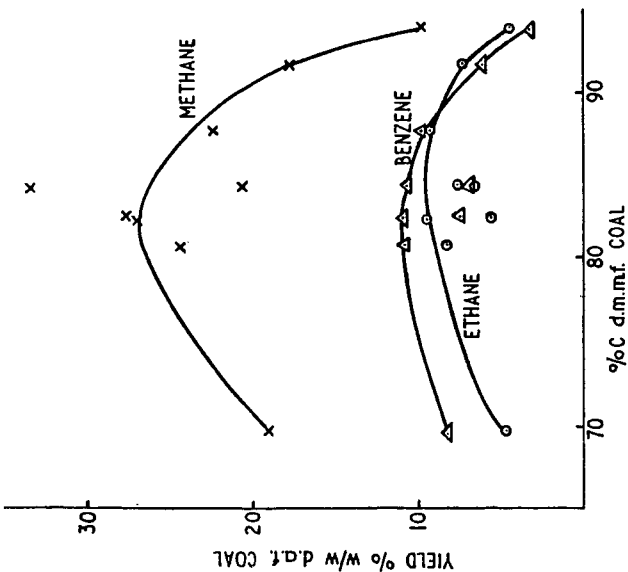
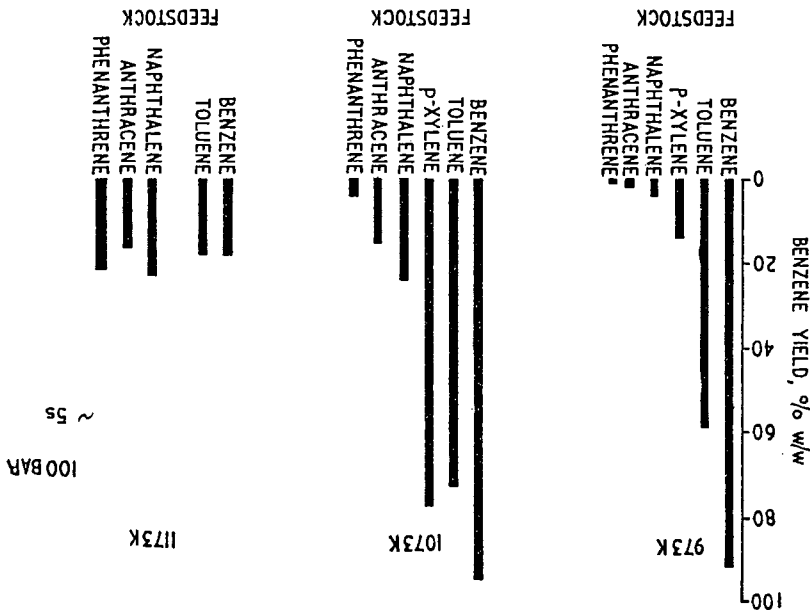


FIGURE 9. THE EFFECT OF COAL RANK ON HYDROLYSIS YIELDS
 CONDITIONS: HEATING RATE 5Ks^{-1} , FINAL CARBONISATION TEMPERATURE 873K , CARBONISATION TIME 15min , CRACKING TEMPERATURE 1123K , HYDROGEN 1.44g min^{-1} , PRESSURE 150BAR , 10g FEEDSTOCK, 8mm ID CARBONISER AND CRACKER.

EFFECT OF CARRIER GAS ON TAR YIELD AND
QUALITY OF OCCIDENTAL FLASH PYROLYSIS

S. C. Che, K. Duraiswamy, K. Blecker
E.W. Knell R. Zahradnik

OCCIDENTAL RESEARCH CORPORATION, IRVINE, CA

ABSTRACT

Occidental Flash Pyrolysis employs recycled heated char as heat carrier to supply the heat of pyrolysis. When nitrogen was used, as transport gas, tar yield decreased due to char-catalyzed tar cracking reactions. When low surface area heat carrier was used, tar cracking reactions was prevented and the tar yield was raised back to the expected level.

The tar was lighter with lower average molecular weight. The improvement of tar yield and quality was attributed to the stabilization of reactive coal fragments by nascent hydrogen produced by char gasification (by CO₂ and steam) and water-gas shift reactions.

INTRODUCTION

Flash Pyrolysis of coal employs very rapid heating to devolatilize pulverized coal in the absence of air to partition the coal into hydrogen-rich tar and carbon-rich char residue. It has been studied in both batch and continuous reactors. (1-5)

Occidental Research Corporation (ORC) developed this concept in a novel entrained flow reactor in which hot recycled char provides the heat to pyrolyze the coal. The typical tar yields are approximately twice that obtained from Fischer Assay test from the same coal. The detailed description of ORC process has been provided elsewhere. (6)

During the operation of a 3-ton-per-day process development unit (PDU), tar loss by char-catalyzed tar cracking reactions was uncovered. A smaller scale unit, 1 kg-per-hour bench scale reactor (BSR), was used to study the effects of transport gas and heat carrier on tar yield. Reactive gases such as CO₂ and H₂O instead of nitrogen were used to transport the char. Tar loss was prevented when the high surface area of char was covered by reactive gases. The tar yield was increased to the same level as that predicted by the electrical heating cases. When low surface area aluminum was used as heat carrier tar loss was also prevented. These results and the mechanism to prevent the tar loss were discussed by Duraiswamy et.al. (7)

This paper presents the effect of carrier gas and heat carrier on the tar quality.

EXPERIMENTAL

The experiments for pyrolysis of coal were carried out in a 1 kg-per-hour bench scale reactor as shown in Figure 1. Coal was metered by a screw feeder and carried by transport gas into the reactor. Char was metered by a second screw feeder and carried by nitrogen or desired transport gas. The char was preheated to the desired temperature before it mixed with the coal. Coal particles were brought to the pyrolysis reaction temperature in a few milliseconds.

Coal disproportionated into hydrogen-rich volatiles and carbon-rich char. The char was separated in a series of cyclones and the vapors and gases were cooled to collect the liquid products. The effluent gases were analyzed by gas chromatographs. The condensed liquid product is dissolved in acetone for easy removal from the collection vessels. After evaporation of the acetone under vacuum, tar and water are separated by distillation.

Each of the fractions, namely acetone, water and tar, are analyzed separately to determine water, light oil and tar ($110^{\circ}\text{C}+$). Tar in condensed water, tar left in char, if any, as determined by pyridine solubility and tar adsorbed in the activated charcoal, as determined by Fischer Assay are all included in the total tar yield.

For the purpose of this study, the characterization of tar properties was only carried out on the $110^{\circ}\text{C}+$ fraction material which is usually over 90% of the "tar".

The analyses of coal and char are given in Table 1. The molecular weight distribution profiles were determined by using gel permeation chromatography performed on tar samples using a Waters 244 ALC/GPC Liquid Chromatograph equipped with a refractive index detector. The columns employed were Waters styragel-columns 30 cm x 7.8 mm ID consisting of 1-1000A, 1-500A and 3-100A pore size packings. Tetrahydrofuran, THF from Burdick and Jackson, was used as the solvent at a pressure of 1000 psig. Calibration of the instrument used the polystyrene standards ranging in molecular weight from 100 to 33,000 AMU. Therefore, the molecular weight labeling of GPC chromatograms was for reference and comparison purpose.

GPC samples were prepared by adding 8 drops of 15% solution of tar in THF to 5 ml THF and filtering through a 0.65 micron filter sample sizes were 125 μl .

The tar was subjected to a solvent fractionation procedure to yield oils, asphaltenes and preasphaltenes. The solubility classes were defined as: oils (hexane soluble), asphaltenes (hexane insoluble/toluene soluble) and preasphaltenes (toluene insoluble/pyridine soluble). Separation was obtained according to the procedure described in Ref. (6).

RESULTS AND DISCUSSIONS

For the purpose of this study, the initial pyrolysis experiments were performed using subbituminous coal, nitrogen carrier gas and electrical heating; i.e., no preheated char was used. A series of runs ranging from 1000°F to 1400°F was carried out. The yields and properties of tar for these runs are given in Table 2.

Effect of Residence Time

Tar produced at the longer residence time contained a higher proportion of oil, and was also characterized by a lower specific gravity, lower viscosity and lower sulfur content than that produced at the lower residence time. These improved tar properties were attributed to the additional cracking that occurs at the longer residence time.

The evidence of the additional tar cracking due to longer residence time is provided by GPC chromatograms, Figure 2. They show that at longer residence times, the concentrations of high molecular weight species decreased while the concentrations of lower molecular species increased.

The oil content of tar was relatively independent of the pyrolysis temperature but was affected by the residence time as shown in Figure 3. The oil content increased from an average value of 43% to 54% when the residence time increased from 1.5 to 3 seconds with a corresponding decrease in the preasphaltenes content. The data suggested that asphaltenes and preasphaltenes underwent cracking at longer residence times and thus the proportion of oil increased. These results indicate that chemical transformations of the tar which occurred during the process enhanced its properties without suffering significant loss in yields. More importantly, these reactions apparently occurred over a practical and controllable range of residence times.

Effect of Heat Carrier: Char and Alumina

When preheated char was used as heat carrier, the tar yields decreased as the ratio of char-to-coal increased, as shown in Figure 4. This effect has been attributed to the char-catalyzed tar cracking reaction by DuraiSwamy et. al.⁽⁷⁾ Due to the secondary cracking reactions, the tar is lighter compared to the tar produced in the electrical heating mode as shown in Table 3. The higher atomic hydrogen-to-carbon ratio and oil content were indications of tar cracking.

When the low surface area (0.23 m²/g) alumina was used as heat carrier, the tar yield was higher than the case which used char as heat carrier. The tar is lightest among the three as shown in GPC of Figure 5. The tar loss reaction by char-catalyzed cracking was prevented when alumina was used as heat carrier. However, a different catalytic reaction might have taken place on the surface of alumina to improve the tar quality, as shown by the GPC.

GPC of tar from the alumina run showed significant reduction of heavy species. This could be attributed to a second possibility that the tar could not lay down on the surface of heat carrier polymerization or condensation to form heavy tar was prevented. The effect on tar yield and quality can be summarized in the following:

Tar Yield: Electrical > Alumina > Char

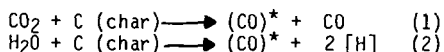
Tar Quality: Alumina > Char > Electrical

Petroleum fluid coke was used in PDU tests instead of alumina and it was found to be in between alumina and char for improving the tar yield and quality.

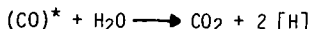
Effect of Reactive Carrier Gases

When different kinds of carrier gases such as CO, CO₂ and steam were used, the tar produced were lighter. The properties are summarized in Table 4. The molecular weights of tars were reduced as shown by vapor phase osmometric analysis and GPC profiles of Figure 6. The high polymeric species such as asphaltenes and preasphaltenes also decreased.

The tar yields were as high as the electrical heating case. The improvement of tar yield and quality were due to the adsorption of reactive gases on the char. When the surface area of char is occupied, tar vapor will not get adsorbed and get cracked on the surface of char to form coke and gases. Additionally by CO₂ and steam char gasification takes place producing CO and [H].



Where (CO)* is surface adsorbed carbon oxides. Nascent hydrogen can be formed on the surface of char by water-gas-shift reaction.



When the primary pyrolysis fragments (free radicals) are formed, they are seeking for stabilization by either reacting with the nascent hydrogen in the gas phase or on the char surface or recombining (polymerizing) stabilization of reactive fragments by nascent hydrogen prevents polymerization reaction to form heavy molecular weight species and coke.

CONCLUSION

Both carrier gas and heat carrier were found to affect the tar yield and tar quality in the Flash Pyrolysis of coal. Preheated char of high surface area provided adsorption sites for tar vapor. Tar either polymerized or cracked on the char to form gases and coke thus lowering the tar yield. When low surface area heat carrier were used, tar loss was reduced significantly. When the active sites of preheated char were occupied by reactive gases such as CO₂ and tar loss was prevented, and the tar quality was also improved. This improvement was attributed to the stabilization of pyrolysis free radicals by the nascent hydrogen produced from carbon gasification between char and reactive gases.

REFERENCE

1. D.B. Anthony, "Rapid Devolatilization and Hydrogasification of Pulverized Coal," Sc.D. Thesis, MIT, Cambridge, Mass (1974).
2. E.M. Suuberg, "Rapid Pyrolysis and Hydropyrolysis of Coal", Sc. D. Thesis, MIT, Cambridge, Mass (1977).
3. A. Sass, Mineral Science Engg. 1972, 4 (4) P. 18-27.
4. A Sass, CEP. 1974, 79 (1), 72-23.
5. J.H. Edwards, I.W. Smith and R.J. Tyler, "Coal to Oil by Flash Pyrolysis", Chemeca 77, Canberra, 14-16, Sept. 1977.
6. "Flash Pyrolysis Coal Liquefaction Process Development" DOE Final Report FE-2244-26, 1979.
7. K. Duraiswamy, S.C. Che, E.W. Knell, N.W. Green and R. Zahradnik, "Tar Yields in ORC Flash Pyrolysis Process", presented in Fuel Chemistry Symp. ACS Nat'l meeting. Honolulu, Hawaii, April, 1979.

TABLE 1
ANALYSES OF FEED COAL AND CHAR

	<u>Feed Coal</u>	<u>Feed Char</u>	<u>Product Char</u>
<u>Proximate Analysis, Wt.%</u>			
Moisture	11.59	1.18	0.7
Ash	5.00	11.40	10.00
Volatile Matter	37.01	7.02	7.88
Fixed Carbon	46.40	80.40	81.42
<u>Ultimate Analysis (Dry), Wt.%</u>			
Carbon	69.12	82.27	82.63
Hydrogen	4.95	1.87	2.13
Oxygen	18.32	2.52	3.29
Nitrogen	1.29	1.14	1.11
Sulfur	0.66	0.66	0.57
Ash	5.66	11.54	10.27
<u>Fischer Assay, Wt.%</u>			
Char	60.4	-	-
Water	21.4	-	-
Tar	9.3	-	-
Gas	8.9	-	-

Table 2
YIELDS AND PROPERTIES OF SUBBITUMINOUS COAL TAR

<u>Pyrolysis Conditions</u>		1.5		3.0	
Residence time, seconds					
Run Number	132	130	134	135	131
Temperature, °F	1000	1200	1400	1000	1400
Tar Yield, wt % MAF	8.7	17.3	15.2	15.2	14.7
					9.7
<u>Tar Properties</u>					
I. Physical Data:					
Specific Gravity, (80/80°F)	1.170	1.171	1.250	1.097	1.090
Viscosity, Centipoises (@ 415°F and extrapolated to)	45	54	23	16	12
0 sec-1 shear)					18
Melting Point, °F	230-265	194-230	-	-	68
					86-104
II. Ultimate Analysis, wt% (Dry Basis)					
Ash	0.7	0.15	0.05	0.02	0.04
Carbon	79.34	80.41	80.86	79.41	79.46
Hydrogen	7.44	7.47	6.35	7.75	6.73
Sulfur	0.51	0.65	0.49	0.39	0.51
Nitrogen	1.25	1.42	1.45	1.04	1.41
Oxygen (by difference)	11.39	9.90	10.80	11.39	11.85
Atomic H/C	1.13	1.11	0.95	1.17	1.02
III. Solubility Classification, wt%					
Oil	43	42	44	56	53
Asphaltenes	29	30	28	27	30
Preasphaltenes	28	28	28	16	17
					21
					24

TABLE 3
COMPARISON OF TAR PROPERTIES
EFFECT OF CHAR HEAT CARRIER

Run No.	<u>175</u>	<u>139</u>	<u>141</u>
Carrier Gas	N ₂	N ₂	N ₂
Preheater Temp °F	----	1200	1200
Pyrolysis Temp. °F	1200	1255	1255
Residence Time, Sec.	2.0	1.2	1.5
Char/Coal Ratio	0 (electric)	3.3	5 (Alumina)
Tar Yield (wt.%)MAF	18.0	9.7	14.1
Sp. Gravity, 60/60°F			
g/cc	1.218	1.191	-
Ultimate Analysis %Wt.			
C	81.47	80.00	76.81
H	6.32	6.68	6.75
N	1.14	1.48	1.12
S	0.55	0.43	0.38
O	10.52	11.40	14.94
Atomic H/C	0.93	1.00	1.05
VPO MW	285	--	--
Solubility Classification, Wt.%			
Pre-asphaltenes	25.6	17.1	--
Asphaltenes	33.0	24.6	--
Oil	41.4	58.3	--

TABLE 4
PROPERTIES OF TARS USING REACTIVE CARRIER GASES

BSR Run	176	177	178
Temperatures, °F char preheater	1500	1500	1500
Reactor	1191	1200	1200
Char/Coal Ratio	3	3	3.3
Carrier Gas	Steam (50%) CO (50%)	Steam (10%) CO ₂ (90%)	CO ₂
Residence Time, sec	1.9	1.94	2.0
Tar Yield, %MAF coal	15.2	19.2	18.3
Ultimate Analysis, % Wt			
C	80.78	81.22	80.15
H	6.25	6.48	6.34
N	1.47	1.43	1.58
S	0.66	0.56	0.61
O (by diff)	10.77	10.31	11.39
Ash	0.07	-	-
Atomic H/C	0.928	0.957	0.949
Sp. Gravity, 60/60°F			
g/cc	1.195	1.183	1.183
°API	-13.1	-11.9	-11.9
VPO MW	275	254	245
Solubility Classification, Wt%			
Preasphaltenes	16.9	16.3	17.4
Asphaltenes	28.6	28.4	27.2
Oil (by diff)	54.5	55.3	55.4

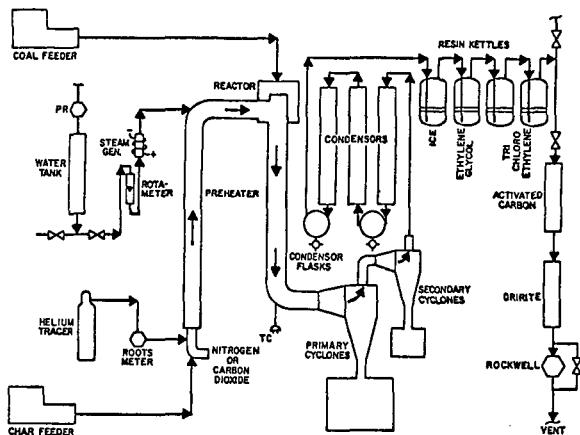


FIGURE 1 FLOW DIAGRAM OF 1 Kg-PER HOUR BENCH SCALE REACTOR

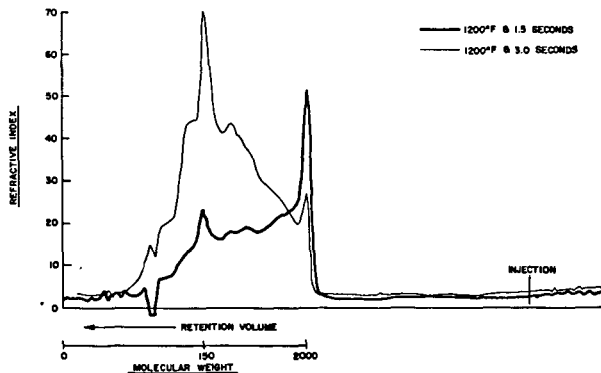
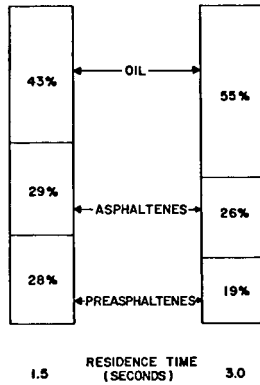


FIGURE 2 GEL PERMEATION CHROMATOGRAMS OF SUBBITUMINOUS COAL TARS PRODUCED AT 1200°F.



YIELDS, RELATIVELY TEMPERATURE INDEPENDENT, WERE AVERAGED FROM RUNS AT 1000-1200-1400°F

FIGURE 3 SOLUBILITY CLASSIFICATION OF SUBBITUMINOUS COAL TARS AS A FUNCTION OF RESIDENCE TIME.

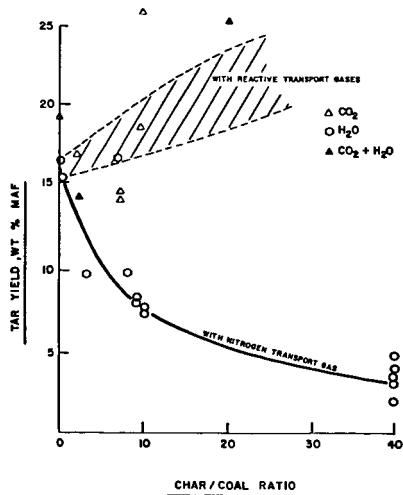


FIGURE 4 EFFECT OF RECYCLED CHAR ON TAR YIELD

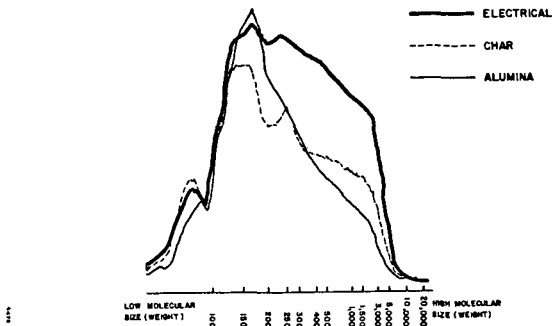


FIGURE 5 EFFECT OF SOLID HEAT CARRIER ON THE MOLECULAR SIZE DISTRIBUTION OF TARS.

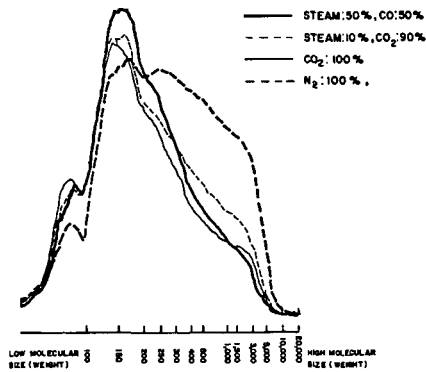


FIGURE 6 EFFECT OF CARRIER GASES ON THE MOLECULAR SIZE DISTRIBUTION OF TARS.

ISOTHERMAL FURNACE STUDIES OF THE KINETICS OF LIGNITE PYROLYSIS

A. W. Scaroni, P. L. Walker, Jr. and R. H. Essenhigh*

Fuels and Combustion Laboratory
The Pennsylvania State University, University Park, PA 16802

INTRODUCTION

In practical pulverized coal combustors and gasifiers, pyrolysis occurs in conjunction with rapid heating of the coal; heating rates in excess of 1,000°C/s being common. One apparent consequence of rapid heating is that crucial reactions occur in the first few seconds or even milliseconds (1-3). This is partially responsible for the stringent requirements associated with an acceptable experimental technique for studying the kinetics of rapid coal pyrolysis. The requirements include controlled rapid heating, isothermal reaction, variation of reaction time and rapid quenching. In essence, it is essential to have unambiguous reaction history.

Two of the techniques currently in use more or less satisfy the requirements. One employs essentially monolayer samples heated on an electrical grid (1), and the other utilizes a flow of coal particles injected into a preheated gas stream (2,3). The latter technique is used in this laboratory. The kinetics of pyrolysis are most conveniently studied using an inert atmosphere as the pyrolyzing medium. This has the effect of decoupling pyrolysis reactions from other heterogeneous gas/solid reactions that occur when a reactive atmosphere such as H₂ is used. Present data are for isothermal pyrolysis in N₂ of a lignite from the Darco Seam in Texas. Temperatures vary from 700 to 1,000°C and particle size fractions, from 60 x 80 to 270 to 400 mesh.

EXPERIMENTAL

Pyrolysis is performed in an entrained flow, isothermal furnace similar to that described by Nsakala and co-workers (3) which, in turn, is based on the design of Badzioch and Hawksley (4). It is, in essence, a vertical reactor heated electrically and for the injection of a dilute coal stream into the center of a preheated gas stream. The ensuing mixing heats the injected stream at a rate of about 10,000°C/s. The injector is designed to minimize migration and adherence of coal particles to the furnace tube wall. A water-cooled sampling probe, which is inserted up the axis of the furnace, collects and rapidly quenches the particle stream. The reactor tube is heated uniformly so that pyrolysis is essentially contained in an isothermal region. Variable positioning of the sampling probe adjusts the reaction time. A schematic of the equipment is shown in Figure 1 and the operating conditions are given in Table 1.

Weight loss due to pyrolysis is determined using proximate ash as a tracer. Data are corrected for the error associated with this technique. For the Darco lignite the error is less than 10% and is thought to result from the loss of sulfur during pyrolysis (5). The proximate analysis of the lignite is given in Table 2. Particle size fractions are separated by dry sieving and characterized by the Rosin-Rammler technique (6).

*Present Address: Department of Mechanical Engineering, The Ohio State University, Columbus, OH 43210

TABLE 1. OPERATING CONDITIONS

	<u>Gas and Wall Temperature, °C</u>			
	<u>700</u>	<u>800</u>	<u>900</u>	<u>1,000</u>
Coal Feed Rate, g/min	1.0	1.0	1.0	1.0
Mean Gas Velocity, m/s	1.12	1.12	1.12	1.12
Secondary/Primary N ₂	16.7	15.0	13.7	12.5
Coal Loading, wt%	2.2	2.5	2.7	2.9
Gas Reynolds Number	458	391	339	298

TABLE 2. PROXIMATE ANALYSIS OF THE DARCO LIGNITE

	<u>as-received</u>	<u>dry</u>	<u>daf</u>
Moisture, %	22.4	-	-
Ash, %	12.4	15.9	-
Volatile Matter, %	33.3	43.0	50.2
Fixed Carbon, %	31.9	41.1	49.8

Equilibrium Moisture = 39.8%

RESULTS

A typical weight loss versus time curve is shown in Figure 2 for isothermal pyrolysis at 900°C. Weight loss, hence pyrolysis rate, is independent of particle size over the range 60 x 80 to 270 x 400 mesh. The corresponding range in mean particle size is 40 to 200 μm. Similar curves are obtained at 700, 800 and 1,000°C.

The maximum potential weight loss in the isothermal furnace is not measurable by a single pass because of the restricted residence time. It is calculated by the method of Badzioch and Hawksley (4). This involves establishing a relationship between the change in proximate volatile matter between the original dry-ash-free coal and char and weight loss due to pyrolysis. The derived relationship is linear; it is essentially particle size (Figure 3) and temperature independent (Figure 4) for the range of operating conditions. The maximum weight loss is 66% of the daf coal, representing a fractional increase of 1.3 over the proximate volatile matter. The weight loss achieved by a single pass in the isothermal furnace at 1,000°C and a total residence time of 0.4 s is 50% of the daf coal, indicating about 80% completion of pyrolysis.

A first-order plot for pyrolysis at 900°C is shown in Figure 5. A feature of the curve is the apparent delay in the onset of pyrolysis during heat-up of the particles. This is in agreement with the findings of Jüntgen and Van Heek (7). Correlating first-order rate constants by the Arrhenius expression (Figure 6) yields a pseudo activation energy of 7.7 kcal/mole and a pre-exponential factor of 92 s⁻¹.

DISCUSSION

Successful description of the kinetics of pyrolysis up to 80% completion by a single first-order reaction equation is not inconsistent with the need for a second equation to describe the completion of pyrolysis as postulated by Nsakala and co-workers (3). This derives from the fact that the second component devolatilization is associated mainly with H₂ liberation (8), which on a weight basis accounts for only about 5% of the daf coal.

The relatively low pseudo activation energy is consistent with the data presented by Anthony and Howard (9). The absence of particle size effects on the rate of pyrolysis for the Darco lignite essentially implies the absence of significant heat and mass transfer effects. Since low activation energies are usually associated with these physical factors, an alternative explanation is required here. Howard and co-workers (1,9) provide a probable explanation in terms of a distribution of activation energies for the generation of different volatile species. They obtain an activation energy of about 10 kcal/mole in a single-step correlation and about 50 kcal/mole in a multistep model.

SUMMARY

The present work further demonstrates the suitability of the entrained flow isothermal furnace for studying the kinetics of lignite pyrolysis. Under rapid heating conditions there is a delay in the onset on significant pyrolysis during particle heat-up. For the Darco lignite, pyrolysis up to 80% completion follows a single first-order reaction equation; but a second equation may be necessary to describe the completion of pyrolysis. The relatively low activation energy of less than 10 kcal/mole and the absence of significant particle size effects are not necessarily inconsistent, as the former may not necessarily indicate physical rate control.

ACKNOWLEDGEMENTS

This research was supported by DOE on Contract EX-76-C-01-2030.

REFERENCES

1. Anthony, D. B., Howard, J. B., Hottel, H. C., and Meissner, H. P., Fifteenth Symposium (International) on Combustion, The Combustion Institute, Pittsburgh, Pa., 1974.
2. Kobayashi, H., Howard, J. B. and Sarofin, A. F., Sixteenth Symposium (International) on Combustion, The Combustion Institute, Pittsburgh, Pa., 1976.
3. Nsakala, N., Essenhigh, R. H. and Walker, P. L., Jr., Comb. Sci. and Tech., 16, 153, 1977.
4. Badzioch, S. and Hawksley, P. G. W., Ind. Eng. Chem. Process Des. Develop., 9, 521, 1970.
5. Scaroni, A. W., M.S. Thesis, Pennsylvania State University, 1979.
6. Rosin, P. and Rammler, E., J. Inst. Fuel, 7, 29, 1933.
7. Jüntgen, H. and Van Heek, K. H., Fuel, 47, 103, 1968.
8. Essenhigh, R. H. and Howard, J. B., "Combustion Phenomena in Coal Dusts and the Two Component Hypothesis of Coal Constitution," The Pennsylvania State University Studies No. 131, 1965.
9. Anthony, D. B. and Howard, J. B., A.I.Ch.E. Journal, 22, 625, 1976.

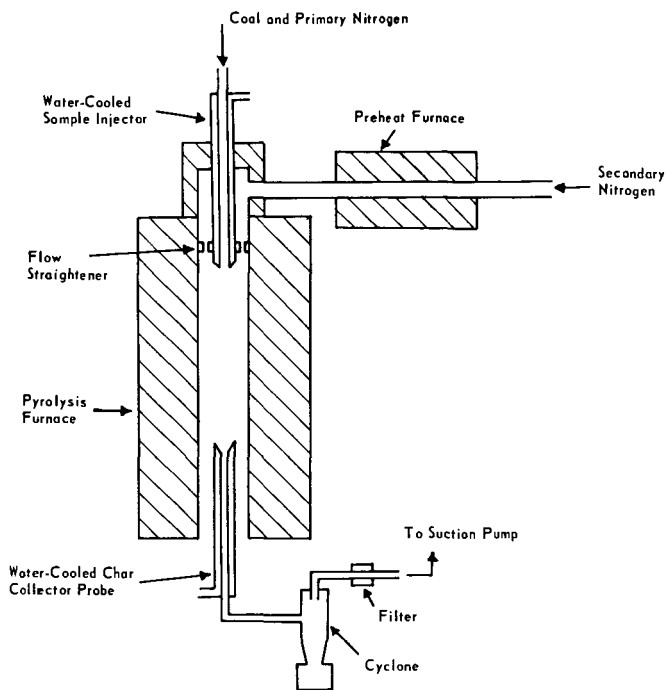


Figure 1. SCHEMATIC OF EQUIPMENT

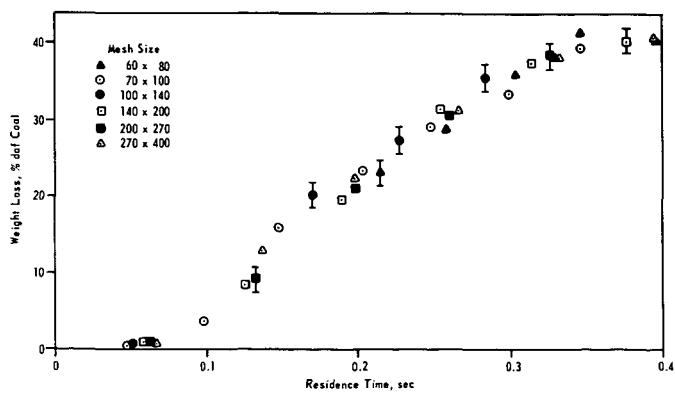


Figure 2. WEIGHT LOSS AS A FUNCTION OF RESIDENCE TIME OF LIGNITE IN REACTOR AT 900°C

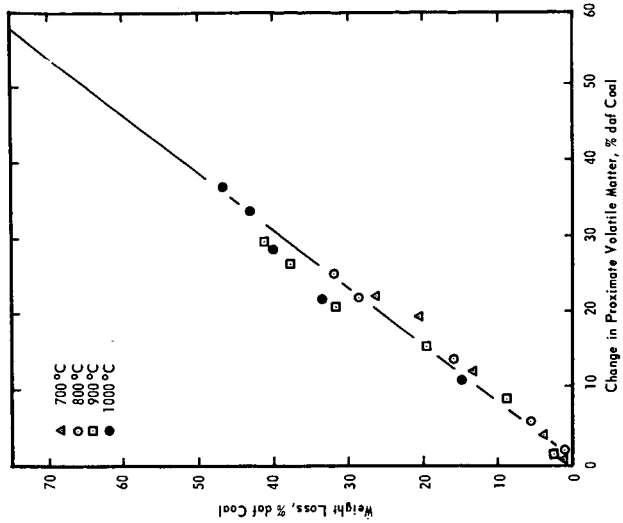


Figure 4. VARIATION OF WEIGHT LOSS IN ISOTHERMAL FURNACE WITH CHANGE IN PROXIMATE VOLATILE MATTER BETWEEN COAL AND CHAR FOR 140 x 200 MESH SIZE FRACTION

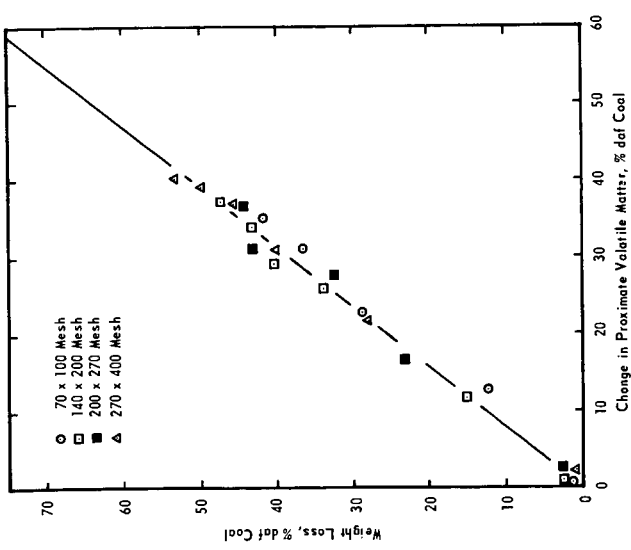


Figure 3. VARIATION OF WEIGHT LOSS IN ISOTHERMAL FURNACE AT 1,000°C WITH CHANGE IN PROXIMATE VOLATILE MATTER BETWEEN COAL AND CHAR

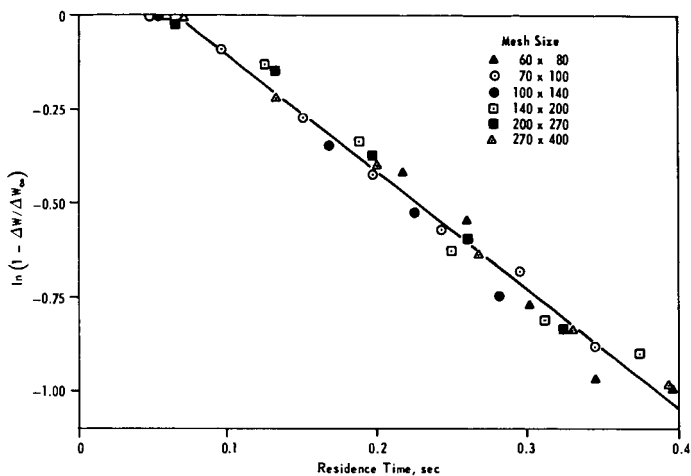


Figure 5. FIRST ORDER PLOT FOR DEVOLATILIZATION WEIGHT LOSS FOR LIGNITE AT 900°C

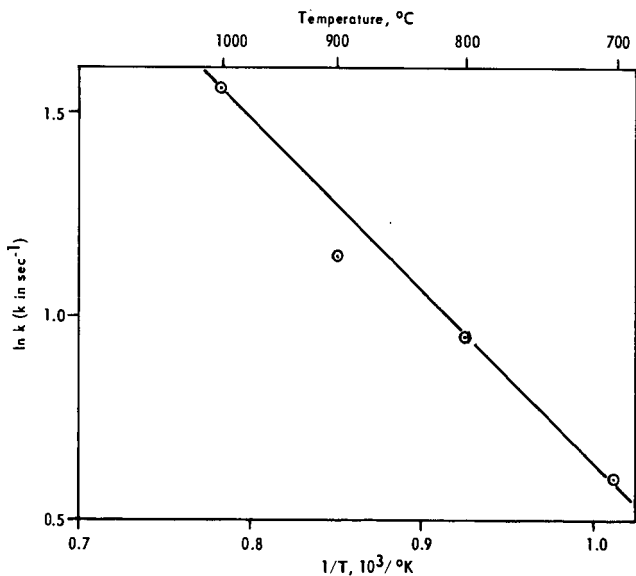


Figure 6. ARRHENIUS PLOT FOR LIGNITE DEVOLATILIZATION TREATED AS ONE STEP, FIRST-ORDER REACTION

RATES OF LIGHT GAS PRODUCTION BY DEVOLATILIZATION OF COALS AND LIGNITE

R. F. Weimer and D. Y. Ngan

Air Products and Chemicals, Inc.; Allentown, Pennsylvania, 18105

INTRODUCTION

The kinetics of coal pyrolysis are important in many coal conversion processes which operate under conditions of relatively moderate temperatures (400° to 1000°C). Such processes range from in situ coal gasification (1) to flash hydropyrolysis (3), having anticipated coal residence times in the region of pyrolysis temperatures of between 10^{-1} and 10^4 seconds - a range of five orders of magnitude.

Although many models have been postulated for coal devolatilization (4), Howard and his co-workers (2,4) have shown that the use of a statistical distribution of activation energies can provide "valuable insight into the overall or global kinetics of the [pyrolysis] process," particularly with regard to explaining the effects of heating rate. They therefore state (4) that, "For a designer seeking a correlation of devolatilization yields, [the distributed activation energy model] combined with a description of secondary reactions is presently the best recommendation." Ciuryla et al. (6) have since shown that the parameters (mean activation energy, standard deviation of the energy distribution, and total potential volatilization) obtained by fitting total weight loss data obtained at heating rates of 40 and 160°C/min, for a Montana lignite and a Pittsburgh Seam bituminous coal, are close to the values reported by Anthony and Howard for the same coals at heating rates of 100 to 10,000°C/sec.

The distributed activation energy model has not previously been applied to data for the yields of individual molecular species from coal pyrolysis. It has normally been assumed (with good results for data obtained over a narrow range of heating rates) that the yields of individual species can be modelled by a small set of individual reactions representing the major mechanisms for their production. However, it has been recognized (2) that the parameters obtained from such models are only "effective" values which may have no fundamental significance. It can be shown (see below) that the values typically obtained from models having a small number of individual reactions cannot be applied over a wide range of heating rates.

EXPERIMENTAL

Coal Samples

The North Dakota lignite and Illinois No. 6 bituminous coal samples used in this study were provided by the Pennsylvania State University. The Pittsburgh Seam bituminous and Wyodak subbituminous coal samples were obtained from Commercial Testing and Engineering Company; these samples were ground under inert atmosphere. Proximate and ultimate analyses of the coals studied are given in Table 1. Sized, 40 x 80 mesh, samples were used in all runs.

Apparatus

The primary apparatus used in obtaining the results reported herein was a 6-gram-capacity thermobalance built specifically for Air Products' laboratories by Spectrum Products, Inc. This apparatus is essentially identical to equipment which was previously in existence at Case-Western Reserve University (5). The apparatus consists of a cylindrical basket, containing the coal sample, which is suspended from a balance arm into an externally heated Haynes 25 superalloy tube. Although the apparatus is capable of operation at pressures up to 1500 psi, only results obtained at atmospheric pressure, in helium, are reported here. Heating rates were monitored by thermocouples

on the tube wall, and also inside the tube near the basket, it having been determined (by placing a thermocouple in the basket itself) that the differences between the sample temperature and the wall temperature were small.

Experimental Procedure

Approximately 3 gms of dry, 40 x 80 mesh, coal were placed inside the sample basket and lowered into the reactor at room temperature. After purging the system with helium, the reactor was heated. The temperature, monitored by a thermocouple located immediately below the sample basket, the helium flow rate, and the sample weight were continuously recorded. Gas samples were periodically collected by syringes through a septum in the heated exit line. These samples were subsequently analyzed using a Perkin-Elmer Sigma-1 gas chromatograph.

The helium flow rate was maintained at approximately 700 cc/min. Due to the heat capacity of the tube and furnace, and to heat losses from the furnace, the heating rate was not constant during the experiments; however, the observed rates can be approximated by the formula

$$\frac{dT}{dt} = 10.8 - 0.00642 \cdot T$$

where T = sample temperature, °C, and t = time, minutes. The actual recorded time/temperature data were used in the computer analysis of the results.

Kinetic Model

Coal pyrolysis has frequently been assumed to be described by a set of parallel first-order reactions (1,2,4). For each reaction, i, the corresponding devolatilization rate is

$$\frac{dV_i}{dt} = k_i e^{-\frac{E_i}{RT}} (V_i^* - V_i) \quad 1)$$

where k_i is the preexponential factor and E_i is the activation energy of reaction i; V_i is the amount of volatile product produced by reaction i up to time t; V_i^* is the amount of product which could potentially be produced; T is the absolute temperature, and R is the gas constant. The total yield from reaction i at time t is therefore

$$\frac{V_i^* - V_i}{V_i^*} = \exp \left\{ -k_i \int_0^t e^{-\frac{E_i}{RT}} dt \right\} \quad 2)$$

For the case of constant heating rate, $m = dT/dt$, it has been shown (2) that, since $E_i/RT \gg 1$ for coal pyrolysis reactions, the solution of Equation 2 is

$$\frac{V_i^* - V_i}{V_i^*} = \exp \left\{ -\frac{k_i RT^2}{mE_i} e^{-\frac{E_i}{RT}} \right\} \quad 3)$$

(This equation may be extended to include a holding period at pyrolysis temperature and/or the subsequent cool-down period, as shown in the Appendix.)

Integration of Equation 2 for the case of nonconstant heating rate may easily be done numerically; however, provided that

$$\frac{RT}{E_i} \cdot \frac{T}{m} \cdot \frac{dm}{dT} \ll 1$$

Equation 3 with $m = m(T)$ can be used.

The distributed activation energy model assumes that the activation energy for producing volatile material (or a specific volatile product) is normally distributed about a mean value, E_{i0} , with k_i constant. The result, analogous to Equation 3, is

$$\frac{V_i^* - V_i}{V_i^*} = \frac{1}{\sigma\sqrt{2\pi}} \int_0^{\infty} \exp \left[-\frac{k_i RT^2}{mE} e^{-\frac{E}{RT}} \right] \exp \left[-\frac{(E-E_{i0})^2}{2\sigma^2} \right] dE \quad 4)$$

where σ is the standard deviation of the energy distribution. (In practice, integration from $E = 1$ kcal/mol to $E = E_{i0} + 4\sigma$ is adequate for analyzing the data.)

The rate of devolatilization at temperature T is

$$\frac{1}{V_i^*} \frac{dV_i}{dt} = \frac{k_i}{\sigma\sqrt{2\pi}} \int_0^{\infty} e^{-\frac{E}{RT}} \exp \left[-\frac{k_i RT^2}{mE} e^{-\frac{E}{RT}} \right] \exp \left[-\frac{(E-E_{i0})^2}{2\sigma^2} \right] dE \quad 5)$$

RESULTS AND DISCUSSION

Figures 1 through 5 present the pyrolysis rate data, for each of the five coals, for the four major noncondensable products of pyrolysis (hydrogen, carbon monoxide, carbon dioxide, and methane). The total weight loss is also shown. The initial appearance of these species occurs in the same order for all of the coals: CO_2 appears first, followed by CO , CH_4 , and, finally, H_2 . However, the maximum rate of CO production does not occur until well after that of methane; the temperature of the maximum rate of CO production is nearly coincident with that of the maximum rate of hydrogen production (about $700^\circ C$). (The CO production rate is actually bimodal, with a small peak at about $450^\circ C$ and a larger peak at about $700^\circ C$, for the low-rank coals.) The observed peaks for C_2 and C_3 hydrocarbons (not shown) occur at the same temperature as those for methane. The major differences among the coals are in the amounts of CO and CO_2 produced, which are, of course, related to the vastly differing oxygen contents of the feed coals.

These results are similar to data reported by Campbell (1) for the slow ($3.3^\circ C/min$) pyrolysis of 50-gram samples of 6 x 12 mesh Wyodak coal, although his total yields of light hydrocarbons were greater than those reported here.

The values found by fitting the Gaussian distributed activation energy model to the data are listed on Table 2. Except for the CO data, which are clearly bimodal, the single Gaussian distribution provides a reasonable first approximation of the data. Except for the Pittsburgh Seam bituminous coal (which yielded very little CO and CO_2), the mean activation energies increase in the order CO_2 , CO (first peak), CH_4 , CO (second peak), and H_2 . The surprising result is the close correspondence of the values obtained for both E_0 and σ for each component from coals of widely differing rank. This suggests that the major mechanisms for the production of these materials are the same for all of the coals.

Table 3 lists, for comparative purposes, the parameters obtained by Campbell by fitting his data to one to three first-order reactions per compound. Since σ is zero in this model, it is necessary to allow k_j for each reaction to vary. The result is a set of extremely low values for both k_j and E_j for all of the reactions. For example, Campbell's value of E_j for hydrogen production is 19.5 kcal/g mole, compared to the E_0 's of 73 to 75 kcal/mol in Table 2, and a typical value (1) of 88 kcal/mol for C-H bond breakage. The small absolute values of k_j and E_j in Campbell's model result from fitting a yield distribution which is spread broadly over temperature with a small number of reactions.

The effect of temperature on flash pyrolysis yields has been studied by Suuberg *et al.* (2) for a Montana lignite. Suuberg's results (Figures 6 and 7), which are total yield data for heating small (15 mg) samples at 1000°C/sec to the indicated peak temperature, and then cooling immediately at a rate of 200°C/sec, show the same trends in the order of the appearance of the various species as do the slow pyrolysis data; in addition, Suuberg's ultimate yields of each of the light gases are similar to those observed upon slow pyrolysis of lignite and subbituminous coal in our experiments.

Suuberg also fit his results using a small number of first-order reactions to describe the yields of each species; his parameters are shown in Table 4. Reasonable values of E_0 were obtained, but the predicted yield curves, as shown on Figures 6 and 7, are notably stepwise in appearance. Also plotted on Figures 6 and 7 are the curves obtained by using the lignite pyrolysis parameters of Table 2, and the distributed activation energy model, to predict the flash pyrolysis yields. The predictions fit the data almost as well as Suuberg's own model, provided only that V_j^* for each species is allowed to vary. This illustrates the ability of the distributed activation energy model to fit both slow and fast pyrolysis data with the same values for the activation energy parameters. In contrast, the slow pyrolysis parameters reported by Campbell would predict almost no reaction under Suuberg's conditions, since his values of k_j are too small to permit any significant reaction in a time of the order of one second.

Finally, the problem inherent in applying Suuberg's model and parameters to slow pyrolysis rate data is illustrated - for the case of CO₂ formation from lignite - by Figure 8. The use of a small number of individual equations requires that the products appear in a few sharply defined peaks (corresponding to the steep steps in the yield curves) in contrast to the broadly distributed slow pyrolysis data.

CONCLUSIONS

A first-order model with distributed activation energies has the potential for explaining the effect of heating rate on the primary production of light gases (H₂, CO, CO₂, CH₄) during the devolatilization of coal; models based on small sets of first-order reactions with nondistributed activation energies do not have this potential. The activation energy distributions for the production of these species obtained from atmospheric-pressure pyrolysis, under inert atmosphere, are remarkably insensitive to coal rank. Data on identical samples of coal, over a wide range of heating rates, would be needed to confirm the validity of this approach to understanding pyrolysis kinetics.

ACKNOWLEDGEMENTS

Dr. K. J. Anselmo of the Management Information Department of Air Products and Chemicals, Inc., is acknowledged for his assistance in developing the computer curve-fits of the data. Mr. S. A. Motika of the Corporate Research and Development Department of Air Products and Chemicals, Inc., is acknowledged for his work in the preparation of coal samples and the operation of the apparatus used in this research.

APPENDIX

Extension of Model Beyond Heating Period

The time-temperature history of much of the published data on coal pyrolysis may be divided into three regions:

1. Heat-up at a constant rate, m_1 , to a peak temperature, T_1 .
2. Holding at temperature, T_1 , for a time, t_H .
3. Cooling at a constant rate, m_3 (often slower than the heating rate), until the reactions are quenched.

Under these conditions, the basic first-order rate equation for a single reaction,

$$\frac{dV_i}{dt} = k (V_i^* - V_i) e^{-\frac{E}{RT}}$$

may be integrated, subject to the approximation $E/RT \approx 1$, to yield

$$\frac{V_i^* - V_i}{V_i^*} = \exp \left\{ -k \left[\frac{RT_1^2}{E} \left(\frac{1}{m_1} + \frac{1}{m_3} \right) + t_H \right] e^{-\frac{E}{RT}} \right\}$$

where V_i is now the total yield from the reaction.

For the distributed activation energy model, the corresponding equation is

$$\frac{V_i^* - V_i}{V_i^*} = \frac{1}{\sigma \sqrt{2\pi}} \int_0^{\infty} \exp \left\{ -k_0 \left[\frac{RT_1^2}{E} \left(\frac{1}{m_1} + \frac{1}{m_3} \right) + t_H \right] e^{-\frac{E}{RT}} \right\} \cdot \exp \left\{ -\frac{(E-E_0)^2}{2\sigma^2} \right\} dE$$

This latter equation may be applied to the yield of any individual component, provided that the yield can be approximated by the assumed Gaussian distributions.

In the event that a more complex time-temperature history is followed (e.g., if m_1 and m_3 are not constants), then recourse may always be had to numerical methods for calculating the final integrated yield from the model.

REFERENCES

1. J. H. Campbell, "Pyrolysis of Subbituminous Coal in Relation to In Situ Coal Gasification," Fuel 57, 232 (1978).
2. E. M. Suuberg et al., "Product Composition and Kinetics of Lignite Pyrolysis," ACS National Meeting, New Orleans, March 1977.
3. W. B. Russell et al., "The Cities Service Model for Short Residence Time Hydro-pyrolysis of Coal," presented at 70th Annual AIChE Meeting, New York City, 14 November 1977.
4. D. B. Anthony and J. B. Howard, "Coal Devolatilization and Hydrogasification," AIChE Journal 22 (4), 625 (1976).
5. N. Gardner et al., "Catalyzed Hydrogasification of Coal Chars," Advances in Chemistry Series, No. 131, p. 217 (1974).
6. V. T. Ciuryla et al., "Ambient-Pressure Thermogravimetric Characterization of Four Different Coals and Their Chars," Fuel, to be published.

TABLE 1

ANALYSIS OF COALS

<u>ASTM Rank</u>	<u>State</u>	<u>Ultimate Analysis (% Dry)</u>					
		<u>C</u>	<u>H</u>	<u>N</u>	<u>S</u>	<u>Ash</u>	<u>O</u> (By Difference)
Lignite	ND	61.6	4.1	1.1	0.6	10.0	22.6
Lignite	TX	64.5	4.2	1.4	0.9	10.0	19.0
Subbituminous	WY	66.4	4.6	1.0	0.8	6.0	21.2
HVC Bituminous	IL	66.4	4.6	1.1	4.5	10.6	12.8
HVA Bituminous	PA	80.5	5.0	1.2	1.1	5.0	7.2

TABLE 2
KINETIC PARAMETERS

Component	Parameter ⁺	Coals				
		North Dakota Lignite	Texas Lignite	Wyodak	Illinois No. 6	Pittsburgh
H ₂	E ₀ , kcal/mol	72.8	76.9	73.1	73.7	74.6
	σ, kcal/mol	8.8	9.8	8.0	8.6	8.2
	v*	0.010	0.009	0.009	0.010	0.011
CO (1st Peak)	E ₀ , kcal/mol	51.9	52.2	50.8	--	--
	σ, kcal/mol	7.8	6.8	6.0	--	--
	v*	0.025	0.018	0.022	--	--
CO (2nd Peak)	E ₀ , kcal/mol	70.3	72.7	71.2	66.7	71.1
	σ, kcal/mol	6.5	5.1	7.5	13.4	11.6
	v*	0.043	0.036	0.053	0.038	0.021
CO ₂	E ₀ , kcal/mol	48.9	53.0	50.3	55.6	61.8
	σ, kcal/mol	9.5	11.4	9.6	14.2	18.1
	v*	0.134	0.123	0.100	0.040	0.015
CH ₄	E ₀ , kcal/mol	57.7	60.1	58.2	58.8	58.7
	σ, kcal/mol	6.0	7.0	5.9	5.8	4.8
	v*	0.016	0.021	0.021	0.022	0.030
Total Weight Loss	E ₀ , kcal/mol	52.7	52.5	53.2	53.0	51.8
	σ, kcal/mol	11.3	10.0	9.7	9.3	5.7
	v*	0.40	0.40	0.41	0.34	0.30

⁺k₀ is fixed at 10¹⁵ min⁻¹ in all cases.

TABLE 3
CAMPBELL'S PARAMETERS FOR WYODAK COAL

<u>Component</u>	<u>E₀, kcal/mol</u>	<u>k₀, min⁻¹</u>	<u>V[*], g/g coal</u>
H ₂	22.3	1200	0.0102
CO, Reaction 1	18.0	3300	0.016
Reaction 2	30.1	1.5 x 10 ⁵	0.037
CO ₂ , Reaction 1	19.5	3.3 x 10 ⁴	0.055
Reaction 2	23.0	1.4 x 10 ⁴	0.047
CH ₄ , Reaction 1	31.1	1.0 x 10 ⁷	0.014
Reaction 2	31.1	1.7 x 10 ⁶	0.016
Reaction 3	35.4	1.8 x 10 ⁶	0.014

TABLE 4
SUUBERG'S PARAMETERS FOR NORTH DAKOTA LIGNITE

<u>Component</u>	<u>E₀, kcal/mol</u>	<u>k₀, min⁻¹</u>	<u>V[*], g/g coal</u>
H ₂	88.8	9.5 x 10 ¹⁹	0.0050
CO, Reaction 1	44.4	1.1 x 10 ¹⁴	0.0177
Reaction 2	59.5	1.6 x 10 ¹⁴	0.0535
Reaction 3	58.4	3.5 x 10 ¹¹	0.0226
CO ₂ , Reaction 1	36.2	1.3 x 10 ¹³	0.0570
Reaction 2	64.3	3.5 x 10 ¹⁵	0.0270
Reaction 3	42.0	3.3 x 10 ⁸	0.0109
CH ₄ , Reaction 1	51.6	9.7 x 10 ¹⁵	0.0034
Reaction 2	69.4	2.8 x 10 ¹⁶	0.0092

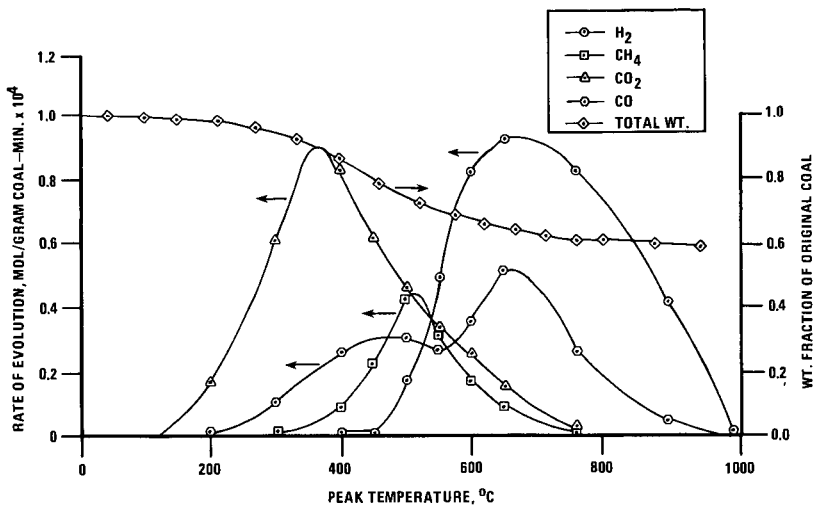


FIGURE 1.
PYROLYSIS YIELDS FROM A NORTH DAKOTA LIGNITE

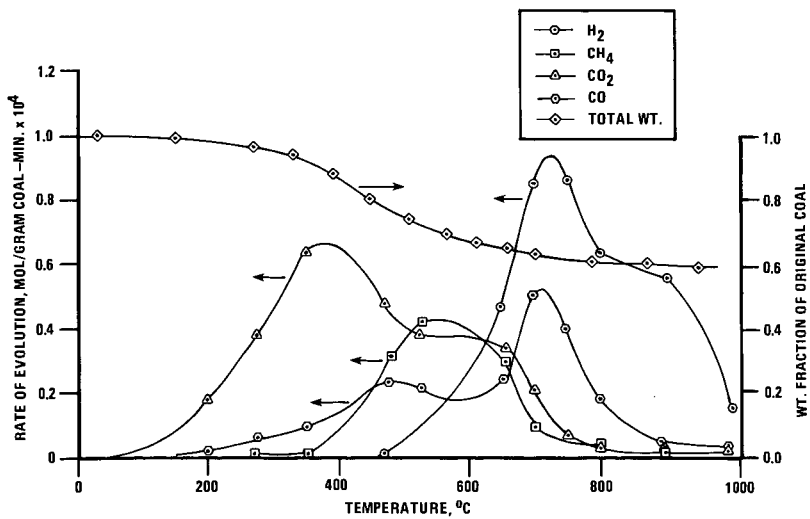


FIGURE 2.
PYROLYSIS YIELDS FROM A TEXAS LIGNITE

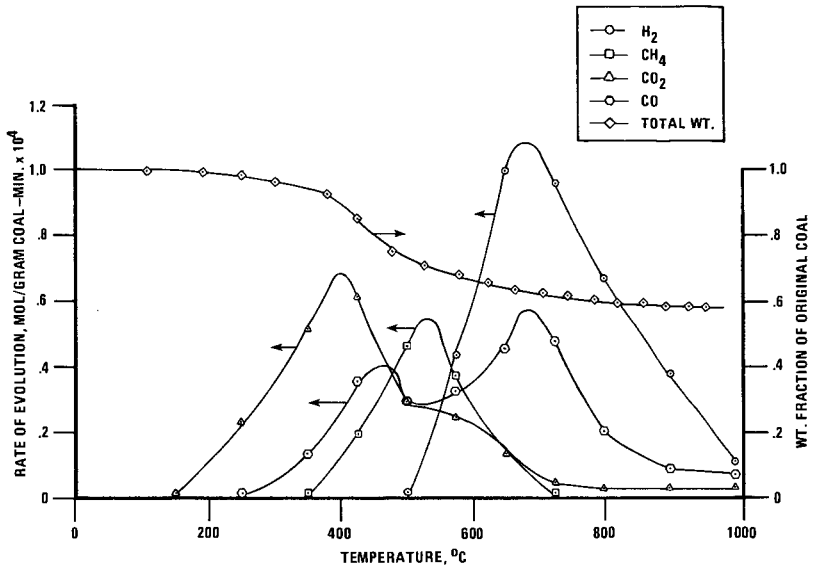


FIGURE 3.
PYROLYSIS YIELDS FROM A WYODAK COAL

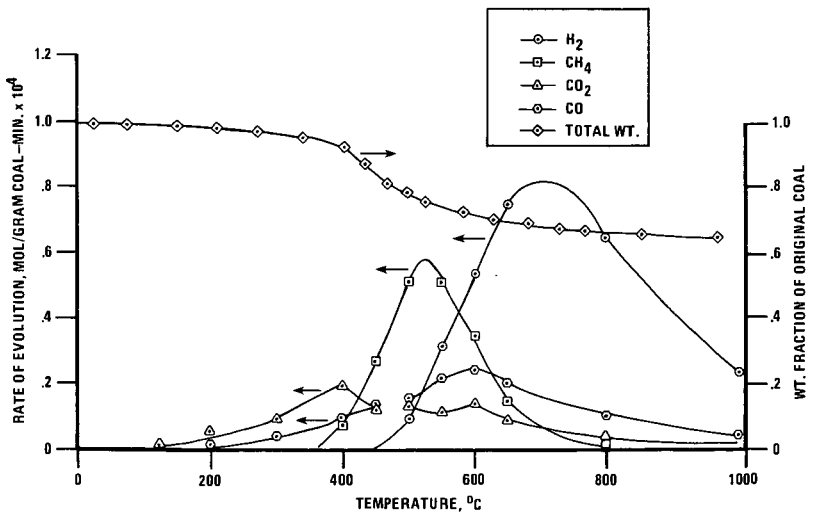


FIGURE 4.
PYROLYSIS YIELDS FROM AN ILLINOIS NO. 6 COAL

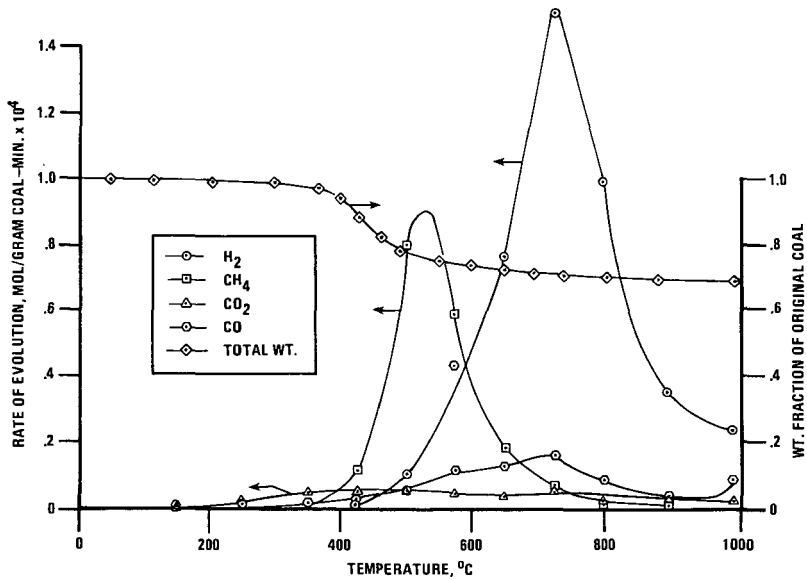


FIGURE 5.
PYROLYSIS YIELDS FROM A PITTSBURGH SEAM COAL

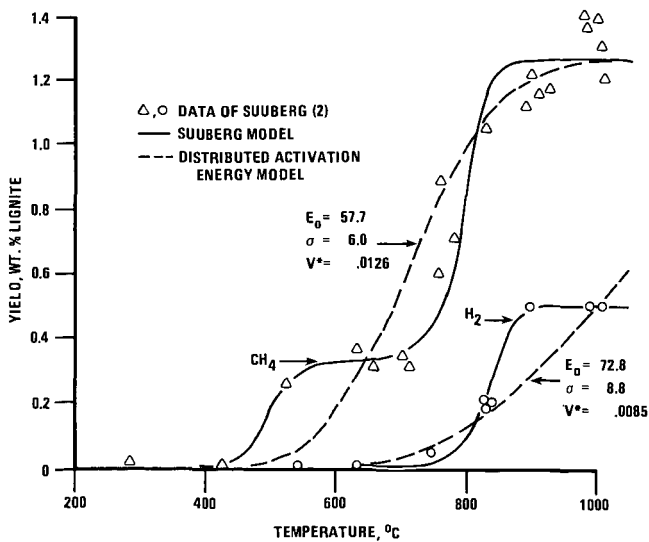


FIGURE 6.
YIELDS OF METHANE AND HYDROGEN VIA FLASH
PYROLYSIS OF MONTANA LIGNITE

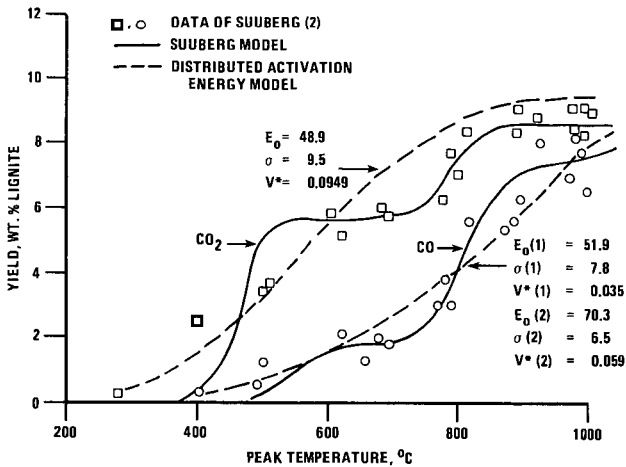


FIGURE 7.
 YIELDS OF CO AND CO₂
 VIA FLASH PYROLYSIS OF MONTANA LIGNITE

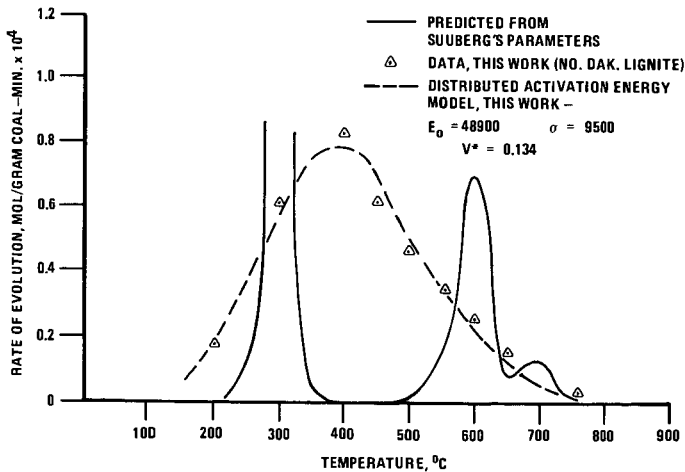


FIGURE 8.
 CO₂ PRODUCTION RATE
 VIA SLOW PYROLYSIS OF LIGNITES

A MODEL FOR COAL PYROLYSIS

by

L. H. Chen and C. Y. Wen
Department of Chemical Engineering
West Virginia University
Morgantown, WV 26506

INTRODUCTION

Pyrolysis of coal occurs in all coal conversion processes and is perhaps the most difficult to model mathematically. A number of models on coal pyrolysis have been proposed during the past several decades. However, very few of these models address the simultaneous changes in product distribution and particle weight loss (or conversion) over a wide range of operating conditions. Such a mathematical model which could take into consideration the effects of residence time, final temperature, heating rate and pressure is needed for design and scale-up of coal pyrolysis and gasification reactors. The purpose of this study is to develop such a mathematical model for simulation of the pyrolysis phenomena of a coal particle. The model to be developed should be general enough to be applicable to other pyrolysis system such as the pyrolysis of wood.

MODEL DEVELOPMENT

The assumptions used to formulate the single particle model are as follows:

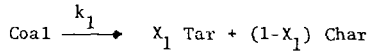
- (a) pseudo-steady state concentration profiles
- (b) negligible increase in internal pressure
- (c) equal binary diffusivities

This model combines the chemical reactions and the transport processes occurring during pyrolysis.

1. Chemical Reactions:

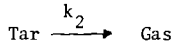
Three chemical reactions are assumed to simultaneously occur within a coal particle which is undergoing pyrolysis in an inert atmosphere. These are devolatilization, cracking and deposition. For convenience, the products of pyrolysis are categorized as char, tar and gas. Char is defined as the undistillable material which remains in the form of a solid. Tar is defined as the distillable liquid which has a molecular weight larger than C_6 . Gas is defined as those components lighter than C_6 , i.e., CO , CH_4 , CO_2 , C_2H_6 , H_2O , etc. Both tar and gas occur in the form of vapor when coal is pyrolyzed. A similar treatment was applied to the catalytic cracking of petroleum⁽¹¹⁾. During pyrolysis all of the chemical reactions are assumed to be first order with respect to the concentration of reactants and rate constants are expressed in Arrhenius form. The chemical reactions and the rate expressions for the pyrolysis of a coal particle are formulated as follows:

A. Devolatilization



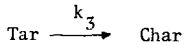
$$\text{Rate} = k_{10} \cdot \exp(-E_1/\overline{RT}) C_{\text{coal}}$$

B. Cracking



$$\text{Rate} = k_{20} \cdot \exp(-E_2/\overline{RT}) C_{\text{tar}}$$

C. Deposition



$$\text{Rate} = k_{30} \cdot \exp(-E_3/\overline{RT}) C_{\text{tar}}$$

The net production rates of tar, gas and inert gas can be obtained as:

$$R_{\text{tar}} = X_1 k_1 C_{\text{coal}} - (k_2 + k_3) C_{\text{tar}} \quad (1)$$

$$R_{\text{gas}} = k_2 C_{\text{tar}}$$

and $R_{\text{inert gas}} = 0$

While the solid concentrations, C_i , and the net production rates of coal and char can be obtained as:

$$\frac{dC_i}{dt} = R_i \quad (2)$$

where

i is the coal or char

and

$$R_{\text{coal}} = -k_1 C_{\text{coal}}$$

$$R_{\text{char}} = (1-X_1)k_1 C_{\text{coal}} + \frac{1}{\left(\frac{4}{3} \pi R^3\right)} \int_0^R k_3 C_{\text{tar}} 4\pi r^2 dr$$

2. Transport Processes:

Both mass and heat transfer affect the pyrolysis of a single coal particle. This is particularly significant for large particles.

2-1. Mass transfer

A. Gas phase

The coal particle can be considered as a porous sphere which retains its integrity as the pyrolysis reaction proceeds. The conservation equation for the gaseous species, i , tar, gas or inert gas, inside the particle having a mass concentration, C_i , can be formulated as⁽⁸⁾:

$$\frac{1}{r^2} \frac{\partial}{\partial r} (r^2 N_i) = R_i \quad (3)$$

where R_i is the rate of generation of the species i due to the chemical reactions.

N_i is the mass flux of the species i and can be expressed as the sum of the diffusion flux in the radial direction and the bulk flow through the pores. Thus

$$N_i = - D_{\text{eff},i} \frac{\partial C_i}{\partial r} + \bar{W}_i \sum_j N_j \quad (4)$$

\bar{W}_i , the weight fraction of the species i in the gas phase, can be expressed as:

$$\bar{W}_i = C_i / \sum_j C_j \quad (5)$$

B. Gas film

The conservation equation for the gaseous species, i (tar, gas or inert gas) across the gas film can be written as:

$$N_i \Big|_R = k_{gi} [C_{i,s} - C_{i,b}] \quad (6)$$

where,

$C_{i,s}$ and $C_{i,b}$ are the concentrations of species i at the particle surface and at the bulk gas stream outside, respectively.

k_{gi} is the mass transfer coefficient across the gas film and can be estimated from an appropriate mass transfer correlation.

2-2. Heat transfer

The energy balance equation for the particle is derived by taking into account convective, radiative and conductive heat transfer with the heating devices and the heat of reaction of the pyrolysis process. The temperature gradient which occurs inside of the particle due to the conduction is negligible for small particles and is neglected. (For a 1000 μm particle, the maximum temperature gradient is 20 °C at 0.5 sec and less than 5 °C at 1 sec. This is the case, if the particle at room temperature is dropped into a pyrolyzer maintained at 1000 °C. The heating rate of the particle is 1000 °C/sec which is in the range usually encountered in pyrolyzers or gasifiers). Accordingly,

$$C_{ps} \cdot \rho_s \cdot \frac{dT}{dt} = \frac{3}{R} h_c (T_w - T) + \frac{3\sigma Fe}{R} (T_w^4 - T^4) + \frac{3 k a}{R^2} (T_w - T) + \sum_i (-\Delta H_i) R_i \quad (7)$$

where, a represents the fraction of the surface area of the particle that comes in contact with the heating elements. T_w , is the temperature of the heating elements and can be characterized by the following equation:

$$C_{pw} \cdot \rho_w \cdot \frac{dT_w}{dt} = h_{ov}' (T_f - T_w) \quad (8)$$

Since the heating rate of a heating device is specified in the experimental work the wire temperature, T_w , can be obtained by substituting a relative overall heat transfer coefficient, h_{ov}' , into Equation 8.

DETERMINATION OF PARAMETERS

Sensitivity analysis of each parameter of the model on the weight loss of the particle under different operating conditions shows that the value of k_1 for different types of coal can be estimated by comparing the weight loss history, the value of k_2 can be estimated based on product distribution of tar and gas under different temperatures and the value of k_3 can be estimated based on the pressure effect on the weight loss.

The pyrolysis data of Anthony and Howard^(1,2,3) for bituminous coal and those of Suuberg et al.⁽¹⁰⁾ for lignite coal were used to determine the reaction rate constants for the devolatilization step and the deposition step. For sub-bituminous coal, due to the lack of data on weight loss history and pressure effects, an average value between the rate constant of bituminous coal and that of lignite is used. The cracking reaction rate constants for each type of coal were chosen based on the product distribution data of Solomon et al.⁽⁹⁾. The reaction rate constants obtained for different ranks of coals are tabulated in Table 1.

A comparison between the calculated results and the experimental data for the weight loss history and the effect of pressure on bituminous coal is shown in Figure 1 and 2. The effect of pressure on weight loss for lignite has been reported to be negligible for pressures ranging from 0.01 to 100 atmospheres⁽³⁾. Figure 2 also demonstrates this trend. Figure 3 shows the effect of the heating rate on the weight loss history for lignite. Good agreement between the calculated lines and the experimental data indicates that the proposed model can represent the pyrolysis process successfully. The comparisons of the product distribution of tar and gas are shown in Figures 4, 5, and 6 for bituminous, sub-bituminous and lignite coal, respectively. The calculated tar yield is slightly higher than the observed yield especially in the low temperature range. Figures 7 to 9 show the application of the model with the predetermined reaction rate constants for bituminous, sub-bituminous and lignite coal. X_1 , the amount of tar formed in the devolatilization step, is correlated with the volatile matter content for each type of coal and is shown in Figure 10. The correlation equations for X_1 with different types of coals can be seen to represent this value closely for bituminous coal. This results from the aforementioned lack of data necessary for accurately determining the chemical reaction rate constants. The relation of X_1 with volatile matter content (dry ash free basis) are listed below:

$$\text{Bituminous } X_1 = 1.3 (\text{V.M.}) + 0.025 \quad (9)$$

$$\text{Lignite } X_1 = 0.95 (\text{V.M.}) + 0.025 \quad (10)$$

DISCUSSION AND CONCLUSIONS

Although the rate of heating affects the weight loss history of lignite coal as shown in Figure 3, it appears that the ultimate weight loss is not affected by the heating rate over the range between 650 to 10^4 °C/sec. However, Badzioch and Hawksley⁽⁴⁾ reported the ultimate weight loss of the particle at a rapid heating rate ($>2.5 \times 10^4$ °C/sec) may be 1.2 to 1.4 times higher than that at slow heating rate ($< 1/20$ °C/sec). There is a concern that their results might be attributable to the experimental conditions employed to achieve the rapid heating rate by use of small particles in an entrained reactor. For a slow heating rate, the ultimate weight loss is approximately the same as the proximate volatile matter content of the coal⁽⁵⁾. Additional studies are needed to clarify the effect of heating rate on the ultimate weight loss.

The estimation of the amount of tar formed at low temperatures based on the model is higher than those observed experimentally. This is shown in Figures 4 to 6. A minor adjustment was attempted in the cracking reaction rate constants, but this did not improve on the result. Hence, the model cannot adequately represent the pyrolysis at low temperatures (< 600 °C).

The weight loss curves at different temperatures for bituminous, sub-bituminous and lignite coals show that the calculated weight loss of the particle at temperatures higher than 800 °C tends to peak rather than continuously increase as seen in some of the experimental data. The validity of the model above 1000 °C is still undetermined due to the lack of experimental data above this temperature.

The phenomena of coal pyrolysis between bituminous and lignite coals are apparently quite different. Bituminous coal is more pressure dependent and has a lower proportion of gas in the pyrolysis products than lignite. The effect of pressure on the weight loss, according to the model, is primarily related to the rate of tar deposition. Since the rate of tar deposition is higher for the bituminous coal compared to that of lignite, the effect of pressure on the weight loss during pyrolysis is also more appreciable for bituminous coal than lignite. Furthermore, the ratio of the cracking rate to the deposition rate has an important effect on the amount of gas and tar formed. Since this ratio is greater for lignite than bituminous coal, lignite produces more gas than bituminous coal under similar pyrolytic conditions. This implies that the fraction of tar formed during the devolatilization step, X_1 , is smaller for lignite than that for bituminous coal as indicated by Equations 9 and 10.

The model developed is applicable within the operating range of pyrolysis process listed below:

$$\begin{aligned} 400 \text{ }^\circ\text{C} &< \text{Temperature} < 1000 \text{ }^\circ\text{C} \\ 25 \text{ } \mu\text{m} &< \text{Particle size} < 1000 \text{ } \mu\text{m} \end{aligned}$$

$1/180 \text{ } ^\circ\text{C}/\text{sec} < \text{Heating rate} < 10^4 \text{ } ^\circ\text{C}/\text{sec}$

$0.01 \text{ atm} < \text{Pressure} < 100 \text{ atm}$

For large particles beyond 1000 μm , temperature gradient within the particle may not be neglected requiring an additional term on heat condition within the particle to be included in Equation 7.

BIBLIOGRAPHY

1. Anthony, D. B., J. B. Howard, H. C. Hottel and H. P. Meissner, "Rapid Devolatilization of Pulverized Coal," Fifteenth Symposium (International) on Combustion, pp. 1303-1317, The Combustion Institute, Pittsburgh, PA (1975).
2. _____, "Rapid Devolatilization and Hydrogasification of Bituminous Coal," 55, 121-128 (1976).
3. Anthony, D. B., and J. B. Howard, "Coal Devolatilization and Hydrogasification," *AIChE Journal*, 22, No. 4, 625-656 (1976).
4. Badzioch, S. and P. G. W. Hawksley, "Kinetics of Thermal Decomposition of Pulverized Coal Particles," *Ind. Eng. Chem. Process Des. Develop.*, 9, No. 4, 521-530 (1970).
5. Goodman, J. B., M. Gomez, and V. F. Parry, "Laboratory Carbonization Assay of Low-Rank Coals at Low, Medium and High Temperatures," Report of Investigations, No. 5383, U.S. Bureau of Mines (1958).
6. Jones, J. F., M. R. Schmid, and R. T. Eddinger, "Fluidized Bed Pyrolysis of Coal," *Chem. Eng. Progr.*, 60, No. 6, 69-73 (1974).
7. Pyrcioch, E. J., H. L. Feldkirchner, C. L. Tsaros, J. L. Johnson, W. G. Bair, B. S. Lee, F. C. Schora, J. Huebler, and H. R. Linden, "Production of Pipeline Gas by Hydrogasification of Coal," *IGT Res. Bull.*, No. 39, Chicago (1972).
8. Russel, W. B., D. A. Saville, and M. I. Greene, "A Model for Short Residence Time Hydrolysis of Single Coal Particle," *AIChE Journal*, 25, No. 1, 65-80 (1979).
9. Solomon, P. R., "The Evolution of Pollutants During the Rapid Devolatilization of Coal," Project R77-952588-3 Report for the period April 1, 1976 through September 30, 1977, NSF Grant No. AER75-17247 U.S. ERDA, pp. i-ix, IV-1-10 (1977).
10. Suuberg, E. M., W. A. Peters, and J. B. Howard, "Product Composition and Kinetics of Lignite Pyrolysis," *Ind. Eng. Chem. Process Des. Develop.*, 17, No. 1, 37-46 (1978).
11. Weekman, V. W., Jr., "Kinetics and Dynamics of Catalytic Cracking Selectivity in Fixed-Bed Reactors," *Ind. Eng. Chem. Process Des. Develop.*, 8, No. 3, 385-391 (1969).

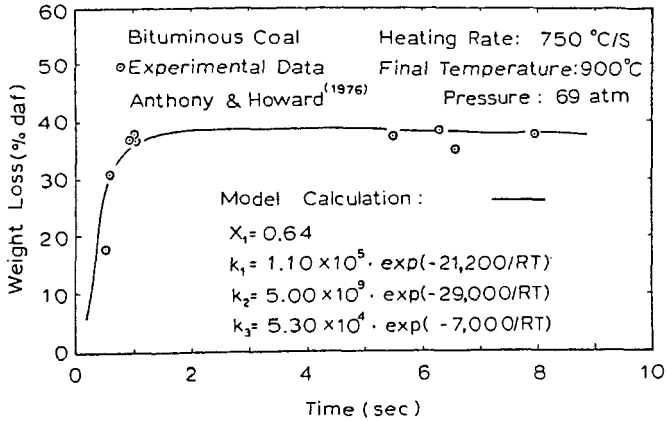


FIG. 1. PYROLYSIS WEIGHT LOSS HISTORY OF BITUMINOUS COAL

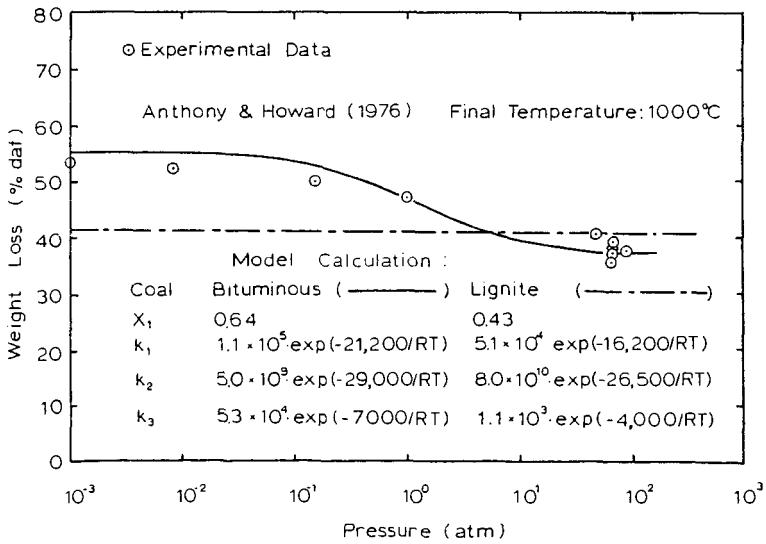


FIG. 2. EFFECT OF PRESSURE ON THE WEIGHT LOSS OF BITUMINOUS AND LIGNITE COALS

Table 1
Reaction Rate Constants for Coal Pyrolysis Model

Reaction Rate Constants	Coal	Bituminous	Sub-bituminous	Lignite
k_{10} 1/sec		1.1×10^5	7.5×10^4	5.1×10^4
E_1 J/mole cal/gmole		88,700 21,200	78,200 18,700	67,800 16,200
k_{20} 1/sec		9.7×10^9	3.5×10^{10}	8×10^{10}
E_2 J/mole cal/gmole		121,500 29,000	116,100 27,750	110,900 26,500
k_{30} 1/sec		5.3×10^4	2.5×10^4	1.1×10^3
E_3 J/mole cal/gmole		29,500 7,000	23,000 5,500	16,700 4,000

Uncertainty of E_i : ± 100 J/mole or cal/gmole

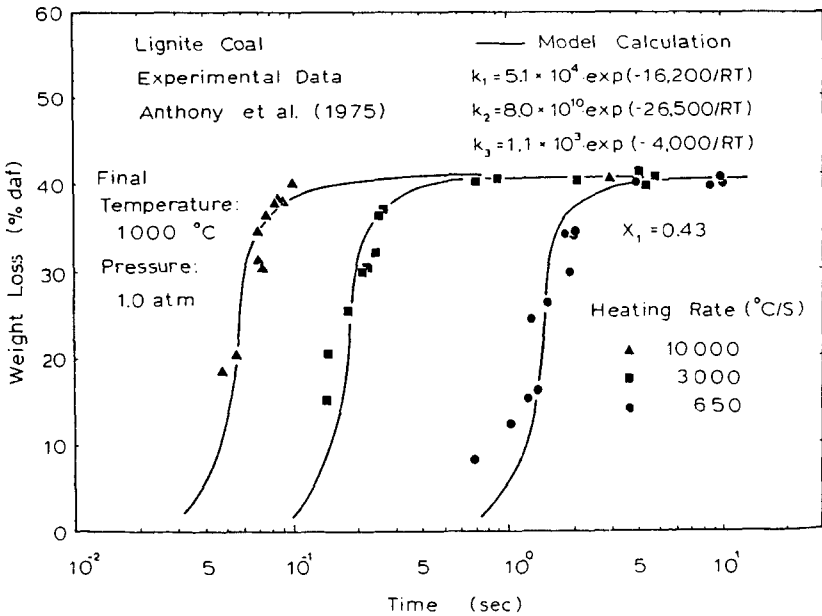


FIG. 3. EFFECT OF HEATING RATE ON THE WEIGHT LOSS HISTORY OF LIGNITE COAL

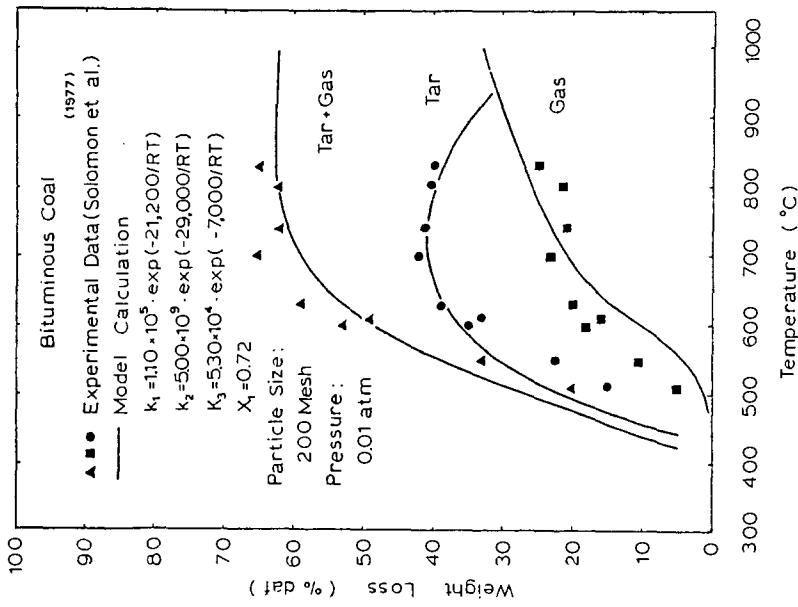


FIG. 4. PRODUCT DISTRIBUTION FROM BITUMINOUS COAL PYROLYSIS

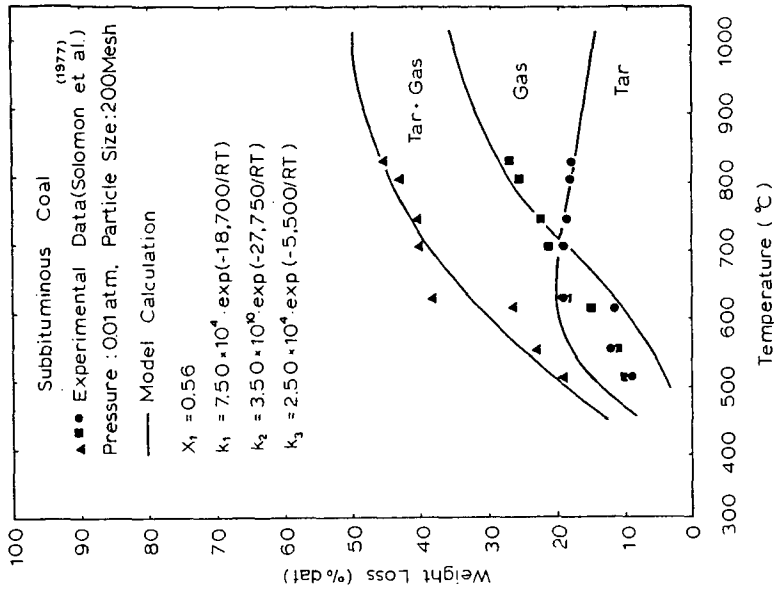


FIG. 5. PRODUCT DISTRIBUTION FROM SUB-BITUMINOUS COAL PYROLYSIS

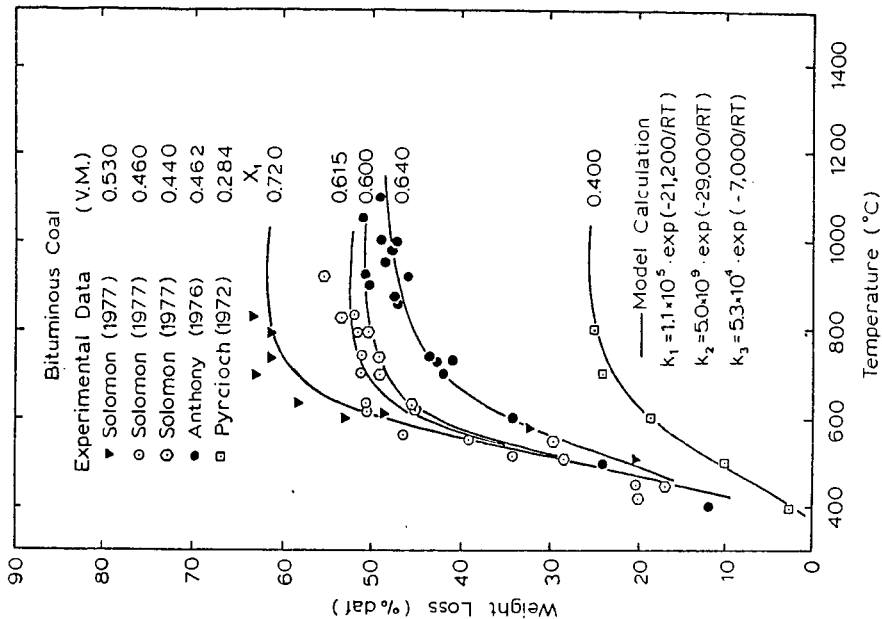


FIG. 7. EFFECT OF TEMPERATURE ON THE WEIGHT LOSS OF BITUMINOUS COAL

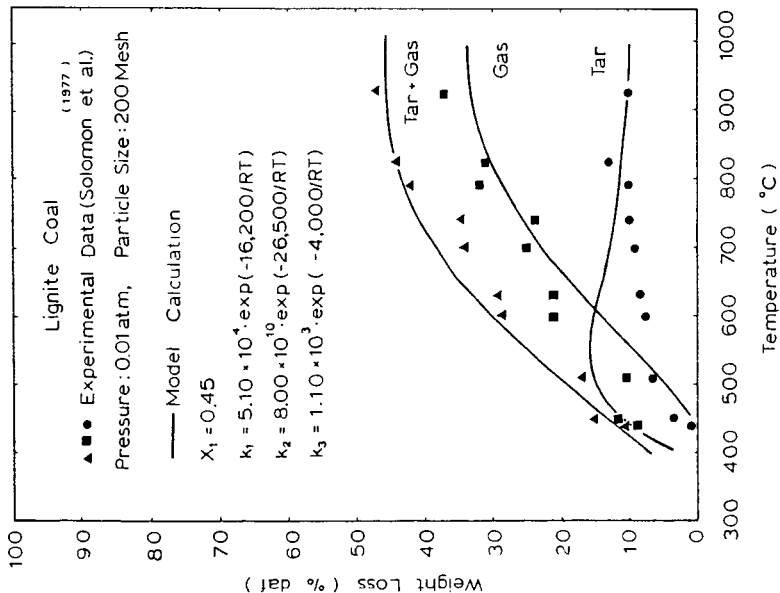


FIG. 6. PRODUCT DISTRIBUTION FROM LIGNITE COAL PYROLYSIS

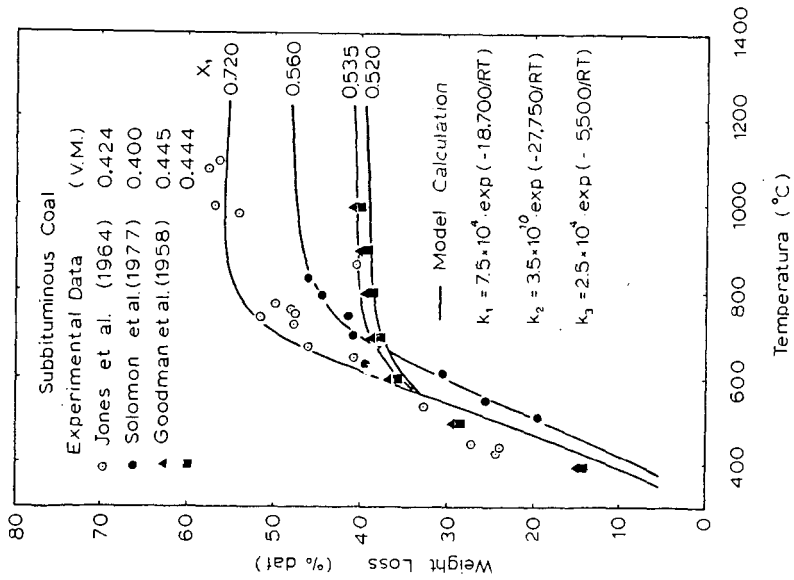


FIG. 8. EFFECT OF TEMPERATURE ON THE WEIGHT LOSS OF SUB-BITUMINOUS COAL

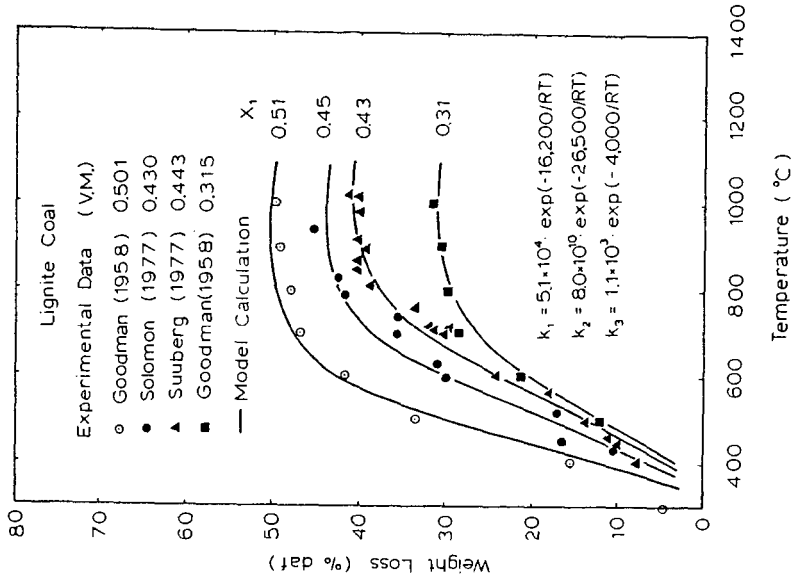


FIG. 9. EFFECT OF TEMPERATURE ON THE WEIGHT LOSS OF LIGNITE COAL

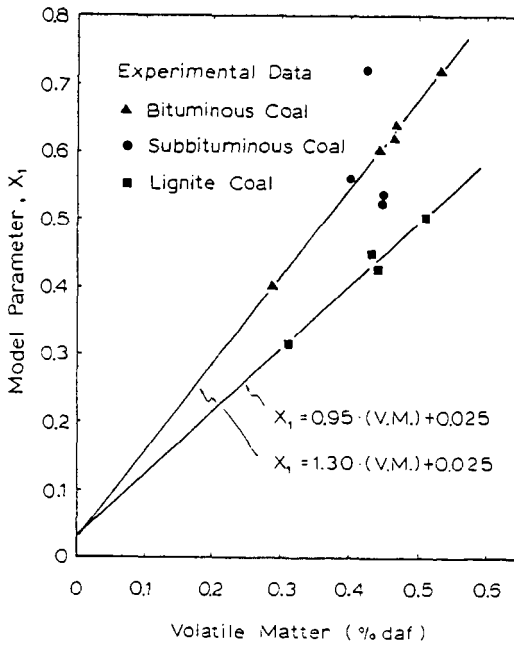


FIG. 10. THE RELATION OF THE MODEL PARAMETER, X_1 , WITH THE VOLATILE MATTER CONTENT FOR BITUMINOUS, SUB-BITUMINOUS AND LIGNITE COALS

MATHEMATICAL MODEL OF BITUMINOUS COAL PYROLYSIS--TAR FORMATION AND EVOLUTION. M.W. Zacharias and J.B. Howard. Department of Chemical Engineering, Massachusetts Institute of Technology, Cambridge, Massachusetts 02139

A mathematical model of the rapid pyrolysis of caking coal has been fitted to extensive data on a Pittsburgh Seam coal pyrolyzed under wide ranges of conditions in a laboratory batch-sample reactor. The model includes an improved description of the role of mass transfer and secondary reactions and offers a means for the prediction of pressure effects on product yields. According to the model, a coal particle decomposes to form tar, lighter volatiles and char. The primary tar may evaporate and diffuse away from the particle or undergo secondary reactions leading to lighter volatiles and coke. The model is quite successful in predicting tar yields at pressures ranging from vacuum to 69 atm, although the predictions at the highest pressure are lower than the experimental yields, particularly at low temperatures. Possible explanations for this discrepancy will be presented. Results from application of the model indicate that mass transfer limitations are negligible under vacuum conditions. As the pressure is increased, tar evolution becomes limited by diffusion into the bulk reactor gas.

EXPERIMENTAL STUDY AND MODELING OF COAL PYROLYSIS AT HIGH TEMPERATURES*

P. R. Solomon

United Technologies Research Center, East Hartford, CT 06108

INTRODUCTION

In a recent study, the vacuum pyrolysis behavior of a lignite and twelve bituminous coals was measured over the range 300 to 1000°C (1,2,3). The results were successfully simulated using a model which predicts the time and temperature dependent product evolution from a knowledge of the function group composition of the coal and a general set of kinetic rates which vary with evolved product but not with coal type.

This paper reports the extension of this investigation to temperatures up to 1450°C and to a wider number of measured and modeled pyrolysis products. Experiments have been performed in an apparatus which employs a Fourier Transform Infrared Spectrometer (FTIR) for on-line analysis of gas species. The FTIR allows the direct accumulation of release rate data for major species by monitoring the gas concentration during a pyrolysis run. Results have been obtained with a Pittsburgh seam bituminous and a Montana lignite. The temperature dependent evolution of corresponding products are similar for the two coals indicating that the use of coal independent kinetic rates is applicable for the additional products and higher temperatures. The dominant effect observed at higher temperatures is the trend toward increased yields of hydrogen gas and unsaturated compounds (olefins, acetylene and probably soot) at the expense of paraffins. These effects are being modeled by including additional parallel reaction paths for the decomposition of the aliphatic content of the coal.

EXPERIMENTAL

The apparatus is illustrated in Fig. 1. It consists of a small chamber in which the coal is pyrolyzed connected through a glass wool filter to a large gas cell for infrared analysis. The coal is evenly distributed between the folds of a stainless steel, molybdenum or tungsten screen and a current is passed through the screen to heat the coal. Coal temperatures of 1450°C and heating rates of 2000°C/sec were achieved using the tungsten screen. Gas analysis is performed with a Nicolet (FTIR) which permits low resolution analysis at 0.5 second intervals. The low resolution analysis can determine CO, CO₂, H₂O, CH₄, COS, SO₂, CS₂, HCN, C₂H₂, C₂H₄, C₃H₆, benzene and heavy paraffins and olefins. A high resolution analysis made at the completion of a run can determine all of the above plus C₂H₆, C₃H₈, C₄H₈, NH₃ and potentially many other species which have not yet been observed. H₂ is determined by difference. Other features of the apparatus are similar to those described previously (1,2,3).

Calibration of the FTIR has been made using pure gases or prepared gas mixtures. Unfortunately, most of the gases of interest show a marked increase in absorbance with dilution. The explanation for this effect is that the absorption lines for these gases are extremely sharp and for moderate concentrations all the infrared energy is

*Work supported by the Department of Energy under Contract ET-78-C-01-3167

absorbed at the line center in a path shorter than the absorption cell. The instrument resolution is substantially broader than the line width so the lines do not appear to be truncated. Dilution of the gas broadens the line, reducing the absorbance at line center so that a longer path contributes to the absorptivity, thus increasing the average absorbance. This effect makes calibration of these gases in the pyrolysis gas mixture difficult. The solution has been to dilute the mixture with nitrogen to a fixed pressure at which calibrations have been made.

Figure 2 shows the spectra obtained at several time intervals during an 80 second devolatilization run at about 500°C. Kinetic rate data for major species can be determined from such scans as indicated in Fig. 3 which shows the methane yield and the pressure rise in the system as a function of time.

Pyrolysis data were obtained up to temperatures of 1450°C for a Pittsburgh seam coal (PSOC 170) and a Montana lignite. For the Pittsburgh seam coal 80 second pyrolysis runs were made with 200 mg samples at temperatures from 400 to 1000°C. For these conditions, the temperature rise takes on the order of two seconds. More rapid heating (less than one second) was achieved using smaller (50 mg) samples. Ten second pyrolysis runs were made with 50 mg samples for both coals.

RESULTS

Using the procedure shown in Fig. 3 the methane kinetic constants were determined for the 10 and 80 runs. These data are plotted in Fig. 4 along with a line for the temperature dependent kinetic rate for methane previously determined (2). As can be seen the lignite and bituminous data are quite close and all data are in reasonable agreement with the previously determined line. The high temperature points for the 80 second runs are low because of the slow heating described above and presumably the same sort of limitations are affecting the 10 second runs at the very high temperatures.

Pyrolysis data for the 10 second runs are plotted in Fig. 5. Figs 5a and b show the product distribution. Included in the light gases are all the species listed except for those heavier than C_3 , which are included with the heavier hydrocarbons (HC). An interesting feature of these data are the high volatile yields obtained at high temperatures. Volatile yields of up to 70% were observed as compared with ASTM volatile yields of 46% and 59% for the bituminous coal and lignite respectively.

Several of the gaseous species are shown in Figs. 5c-h. The similarity between lignite and bituminous coal is apparent in the temperature dependence of the evolution of each species. Figs. c to f show results for H_2 , CH_4 and C_2H_2 and heavy olefins and paraffins. These figures illustrate the tendency for high temperature pyrolysis to favor molecular hydrogen and unsaturated compounds. Figures g and h show the distribution of oxygen containing species.

PYROLYSIS MODEL

A successful model was developed to simulate the pyrolysis behavior of the thirteen coals previously studied at low temperature (1,2,3). The model assumes that large molecular fragments ("monomers") are released from the coal "polymer" with only minor alteration to form tar while simultaneous cracking of the chemical structure forms the light molecules of the gas. Any chemical component of the coal can, therefore, evolve as part of the tar or as a species in the gas. The mathematical

description presented in detail in Refs. 2 and 3 represents the coal as a rectangular area with X and Y dimensions. The Y dimension is divided into fractions according to the chemical composition of the coal. Y_i^0 represents the initial fraction of a particular component (carboxyl, aromatic hydrogen, etc) and $\sum Y_i^0=1$. The evolution of each component into the gas (carboxyl into CO_2 , aromatic hydrogen into H_2 , etc) is represented by the first order diminishing of the Y_i dimension, $Y_i=Y_i^0 \exp(-k_{i1}t)$. The X dimension is divided into a potential tar forming fraction X^0 and a non-tar forming fraction $1-X^0$ with the evolution of the tar being represented by the first order diminishing of the X dimension $X=X^0 \exp(-k_{tar}t)$. The amount of a particular component in the char is $(1-X^0+X)Y_i$ and the amounts in the gas and tar may be obtained by integration. It was found that a general set of kinetic constants (k_{i1} 's and k_{tar}) could be used for all the coals. The differences among coal results solely from the different mix of chemical groups (the Y_i^0 's). As described in Ref. 3 many of the Y_i^0 's may be determined from ultimate and infrared analysis.

Modifications of the model were made to include the high temperature production of unsaturated compounds. An example, the production of acetylene and H_2 is assumed to be a third independent path for the evolution of an aliphatic component. The component is represented as a volume and the evolution of acetylene and H_2 is represented by the diminishing of the X dimension, $Z=Z^0 \exp(-k_{ac}t)$ where $Z^0=1$. The amount of the component in the char is then $(1-X^0+X)Y_iZ$. The evolved amounts may be obtained by integration. Further competitive processes such as the production of olefins plus H_2 from paraffins and the production of soot and H_2 from aliphatics were incorporated in a like manner.

The results are the lines shown in Fig. 5. The kinetic constants are the same as those used in Ref. 2 with the exception of: $k_{H_2O} = 45 \exp(-4950/T)$, $k_{al} = 750 \exp(-8000/T)$ and the addition of: $k_{ac} = 2.19 \times 10^{10} \exp(-35000/T)$, $k_{o1} = 2.0 \times 10^7 \exp(-20000/T)$, $k_{soot} = 9.5 \times 10^{10} \exp(-35000/T)$. The model is in reasonable agreement with experiment for most species. Exceptions are H_2O and H_2 . The decrease in H_2O at high temperatures has not been modeled. The effect could be a steam char reaction to form CO and H_2 . Inclusion of this reaction would improve the agreement for CO and H_2 as well.

CONCLUSIONS

1. Using a heated grid apparatus with on-line gas analysis by FTIR, data has been obtained for a large number of pyrolysis products from a lignite and a bituminous coal at temperatures up to 1450°C.
2. The temperature dependent evolution of corresponding products from the lignite and bituminous coal vary in magnitude but are otherwise quite similar.
3. The pyrolysis behavior has been simulated by modifying a previously developed model which uses the same kinetic rates for all coals. Modifications of the model were made to include the high temperature evolution of H_2 and unsaturated compounds (olefins, acetylene, and soot) from the aliphatic material in the coal.
4. The coal parameters of the model are related to the functional group composition of the coal.

REFERENCES

1. Solomon, P. R. and Colket, M. B., Fuel, 57, 749 (1948).
2. Solomon, P. R. and Colket, M. B., Seventeenth Symposium (Int'l) on Combustion, the Institute 1979, to be published.
3. Solomon, P. R., A.C.S. Division of Fuel Chemistry preprints 24, No. 2, 185 (1979).

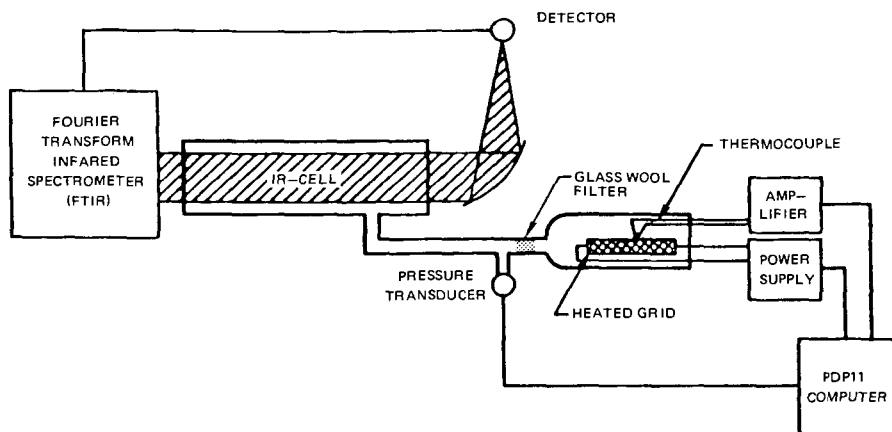


FIG. 1 PYROLYSIS APPARATUS

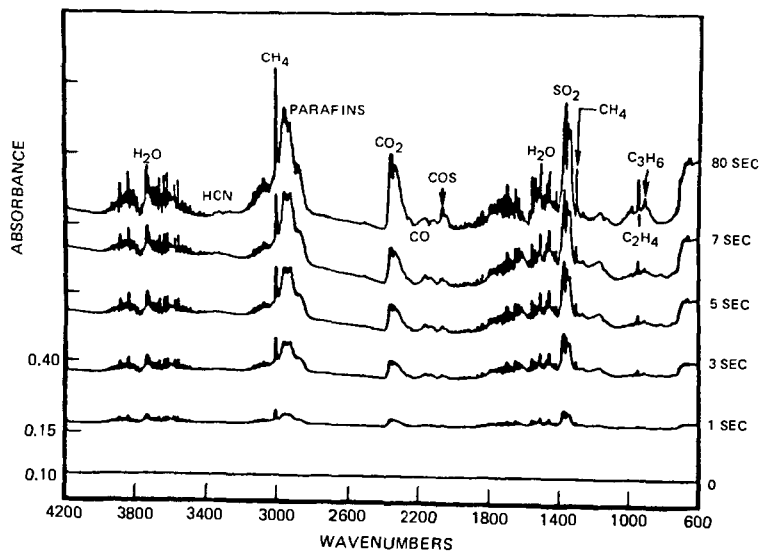


FIG. 2 INFRARED SPECTRA OF EVOLVING PYROLYSIS GAS

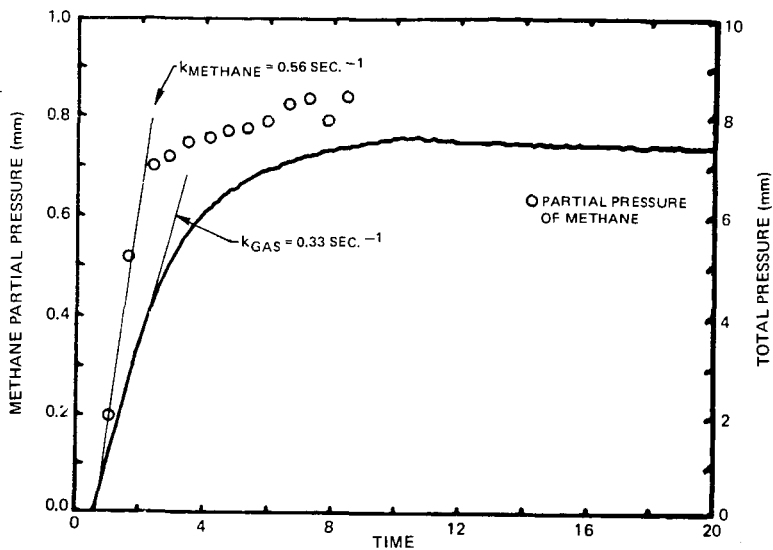


FIG. 3 TIME DEPENDENCE OF METHANE PARTIAL PRESSURE AND TOTAL PRESSURE DURING PYROLYSIS

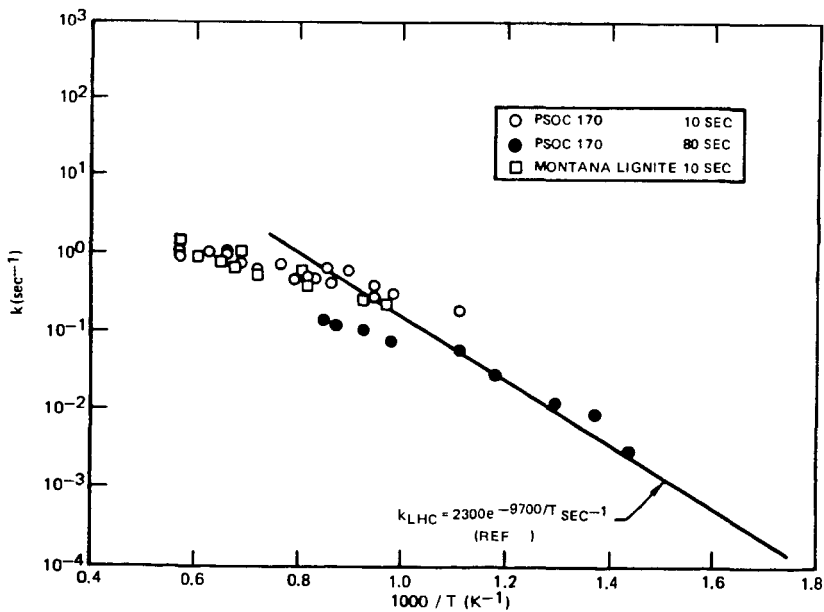


FIG. 4 RATE CONSTANT FOR METHANE EVOLUTION

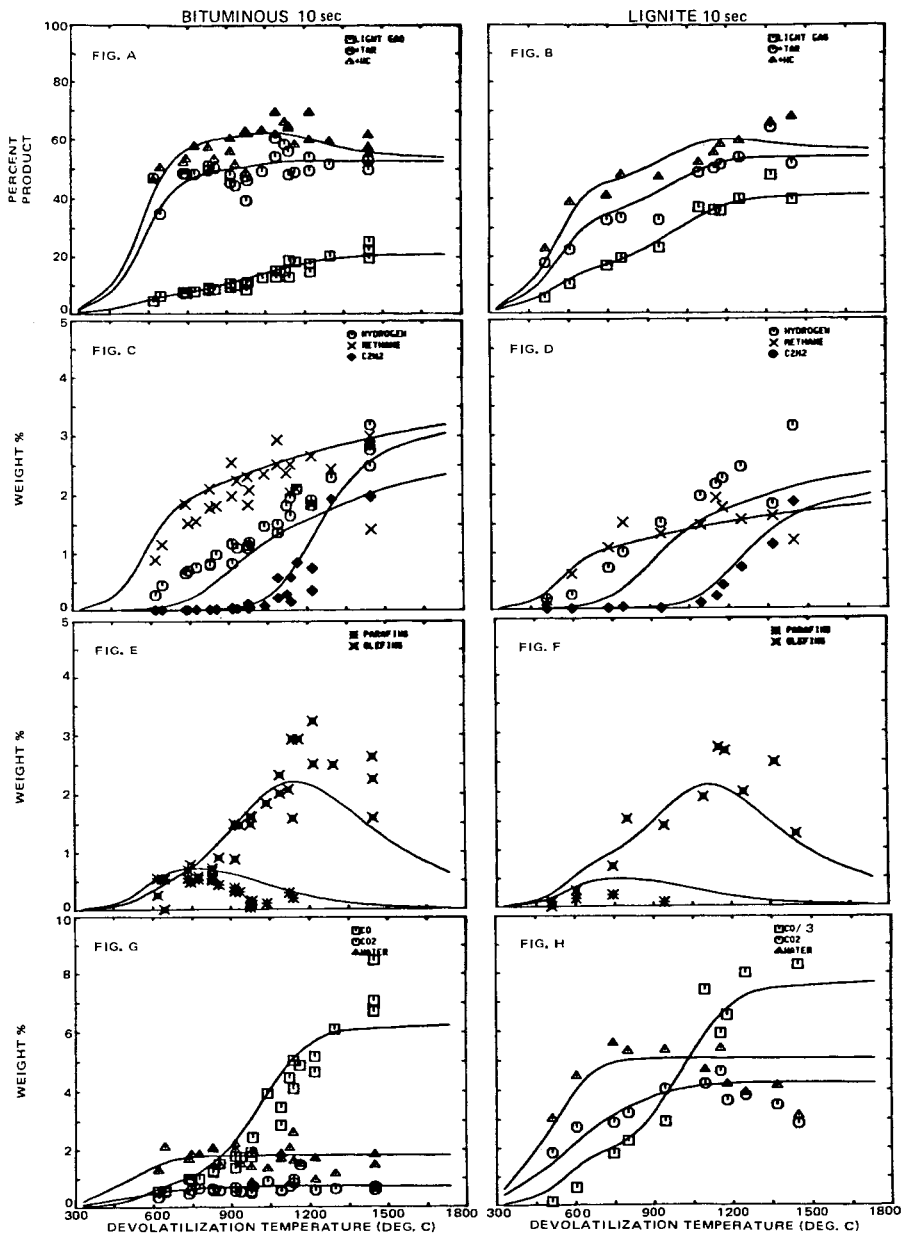


FIG. 5 PYROLYSIS PRODUCT YIELDS

THE GOVERNMENT ROLE IN FUELS RESEARCH AND DEVELOPMENT. Robert C. Ketcham, U.S. House of Representatives, Committee on Science and Technology, Washington, D.C. 20515.

The seventies have seen the multi-fold increase in federal support for non-nuclear R&D. At the same time, major institutional changes have occurred within the Legislative and Executive Branches of the Federal Government. This same period has also witnessed the emergence of environmental regulation and review, which added another dimension to decision making.

The U.S. needs a sense of adventure to solve its energy supply shortfall, energy rough-riders, as it were, to focus our technological talent and bring together our industrial and governmental players. Some of the key ingredients for success require: (1) overcoming technological timidity by setting goals for programs and committing necessary funds; (2) making hard choices between competing technologies; (3) budget support at the time a favored technology requires funding for large scale demonstration; (4) support for U.S. industry, profit-making, and aggressive pursuit of world markets; and (5) a recognition that the environment and health and safety are matters that must not be scaled down to obtain energy production, but the existing weapons used by obstructionists must be melted into plowshares for production.

SYNTHETIC FUELS: LET'S GET ON WITH THE JOB. R.E. Balzhiser. Electric Power Research Institute, P.O. Box 10412, Palo Alto, California 94303.

The government has been and should continue to be an active funder of fossil fuel research and development, particularly as it relates to syn-fuels from coal and shale. Work should continue to be supported in universities and industry as well as government facilities, with the principal support of pilot scale development work performed and managed by industry utilizing the cooperative agreement form of government participation. The most urgent need facing the nation relates to the need to develop a synthetic fuels production capability. Uncertainties arising from past regulatory practices have inhibited industry from making the large investments necessary to commercialize these technologies. Government options include: 1) funding demonstration plants, such as the Solvent Refined Coal projects; 2) use of loan guarantees and/or tax incentives; 3) establishment of government owned industry operated plants as was done for synthetic rubber; 4) government purchase of synfuels output; and 5) government mandated production levels with industry selecting the technologies and providing funds in lieu of an excess profits tax. While each approach has its advocates, I believe the latter best fixes responsibility on the government and industry to make those decisions that they are institutionally most qualified to make.

ENVIRONMENTAL REGULATIONS - PRESENT AND FUTURE. S. R. Reznick. U. S. Environmental Protection Agency, Office of Energy, Minerals and Industry, 401 M Street, S. W., Washington, D. C. 20460

Three major pieces of environmental legislation are affecting, and will continue to affect fossil fuel combustion. These are, the Clean Air Act, the Clean Water Act, and the Resource Recovery and Conservation Act. This paper will summarize the new goals established for the Environmental Protection Agency by this legislation and will discuss the major revisions to regulations which will affect fossil fuel combustion for power generation. Proposed standards to reduce airborne emissions from power and utility boilers and to reduce the discharge of waterborne "toxic" pollutants are presented. The requirements of the RCRA, as they are being applied to utility industry sludges, are also discussed.

SOME PERSPECTIVES ON THE VIEWS OF COAL PRODUCERS TOWARDS THE ROLE OF THE FEDERAL GOVERNMENT IN COAL MINING RESEARCH AND DEVELOPMENT. Dr. Joseph J. Yancik, 1130 17th Street, Washington, D.C. 20036

The commercial use of significantly new or improved coal mining technologies requires a long-term commitment from a mine operator. The route to commercialization of new technology begins with the initial concept development and from there it must proceed in an orderly fashion in order to culminate in a mine-worthy system capable of producing coal on a daily basis. The time span may be from 15 to 30 years depending upon a large number of factors that can be grouped under two general headings. The first group includes those considerations which are related to the complexity and degree of innovation involved in the new technology. The second grouping involves factors which are specific to the mining operation, such as its location, life cycle and production requirements. It is important that research and development programs for new mining systems take into account the unique nature of the relationship between the mine site and the extraction system. Since mining occurs under a wide variety of geologic and geographic conditions, there are many different "sets" of requirements for extraction systems. This paper discusses the various roles which the federal government could best assume in the development of new mining systems with special emphasis placed on those aspects which are pertinent to the unique site specific demands of mining R&D. The paper also offers suggestions on how these roles should be planned and implemented to conduct cost effective programs and improve the chances of commercialization.

THE ACADEMIC VIEW OF THE GOVERNMENT ROLE IN FUELS RESEARCH AND DEVELOPMENT
J. H. Gary. Colorado School of Mines, Golden, Colorado 80401

The role of government in fuels research and development is characterized by division into three areas: university research, federal laboratory research and development, and joint government-industry development.

The federal government should fund basic and applied research at the universities to find new sources and processes to produce liquid and gaseous fuels, improvements in known reactions and processes, and ways of eliminating or minimizing undesirable reactions or features of known or new methods.

Federal laboratories should be directed mainly to pilot plant and field development, but should include monitoring of university basic and applied research. Greater interaction between university and federal laboratory programs will improve efficiency and give better and more timely results by greater utilization of the unique strengths of each.

Government-industry efforts should be in the joint sponsoring of large pilot units or process development units after research and development work has shown a process to be sufficiently promising.

It is essential to view and finance programs from a program viewpoint and not on a fiscal year basis. In-depth annual reviews would decide on continuation or termination of a given grant.

A ROLE FOR THE GOVERNMENT IN PETROLEUM FUEL R&D

E. J. Gornowski

Exxon Research and Engineering Company
Florham Park, New Jersey

Deriving a national benefit from petroleum fuel involves many steps:

- Finding the resource - Exploration
- Getting it out of the ground - Production
- Bringing it to the refinery - Transportation
- Converting it to useful products - Refining
- Delivering it to the customer - Marketing
- Burning it in suitable equipment - Utilization

as well as the setting of standards that protect the national welfare. The overall role of petroleum fuel R&D is to provide better ways to carry out all these steps--where "better" means cheaper, safer, cleaner, more efficient, more convenient, more timely or any other positive comparative.

Who should control this R&D?

Obviously those who can do it in the best, that is in the cheapest, safest, cleanest, most efficient, most convenient, most timely manner.

In this country, we have basically four choices:

- The Government
- The Universities
- Non-profit Institutes
- Private Industry

and each of these four has its particular areas of expertise, activities in which it is "best." So we really need all four and our present goal must be to suggest a way in which to carve up the R&D function to assure that the overall result is optimal for the country.

Retrospectively, our private and highly competitive industry has funded, performed and controlled by far the greatest part of petroleum fuel R&D--with a very able assist from the Universities in the basic research area. Private industry has carried the ball and has carried it well. U.S. technology for all the steps involved--from exploration through refining to utilization--tends to be the model that other nations strive to emulate.

That has been the picture in the past.

What of the future?

A different factor is affecting the desire for new technology, a factor that does not necessarily make itself felt through the marketplace, a factor that does not elicit a prompt R&D response from private industry: the factor of national security.

To the extent that national security considerations override commercial driving forces, to that extent governmental intervention in petroleum fuel R&D is not only warranted but required. Thus if production of otherwise commercially unattractive resources such as shale oil or coal liquids is considered to be a national requirement, Government involvement in developing the requisite technology is called for. The ideal role here, as we see it, is a cooperative one where the Government and the private sector combine to fund and to control the R&D.

But what of the other steps--the steps beyond production? Transportation, refining, marketing and utilization of fuel products from synthetic feeds like shale oil and coal liquids will differ from these same operations using "normal" crude oils. Here we see no need for Government involvement in developing new technology. Private competitive industry has amply illustrated that it can well handle such a change in feedstocks. The driving forces to make, market and use the products will remain the same. We believe that it would be unwise to change a competitive innovation system that has worked well in the past if there is no change in the driving forces.

Similar reasoning applies wherever any societal factor overrides "normal" market forces: government intervention in R&D should parallel government intervention thru other mechanisms (penalties, grants, subsidies, tax-relief or whatever) to facilitate initiating the desired change. Once the new incentives and new criteria exist, the private sector is best able to uncover the technology needed to optimize meeting the perceived societal goals.

Of course, we also see other roles that the Government can and should play in indirect support of the development of new petroleum fuel technology.

First, is an obligation to help in the development of a pool of well-trained technical professional personnel. This is a national need. The best way to train good technical people is still to have them participate in good research and the Universities can hardly be expected to find adequate financing for meaningful research programs on their own.

The Government is also well placed to undertake large-scale basic research programs which the universities cannot afford and to build special facilities that can be shared by a number of organizations.

Basically, the role of all R&D is to find better ways of doing things and the Government's "things" have been well defined for us:

- To establish justice
- To ensure domestic tranquility
- To provide for the common defense
- To promote the general welfare
- To secure the blessings of liberty to ourselves and our posterity.

The appropriateness of any proposed Governmental R&D should be tested against those objectives.

Government Role in Fuels R&D -- DOE Perspective.

Roger W. A. LeGassie. U.S. Department of Energy, 1000 Independence Ave.,
Washington, D.C. 20585

The Federal government's perspective on the national energy problem and the role of the Department of Energy in dealing with the problem will be discussed. The basic problem is seen as the increasing U.S. dependence on foreign oil to meet its energy demands and the resultant need to reduce U.S. levels of energy imports.

The Federal government, through the Department of Energy, has three primary tools at its disposal to accomplish its energy policy objectives: tax incentives, regulatory actions, and support of R&D. The problem in any particular situation is to find the most suitable mix of these three tools. The mix will be different for each program, fuel, and technology area. The valid bases for government involvement in R&D in various situations will be discussed.

Specific examples from current DOE fuels programs will be cited to show how the various mixes of these tools are being applied and what the appropriate role is for Federal support of R&D in each case.

FEDERAL FUELS R&D AS AN ARM OF ENERGY POLICY

Henry R. Linden

Gas Research Institute
10 West 35th Street
Chicago, Illinois 60610

It would be a truism to state that Federal support or lack thereof of energy research, development and demonstration (RD&D) has become one of the key elements in the implementation of energy policy. Examples abound. They range from the cutback and restructuring of nuclear breeder R&D in line with the Administration's non-proliferation policy, to growing support for unconventional natural gas R&D in line with the Administration's recognition that increased domestic pipeline quality gas supply and use is one of the most effective means to constrain oil imports.

In the fossil fuel or, more generally, the non-nuclear area, the role of Federal energy R&D as an energy policy tool is of relatively recent vintage. The step-up in the scope and magnitude, and the shift to relatively near-term commercialization goals, dates roughly from the consolidation of all energy-related RD&D programs under the Energy Research and Development Administration (ERDA) in January 1975. Prior to that time the technical data base for fossil energy policy came largely from private R&D sources. In contrast with nuclear energy policy and RD&D, which was under Federal control from its inception, most early attempts of major Federal intervention in fossil fuel RD&D failed. The fossil energy industry with its large and effective in-house R&D programs successfully bypassed such Federal initiatives as the abortive post-World War II synthetic fuels effort. Prior to the official recognition of an "energy crisis" in 1971 in the form of the first pronouncement of a comprehensive energy policy by a U.S. president, only the coal industry actively sought Federal support for relatively short-term commercial applications-oriented fossil fuel R&D. Some minor exceptions were co-operative programs with the gas industry in such areas as nuclear stimulation of tight gas formations and the production of pipeline quality gas from coal.

The coal industry initiative led to the establishment in 1963 of the relatively small program of the Office of Coal Research in the Department of the Interior which became the nucleus of the vastly expanded ERDA and Department of Energy (DOE) fossil energy RD&D programs developed with the urging of Congress. The blueprint for integrating nuclear and fossil fuel R&D, and developing a better balance between the two, was prepared in 1973 under the direction of Dixy Lee Ray, the last Chairman of the Atomic Energy Commission (AEC). In this blueprint, the AEC RD&D model was followed closely because of its success in moving government-developed technology into the private sector

following World War II. Although defense-related and nuclear material supply activities continued to be a major share of the Federal nuclear program, civilian RD&D by the National Laboratories and industry grew rapidly and formed the foundation for the development of commercial nuclear power.

The expansion of the Federal role in energy RD&D was, of course, greatly accelerated by the 1973/74 oil embargo and led to the increase of Federal energy RD&D budgets from less than \$1 billion to more than \$3 billion today. However, even during the short ERDA days, it became apparent that the AEC model could not be successfully applied to fossil fuel RD&D and to non-nuclear R&D in general. Nuclear RD&D, nuclear energy policy, and nuclear power commercialization were always fully integrated under Federal control. This is not true in any sense in the fossil fuel area. In fact, with some notable exceptions, relationships between the Administration, Congress and industry in this area could be better characterized as adversary rather than as cooperative.

Thus, the basic objective of Federal fossil fuel RD&D — commercialization of new technologies leading to increased use of domestic resources and a reduction of oil imports — has become increasingly elusive. The difficulty extends far beyond the government/industry interface. Whereas, until the relatively recent doubts concerning safety, the goal of nuclear programs was to reduce electric power cost and environmental impact while simultaneously relying on abundant domestic resources, the goal in much of fossil fuel RD&D has been to substitute more costly, environmentally more difficult energy sources for conventional oil and natural gas. The direct benefits often defy conventional economic or social justifications. Rather they are of broad national scope — improved military security and monetary stability, greater freedom to implement foreign policy and trade objectives, etc., not cheaper energy.

The synthetic fuels program is, of course, the best example of the difficulty of applying the lessons of the civilian nuclear reactor program, the wartime synthetic rubber program, the civilian air transport program, etc., to commercialization of Federally developed fossil fuel technology. Various administrative, legislative and regulatory approaches so far have either failed or have poor prospects. This includes loan guarantees, cost sharing, construction grants, tax credits, favorable regulatory treatment in case of synthetic pipeline gas, and several combinations and permutations of these means to compensate the producer, user and investor for higher costs and risks. It has been next to impossible to have the stockholder, tax payer and consumer or rate payer assume costs or risks on behalf of the national interest which they perceive to be inequitable. Thus, in spite of a lot of good R&D and widespread acceptance of the overall goal of increased energy self-sufficiency, little progress has been made. Apparently, the model, the logic and the entire approach have been faulty. The biggest problem is, of course, that synthetic fuels continue to cost about twice as much as their fossil fuel counterparts as has been the case since World War II.

As an alternative, I would like to propose a plan for new fossil fuel technology development and commercialization modeled after the legislatively

mandated automotive fuel efficiency standards. Evidence abounds that they have indeed been successful. Without National Laboratories, any major Federal RD&D programs, loan guarantees, special tax treatment or other forms of Federal intervention, the automotive industry has risen to the challenge and is indeed far along the road to meeting the efficiency standards. In the process, they are probably now building domestic automobiles which will again be competitive in the world market.

This is not an original idea, of course, but why not legislate that by 1990, say, 5 percent of total pipeline gas and total liquid fuels marketed must consist of the domestic supplemental source of the wholesaler's choice, i.e., it can be derived from coal, oil shale, unconventional natural sources, or biomass, by whatever process that gives the desired results. Purchase of entitlements should be encouraged to ensure optimum economy of scale, etc. This would drive the system to the quickest and lowest cost solutions. It would take government largely out of the process of developing and commercializing synthetics and biomass fuels, a task at which government so far has an unbroken record of failure. It would mandate industry, including its regulated utility component, to do the job instead, under conditions which distribute the financial burdens and risks equitably, thereby eliminating the need for complex systems of selective subsidies. If, through some miracle, further expansion of synthetics and other supplementals after 1990 is not needed, the consumer impact of 5 percent of supply at, say, double conventional fuel price, would have been marginal. If, as many believe, supplementals will be essential to the survival of the United States, then this investment would have untold benefits at relatively little cost.

GENERAL MOTORS' VIEW ON ALTERNATE FUELS. Alex C. Mair, GM Research Laboratory,
Warren. Michigan 48090

General Motors' outlook regarding utilization of domestic energy resources to provide alternative fuels for transportation will be discussed. Alternative fuels production is needed to complement energy conservation programs now in effect. The Government's role in spurring production of alternative fuels will be addressed.

DEFENSE MOBILITY FUELS AND GOVERNMENT R&D. Dr. R. M. Davis, Deputy Under Secretary of Defense for Research and Advanced Technology, Room 3E114, Pentagon, Washington, D.C. 20301

Our national security objectives can be achieved only if we are thoroughly prepared to meet essential military energy requirements. The continuation of our ability to deter armed conflict, to produce modern weapon systems, to maintain the readiness of our military forces, and to support worldwide commitments on the seas, in the air, and on the ground depends on energy, particularly liquid hydrocarbon fuels. As evidenced by the fact that crude oil imports now comprise nearly 50 percent of the U.S. petroleum demand, our most serious near term energy problem is our growing reliance upon foreign oil to compensate for the inability of domestic energy production to keep pace with domestic energy demand. Considering the practical reality of DOD's continued dependence upon liquid hydrocarbon fuels, this pattern of ever increasing dependence upon foreign oil poses a most serious threat to our ability to guarantee adequate energy supplies to meet essential military requirements, particularly for mobility fuels. In response to this current and most critical energy issue, the Department of Defense has undertaken a series of actions which are intended to provide the basic framework upon which it can formulate a comprehensive, fully coordinated defense mobility fuels strategy. These actions will be discussed with particular emphasis on DOD's efforts to develop the capability to transition to synthetic mobility fuels.

A NEW OUTLOOK ON COAL LIQUEFACTION THROUGH SHORT CONTACT TIME THERMAL REACTIONS -- CHEMICAL FACTORS WHICH LEAD TO HIGH REACTIVITY, D. D. Whitehurst, Mobil Research and Development Corporation, P. O. Box 1025, Princeton, New Jersey 08540

In the presence of certain solvents and at elevated temperatures ($\sim 400^{\circ}\text{C}$), coals can be transformed to soluble products in high yields in less than 5 minutes. This observation has led to a number of potentially new coal liquefaction processes.

The ease of coal transformation is dependent on the chemical and physical nature of the coal and the chemical nature of the solvent. Contrary to past reports, the rate of coal solubilization was observed to be dependent on the hydroaromatic content of the solvent. With a solvent having limited hydroaromatic content, maximum conversions were observed for coals having $\sim 85\%$ carbon (maf). High conversion was associated with low hydrogen consumption.

High reactivity was found to be associated with coals which swell with solvents or become plastic easily. The significant chemical properties of highly reactive coals were observed to be an intermediate aromatic carbon content, and the presence of Ar-CH_2- or $\text{ArCH}_2\text{-CH}_2\text{-Ar}$ groups.

POTENTIAL OF FURTHER CONVERSION OF SHORT CONTACT TIME SOLVENT REFINED COALS BASED ON CHEMICAL STRUCTURE. M. Farcasiu. Mobil Research and Development Corporation, Central Research Division, P. O. Box 1025, Princeton, New Jersey 08540.

Chemical structures present in short contact time solvent refined coals are different from the corresponding long contact time liquefaction products. The differences will be presented in a comparative way for both bituminous and subbituminous coals. The short contact time products contain comparatively more hydroaromatic structures and phenolic groups, but are similar in molecular size to the long contact time products. The implication of these structural features on further upgrading of the products and on possible regressive reactions should be considered in connection with choosing the right parameters: temperature, pressure, solvent and catalyst for further processing. A discussion of the thermodynamic constraints due to the chemical structures present in short contact time liquefaction products will be also presented.

UPGRADING OF SHORT CONTACT TIME SOLVENT REFINED COAL. R. H. Heck, T. O. Mitchell, T. R. Stein and M. J. Dabkowski. Mobil Research and Development Corporation, Central Research Division, P. O. Box 1025, Princeton, New Jersey 08540.

In the production of Solvent Refined Coal for use as a solid low sulfur boiler fuel, the residence time of the coal in the dissolver is dictated by the desired sulfur content of the SRC product. The coal can, in fact, be liquified at significantly shorter dissolver residence times. This short contact time (SCT) operation results in significantly lower gas make and hydrogen consumption for the SRC process.

SRC from the SCT operation contains more sulfur and oxygen than conventional SRC from the same coal. It also contains a much higher fraction of high molecular weight, highly polar asphaltenic molecules. Both thermal and catalytic upgrading of SCT-SRC were investigated. Thermal treatment reduces the molecular weight, functionality and heteroatom content, but is accompanied by excessive gas make and a decrease in product hydrogen content. However, catalytic hydroprocessing results in a significantly higher quality liquid product with a minimum of light gas production.

The use of a SCT-SRC process coupled with hydroprocessing of the SRC product provides an efficient route for producing high yields of high quality liquid fuels from coal.

PROCESSING SHORT CONTACT TIME COAL LIQUEFACTION PRODUCTS. W. C. Rovesti and H. E. Lebowitz. Electric Power Research Institute, 3412 Hillview Avenue, Palo Alto, California 94303

The authors believe that there are substantial practical applications to the use of the primary coal liquefaction products (i.e., made at short contact times) as an intermediate in the production of clean solid and liquid fuels from coal. The theme of these applications is selective treatment of the primary products to meet specific end-product requirements. Traditional coal liquefaction practice has tended toward combination of the initial liquefaction, product upgrading, and recycle media generation into a single reaction step.

A key element in the envisioned process applications is the Kerr-McGee Critical Solvent Deashing (CSD) Process. The primary liquefaction effluent is quite viscous and would be a poor candidate for filtration. Further, process solvent is imbibed in the products and cannot be recovered for recycle by vacuum distillation. Data are presented in which the CSD unit has been used to recover the ash free vacuum resid product and imbibed process solvent. In addition, the streams have been generated for internal recycle and catalytic upgrading.

Continuous bench data are presented on short contact time liquefaction of bituminous and subbituminous coals. Pilot plant data are also presented.

HYDROLIQUEFACTION OF AUSTRALIAN COALS

Norbert V.P. Kelvin

Australian Coal Industry Research Laboratories Limited,
North Ryde, N.S.W. 2113. Australia.

Introduction

Australia, like many other nations, faces an increasing demand for liquid transportation fuels with decreasing domestic crude oil production. Accordingly, efforts are now under way to investigate the liquefaction of Australian coals. Hydroliquefaction processes are considered to be likely candidates for initial commercial development because of the abundance of brown and high volatile black coals which are good hydroliquefaction feedstocks. Initial work by ACIRL indicates that a number of Australian coals can be hydrogenated to produce high liquid yields.

Batch Autoclave Screening Tests

Batch autoclave tests were done on several Australian coals ranging from low-volatile high rank to Victorian brown coals (sub lignites) (1-8). These were conducted in 4 litre stirred autoclaves in tetralin solvent under hydrogen pressure at the following conditions:

Total autoclave volume, L		3.78
Coal charge, g		500
Tetralin charge, g		1500
Initial hydrogen pressure (cold), MPa		8.3
Max. temperature °C		400
Hold time at 400°C, h		4

The yields of toluene-soluble oils are plotted against coal composition and petrography in Figures 1, 2 and 3. As expected these data clearly show that coals with high reactive maceral contents, high hydrogen/carbon ratios and high volatile matter are likely to give the highest liquid yields.

Abundance and ease of mining of the highest liquid yielding coals as determined in the batch autoclave tests indicated the most suitable coals for further testing in ACIRL's continuous bench scale reactor unit.

Continuous Reactor

ACIRL's continuous reactor unit has been described in an ACIRL report (8). The flow diagram of the unit is shown in Figure 4. Coal-solvent slurry and hydrogen are fed into the unit which produces a cooled product slurry containing all the water and light oil which is then flash-distilled in 4 kg batches in separate glass-ware. High-pressure exit gases are vented at low pressure through meters and representative samples analysed by GC.

The distillation is carried out in stages to produce light oil, water, medium (atmospheric) distillate, vacuum distillate and a residue of high boilers plus all the unconverted coal solids. Recycle solvent is made by recombining the medium and vacuum distillates. For nearly all runs conducted so far, sufficient solvent has been produced to maintain solvent balance plus a net liquid yield.

The actual excess liquids produced end up as samples for further analysis and evaluation.

The conditions under which the continuous reactor operates are :

Slurry feed rate	0.5 - 3.0 kg/hr
Hydrogen feed rate	0 - 300 g/hr
Solvent:coal ratio	1.7 - 3.0:1
Pressure	10 - 21 MPa
Temperatures :	
- preheater	500 ^o C max.
- stirred reactor	425 ^o C max.
Preheater tube dimensions	6-20 m x 6 mm I.D. x 9.5 mm O.D.
Preheater volume	0.2 - 0.6 L
Stirred reactor liquid holdup	1.5 - 3.6 L

Results

Run conditions and yield data from a batch test and a series of continuous recycle runs on a typical coal selected for continuous tests are presented in Table 1. Analyses of this coal are given in Table 2.

These data indicate that hydrogenation of this coal under recycle solvent conditions will produce about 40% distillate liquids on dry ash-free coal.

Further work is being carried out now to improve these yields to around 50% or better. The configuration of the unit and equipment limitations (temperature, pressure, hydrogen compressor capacity, etc.) for the tests reported here are considered to be in need of upgrading to achieve the higher yields. Moreover, some operational problems are also considered to contribute to lower than desired yields. These problems are discussed below.

Operability

Apart from mechanical and electrical problems that have nothing to do with what goes through the system, the major problem areas are -

1. Large losses relative to the small scale of operation (mainly in distillation).
2. Difficulty in pumping thicker slurries than 2:1 solvent:coal ratio at this small scale.
3. Preheater blockage.
4. High-pressure slurry let-down valve wear.

Losses

Generally, material balances from feed to product slurry and gases over the high-pressure system are good, 97 - 103%. Distillation losses of the order of 5% on coal are usual and almost unavoidable at this small scale. These losses are believed to be caused mainly by evaporation of light hydrocarbons and water from collecting vessels and vaporisation and inadequate trapping of medium boiling materials during vacuum distillation. In addition, some pyrolysis occurs at the later stages (at 400 - 450^oC) of vacuum distillation releasing gases which are not

easy to meter and analyse under vacuum conditions.

Slurry Pumping

We have found that our slurry circulating gear pumps can only handle slurries up to 35% solids loadings. On a larger scale 45% would be possible. At this scale the larger pumping and piping required would entail too much variable hold up of feed slurry to be able to obtain satisfactory material balances.

Preheater Blockages

Our preheater, a 20 metre length of 9.5 mm O.D. by 6.0 mm I.D. stainless steel tube wound into spirals, is heated in a cylindrical sand bath 270 mm diameter x 300 mm sand depth. We have found that preheater blockage can result from a number of factors including :

- (i) temperatures above 460°C.
- (ii) accidental pressure reduction so that too much solvent evaporates.
- (iii) sudden surges of feed hydrogen which dry out the solvent.
- (iv) stagnant slurry at above 380°C due to pumping stoppage.
- (v) attempting to pump slurry through the preheater when its whole length is at 360 - 390°C, that is when the preheater is full of gelling slurry.

Slurry valve wear

Wear of high pressure slurry let-down valves has been a very serious problem. After discharging about 20 - 100 kg slurry from 21 MPa to atmospheric pressure through our slurry let-down valves these valves are unable to hold pressure satisfactorily. At our small scale, this problem can only be solved by using gas pressure equalisation to reduce the pressure drop across the slurry valves.

Acknowledgments

Financial support for this work was provided by the National Coal Research Advisory Committee. Permission by Mr. A.H. Hams, ACIRL's General Manager and Director of Research, to present this paper is gratefully acknowledged.

The assistance of J.F. Cudmore, R.E. Guyot, I.S. Fletcher, P.A. Bennett and B.P.K. Lim is also gratefully acknowledged.

References

1. ACIRL Ltd. (1975)
"Production of Synthetic Oil and Chemicals from Coal - Batch Autoclave Hydrogenation Studies - Part 1" by R.E. Guyot and J.F. Cudmore. Report P.R.75-6
2. ACIRL Ltd. (1975)
"Production of Synthetic Oil and Chemicals from Coal - Batch Autoclave Hydrogenation Studies - Part 2" by R.E. Guyot. Report P.R.75-14
3. ACIRL Ltd. (1976)
"Production of Synthetic Oil and Chemicals from Coal - Part 3 - Relationships between Coal Properties and Hydro-Liquefaction Potential" by R.E. Guyot. Report P.R.76-8

4. ACIRL Ltd. (1977)
"Production of Synthetic Oil and Chemicals from Coal - Part 4 - Relationships between Coal Properties and Liquefaction Potential" by R.E. Guyot. Report P.R.77-1
5. ACIRL Ltd. (1977)
"Production of Synthetic Oil and Chemicals from Coal - Part 5 - Relationships between Coal Properties and Liquefaction Potential" by R.E. Guyot. Report P.R.77-8
6. ACIRL Ltd. (1978)
"Influence of Coal Characteristics on the Yields and Properties of Hydrogenation Products" by R.E. Guyot. Report P.R.78-8
7. ACIRL Ltd. (1979)
"Relationship between Coal Properties and Liquefaction Potential" by R.E. Guyot. Report P.R.79-1
8. JOINT COAL BOARD and QUEENSLAND COAL BOARD
"Survey of Australian Black Coals of Conversion Potential"
Report November 1976
9. ACIRL Ltd. (1978)
"Oil and Chemicals from Coal - Construction and Commissioning of a 1 kg/hr Continuous Reactor Unit" by N.V.P. Kelvin. Report P.R.78-2

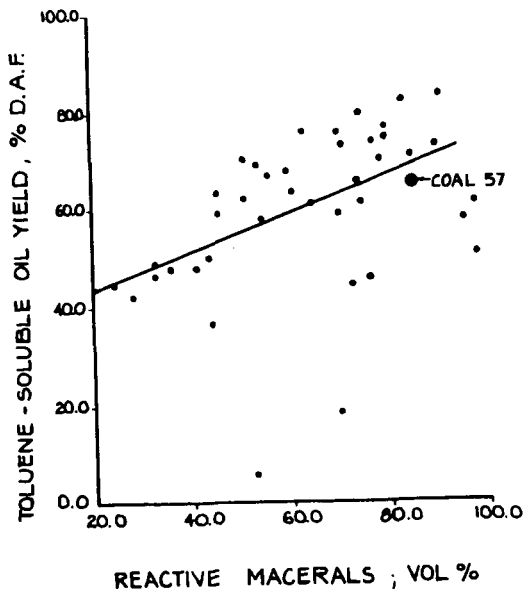


FIGURE 1 - BATCH AUTOCLAVE OIL YIELD VERSUS REACTIVE MACERALS

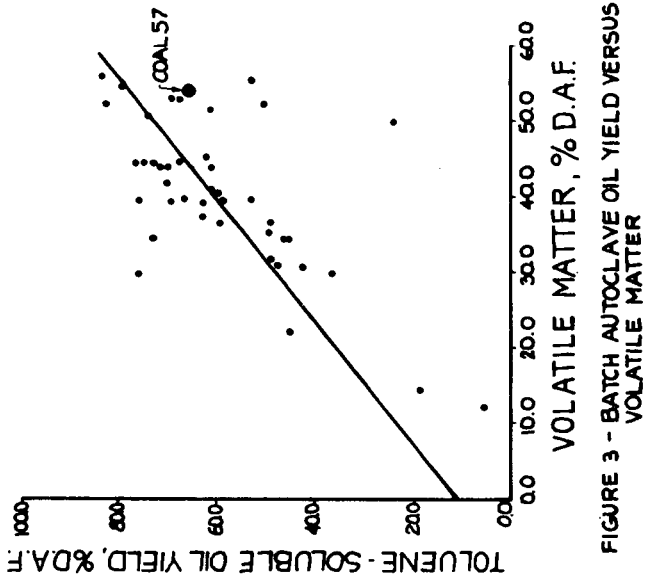


FIGURE 3 - BATCH AUTOCLAVE OIL YIELD VERSUS VOLATILE MATTER

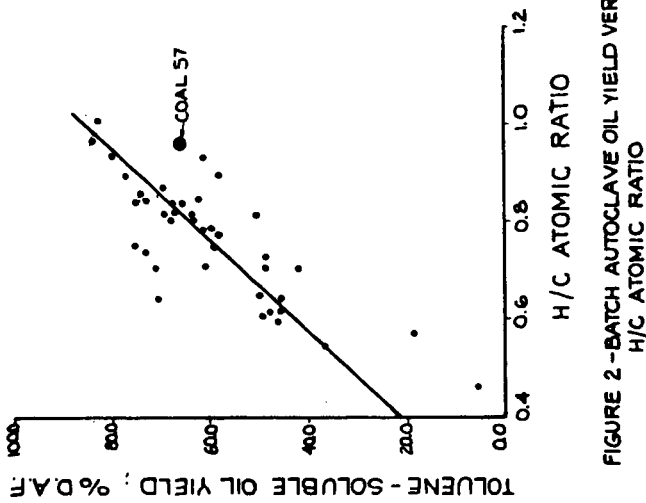


FIGURE 2 - BATCH AUTOCLAVE OIL YIELD VERSUS H/C ATOMIC RATIO

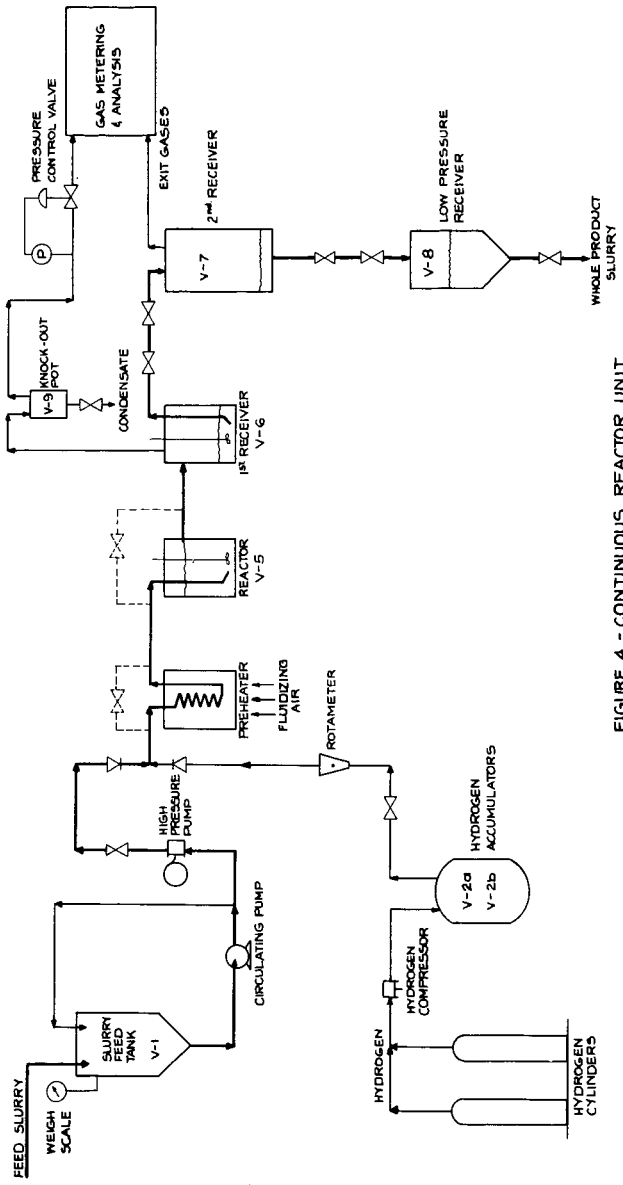


FIGURE 4 - CONTINUOUS REACTOR UNIT FLOW DIAGRAM

TABLE 1

Yield Data for Coal 57

Process Parameters	Batch	Continuous Reactor Runs			
	Test	23	25	26A	26B
Run time, h	4	83	100	216	(216)
Solvent	(T)	(R)	(R)	(R)	(R)
Solvent:coal ratio	3	2	2	2	2
Red mud, % coal	0	3	3	3	3
Feed H ₂ , % d.a.f. coal	2.6	5.5	9.6	27	43
Pressure MPa	~19	21	21	21	21
Temperatures, °C					
- preheater	-	425	440	425	425
- reactor	400	425	425	400	400
Est.slurry hold time,h	4	2	3.2	4.2	4.2
Slurry feed rate,kg/h	static	1.0	1.0	0.5	1.0
<u>Results</u>					
Product recovery,					
% of feeds	~95	100	93	99	99
Toluene conversion,	91	75	82	87	80
(% d.a.f.)					
Total distillate oil	20	30.4	29.4	36.8	35.1
yield, (% d.a.f.)					
Distillation residue,	54	61.3	47.9	41.8	54.2
(% d.a.f.)					
Water & Gases, (% d.a.f.)	26	8.2	9.7	16.2	8.4
Losses (% d.a.f.)	(N)	0.1	13.0	5.2	2.3
Est. residue pyrolysis	3	3.1	2.4	2.1	2.7
oil yield, % d.a.f.					
Total estimated oil	23	33.5	38.3	41.5	39.0
yield, % d.a.f. (E)					

Notes: (T) Tetralin solvent
 (R) Recycled distillate (ca. 200 - 600°C B.P.)
 (N) Batch data normalised to 100%
 (E) Sum of total distillate yield, 50% of losses and estimated pyrolysis oil.

TABLE 2

Analyses of Coal 57

<u>Proximate</u>	%	<u>Elemental</u>	% d.a.f.
Moisture	2.0	Carbon	78.7
Ash	18.3	Hydrogen	6.38
Volatile Matter	42.2	Nitrogen	1.25
Fixed carbon	37.5	Sulphur	0.63
		Oxygen	13.0
		(by diff.)	
<u>Petrography</u>	Vol. %	<u>Forms of Sulphur</u>	% d.a.f.
Vitrinite	67	Pyritic	0.09
Suberinite	15	Sulphate	0.01
Exinite	4	Organic	0.43
Inertinite	4		
Mineral Matter	15		

Mean maximum reflectance of vitrinite 0.54%

The Effect of Solvent Quality on Coal Conversion

C.W. Curtis, J.A. Guin, J.F. Jeng and A.R. Tarrer

Chemical Engineering Department
Auburn University
Auburn, Alabama 36830

Introduction

One factor governing the success or failure of a coal liquefaction process is the ability of the process to generate and sustain an adequate amount of a sufficiently high quality recycle solvent for continuous operation. To insure continued operability of the plant and to recognize when solvent quality is declining it is useful to have a quantitative measure of the solvent's ability to liquefy some given coal under a prescribed set of operating conditions, i.e. the solvent quality. It is obvious that the solvent quality will depend to a high degree on the solvent composition - as determined by a variety of techniques - however, the solvent's performance will also vary with coal type and operating conditions. That is, the best solvent for coal A will not necessarily be the best solvent for coal B. Extension of this idea to temperature, pressure, residence time, etc. is obvious. Thus, when speaking of solvent quality, one must, of necessity refer to a prescribed set of conditions. In general, however, there will be some finite range of solvent parameters which are more beneficial for coal conversion for a rather wide variety of coals and processing conditions.

The purpose of this study is to begin to define such a range of solvent parameters. While this set of parameters will not apply to all situations, it is hoped that they will allow a distinction to be made between a truly poor solvent and one which is satisfactory for coal liquefaction operations and perhaps some inclination as to the efficacy of a particular solvent under certain conditions.

Experimental

Coal Dissolution

Coal dissolution reactions were performed in a tubing bomb reactor which has previously been described. (1) These reactions used Western Kentucky 9/14 and Amax coals under the following conditions: temperatures - 385°C, 410°C and 450°C; reaction time - thirty minutes; agitation rate - 1000 rpm; solvent to coal ratio - 2 to 1; and an air atmosphere. The conversion of the coal was determined by comparison of the ash content of the cresol insoluble filter cake with the original ash content of the coal.

Solvents and Solvent Preparation

Four light recycle oils (LRO) from the SRC processing of Indiana V, Monterey and Amax coals were obtained from the Wilsonville SRC Pilot Plant and were used in this study. Three distillation cuts were obtained from Western Kentucky LRO: <140°C, 140°-200°C, 200°-290°C pot temperature at 1 torr. Creosote oil was successively hydrogenated to hydrogen contents between 7% and 10% in a commercial 300 cc magne-drive autoclave (Autoclave Engineers) using a commercial Co-Mo-Al catalyst and hydrogen pressures from 1000 to 3500 psi for periods of time ranging from 1 to 13 hours. Also, one solvent was prepared by dehydrogenation of cresote oil under nitrogen atmosphere.

Solvent Characterization

The solvents were characterized using standard analytical techniques. Carbon and hydrogen percentages in each solvent were determined using a Perkin Elmer 240 Elemental Analyzer. The infrared spectra of the solvents were obtained neat, in CCl_4 and in CS_2 using a Digilab FTS10 Fourier Transform Infrared Spectrometer. A Varian EM390 NMR spectrometer was used to obtain the ^1H nmr spectrum of each solvent both neat and in CCl_4 .

Results and Discussion

Dissolution Behavior of Western Kentucky Coal

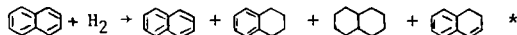
The dissolution behavior of Western Kentucky 9/14 coal was examined in the solvents listed in Table I. The dissolution behavior in each solvent is reported together with the hydrogen content of each solvent. Other conditions were the same for all reactions. Both the creosote oil solvent series and the light recycle oils are listed in order of increasing conversion.

Solvent Character

The solvents used in this study were characterized by infrared analysis, by NMR and by gas chromatographic analysis. For each solvent, the infrared aromatic C-H stretch at 3050cm^{-1} , methyl asymmetric C-H stretch at 2960cm^{-1} , and methylene in-phase stretch at 2925cm^{-1} were measured. The infrared absorbance ratios of aromatic/aliphatic (CH_3) and aromatic/aliphatic (CH_2) were calculated and are given in Table II. In every solvent, except the 90-weight petroleum oil, the aromatic absorption at 3050cm^{-1} is present. The methylene absorption at 2925cm^{-1} is present in both the creosote oil solvent series and in the light recycle oils. The methyl absorption at 2960cm^{-1} is present in the light recycle oils and in the original creosote oil, HCl, HClI and HClII, all of which contain 7% hydrogen or less. The methyl absorption is absent in the neat spectra of the more highly hydrogenated oils.

The hydrogen distribution of each solvent is given in Table III. The hydrogen distributions range from being predominately aromatic as in the creosote oil and HCl solvent to being nearly totally aliphatic as in the 90-weight petroleum oil. Average hydrogen values for three ranges of conversion, 32.8% to 48.1% (low), 64.2% to 70.0% (medium) and 79.7% to 84.5% (high) are shown in Table IV. At low conversion levels, the aromatic hydrogen is the greatest compared to other conversion levels. The α and β hydrogens increase substantially from low conversion to high conversion levels; a significant increase is also seen for the γ hydrogens. Calculation of the average chemical shift from the integrated hydrogen distribution provides a means for determining the effect of the total hydrogen distribution on conversion as shown in Figure 1. A roughly normal shaped distribution is observed for the hydrogenated creosote solvent series. As the hydrogen distribution becomes predominately aliphatic (low ppm) or aromatic (high ppm) coal conversion is adversely affected.

The weight percents of naphthalene, hydrogenated naphthalenes and decalin, in selected solvents were determined by gas chromatographic analysis. This compound series was chosen to provide an indication of the effect of degree of hydrogenation on an aromatic species that readily accepts hydrogen to form hydroaromatic and alicyclic compounds. In the oils studied, the naphthalene appeared to produce three reaction products



The weight percents of these compounds in the selected oils are shown in Table V. The original creosote oil contains 11% naphthalene with no tetralin present. As

*Retention behavior similar to dihydronaphthalene. Further identification work planned.

the creosote oil becomes increasingly hydrogenated, tetralin, decalin and a compound with retention behavior similar to dihydronaphthalene is formed. (Further work is being conducted to identify this compound.) The most hydrogenated oils, HCIV and HCIX, contain a significant percentage of decalin, 7.6% and 5.7%, respectively.

Solvent Character and Coal Dissolution

Coal dissolution behavior is a function of the character of the solvent. The solvents used in this study, characterized by the methods described, provide some indication as to the type of solvent necessary for effective coal dissolution.

The infrared ratios of the hydrogenated creosote oil series obtained from CCl_4 solution spectra show that solvents which produce conversions in the 80% range have IR aromatic to aliphatic methylene ratios ranging 0.42 to 0.27. Solvents with infrared ratios either greater or less than these values show poorer coal conversion. In general, the light recycle oils show lower conversions than do the hydrogenated creosote oils and have infrared ratios obtained from CCl_4 solution spectra ranging from 0.15 (Indiana V) to 0.50 (Western Kentucky II).

Through the hydrogen distribution of the solvents, the aromatic and aliphatic nature of the oils can be examined. From Figure 1, it is apparent that an optimum combination of aromatic and aliphatic hydrogens exists to dissolve ~80% of the Western Kentucky coal.

Brown and Ladner (2) determined that a quantitative relationship between the hydrogen distributions obtained through NMR and the infrared ratios supports the value of 0.5 which they adopted for the ratio of the extinction coefficient of the aromatic C-H stretch to the aliphatic C-H stretch. We performed a similar calculation using IR absorbance ratios obtained from neat spectra:

$$\frac{A_{AR}}{A_{CH_2}} = \frac{\epsilon_{AR}}{\epsilon_{CH_2}} \frac{(C-H_{AR})}{(C-H_{CH_2})} = \frac{\epsilon_{AR}}{\epsilon_{CH_2}} \frac{H_{AR}}{H_{\alpha+\beta}}$$

All of the light recycle oils have extinction coefficient ratios ranging between 0.59 and 0.44. Indiana V LRO has a higher ratio value of 0.77.

Through the study of the naphthalene + tetralin hydrogen donor system, the effect of the level of hydrogen donor within one such series on coal dissolution can be examined. The naphthalene-tetralin compound series is a dynamic system within the hydrogenated creosote oils in that the total weight percent of these compounds changes with degree of hydrogenation. The total amount present in the original creosote oil is 11.3% while in oils HCIV, and HCIX the total weight present is 19.78 and 14.95, respectively. Solvents with high hydrogen contents like HCIV and HCIX are likely forming naphthalene from higher molecular weight compounds. The hydrogenated creosote oils which showed coal dissolution of ~80% have a larger portion of hydrogen donors in the two ring series than do the less effective solvents.

A plot of coal conversion vs. H content is presented in Figure 2. For the creosote oil series there is an optimum in the degree of hydrogenation, probably corresponding to maximum H-donor content. For the LRO solvents, there is no clear optimum and all conversions lie below those of the hydrogenated creosote oils. The implications of the optimum range of solvent hydrogenation in plant operations are obvious. A balance between aromatic and aliphatic character must be maintained for acceptable solvent quality.

Effect of Coal Type and Temperature on Coal Dissolution Behavior

The effect of coal type on the dissolution behavior of coal was studied through a comparison of the dissolution behavior of a slow dissolving coal, Amax, and a faster dissolving coal, Western Kentucky (3). For the creosote oil solvent series, the conversion of Western Kentucky coal is consistently higher than for the Amax coal as shown in Figure 2. In addition, two light recycle oils, Indiana V and Amax, were also tested with the two coals. Indiana V shows essentially the same dissolution for both coals 54.3% for Amax and 53.1% for Western Kentucky. Amax LRO, however, was a better solvent for Amax coal (44.5% conversion) than for Western Kentucky (38.4% conversion).

Three solvents, creosote oil, HCIV and HCIX, were used to examine the effect of reaction temperature on the conversion behavior of Amax and Western Kentucky coal. Figure 3 shows that the dissolution for both coals was minimal in the creosote oil with maximum conversion occurring at 410°C. The conversion of Amax increased with increasing temperatures for both HCIV and HCIX. In contrast, in the HCIV solvent Western Kentucky coal shows lower conversion at 450°C than at 410°C. In HCIX, the conversion of Western Kentucky appears to level out between 410°C and 450°C. Even though HCIV and HVIX differ by only 0.5% hydrogen, the conversion of both Amax and Western Kentucky is lower in HCIV at the three different temperatures than HCIX. The solvent character of HCIV is somewhat more aliphatic than HCIX according to Table V and falls outside the optimum range of aromatic and aliphatic hydrogen combinations (Figure 1).

Conclusions

From the results presented above it is seen that solvent quality can be adversely affected by limited or excess hydrogenation, for example, HCl vs. HCIV. In the hydrogenated creosote oil series the decalin content provides a fairly good indication of the degree of solvent hydrogenation. However, this is not a general result since the most hydrogenated light recycle oil, Indiana V, contains no decalin and virtually none of the two ring system, in contrast to the other light recycle oils studied. Since Indiana V is the best LRO solvent for Western Kentucky coal, the absence of the two ring system strongly indicates the probable presence of additional donor species.

Examination of the various solvent parameters: hydrogen content, infrared absorbance ratio, average proton chemical shift, and proton distribution shows an optimum range for maximal conversion and are given in Table VI. It is hoped that these ranges will provide a means for evaluating solvents for effective coal dissolution.

Acknowledgements

The authors are grateful to the U.S. Department of Energy Fossil Energy Division for support of this work.

References

- 1) Guin, J.A., Tarrer, A.R., Lee, J.M., Lo, L., Curtis, C.W., I. & E.C. Proc. Des. and Devel., in press, (1979).
- 2) Brown, J.K. and Ladner, W.R., Fuel, 39, 87 (1960).
- 3) Curtis, C.W., Tarrer, A.R. and Guin, J.A., I. & E.C. Proc. Des., and Devel., in press, (1979).

Table I
Dissolution Behavior of Western Kentucky Coal in Creosote Oil,
Hydrogenated Creosote Oil and Light Recycle Oil

Experimental Conditions: Temperature = 410°		Reaction Time = 15 minutes
Creosote Oil and Hydrogenated Creosote Oil	Hydrogen Content of Solvent H %	Dissolution Behavior of Solvent % Conversion
Creosote Oil	6.74 ± 0.26	32.8 ± 2.37
HC I ^a	6.24 ± 0.13	36.9 ± 0.24
HC II	6.98 ± 0.22	48.1 ± 0.93
HC III	7.20 ± 0.30	64.2 ± 1.82
HC IV	10.00 ± 0.22	66.3 ± 1.11
HC V	7.78 ± 0.07	70.0 ± 1.11
HC VI	8.14 ± 0.22	79.7 ± 0.15
HC VII	9.41 ± 0.21	81.5 ± 0.94
HC VIII	8.34 ± 0.19	82.3 ± 0.61
HC IX	9.54 ± 0.09	82.4 ± 0.63
HC X	8.00 ± 0.22	84.5 ± 0.06
Light Recycle Oil		
Amax	7.97 ± 0.10	38.4 ± 1.4
Monterey	7.26 ± 0.49	40.0 ± 0.55
Western Kentucky I	8.74 ± 0.09	44.2 ± 0.61
Western Kentucky II	8.31 ± 0.40	46.0 ± 1.24
Indiana V	9.72 ± 0.26	53.1 ± 0.14
Western Kentucky Distillation Cuts		
I. < 140°	8.76 ± 0.09	41.0 ± 0.34
II. 140° - 200°	8.08 ± 0.14	57.9 ± 0.58
III. 200° - 290°	8.17 ± 0.27	59.1 ± 3.1
90 - Weight Petroleum Oil	12.47 ± 0.10	28.8 ± 1.4

a) reacted under N₂ atmosphere b) pot temperature, 1 mm of Hg

Table II
Infrared Absorbance Ratios of the Hydrogenated Creosote Solvents and the
Light Recycle Solvents in order of Increasing Dissolution

Solvent:	IR Absorbance Ratios ^e		
	$\frac{\text{Aromatic C-H}}{\text{Aliphatic CH}_3}$ 3050/2960	$\frac{\text{Aromatic C-H}}{\text{Aliphatic CH}_2}$ 3050/2925 ²	$\frac{\text{Aliphatic CH}_3}{\text{Aliphatic CH}_2}$ 2960/2925 ²
Creosote Oil and Hydrogenated Creosote Oils ^e			
Creosote Oil	2.23 ^b	1.54	0.68
HC I ^a	2.30 ^b	1.70	0.74
HC II	1.89 ^b	1.24	0.66
HC III	-- ^c	0.76	-- ^c
HC IV	--	0.18	--
HC V	--	0.62	--
HC VI	--	0.42	--
HC VII	--	0.27	--
HC VIII	--	0.36	--
HC IX	--	0.27	--
HC X	--	0.32	0.24
Light Recycle Oils ^f	3050/2960	3050/2925	2960/2925
Amax	0.70	0.62	0.89
Monterey	0.59	0.54	0.90
Western Kentucky I	0.55	0.48	0.88
Western Kentucky II	0.67	0.59	0.88
Indiana	0.38	0.34	0.88
Distillation Cuts			
<140° C I	0.56	0.51	0.90
140° - 200° C II	0.52	0.45	0.87
200 - 290° C III	0.43	0.34	0.79
90 Weight Petroleum Oil	-- ^d	-- ^d	0.76

- a) reacted under N₂ atmosphere
b) 2960 cm⁻¹ peak is a shoulder
c) 2960 cm⁻¹ is absent
d) 3050 cm⁻¹ peak is absent
e) solution spectra in CCl₄
f) neat spectra

Table III
Hydrogen Distribution (% H) of Hydrogenated
Creosote Solvents and Light Recycle Solvents

Solvent Creosote Oil Hydrogenated Creosote Oils	% Conversion	Hydrogen Distribution Actual Hydrogen Content in Each Fraction			
		H _{AR}	H _α	H _β	H _γ
Creosote Oil	32.8	5.0	0.74	0.74	0.22
HC I	36.9	4.7	0.75	0.75	0.13
HC II	48.1	5.0	1.0	0.70	0.26
HC III	64.2	4.5	1.2	1.1	0.43
HC IV	66.3	2.3	2.0	4.0	1.6
HC V	70.0	4.7	1.5	1.2	0.39
HC VI	79.7	4.3	1.6	1.6	0.55
HC VII	81.5	2.9	2.1	3.1	1.2
HC VIII	82.3	4.2	1.6	1.8	0.72
HC IX	82.4	2.6	2.3	3.5	1.2
HC X	84.5	3.8	1.8	1.8	0.59
Light Recycle Oils					
Amax	38.4	3.7	1.4	1.8	0.96
Monterey	40.0	3.6	1.3	1.6	0.73
Western Kentucky I	44.2	3.4	1.7	2.4	1.1
Western Kentucky II	46.0	4.3	1.5	1.8	0.66
Indiana	53.1	2.4	2.4	3.5	1.7
Western Kentucky Distillation Cuts					
I	41.0	3.7	1.8	2.2	1.1
II	57.9	3.2	1.8	2.5	0.5
III	59.1	2.5	2.2	2.5	1.1
90 Weight Petroleum Oil	28.8	0.87	0.5	5.4	3.6

H_{AR} = 6.0 to 9.2 ppm

H_β = 1.0 to 2.0 ppm

H_α = 2.0 to 3.3 ppm

H_γ = 0.5 to 1.0 ppm

Table IV
Average Hydrogen Distributions for
the Three Conversion Ranges

Conversion Range % Conversion	Average Hydrogen Distributions			
	H _{AR}	H _α	H _β	H _γ
32.8 to 48.1	4.9	0.83	0.69	0.20
64.2 to 70.0	3.8	1.3	1.8	0.81
79.7 to 84.5	3.5	1.9	2.4	0.85

Table V
Weight Percent of Decalin, Tetralin, Naphthalene and a
Hydrogenerated Naphthalene in Creosote Oils and Light Recycle Oils

Creosote Oil		Hydrogenerated			
Solvent Series	% Conversion	Naphthalene	Naphthalene	Tetralin	Decalin
Creosote Oil	32.8	11.2	0	0	0.11
HC I	36.9	10.2	0	0	0
HC II	48.0	5.7	0.45	0	0
HC III	64.2	8.4	0.25	1.7	0.085
HC IV	66.3	2.4	2.66	7.14	7.58
HC V	70.0	6.9	0.99	3.2	0.093
HC VII	81.5	1.92	1.87	7.64	5.70
HC IX	82.4	0.082	4.05	8.88	1.20
HC X	84.5	2.67	1.40	4.01	1.40
Light Recycle Oil					
Amax	38.4	18.1	0.438	4.4	0.77
Monterey	40.0	14.5	0.43	5.62	1.71
Western Kentucky I	44.2	12.3	4.8	6.03	0.61
Western Kentucky II	46.0	15.8	0.55	5.50	0.83
Indiana	53.1	2.81	0	0.093	0

Table VI

Optimum Parameter Ranges for Effective Dissolution (Conversions > 80%)
for the Hydrogenerated Creosote Oil Solvent Series

<u>Parameter</u>	<u>Range</u>
Hydrogen Content (H%)	8.00 to 9.60
Aromatic Hydrogen ($H_{AR}\%$)	2.75 to 4.3
Alpha Hydrogen ($H_{\alpha}\%$)	higher 1.7
Beta Hydrogen ($H_{\beta}\%$)	1.6 to 3.55
Gamma Hydrogen ($H_{\gamma}\%$)	0.6 to 1.25
Average Chemical Shift (\bar{H} ppm)	3.15 to 4.55
IR Absorbance Ratios (in CCl_4)	0.27 to 0.36

FIGURE 1
CONVERSION VS. AVERAGE CHEMICAL SHIFT

- CREOSOTE OILS
- RECYCLE SOLVENTS
- △ PETROLEUM OIL

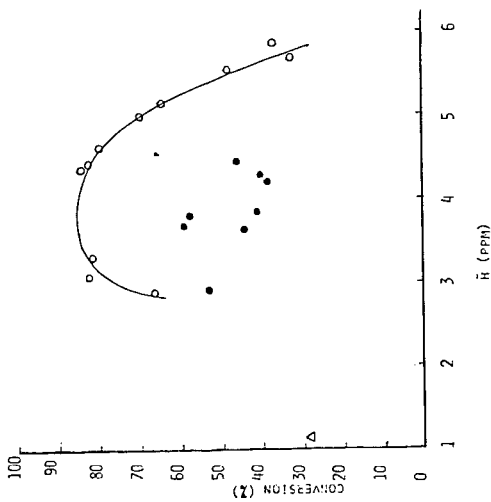


FIGURE 2
CONVERSION VS. HYDROGEN CONTENT

- CREOSOTE OILS WITH WESTERN KENTUCKY COAL
- RECYCLE SOLVENTS WITH WESTERN KENTUCKY COAL
- CREOSOTE OILS WITH AMAX COAL
- RECYCLE SOLVENTS WITH AMAX COAL
- △ PETROLEUM OIL WITH WESTERN KENTUCKY COAL
- ▲ PETROLEUM OIL WITH AMAX COAL

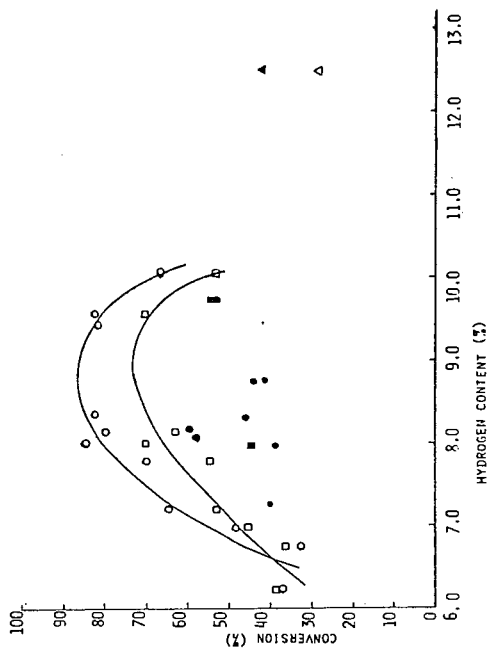
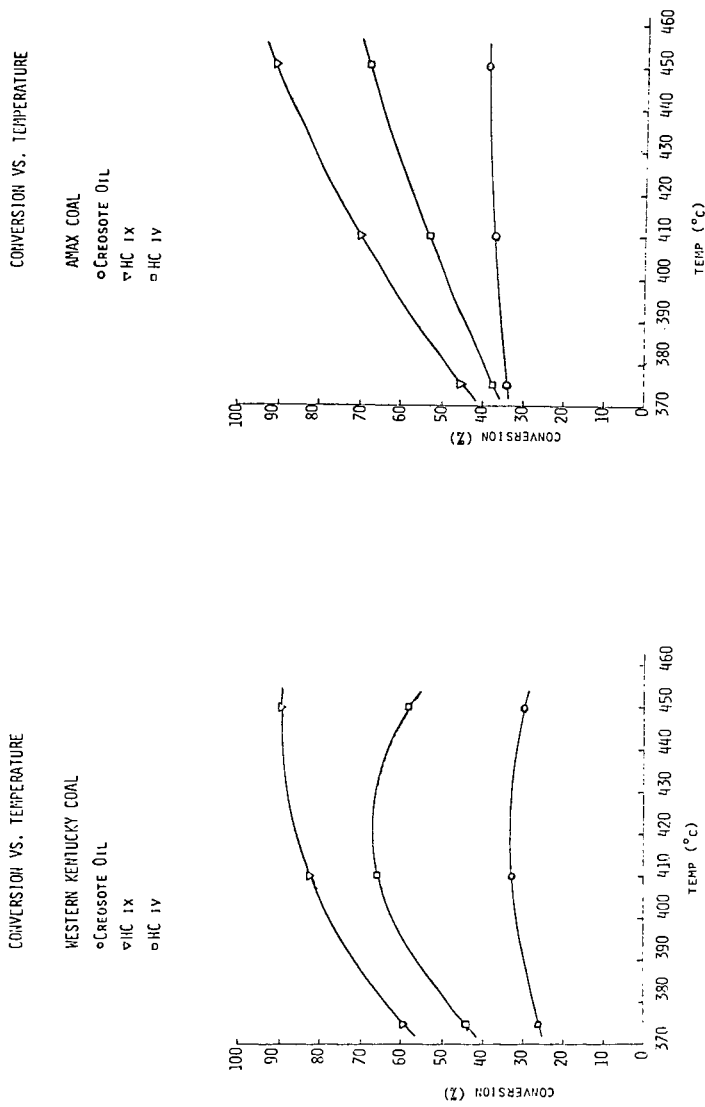


FIGURE 3



PRODUCTS OF LIQUEFACTION OF LIGNITE WITH SYNTHESIS GAS BY PRODUCT SLURRY RECYCLE

Bruce W. Farnum, Curtis L. Knudson and Del A. Koch

Grand Forks Energy Technology Center, U. S. Department of Energy
Box 8213 University Station, Grand Forks, ND 58202

Liquefaction of lignite is under study at the Grand Forks Energy Technology Center using a 5 lb coal per hour continuous processing unit (CPU) with various reactor configurations (1). The objectives of the experiment reported in this paper were (a) to test CPU operability under conditions of extensive product slurry recycle with fresh coal addition, (b) to produce a quantity of "lined out" lignite derived liquids for analytical characterization, and (c) to ascertain the function of reaction yields with the degree of line out or number of slurry passes. Objectives (a) and (c) have been discussed at a recent symposium by Willson et al. (2). A one gallon stirred autoclave reactor was operated at 460°C and 4000 psig with an average residence time of about one hour. Redistilled anthracene oil (IBP 296°C at 10 Torr.) was used as a pasting solvent for the initial pass. A 30% slurry of high ash Beulah seam lignite (10.7% ash, 29.6% fixed carbon, 29.5% moisture, 30.2% volatile matter) in pasting solvent was prepared for each pass. The lignite had been pulverized to 100% minus 60 mesh and 90% minus 200 mesh. Batch recycling was carried out through 34 cycles using the unfiltered product as pasting solvent for each subsequent pass. Gases, water and high pressure volatile oils were removed during each cycle. A mixture of equal parts of carbon monoxide and hydrogen was fed through the system at a rate of 1/2 scfm.

Separation of gas and liquid phases at 4000 psig and 300°C was carried out in the unit after the products exited the reactor (Figure 1). The gas phase was then cooled and depressurized producing a water layer, a high pressure volatile oil layer, and tail gases. Yields calculated on a moisture and mineral free coal basis were: C₁-C₄ hydrocarbons 19%, high pressure volatile oils 19%, vacuum distillate 36%, THF soluble vacuum bottoms 9%, and THF insoluble organic polymers 11%.

During Run 27 (64 hours) a slight leak in the autoclave head closure caused loss of the gas head in the reactor with the result that the liquid level rose above the level of the liquid removal tube, and the relatively poorly stirred liquid contacted the overheated wall surfaces. The reactor filled with coked slurry around the space occupied by the stirrer blade and shaft. The suspended solids (minerals and organic polymers) normally present in the product were deposited in the reactor by a process of polymerization of the organic high molecular weight material with inclusion of the mineral particles. Run 27 was terminated after the sixteenth pass. Operation of the CPU was resumed (Run 28) using product from Run 27 as pasting solvent for the first cycle. After the 34th recycle pass, conditions were changed, doubling the slurry feed rate. Coke was found in the reactor at the end of Run 28 and probably occurred for the same reason as in Run 27. However, as indicated in Figure 2 the disproportionate increase in the amount of THF soluble vacuum bottoms was not observed in Run 28, indicating this coking occurred later in the run.

Figure 2 depicts on an MAF coal basis a summation of the yields of the various product fractions obtained. Ash concentration in the product stream paralleled the THF insoluble values showing the same inclusion of inorganic fraction as coke formed in the reactor.

Gas samples were analyzed by on-line gas chromatography. Effluent water samples were characterized by standard analytical methods for waste water and

standard EPA methods (3,4). The average analysis of four samples of condensate water produced under lined out conditions is reported in Table 1.

The aromatic to aliphatic proton ratio of the high pressure volatile oils was monitored as a function of recycle pass number by infrared spectrophotometry and by proton nuclear magnetic resonance spectrometry. 90MHz proton NMR spectra were integrated over the range 9.7 to 6.4 ppm in the aromatic region (Har), 4.2 to 1.7 ppm in the benzylic region (Halp), and 1.7 to 0.25 ppm in the aliphatic methyl and methylene region (Ho). Water and phenolic OH proton signals were omitted, and solvent (deuteropyridine) contributions were subtracted from the total integrated area. Calculation of molecular parameters, f_a , sigma and Haru/Car were carried out as defined by Brown and Ladner (5).

Figure 3 illustrates the approach to constant composition of the high pressure volatile oils collected during each pass. The discontinuity of the curves following the sixteenth pass was caused by the operational problem previously discussed. Agreement of the two methods of analysis was good. A plot of IR ratio versus NMR ratio was linear with a correlation coefficient of 0.96. NMR data is listed in Tables 2 and 3. Gas chromatographic separation indicated about 269 resolved components using a 50 meter OV-101 glass capillary column. There were 30 components present in 1 to 4% concentration, 23 in 0.5 to 1%, 110 in 0.1 to 0.5%, and 106 in 0.01 to 0.1% concentration. Identification of the components of the light oil is in progress and will be reported at a future date.

Low voltage low resolution mass spectrometry provided an indication of the organic oxygen compound type distribution of the high pressure volatile oils (Figure 4). The build up of phenolic oxygen observed by mass spectrometry was also observed by measuring the phenolic OH proton concentration by NMR. The total oxygen content by neutron activation analysis equaled the organic oxygen content from LVMS plus the water oxygen content measured by Karl Fischer titration in the lined out volatile oil. The computer program for analysis of mass data was originally developed for analysis of gasifier tar (6) and accounted for 76% of the total ion current.

Determination of the molecular weight distribution (MWD) of the THF soluble fraction of the product stream was carried out using gel permeation HPLC with uv detection at 365 nm (7). The startup solvent was mostly replaced by lignite derived oil by pass number 5 (Figure 5). The THF soluble fraction of the product stream yields an average MW of 300 relative to Water's polystyrene standards.

Gel permeation chromatography of the non-distillable but THF soluble fraction of the product stream indicated an increase in molecular weight during passes 6-14 which paralleled the trend in percent vacuum bottoms. This is another indication that organic polymerization was the probable cause of coke formation in the reactor. Temperature was held constant during processing. Reactor temperature has been previously observed to be the predominant factor in lowering molecular weight in both batch autoclave studies (8) and stirred autoclave continuous process unit studies (1,2). Figure 6 illustrates the ratio of uv absorbance at 254 nm of high molecular weight to low molecular weight materials versus reactor temperature in studies carried out with the batch autoclave and the continuous stirred autoclave unit. The strong temperature dependence of the MWD between 400 and 500°C is readily observed. That a CPU yielded similar dependence can also be noted.

The ashes obtained from the feed slurry, product slurry and reactor coke material have been examined to determine if the coke contains any enrichment of Ca, Mg, Fe, or Na content. None was observed, supporting the hypothesis that coking was due to polymerization of the organic phase rather than agglomeration and deposition of minerals. Figure 7 depicts the locations where samples were obtained from coke removed from the reactor after Run 28. Three distinct differ-

ently colored regions were observed. The center (B3-1) was softer and slightly sticky, while the other areas were hard and brittle. Ash and sulfur content indicated little variability in composition of the coke from the reactor (Table 4). Analysis of the ashes of feed slurry, product slurry and coke samples with an inductively coupled argon plasma (ICAP) spectrometer after digestion indicates that the Ca, Fe, Mg and Na contents are essentially identical. The data does indicate that no build up of calcium carbonate occurred in the stirred autoclave reactor to cause reactor plugging as has been observed in tubular reactors (9). The presence of 5.7 wt. percent carbonate was observed by TGA analysis indicating carbonates were present. Since much of the sodium and calcium content of low rank coals is dispersed throughout the organic matrix as humate salts, the formation of bicarbonate-carbonate salts is expected from decarboxylation of the humates early in the process. High CO₂ and water concentrations in the reactor may account for not observing carbonate agglomeration.

Acknowledgement: We are indebted to Dr. Warrack Willson (Liquefaction Project Manager), Gene Baker, Raymond Majkrzak and James Tibbetts for operation of the CPU and calculation of yield data. We also thank Dr. Sylvia Farnum, Dr. Warren Reynolds, William Barton, David Miller, Ed Bitzan, Diane Rindt, George Montgomery and Steven Benson for contributions of data and helpful discussions.

References

1. Sondreal, E. A., Knudson, C. L., Majkrzak, R. S., and Baker, G. G., "Liquefaction of Lignite by the CO-Steam Process", A.I.Ch.E. National Meeting, Miami, Florida, November 12-16, 1978.
2. Willson, Warrack, Baker, G. G., Knudson, C. L., Owens, T. C., and Severson, D. E., "Applications of Liquefaction Processes to Low-Rank Coals." Proceedings of the 1979 Symposium on Technology and Use of Lignite, Grand Forks Energy Technology Center, Grand Forks, ND 58202, May 1979.
3. American Public Health Assn. Standard Methods for Examination for Examination of Water and Wastewater, 14th Ed, APHA, AWWA, and WPCF, Washington (1975).
4. EPA Methods for Chemical Analysis of Water and Wastes EPA #5501-0067 (1976).
5. Brown, J. K. and Ladner, W. R., Fuel (London) **39**, 87-96 (1960).
6. Miller, D. J., Olson, J. K., and Schobert, H. H., Preprints, ACS Div. of Fuel Chemistry, in press.
7. Barton, W. F., Knudson, C. L., Ruud, A. L. and Farnum, B. W. Symposium on Characterization of Coal Derived Materials, Pittsburgh Energy Tech. Ctr, May 10-11, 1979.
8. Knudson, C. L., Schiller, J. E. and Ruud, A. L. "Temperature Effects on Coal Liquefaction", in Organic Chemistry of Coal, American Chemical Society, Washington, DC, J. Larsen, Editor, 1978.
9. Dr. Ray Anderson, Pittsburg and Midway Co., Merriam, KS, Private Communication.

Table 1
Effluent Water Composition^a
(Averages of Recycle Passes 21, 24, 29 and 32)
(Concentrations in ppm)

pH at analysis	8.6
Alkalinity as CaCO ₃	80,400
Ammonia	27,300
Total sulfur	2,380
Total carbon	31,200
Inorganic carbon	12,400
Organic Carbon	18,800
Phenol	6,430
<u>o</u> -cresol	579
<u>m,p</u> -cresols	1,640

a. Analysis carried out under contract by Stearns-Roger, Inc.

Table 2
NMR Analysis of Light Oils^a

Sample	Pass No.	%Har	%H α	%H δ	fa	σ	Haru/Car	%Hphenolic
27L01	0.5	8.0	13.0	79.0	0.167	0.455	1.602	0
L02	4.2	12.7	15.7	71.6	0.264	0.416	1.395	0.79
L03	8.7	19.3	20.1	60.7	0.387	0.364	1.191	1.84
L04	13.6	22.6	20.9	56.4	0.432	0.348	1.182	2.53
28L02	18	21.7	23.2	55.1	0.415	0.393	1.224	2.08
L04	20	17.1	18.3	64.6	0.346	0.404	1.230	1.72
L06	22	19.6	22.0	58.4	0.386	0.413	1.246	2.02
L08	24	19.5	18.8	61.7	0.378	0.380	1.216	2.43
L010	26	21.9	22.8	55.2	0.406	0.392	1.282	2.51
L012	28	20.9	19.5	59.6	0.393	0.370	1.228	2.49
L013	29	21.3	19.7	59.0	0.393	0.373	1.257	2.74
L014	30	22.6	20.7	56.7	0.406	0.383	1.286	2.86
L015	31	21.9	20.7	57.4	0.398	0.376	1.286	2.63
L016	32	22.0	20.4	57.5	0.405	0.384	1.256	2.59
L017A	33	22.5	20.3	57.2	0.410	0.368	1.244	2.74
L018	34	18.6	18.9	62.5	0.351	0.378	1.363	2.07

a. Analyses performed on a Varian EM-390 Spectrometer located at the University of North Dakota Department of Chemistry.

Table 3
NMR Analysis of Unfiltered Product^a

Sample	Pass No.	%Har	%H α	%H β	f α	σ	Haru/Car
27-Y1	1	33.4	28.6	38.0	0.650	0.296	0.762
27-B2B	3	35.8	28.5	35.7	0.670	0.294	0.774
27-B2D	5	38.0	28.6	33.5	0.693	0.304	0.756
28-2B	18	42.6	28.7	28.7	0.730	0.303	0.750
28-4B	20	43.4	29.3	27.3	0.737	0.284	0.741
28-6B	22	42.7	28.8	28.4	0.734	0.287	0.734
8B	24	43.1	28.3	28.6	0.735	0.286	0.741
10B	26	43.5	27.1	29.5	0.739	0.274	0.723
12B	28	43.0	28.6	28.4	0.741	0.289	0.718
13B	29	43.9	27.7	28.5	0.746	0.278	0.713
14B	30	43.1	28.3	28.6	0.745	0.286	0.701
15B	31	42.5	28.0	29.5	0.737	0.291	0.713
16B	32	44.1	28.2	27.7	0.753	0.289	0.697
17B	33	41.5	30.2	28.3	0.718	0.295	0.770
18B	34	41.1	29.3	29.5	0.735	0.317	0.701
22B	38	41.6	30.8	27.6	0.745	0.326	0.687

a. Analyses performed on a Varian EM-390 Spectrometer located at the University of North Dakota Department of Chemistry.

Table 4
Analyses of the Feed Slurry (FS), Product Stream (PB)^a
and Reactor Coke (CK) by ICAP after High Temperature Ashing^a

Run 28										
Element/ Sample ^b	FS4	FS13	FS15	FS16	FS Ave	PB8	PB13	PB15	PB16	PB Ave
Ca, x10 ⁻³ ppm	83.1	80.3	81.6	83.4	82.1	85.0	78.8	83.2	80.7	81.9
Fe	86.2	84.7	84.5	85.5	85.2	89.0	85.4	89.5	86.2	87.5
Mg	23.4	22.8	23.0	23.6	22.9	24.1	23.0	23.2	23.2	23.4
Mg ₂	22.5	22.6	23.2	22.3		23.6	23.2	23.9	22.9	
Na	28.7	29.4	30.9	27.1		26.9	31.3	29.7	29.7	
Na ₂	27.9	29.4	30.7	27.3	28.9	27.9	31.2	29.7	29.8	29.5
Run 28 Coke										
Element/ Sample ^c	CKB1				CKB3-4					
Ca, x10 ⁻³ ppm	83.9				86.3					
Fe	83.4				87.2					
Mg	23.8				24.2					
Mg ₂	22.9				23.7					
Na	29.4				31.3					
Na ₂	24.9				30.6					

a. Determinations.

b. As an example FS4 = feed slurry on the fourth recycle pass.

c. See Figure 7 for locations where coke samples were obtained.

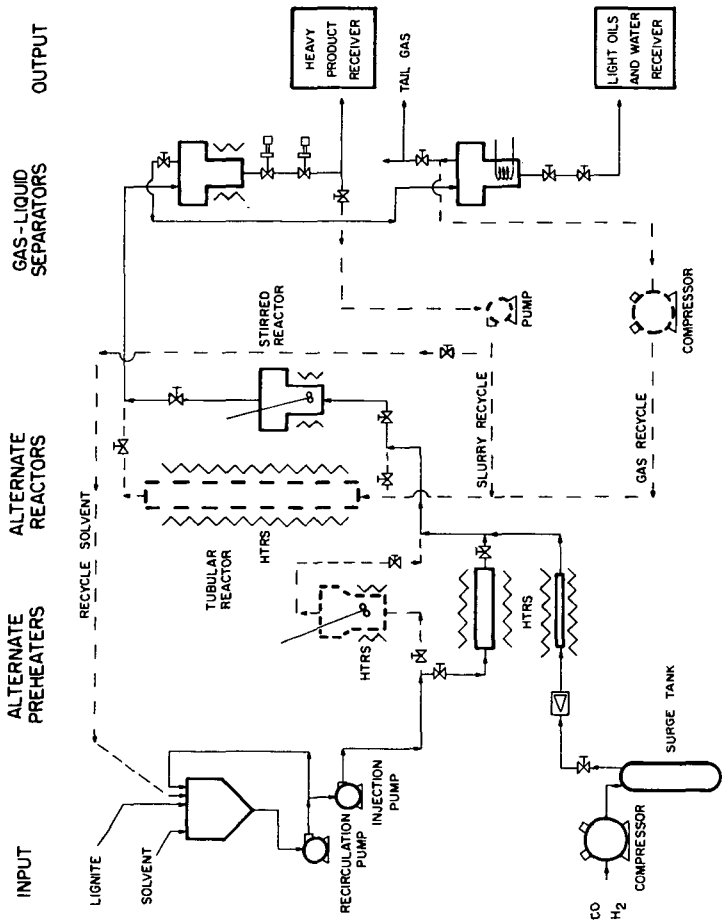


Figure 1. - Schematic diagram of the 6FETC 5-lb coal/hr continuous process unit.

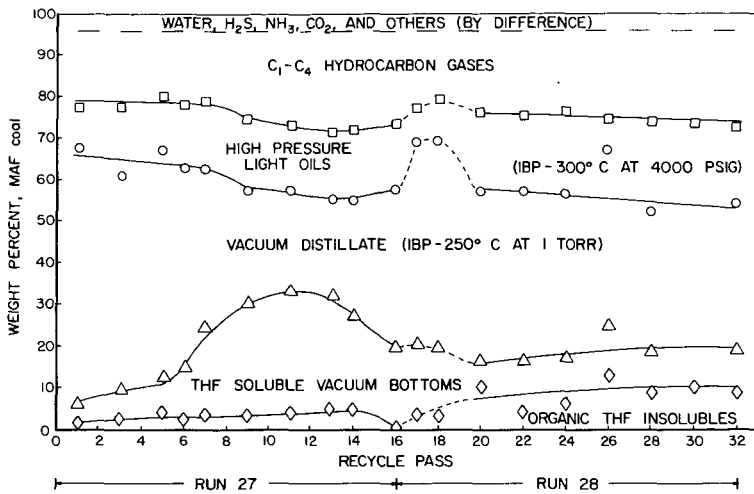


Figure 2. - Runs 27 & 28: Distribution of MAF coal conversion products versus recycle pass.

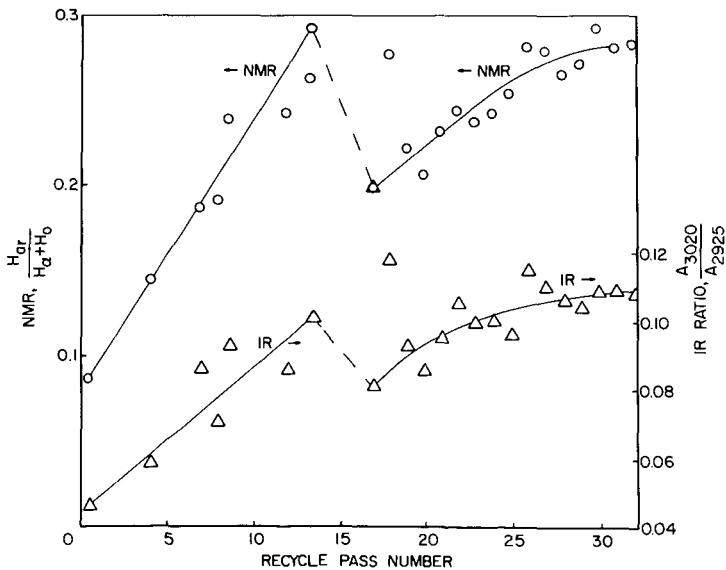


Figure 3. - Aromatic to aliphatic proton ratio by NMR and IR versus recycle pass number.

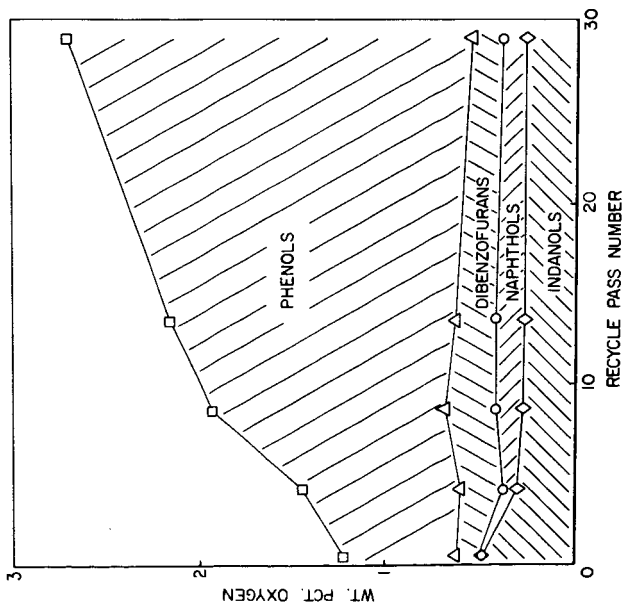


Figure 4. - Oxygen distribution in the high pressure light oils as determined by LVMS.

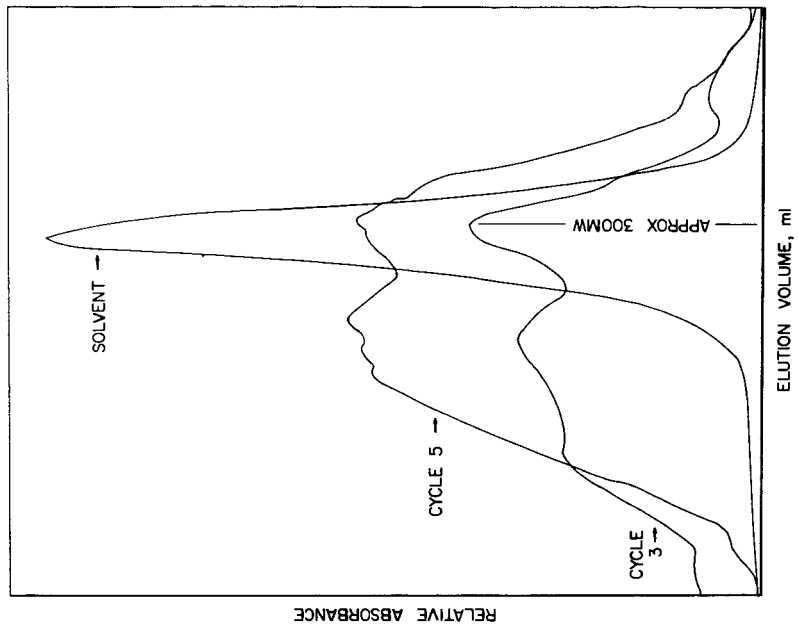


Figure 5. - Changes in the molecular weight distribution with recycle (Run 27). Detection was at 365 nm.

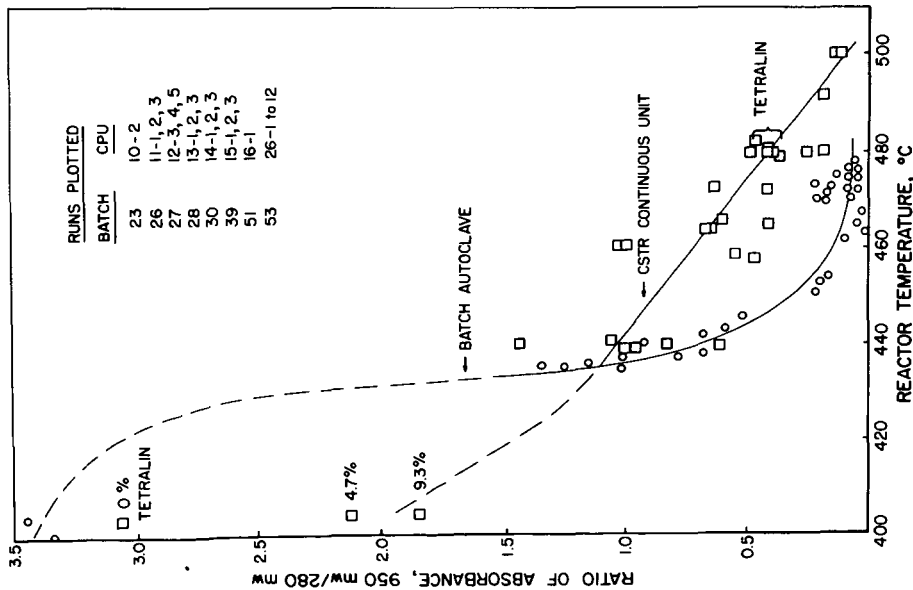


Figure 6. - Ratio of U.V. absorbance at 254 nm of 950 MW to 250 MW material versus reactor temperature for reaction times under 30 minutes.

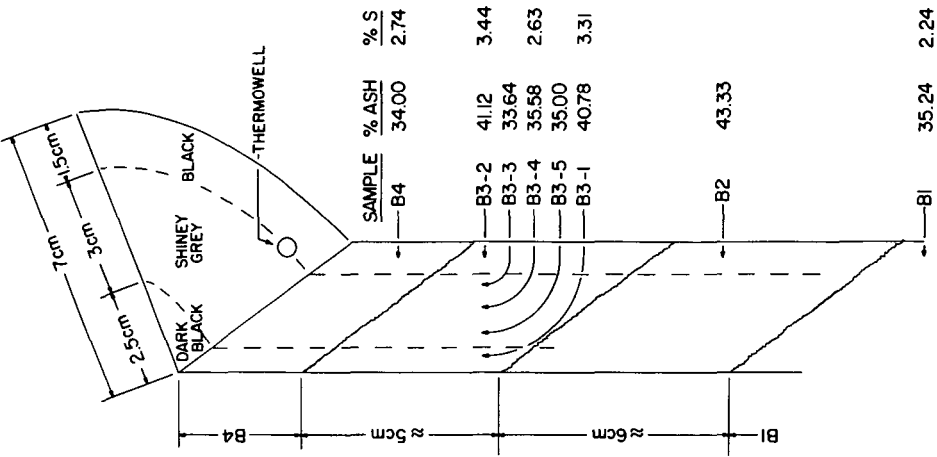


Figure 7. - Location of reactor coke samples from Run 28 and their ash and sulfur contents.

Separation of Coal-Derived Liquids By Gel Permeation Chromatography

C. V. Philip and Rayford G. Anthony

Department of Chemical Engineering
Texas A&M University
College Station, Texas 77843

INTRODUCTION

Characterization and estimation of components in coal derived products are always time consuming and complex due to the number of various constituents present in them. Most of the people working in this area try to separate coal derived mixtures into four or five fractions and each fraction is enriched with chemically similar species (1 to 7). The fractionation is achieved by either using the difference in the solubility of various components in solvents with different chemical affinities or using absorption chromatography, mainly silica gel columns or various ion exchange and ion-pair columns. The latter achieves a cleaner separation than the former. The major disadvantage of both techniques is the loss of material balance at the end of the separation and the time consuming steps involved. Development of technology on hydro-genation and solvent liquefaction of coal requires analytical techniques for the fast reliable monitoring of coal derived fluids. When solvents like tetralin are used for the liquefaction experiments the analysis of the coal derived products is complex due to the large excess of tetralin and tetralin-derived products in the liquid phase of the system. The removal of the solvent system by conventional separation methods like distillation may result in the partial or complete loss of a number of coal-derived components with boiling points close to that of tetralin. This paper discusses the use of gel permeation chromatography followed by high resolution gas chromatography-mass spectrometry for the separation and characterization of coal derived liquids.

GEL PERMEATION CHROMATOGRAPHY (GPC)

Gel Permeation Chromatography uses columns packed with swelled polymer particles with controlled pore size, formed by the copolymerization of styrene and divinylbenzene. GPC separates molecules according to molecular size based upon a distribution between a stationary phase of controlled pore size distribution and mobile liquid phase. Larger molecules elute faster than smaller molecules since larger molecules are less probable to diffuse into the liquid trapped inside the pore. Selecting the columns with proper pore size which varies from 100A to 10⁶A, the technique can be used to separate molecules over a wide range of molecular size, several million to less than 100 molecular weight. The retention volume V_r in a GPC is given by the following equation,

$$V_r = V_i + KV_p$$

where V_i is the column interstitial volume, V_p is the total pore volume and K is the partition coefficient, the ratio of the accessible pore volume to the total pore volume. All solutes elute between V_i and $V_i + V_p$. For Styragel columns the value of the ratio of V_i to V_p is in the order 1-1.3. Consequently the total number of peaks that can be separated on GPC is limited compared to other modes of LC. Relatively larger samples can be separated without sacrificing much of the resolution in about 20

to 40 minutes. Because of its operational simplicity, GPC lends itself as an efficient method for fractionating samples according to molecular size.

EXPERIMENTAL

In the separation of coal derived liquid we used two separate GPC systems. One system consists of four 100 Å μ Styragel columns and THF as the liquid phase, while the other system consists of two 100 Å μ Styragel columns and toluene phase. Two refractometers (Waters Model R 401 and R404) and a UV detector were used for monitoring the effluents from the columns. A flow rate in the range of 0.75 to 1 ml was used for both systems. The samples were injected into the systems as pure liquids or as a concentrated solution. A sample size of about 250 μ l was injected into the column for the separation of coal-derived liquids. Samples from liquefaction experiments using tetralin as hydrogen donor solvent were injected into the columns after filtration using micropore filter without any dilution. Syn-Crude from the Pittsburgh Energy Center pilot plant was obtained as a very viscous material and it was dissolved in THF and injected as a 25% solution after two filtrations using micro-pore filters. Since THF is an excellent solvent for coal-derived liquids, samples were dissolved in THF and used in the GPC system with toluene as the mobile liquid phase. A number of compounds representing various chemical species in coal-derived liquids were obtained from commercial sources and these were used without purification for GPC retention volume studies. When both THF and toluene GPC systems are used for the separation of a coal-derived sample, the fractions from one system were concentrated before injecting into the second system. In certain cases, the samples were completely evaporated and redissolved in the solvent of the second system. Most of these sample manipulations were conducted under dry anaerobic condition. The final characterization of components in various GPC fractions were done using GC and GC-MS. The methodology is expalined in earlier works (8 to 12).

RESULTS AND DISCUSSION

Resolution and percentage of recovery are the two main issues to be solved in order to achieve a successful separation of any complex mixture by chromatographic techniques. The percentage of recovery is very close to 100% for GPC systems using Styragel columns and carrier solvents such as THF and toluene. Figure 1 shows the effect of sample size on peak broadening. Four compounds - octadecane, tetradecane, phenol and tetralin - used in the study represent three major chemical species found in coal-derived products namely straight chain hydrocarbons, phenols and aromatics. The precipitation of octadecane from the mixture was prevented by adding THF (about 15%) to the prepared sample. The use of concentrated or undiluted samples does not affect the specific retention volumes or resolutions. When sample size was increased from a few milligrams to over a hundred milligrams the observed peak broadening was minimal. GPC of a sample with each component over 50 milligram showed unacceptable peak broadening. It was also found that when a sample contained a large amount of one component and other components are not in the over loading range, the resolution of the minor components were unaffected by the overloading effect of the large component.

When THF is used as the mobile liquid phase certain species can hydrogen bond with THF resulting in a larger molecular size and a lower retention volume. When nonpolar solvents like toluene are used the molecular size is more or less unaffected. The retention volume of several compounds in THF and toluene are listed in Tables I and II. The effect of solvent on specific retention volumes of various compounds are illustrated in Figure 2. It is interesting to note that rigid molecules like aromatics have smaller molecular sizes (larger retention volumes) compared to straight chain hydrocarbons of similar molecular weights (8). Phenol hydrogen bonds with THF (1 to 1 complex) resulting in a molecular size larger than a four ring aromatic hydrocarbon. Tetralin, naphthalene and toluene have the same molecular size. It could be inferred that the molecular size in a liquid phase gets a substantial contribution from the

flexible part of the molecules or the bonds with freedom of rotation. No molecular effect resulting from the solute-association with toluene was detected.

The retention volume of known compounds could be used as a guide to fractionate coal-derived liquids. Contrary to the general belief that coal-derived liquids are extremely complex and are formed of several thousands of compounds a simple concept that coal-derived liquids are simple and composed of four or five distinct chemical species such as alkanes, 'asphaltenes', phenols and aromatics was used for GPC separations. By a trial and error method, the technique of fractionating coal-derived liquids by GPC system using THF as the mobile liquid phase was perfected. Figure 3 shows the GPC of a sample from a Texas lignite liquefaction experiment using tetralin as the hydrogen-donor solvent. The sample has about 20% lignite-derived products and the rest composed of tetralin and tetralin-derived products such as naphthalene and decalin. The GPC separates the sample into five fractions. The first fraction is composed of colloidal carbons as well as high molecular weight species. Although the high molecular weight species are not completely characterized, the preliminary test shows that they are mainly of saturated hydrocarbon chains. The second fraction is composed of hydrocarbon chains as well as asphaltenes. Vacuum distillation separates saturated hydrocarbons from the non-volatile asphaltenes. The term asphaltenes is used for a spectra of compounds seen in the GPC with a wide molecular weight distribution but they are relatively non-volatile or decompose at high temperature so that their characterization by GC-MS or MS is so far unsuccessful. Using the elemental analysis of the asphaltene derived from West Virginia sub bituminous coal, can be expressed as $(C_{14}H_{15}O_xN_yS_z)_n$, where values of x, y and z are less than 1. NMR and IR spectra of the asphaltene fraction is similar to those published by other workers (1). The molecular weight distribution, as it is apparent from the GPC pattern resembles to reported values (5).

The aliphatic portion of fraction 2 and fractions 3, 4 and 5 were analyzed by GC-MS and the total ion gas chromatograms of these fractions are shown in figure 4. The peaks are identified in Tables III, IV and V. Since the separation of fractions were made on an arbitrary basis, slight overlapping of some species are expected. The aliphatic fraction is almost free of any phenols and aromatics. A portion of the lower members of alkanes such as dodecane and tridecane are present in the phenolic cut (fraction 3). Although the phenolic cut did not have any aromatics, some of the low molecular weight phenols overlap into the aromatic cut. The cut between the hydrogen donor system namely tetralin and the coal-derived aromatics encounters unavoidable overlapping due to the column overloading effect of the tetralin system, which composes almost 80% of the sample size. Any alkylated aromatic with the exception of toluene (same effective molecular size as naphthalene) has a retention volume lower than that of naphthalene and the overloading causes broadening of the peak resulting from tailing. As a result fairly good separation of aromatics from the tetralin system is obtained. Figure 4e shows the separation of tetralin system. GPC does not separate tetralin from naphthalene or other tetralin-derived products due to their close molecular sizes.

Coal derived liquids from a pilot plant were also separated by GPC followed GC-MS. Since they do not contain a large amount of any hydrogen donor solvent system as in the case of the bench scale experiments, the separation is less complex in appearance. As far as individual components are concerned there is lot of similarity in the general pattern of various coal-derived liquids. Figure 5a shows the GPC of Syn-Crude sample (Pittsburgh Energy Center pilot plant, derived from West Virginia sub-bituminous coal.) Figures 5 b to f show the GPC of the fractions. It could be concluded from these figures that the recovery of the sample injected into the columns is nearly 100%. The components in fraction 1 have a greater tendency for spreading than others.

When the GPC system using THF is used for the separation of coal derived liquids, the GC-MS of various fractions indicate reasonably good separations. But nonvolatile components could still overlap and escape GC-MS detection. If large molecular size aromatics which are nonvolatile are present in the coal-derived liquids, they may be

present in the phenolic fraction. Phenolic fractions of coal-derived liquids from experiments using tetralin contain two isomers of octahydrobinaphthyl (dimeric form of tetralin) as shown in Figure 3b. The phenolic fraction may have overlapping from the low molecular size asphaltenes. Use of a GPC system with toluene as the mobile liquid phase could solve some of these problems. GPC separation of Syn-Crude using toluene is shown in Figure 6a. The fractions were further separated by a GPC system using THF. In the toluene system both phenols and aromatics have more or less similar molecular sizes due to the absence of any hydrogen bonding between the solvent and the coal-derived products. Fraction 3 is composed of phenols and aromatics and Figure 6d shows their separation by the GPC system using THF. It could be assumed that any fraction from the toluene-GPC system should split up in the THF-GPC system if that fraction contains both hydrogen bonding and non-hydrogen bonding species. As expected, all three fractions from Toluene-GPC show signs of spreading due to hydrogen bonding in THF. Ultimately a combined use of two systems using two different solvents such as THF and Toluene can achieve a superior separation for coal derived liquids.

CONCLUSIONS

The analytical techniques have to be developed further for the characterizations of asphaltenes and nitrogen containing species. It is quite likely that the latter could be separated using appropriate solvent manipulations in the GPC systems. It was found that various coal-derived liquids have more or less similar components. Although Texas lignite varies in its BTU value as well as its ash content, a striking similarity in the composition of lignite-derived liquids was observed. Coal-derived liquids from West Virginia sub bituminous coal shows a resemblance to Texas lignite-derived liquids. The amount of aromatic species with three or more rings was detected in relatively small amounts. It could be quite possible that most coal may have a molecular structure made up of loosely bound building blocks such as alkylated phenols and alkylated aromatics (one or two ring-species predominating) and trapped long chain alkanes.

ACKNOWLEDGMENTS

The financial support of the Texas Engineering Experiment Station, the Texas A&M University Center for Energy and Mineral Resources, and Dow Chemical Co., Freeport, Texas, and The Alcoa Foundation, Pittsburgh, PA., is very much appreciated. The lignite was furnished by Alcoa at Rockdale, Texas and by Dow Chemical Co. Collaborative help of Professor Ralph Zingaro of the Chemistry Department is appreciated. Mrs. Argentina Vindiola assisted in collecting some of the data.

REFERENCES

1. Azel, T., Williams, R. B., Pancirov, R. J., and Karchmer, J. H., "Chemical Properties of Synthoil Products and Feeds," Report prepared for U.S. Energy Research and Development Administration, FE8007, 1976.
2. Baltisberger, R. J., Klabunde, K. J., Sternberg, V. I., Woolsey, N. F., Saito, K., and Sukalski, W., *Am. Chem. Soc., Div. of Fuel, Preprints*, 22 (5) 84, 1977.
3. Shultz, H., and Mima, M. J., *Am. Chem. Soc., Div. of Fuel, Preprints*, 23 (2) 76, 1978.
4. White, C. M., Shultz, J. L., and Sharkey, Jr. A. C., *Nature* 268, 620 (1977).
5. Bockrath, B. C., Delle Donne, C. L., and Schweighardt, F. K., *Fuel*, 57, (4), 1978
6. Fugmire, R. J., Grant, D. M., Zilm, K. W., Anderson, L. L., Oblad, A. G., and Wood, R. E. *Fuel*, 56, 1977.
7. Cogswell, T. E., and Latham, D. R., *Am. Chem. Soc., Div. of Fuel, Preprints*, 23, (2), 58, 1978.
8. Cox, J. H., and Anthony, R. G., *J. Appl. Polym. Sci.*, 19, 821. (1975).
9. Philip, C. V., and Anthony, R. G., *Preprints ACS Fuel Div.*, 22 No. 5, 31, Chicago, (Aug. 1977).

10. Philip, C. V., and Anthony, R. G., *TEES PUBLICATIONS, TECH BN.*, 78-2, 10 (1978).
11. Philip, C. V., and Anthony, R. G., "Organic Chemistry of Coal," *ACS Symposium Series, In Press* 258, (1978).
12. Philip, C. V., and Anthony, R. G., *Preprints ACS Fuel Div.* 24 No. 4, 196, Miami, 1978.

Table I Retention Volume in THF

<u>Compound</u>	<u>Retention Vol.</u>
Pyridine	34.7
Quinoline	33.08
Benzoquinoline	32.00
Acridine	32.00
N-Ethyl Carbazol	30.9
Aniline	30.26
Phenol	30.00
p-Cresol	29.3
Trimethyl phenol	29.0
β -Naphthol	28.64
Octanol	26.8
Tetradecane	25.0

Table II Retention Volume in Toluene

<u>Compound</u>	<u>Retention Vol.</u>
Phenol	21.5
p-Cresol	19.7
Naphthol	19.7
Tetralin	18.97
Indol	17.91
Quinoline	16.66
Octanol	16.28
N-Ethyl Carbazol	14.6
Tetradecane	14.0
Octadecane	11.66

Table III Hydrocarbon Chains Separated from GPC Fraction #2

<u>Aliphatic Fraction</u>		<u>Aliphatic Fraction</u>	
<u>Retention Time</u>	<u>Compound</u>	<u>Retention Time</u>	<u>Compound</u>
<u>(Min.)</u>		<u>(Min.)</u>	
8.0	Dodecane	33.5	Heneicosane
9.7	Tridecane	35.9	Docosane
13.7	Tetradecane	38.2	Tricosane
16.7	Pentadecane	40.4	Tetracosane
19.8	Hexadecane	42.7	Pentacosane
22.9	Heptadecane + Pristine	44.8	Hexacosane
25.7	Octadecane	46.9	Heptacosane
28.3	Nonadecane	48.9	Octacosane
31.0	Eicosane	50.7	Nonacosane

Table IV Phenolic Fraction (GFC Fraction, #3)

Retention Time (min)	Compound	Retention Time (min)	Compound
6.0	Phenol	36.9	n-Tetradecane C ₁₄ H ₃₀ + C ₁ -Alkylindanol
7.4	n-Decane	37.3	C ₅ -Alkylphenol + C ₁ -Alkylindanol
9.8	o-Cresol	38.1	C ₅ -Alkylphenol
11.2	p-Cresol + m-Cresol	39.3	C ₅ -Alkylphenol
12.9	n-Undecane	40.7	C ₂ -Indanol
14.9	C ₂ -Alkylphenol	42.4	Dimethyl Benzothiofene
17.1	C ₂ -Alkylphenol	43.2	Dimethyl Indanol
18.2	C ₂ -Alkylphenol	43.7	n-pentadecane + C ₂ -Alkylindanol
19.1	C ₂ -Alkylphenol	45.1	C ₂ -Alkylindanol
20.2	C ₃ -Alkylphenol	46.1	C ₂ -Alkylindanol
20.8	C ₃ -Alkylphenol + n-Dodecane	47.2	C ₂ -Alkylindanol
21.9	C ₃ -Alkylphenol	48.0	C ₃ -Alkylindanol
23.0	C ₃ -Alkylphenol	48.9	C ₃ -Alkylindanol
23.7	C ₃ -Alkylphenol	50.0	C ₃ -Alkylindanol + Hexadecane
24.1	C ₃ -Alkylphenol	50.9	C ₃ -Alkylindanol
24.4	C ₃ -Alkylphenol	51.8	C ₃ -Alkylindanol
25.8	C ₃ -Alkylphenol	53.0	C ₁ -Alkylinaphthol
26.7	C ₃ -Alkylphenol	54.1	C ₄ -Alkylindanol + C ₁ -Alkylinaphthol
26.9	C ₁₃ n-Tridecane	55.3	C ₁ -Alkylinaphthol
28.1	C ₃ -Alkylphenol	56.3	C ₁ -Alkylinaphthol
29.3	n-Tridecane	57.5	C ₄ -Alkylindanol
30.0	C ₄ -Alkylphenol	59.9	Dimethyl Naphthol
30.5	C ₄ -Alkylphenol	61.7	Dimethyl Naphthol
31.3	C ₄ -Alkylphenol	62.7	Dimethyl Naphthol
31.5	C ₄ -Alkylphenol	63.4	Dimethyl Naphthol
33.5	C ₄ -Alkylphenol + Indanol		
33.7	C ₄ -Alkylphenol + C ₅ Alkylphenol		
34.1	C ₄ -Alkylphenol + C ₅ Alkylphenol	81.2	Octahydro 2,2 Binaphthyl
35.3	C ₅ -Alkylphenol	83.2	Octahydro, Binaphthyl
36.2	C ₅ -Alkylphenol		

Table V Aromatic Fraction (GPC fraction #4)

Retention Time (min)	Compound	Retention Time (min)	Compound
6.1	Phenol	29.6	C ₃ -Alkylindan
6.9	C ₃ -Alkylbenzene + Phenol	30.0	C ₁ -Alkyl-naphthalene
8.9	C ₃ -Alkylbenzene	30.7	C ₃ -Alkylindan
10.1	o-Cresol	31.5	C ₃ -Alkylindan + C ₄ - Alkylindan
11.1	p-Cresol	31.9	C ₄ -Alkylindan
11.9	m-Cresol	32.7	C ₄ -Alkylindan
13.0	m-Cresol + C ₄ - Alkylbenzene	33.7	C ₄ -Alkylindan
13.7	C ₁ -Alkylindan	34.5	C ₂ -Alkyl-naphthalene
14.6	C ₂ -Alkylphenol	35.1	C ₄ -Alkylindane + C ₂ - Alkyl-naphthalene
15.6	C ₂ -Alkylphenol	35.6	C ₄ -Alkylindane
16.2	C ₂ -Alkylphenol	36.2	C ₅ -Alkylindane + C ₂ - Alkyl-naphthalene
17.4	C ₂ -Alkylphenol	37.2	C ₃ -Alkyl-naphthalene
18.5	C ₁ -Alkylindan	37.6	C ₅ -Alkylindan
20.8	Naphthalene	38.2	C ₅ -Alkylindan + C ₃ - Alkyl-naphthalene
21.4	Naphthalene + C ₅ - Alkylbenzene	38.4	C ₃ -Alkyl-naphthalene
21.9	C ₅ -Alkylbenzene	39.5	C ₅ -Alkylindan
22.5	C ₅ -Alkylindan	40.5	C ₃ -Alkyl-naphthalene + C ₅ - Alkylindan
22.9	C ₂ -Alkylindan	40.8	C ₃ -Alkyl-naphthalene
23.7	C ₅ -Alkylbenzene	41.4	C ₃ -Alkyl-naphthalene
25.0	C ₂ -Alkylindan	41.7	C ₃ -Alkyl-naphthalene
25.7	C ₂ -Alkylindan	42.1	C ₃ -Alkyl-naphthalene
26.9	C ₂ -Alkylindan	42.9	C ₄ -Alkyl-naphthalene
27.3	C ₃ -Alkylindan	44.6	C ₅ -Alkyl-naphthalene
28.8	C ₁ -Alkyl-naphthalene		

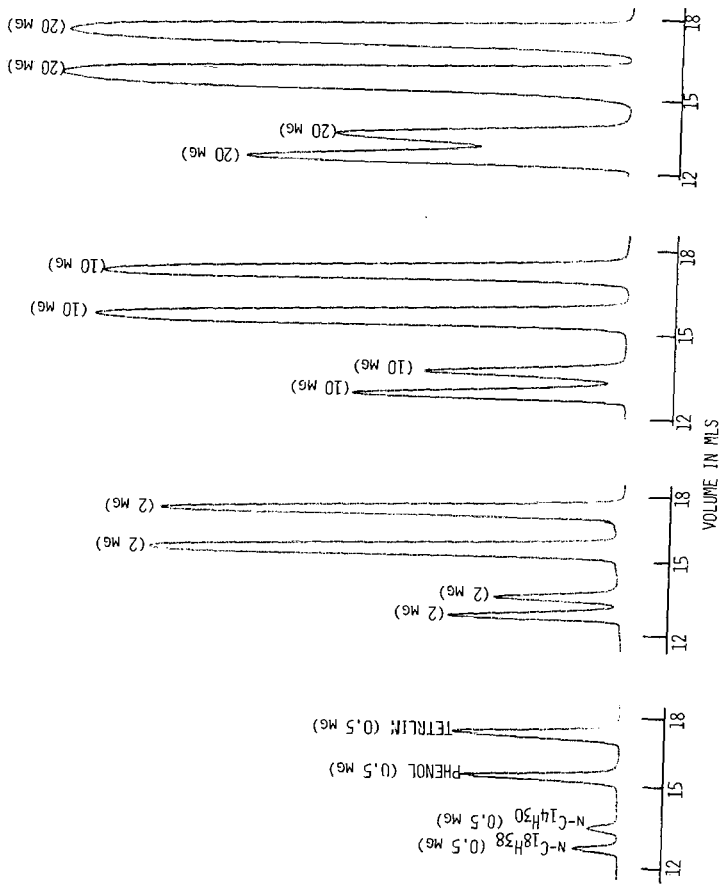


Figure 1. Effect of sample size on retention volume (V_r) and resolution. GPC system used two μ Styragel columns and THF as the liquid phase at a flow rate of 0.75 ml/min.

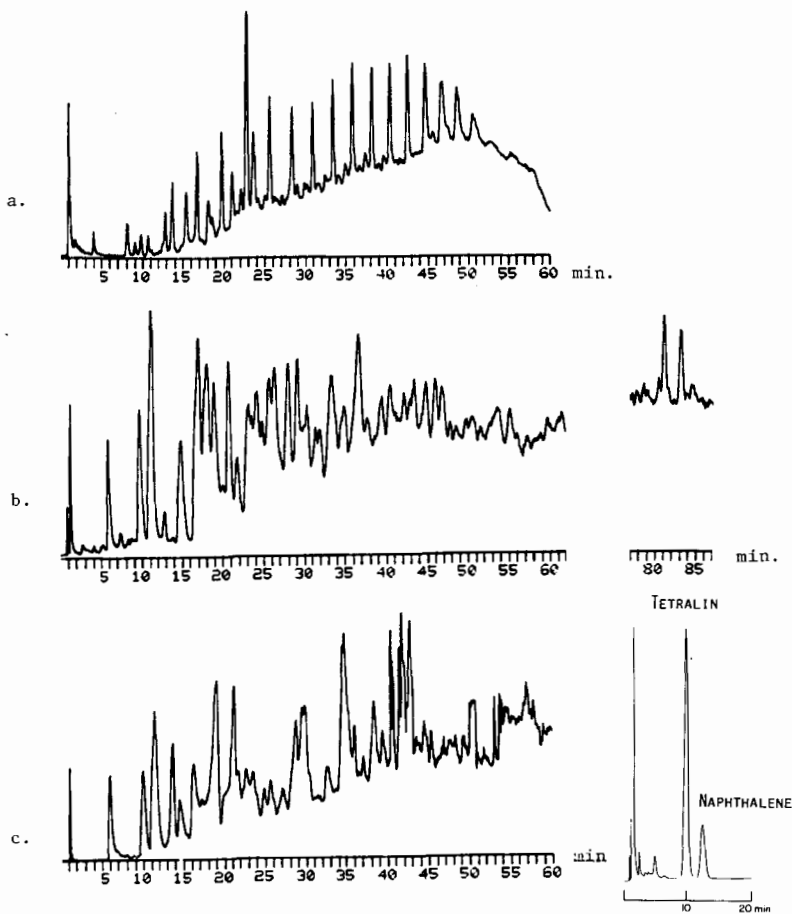


Figure 4. Total ion gas chromatogram of GPC fractions (Figure 3). Column: 5% Dexsil 300 on 100/120 Chromosorb H-WP, 1/8 in. od X 8 ft., carrier gas: 20 ml helium/min., a. Separation of hydrocarbon chains from GPC fraction #2, temperature program 80-270°C at 4 C/min. b. Separation of fraction #3, temperature program: 80-270°C at 2°C/min. for 40 min. followed by 4°C/min., c. Separation of fraction #4, temperature program 50°-270°C at 2°C/min. for 40 min. followed by 4°C/min. d. Fraction #5 was separated on a 10% SP2250 on 100/120 supelcoport 1/4 in. od X 8 ft. SS column at 160°C isothermal. Helium flow rate: 60 ml per min.

Figure 5a. Shows the separation of West Virginia sub bituminous coal-fluid by GPC using four 100 A μ Styragel columns and a flow rate of 1 ml of THF/min. The fraction 1 to 4 reinjected into the same system after concentration and the GPC's of the fractions are shown in Fig. 5b to e in the order.

Figure 6a. Shows the separation of West Virginia sub bituminous coal-derived fluid by GPC using 2 100 A μ Styragel columns and a toluene flow rate of 0.75 ml per min. The fractions were evaporated and redissolved in THF and separated by GPC system using THF solvent (as in Figure 5). The GPC's of the fractions are shown in Fig. b to d in the order. The fractions contained small amounts of toluene.

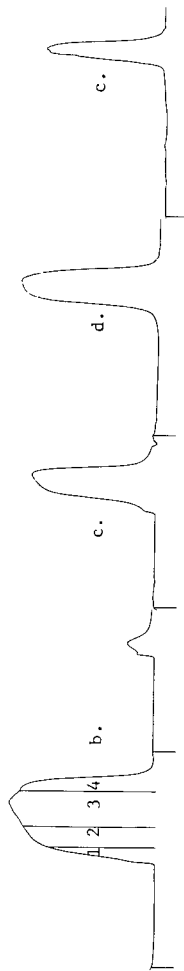


Fig. 5a.

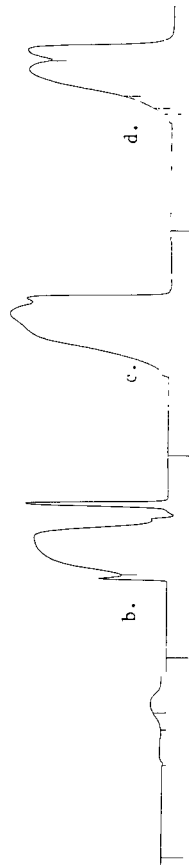


Fig. 6a.

Characterization of Upgraded Coal Liquids
Takao Hara, Krishna C. Tewari, Norman C. Li
Department of Chemistry, Duquesne University, Pittsburgh, PA 15219
Yuan C. Fu
Pittsburgh Energy Technology Center, U.S. Department of Energy
4800 Forbes Avenue, Pittsburgh, PA 15213

INTRODUCTION

The upgrading of coal liquids has become necessary in order to make acceptable fuels for home, transportation and industrial use. Several research groups have stepped up their activities in coal liquid upgrading, as evidenced by a recent symposium (1). However, only a few studies have been reported on characterization and structural analysis of the different fractions obtained in the upgrading of coal-derived liquids.

In this study, upgraded coal liquids from a blend of 30 weight percent of SRC I with 70 weight percent of SRC II, as well as from SRC II, have been studied by IR and NMR techniques. The variation of structural parameters of the upgraded liquids has been determined as a function of reaction temperature and contact time in the catalytic hydroprocessing. The results indicate that along with the decrease in heteroatom contents, asphaltene content, aromatic content and a corresponding increase in aliphatic content, the hydrogen-bonded structure and phenolic OH content of the coal liquids drastically decrease with increase in contact time and temperature. The disappearance of phenolic OH in upgrading process follows a first-order kinetics but no such dependence was observed in case of acidic NH.

EXPERIMENTAL

SRC I and SRC II were made from Kentucky bituminous coal. SRC II was a liquid product with initial boiling point of 453 K and extending into end boiling point of 665K. Elemental analysis of the two products are listed in Table 1, with the results of solvent fractionation based on solubility in toluene and pentane. The blend was prepared by adding 30 parts SRC I to 70 parts SRC II by weight at 413-423 K for 2.5 hrs. under nitrogen pressure.

SRC II and the blend were hydroprocessed over a Ni-Mo catalyst (Nalco NM504) in a trickle bed reactor at hydrogen pressure of 13.8 MPa, liquid hourly space velocities (LHSV) of 0.5, 0.75, and 1.0 hr⁻¹, and temperatures of 672 and 694 K. Prior to the hydroprocessing, the catalyst in the oxide form was presulfided with a H₂/H₂S stream. The hydroprocessing experiments were carried out during a 32-hour continuous operation.

Infrared spectra were recorded on solutions in CS₂ in a 5-mm KBr liquid cell with the solvent in the compensating beam on a Beckman IR-20 infrared spectrometer. The NMR structural parameters (2) were determined before and after hydroprocessing by using a 60-MHz FT NMR spectrometer (Perkin-Elmer R-600).

RESULTS AND DISCUSSION

Several properties, including the results of elemental analysis and solvent analysis for the two kinds of feed materials and their upgraded liquids, are listed in Table 2. The blend and SRC II are sometimes referred as F-1 and F-2, respectively. Hydroprocessed liquids from F-1 are referred as U-1 to U-4, while the upgraded liquid from F-2 is referred as U-5, according to the various hydro-processing reaction conditions as shown in Table 2. With F-1 as feedstock, increase in the H/C ratio is found with increase in contact time at 672 K, but a satisfactory increase in H/C can be obtained at higher temperature of 694 K. Values of H/C and specific gravity of U-5 are comparable to those of light petroleum crude oils such as Kirkuk and Khafji (H/C: 1.68-1.80; specific gravity: 0.85-0.89). Values of U-4 are comparable to heavy petroleum crude oils such as Eocene and Boscan (H/C ratio: 1.51; specific gravity: 0.95 - 0.99 (3). N/C ratio decreases with increase in contact time and temperature.

The IR spectra of F-1 and U-4 are shown in Fig. 1. The decrease of hydrogen-bonded structure after upgrading is seen by the dramatic decrease of broad bands of 3400 cm^{-1} (bonded OH) and 1610 cm^{-1} for U-4. The intense band of 1610 cm^{-1} for F-1 is due to the hydrogen-bonded carbonyl stretching in addition to the skeleton vibration of the aromatic ring (4).

Structural parameters were determined from NMR spectra of the coal liquids in CS_2 . There seems to be no significant difference in the parameters of F-1 and F-2. (Table 3). It should be noted, however, that the CS_2 -soluble fraction of the blend (F-1) is 89.5% and that the toluene-insoluble fraction of F-1 could not be dissolved in CS_2 . In using F-1 as feedstock, there is a gradual decrease in f_a accompanied by an increase in the degree of substitution of aromatic nucleus (σ), with increase in contact time of hydroprocessing at 672 K. At the higher temperature of 694 K, f_a of the upgraded oils from F-1 and F-2 were decreased to 0.33 and 0.17, respectively. Table 3 shows that U-5 is mainly composed of aliphatic compounds, and this is supported by the high H/C ratio (Table 2) as well as IR spectra.

Removal of phenolic OH and acidic NH groups in hydroprocessing of SRC liquids was studied kinetically by measuring the intensity of free OH and NH stretching vibrations at 3600 and 3480 cm^{-1} , respectively. The relative decrease of the OH and NH group intensities is summarized in Table 4 in relation to the contact time of hydroprocessing of F-1 at 672 K. The removal of OH group was found to follow first-order kinetics (Fig. 2). However, no such dependence was observed for the NH group. It must be mentioned that the importance of the effect of mass transfer processes or incomplete catalyst wetting has not been considered in this discussion. As shown in Fig. 2, the relative decrease in the N/C ratio also follows a first-order kinetics under the same reaction conditions. The relative reactivity of oxygen removal to nitrogen removal in hydroprocessing of F-1 at 672 K is estimated to be 2:1, from the slopes in Fig. 2.

Fig. 3 shows partial IR spectra of SRC liquids before and after hydroprocessing in rather concentrated CS₂ solutions of the same concentration (19.2 g/l). After hydroprocessing, the intensity of the 3600 cm⁻¹ peak decreases and new absorption at 2670 cm⁻¹ is found in the upgraded oils. The intensity increases with increase in contact time and temperature of hydroprocessing. The absorption in this region can be ascribed to the proton-transfer NH stretching (N⁺ H...O⁻) (5). We have previously found that when an aliphatic amine as triethylamine is added to the acid/neutral fraction of SRC process solvent, new absorptions were found at 2630, 2610 and 2505 cm⁻¹ (6) and we ascribe these to the formation of proton-transfer ionic species, (N⁺ H...O⁻). The spectrum of U-5 shows that it contains a certain amount of such species, even after almost complete disappearance of NH stretching at 3480 cm⁻¹. The implication is that the proton-transfer ionic species are formed under present hydroprocessing conditions.

Table 5 gives the infrared absorbance ratio of CH₃/CH₂ for the hydroprocessed liquids in dilute CS₂ solution. The ratio decreases from 0.87 to 0.56 with increase in contact time of processing at 672 K, using F-1 as feedstock. The result may indicate that the upgraded oils in the hydroprocessing treatment takes on a saturated cyclic structure (7).

Structural parameters in the asphaltene fractions of the upgraded liquids are given in Table 6. It is interesting to note for the asphaltenes that the values of H_{au}/C_a actually decrease with increase in contact time of hydroprocessing, whereas the reverse is true for the unfractionated liquids. There is also an increase in the number-average molecular weight of the asphaltenes which are isolated from liquids which have been hydroprocessed with a longer contact time. The changes in properties of the various asphaltenes are particularly intriguing, and we plan further experiments with the asphaltenes.

Acknowledgments

The authors thank R. F. Batchelder, J. C. Winslow, and Ray Markby for carrying out the hydroprocessing experiments at the Pittsburgh Energy Technology Center. The work at Duquesne University was supported by the U.S. Department of Energy under Contract No. EY-76-S-02.0063.A003.

References

- (1) Symposium on "Refining of Synthetic Crudes," Div. Petrol. Chem., Am. Chem. Soc. Meeting, Chicago, August, 1977.
- (2) J. K. Brown and W. R. Ladner, *Fuel*, **39**, 87 (1960).
- (3) R. S. Chillingworth, K. E. Hastings, J. D. Potts, and H. Unger, Paper presented at 71st Annual AIChE Meeting, Miami Beach, FL, Nov. 1978.
- (4) J. M. Lee, R. E. Wood, and W. H. Wiser, Preprint, Div. Fuel Chem., Am. Chem. Soc., **23** (1), 275 (1978).
- (5) Th. Zeegers-Huyskens, *Spectrochim. Acta*, **21**, 22,221 (1965).
- (6) K.C. Tewari, T. Hara, L. S. Young and N. C. Li, unpublished work.
- (7) G. Tan and A. J. de Rosset, "Upgrading of Coal Liquids." Interim Report, D. O. E., FE-25 66-12, March, 1978.

Table 1. Elemental and Solvent Analyses of SRC Products

SRC	Elemental Analysis (wt% maf)				atomic H/C ratio	Toluene-insoluble (TI)	Solvent Fractionation Distribution (wt%)		Heavy Oil [†] (HO)
	C	H	O	N			S	Asphaltene** (A)	
SRC I	85.6	6.05	5.6*	2.01	0.84	34.1	48.8	17.1	
SRC II	89.0	8.7	1.16	0.84	1.17	0.0	0.7	99.3	

*by difference, **Toluene-soluble and pentane-insoluble, † pentane-soluble

Table 2. Properties of Hydroprocessed SRC Liquids

Upgrading Conditions Temp. LHSV K hr ⁻¹	Elemental Analysis (wt% maf)				atomic H/C ratio	N/C x10 ²	Solvent Fractionation		Viscosity cp 311 K	Specific Gravity 289/289 K
	C	H	O*	N			S	TI		
F-1	87.9	7.95	2.5	1.32	0.3	1.3	10.2	18.5	71.3	1.068
U-1	672	88.9	9.7	0.7	0.61	1.31	1.6	10.9	87.5	9.5
U-2	672	89.0	10.1	~0.3	0.50	1.36	0.2	7.4	92.4	6.1
U-3	672	89.0	10.4	~0.2	0.24	1.40	0.0	5.1	94.9	5.2
U-4	694	88.5	11.3	~0	0.16	1.53	0.0	0.5	99.5	3.0
F-2	89.0	8.7	1.16*	0.84	0.28	1.17	0.0	0.7	99.3	5.0
U-5	694	87.3	12.7	~0	0.02	1.75	0.0	0.1	99.9	1.5

*by difference, **by direct method

Table 3. Structural Parameters for Hydroprocessed SRC Liquids

Sample	Proton Distribution (Area %)			Structural Parameters			
	Aromatic H_a	Benzylic H_α	Aliphatic H_o	f_a	σ	$H_o/H_\alpha + 1$	H_{au}/C_a
F-1**	38.9	27.7	33.4	0.66	0.28	2.2	0.93
U-1	21.4	29.7	48.9	0.49	0.42	2.6	0.99
U-2	19.3	28.7	52.0	0.45	0.43	2.8	1.03
U-3	15.7	24.6	59.7	0.41	0.44	3.4	0.97
U-4	12.9	19.6	67.5	0.33	0.43	4.4	1.05
F-2	37.3	29.8	32.9	0.63	0.30	2.1	0.98
U-5	4.6	9.6	85.8	0.17	0.51	9.9	0.98

*Separation point between H_α and H_o chosen at $\delta = 2.1$ ppm

**Elemental analysis of the CS_2 -soluble fraction of F-1: C 88.2, H 8.3, O 2.0, N 1.18, S 0.3. The CS_2 -soluble fractions of F-1 and U-1 are 89.5% and 99.2%, respectively. All other samples are completely soluble in CS_2 .

Table 4. Reduction of Phenolic (OH) and Acidic Nitrogen (NH) Groups in Hydroprocessing of the Blend of SRC I with SRC II

Sample	Unfractionated Liquid	
	% OH*	% NH*
U-1	19	88
U-2	11	82
U-3	4.4	48

*% of original OH and NH groups remaining in the upgraded liquids, determined by IR.

Table 5. Infrared absorbance ratio of CH₃/CH₂ for various hydro-processed SRC liquids.

Sample *	F-1	U-1	U-2	U-3	U-4	F-2	U-5
ACH ₃ /ACH ₂	0.87	0.62	0.59	0.56	0.57	0.83	0.53

*Absorbance of symmetrical stretching vibration of

CH₃ group at 2960 cm⁻¹ : ACH₃

CH₂ group at 2925 cm⁻¹ : ACH₂

Table 6. Structural parameters of asphaltene fractions isolated from upgraded SRC liquids.

Source of Asphaltene	Proton Distribution (Area%)		Structural Parameters				Mol. Wt.	
	Aromatic Ha	Benzyllic H _α	Aliphatic H _β	fa	σ	Ho/H _α +1		Hau/C _α
F-1	37.9	38.1	24.0	0.76	0.40	1.6	0.64	820
U-1	33.9	36.0	30.1	0.75	0.39	1.8	0.57	1130
U-2	34.0	32.0	34.0	0.75	0.36	2.1	0.54	1180
U-3	34.0	32.5	33.5	0.75	0.36	2.0	0.54	1160

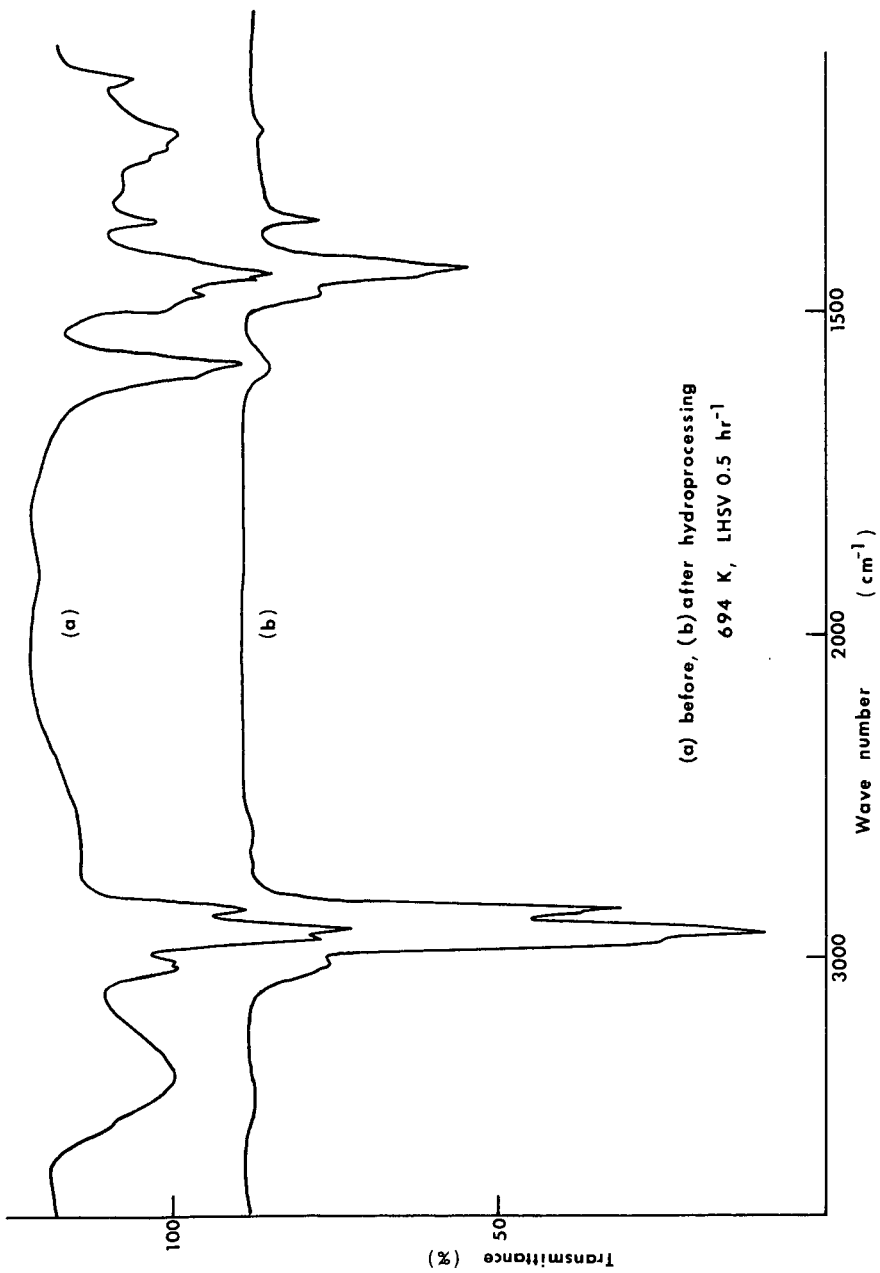


Fig. 1 IR spectra of the blend of SRC I with SRC II before and after upgrading

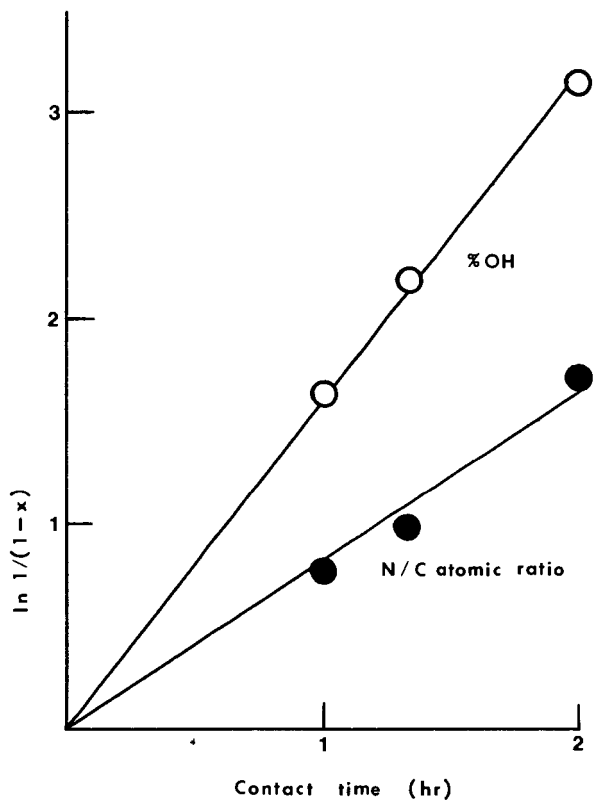


Fig. 2 First-order plot of removal of oxygen and nitrogen

Feed F-1, 672 K

x % conversion

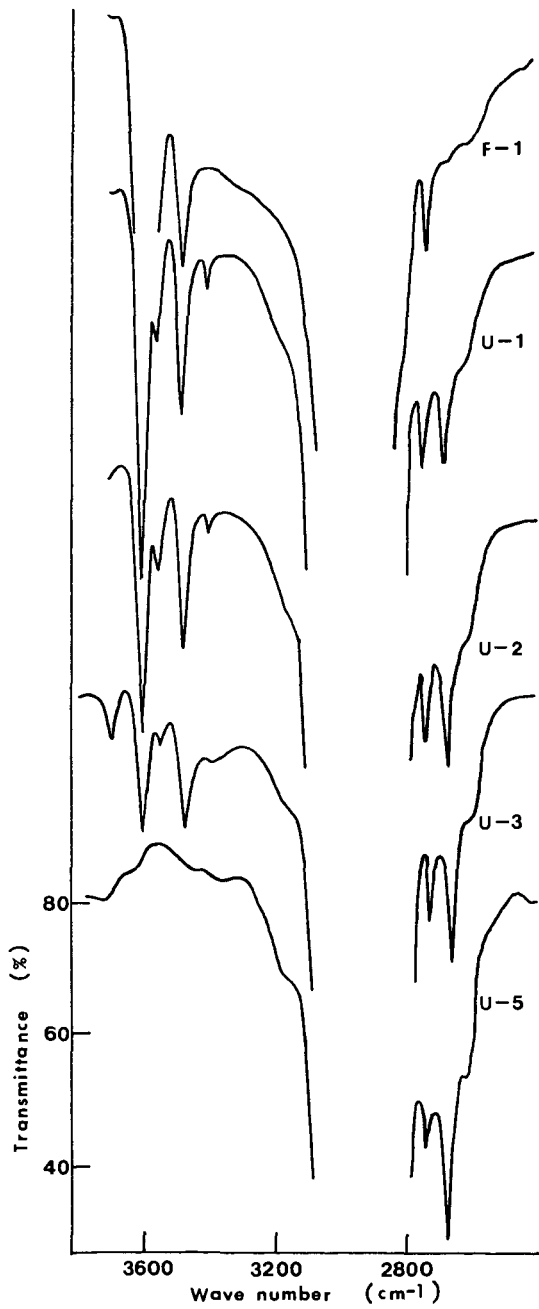


Fig. 3 Formation of proton transfer species (NH⁺) in hydroprocessing
Solvent C₅H₂, 19.2 g/l

A LOW TEMPERATURE REACTION PATH FOR COAL LIQUEFACTION*

M. G. Thomas and R. K. Traeger

Sandia Laboratories, Albuquerque, NM 87185

Introduction

The interaction of coal and solvent to form a gel in the 250-350°C range has significant implications in the efficiency of short residence time or two-stage liquefaction processes and the operation of preheaters in existing coal liquefaction processes. This interaction has been noted (1,2) during the heating of coal slurries in autoclaves where an apparent "endotherm" appears in the time-temperature curve--the "endotherm" is currently believed to be due to a high viscosity gel reducing heat transfer to the thermowell in the autoclave. Evaluation of these transitions leads to the following qualitative results.

1. Coal Effects - As the reactivity (to benzene solubles) toward liquefaction of the coal increases, the temperature of the transition increases;
 - Lignites do not exhibit a measurable transition.
2. Solvent - Transitions are not noted with pure hydrogen donor solvents as tetralin;
 - Magnitude of the transition increases as dissolving ability of the solvent increases.

Work by Cronauer (3) and Whitehurst (4) suggests initial solvent coal reactions which form adducts.

This paper summarizes the results of initial experiments on coal-solvent interactions. Results of low temperature (300°C) batch studies are compared to results obtained from 400-450°C, short residence time continuous reactor studies.

Materials

Three coals of varying reactivity were reacted with pure and coal-derived solvents; analyses are shown in Table 1 (5).

Table 1. Analyses of Coals and Solvents

Ultimate	Illinois #6 Burning Star	West Va. Ireland	Bruceton	SRC II Heavy Distillate	Creosote #4 Cut
Carbon	71.5	73.0	81.3	89.9	90.8
Hydrogen	4.8	5.2	5.3	7.6	5.8
Nitrogen	1.5	1.2	1.6	1.4	1.1
Sulfur	3.3	4.5	1.2	0.4	0.4
Ash	10.0	10.0	3.7	.05	< .05

Three non-coal-derived solvents used were hexadecane, phenanthrene--both C.P. grade--and tetralin, technical grade.

Table 2 summarized results of autoclave liquefaction studies on the three coals.

* This work supported by the U.S. Department of Energy.

Table 2. Coals

Coal	Autoclave Results(5)			Transition Temp.(2) in Creosote Oil, #4 Cut (°C)
	Time	Temp (°C)	% Conv to ØH Sol	
Illinois #6 Burning Star	30	430	-	300
West Virginia Ireland Mine	30	430	64	240
Bruceton	30	430	44	200

Experimental

Two systems were used. The first was a glass system constructed with Schlenk apparatus. A 100 ml flask was topped with an adiabatic (silvered) reflux column. A thermocouple was inserted directly into the slurry and the system was continuously flushed with argon at 1 atmosphere. Slurries contained approximately 9g coal and 22g solvent. The system was stirred with a teflon-coated stir bar in the slurry. (When high viscosities were reached, this method was ineffective.) This apparatus was also employed for heating the dry coals to 300°C. In these cases, a thin layer of coal covered the bottom of the flask and the thermocouple was in direct contact with the flask.

The second system was a four-stage continuous flow reactor. Slurries of 30% coal/70% solvent were employed. Procedures and results are given in reference 6.

Analysis

Products have been analyzed by exhaustive Soxhlet extraction with benzene, followed by a THF extraction of the benzene insols (7) and a separation of benzene sols into pentane sols and insols (7). Some samples were filtered using a pressure filter fitted with #50 Waltman filter paper. Viscosities were measured with a Brookfield LVT viscometer.

Stability of Coal and Solvents

Experiments on the coal and solvent individually were carried out to determine if reactions observed were due to the individual components. Results shown in Table 3 indicate no significant chemical reaction occurs below 370°C and heating to 300°C does not result in THF solubility. However, softening is noted in the 300-330°C range.

Table 3. Thermal Response of Coals and Solvent

Coal	DSC (Broad Endotherm)	Maximum Rate of Wt Loss TGA	Temperature of Maximum Expansion by Dilatometry	Changes in Solubility Observed After Heating to 300°C
Ill #6 BS	~ 370°C	~ 450°C	300°C	None
W. Va.	~ 370°C	~ 450°C	-	None
Bruceton	~ 370°C	~ 450°C	330°C	None
SRC II Heating Dist	Boiling heating to 450°C	Boiling Range 290-550°C; no change noted in heating to 450°C.		

Solvent-Coal Studies at Low Pressures

Results of studies made under inert gas at one atmosphere are shown in Table 4.

Table 4. Low Temperature Liquefaction Results

Coal	Solvent	Temp °C	Time Min.	% Soluble Based on MAF Coal	
				% Benzene	% THF
Solvent Effects					
Bruceton	Hexadecane	200	15	0	0
	Tetralin/ Phenanthrene	200	15	-0.4	11
	SRC II H.D.	200	15	-6.0	25
Coal Effects					
Bruceton	SRC II	200	15	-6	25
W. Va.		260	15	-12	22
Ill #6		300	15	-4	19
Ill #6		300	300	-6	23
Temperature Effects					
Bruceton	SRC II	25	0	0	0
		25	15	4	12
		50	15	8	13
		93	15	7	12
		120	15	6	13
		130	15	4	11
		170	15	3	13
200	15	-6	25		

The data from the low temperature experiments show the following:

- Solvent: (a) A non-reactive solvent as hexadecane does not dissolve the coal. Tetralin/phenanthrene mix is a good hydrogen donor but does not give as large a THF conversion as the SRC II heavy distillate.
(b) Increased THF conversion is accompanied by increasing solvent loss (benzene solubles).
- Coal: The least reactive coal (Bruceton) toward liquefaction at higher temperatures is dissolved more readily at lower temperatures. This agrees with the transition temperatures noted in autoclave heatup curves.
- Temperature: Approximately 13% of the coal can be extracted in 15 minutes with THF and this solubility does not increase with temperature until the autoclave transition temperature is reached; THF solubility increases and solvent is lost.

High viscosity products were noted when the THF solubility exceeded 20%; the products contain a high preasphaltene/oil ratio. This condition was only observed when the temperatures equaled or surpassed temperatures where endotherms had been observed in autoclave experiments with the respective coal/solvent systems.

Continuous Reactor Data

If the reactions are thermally activated and no significant mechanism changes occur between 300 and 400°C, short time 400°C effects should be similar to the 15 minute low temperature data just described. Product distributions from the reactor runs with Ill. #6 coal, Figure 1, show that preasphaltenes are produced at short times, apparently at the expense of solvent. These distributions result in high viscosities.

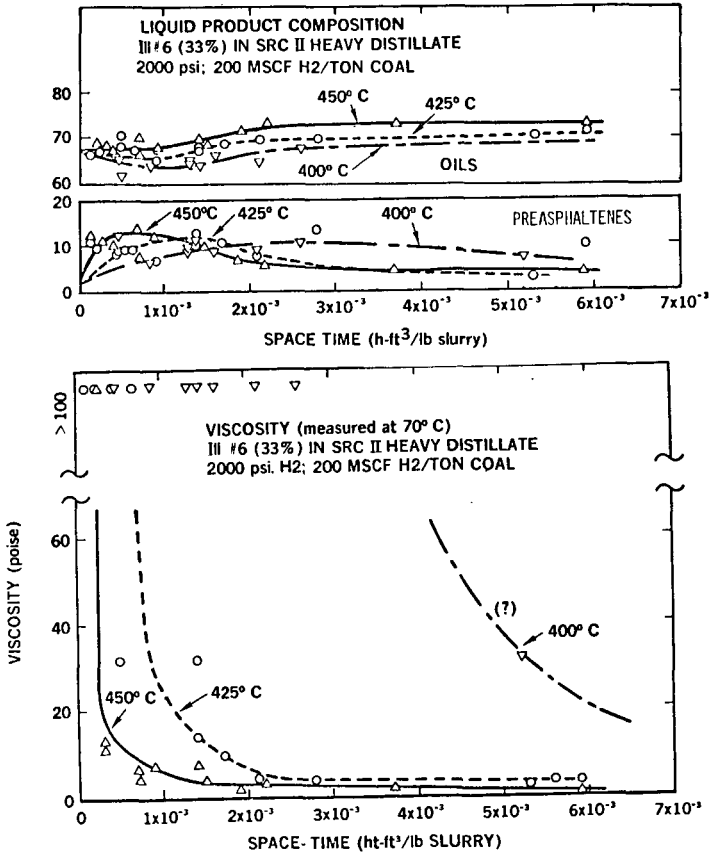


Figure 1

Thus, these continuous reactor data, at short reaction times, agree qualitatively with the low temperature, batch data. Initial regressive reactions have been noted in solvent imbalance during pilot plant short residence time preheater studies (8).

Evaluation of conversion data from the continuous reactor indicate the asphaltene concentration in the slurry product is independent of temperature and dependent on conversion at short times (benzene conversions of 0-55%). These data (Figure 2) suggest a series reaction sequence from coal to asphaltenes.

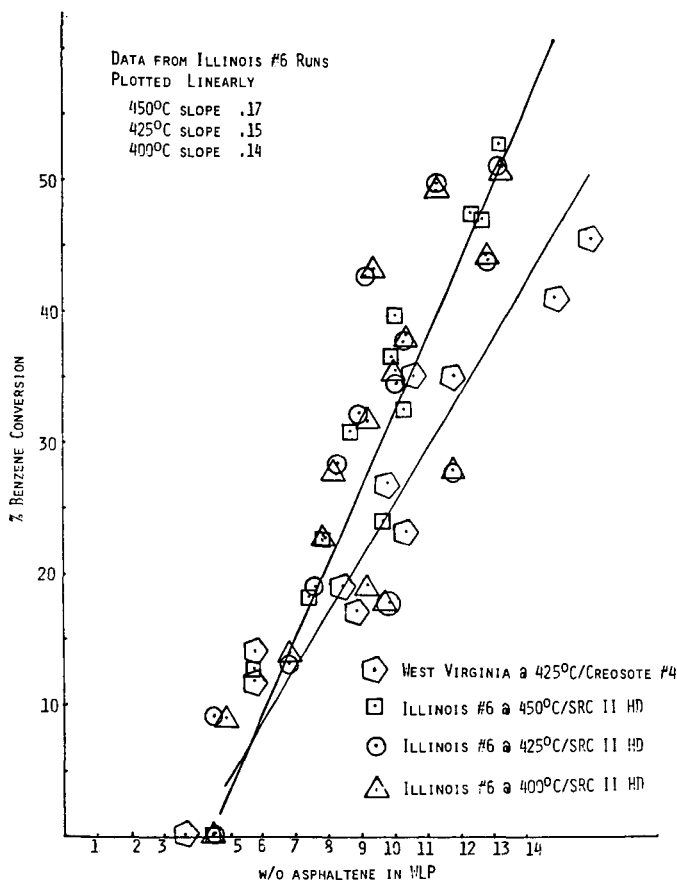
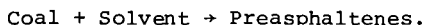


Figure 2

Discussion

Onset of a solvent-coal reaction occurs in the 200-300°C temperature range. The temperature and extent of this reaction are dependent on the coal and solvent. In this initial reaction, THF soluble products increase but solvent is lost indicating formation of a THF soluble, coal-solvent reaction product. This reaction product, defined in the preasphaltene or asphaltol compounds, results in high viscosity products--possibly gels.

A number of kinetic studies of coal liquefaction (Cronauer) processes made at long reaction times (< 10 min) show the liquefaction mechanisms can be represented by parallel reactions of coal to pre-asphaltenes, asphaltenes, oils and gases. However, these data show coal itself does not undergo thermosolvolytic at temperatures to 300°C and free radical processes need not be invoked to explain the reactions observed in the 200-300°C range. The data do suggest an initial series reaction of



The hydrogen donating capability of the solvent does not appear to be critical at this stage, but functional groups that can interact with the coal and cause swelling are important.

This initial series reaction is also indicated in the short time, continuous reactor results, Figure 2, where the preasphaltene content rises along with a solvent loss early in the reaction; subsequent decrease in preasphaltene content is accompanied by an increase in oil and asphaltene concentrations. The asphaltene content (and similarly the oil) is defined by the benzene conversion at 400, 425, and 450°C. The dependence of asphaltene and oil on conversion and not on temperature further suggests that the reaction of coal to preasphaltene goes to completion. Product distributions derived from two sources--coal and preasphaltene--would almost certainly be dependent upon temperature.

Preasphaltene chemistry needs further clarification. The extent, and possibly type, of coal-solvent interaction changes with temperature. Only about 30% THF conversion occurs at low temperatures with 80-95% conversion occurring over 400°C.

Conclusions

Coal liquefaction is initiated at 200-300°C by the reaction of solvent and coal to form preasphaltenes. The temperature of the reaction is a function of the coal type and the solvent. This reaction product imparts high viscosity to the slurry and its chemistry may influence subsequent liquefaction reactions. Understanding of this initial reaction is important to evaluate the applicability of advanced, two-stage liquefaction processes and could lead to the development of new, low temperature and pressure liquefaction schemes.

References

1. C. H. Wright and D. K. Schnalzer, "Short Residence Time SRC-I: Background and Recent Work," Proceedings of the DOE Project Review Meeting on Coal Liquefaction Preheater Studies, Oak Ridge, TN, March 21, 1979.
2. B. Granoff, unpublished data, Sandia Laboratories.
3. D. C. Cronauer, R. G. Ruberto, Y. T. Shah, "Reaction Mechanism Studies of Liquefying of Belle Ayr and Burning Star Coals," Proceedings of EPRI's Conference on Coal Liquefaction, Palo Alto, CA, May 1978.
4. D. D. Whitehurst, "Relationships Between the Composition of Recycle Solvents and Coal Liquefaction Behavior," Proceedings of EPRI's Conference on Coal Liquefaction, Palo Alto, CA, May 1978.

5. B. Granoff, P. M. Baca, M. G. Thomas, and G. T. Noles, "Chemical Studies on the Synthoil Process: Mineral Matter Effects," Sandia Laboratories Report SAND-78-1113, June 1978; R. K. Traeger and R. M. Curlee, "Preheater Effects in Coal Liquefaction Processes," Sandia Laboratories Report SAND-78-0312, March 1978.
6. R. K. Traeger and R. M. Curlee, "Preheater Studies in Coal Liquefaction," Sandia Laboratories Report SAND-78-1124, June 1978.
7. M. G. Thomas and G. T. Noles, "Sandia Fossil Fuel Analytical Laboratory Procedures Used in Coal Liquefaction Analyses," Sandia Laboratories Report SAND-78-0098, April 1978.
8. G. A. Styles and W. H. Weber, "Short Residence Time Studies Utilizing the Dissolver Preheater at the Wilsonville SRC Pilot Plant," Proceedings of the EPRI Contractor's Conference on Coal Liquefaction, Palo Alto, CA, May 1978.

THE SELECTIVITY OF COAL MINERALS AND SRC RESIDUE
ASHES FOR HYDRODESULFURIZATION IN THE SRC PROCESS

D. Garg, A. R. Tarrer, C. W. Curtis,
J. M. Lloyd, and J. A. Guin

Chemical Engineering Department
Auburn University
Auburn, Alabama 36830

INTRODUCTION

Many improvements have been made in the Solvent Refined Coal (SRC) process over the past year. During this time period, several solid/liquid separation techniques have evolved that offer promise for cost reduction in ash removal. Concurrently, technical feasibility for the Kerr-McGee's process for critical solvent deashing has been demonstrated on a pilot scale at the Wilsonville SRC facility. Since this separation process can be used to fractionate liquified coal as well as for deashing, a fraction of the liquefied coal could be used as make-up process solvent. As a result, process solvent regeneration appears no longer to be a limiting operational factor for the dissolver stage (1). Now the dissolver performs three basic functions: liquefaction of coal, regeneration of the process solvent and desulfurization of coal liquids. Several studies have shown that liquefaction occurs very rapidly while desulfurization occurs slowly. Thus, now that the Kerr-McGee's process can be used to offset solvent deficiencies, desulfurization may limit dissolver operations, particularly when a solid SRC is produced.

Hydrogen generation for SRC processing is a major operational cost, making short reaction times with minimum hydrogenation severity desirable. The overall objective of this study is to develop a methodology for using mineral additives to increase the rate of desulfurization during coal liquefaction. Some iron containing minerals, including the ash of SRC residue, have been shown to act as in situ sulfur scavengers (2). The addition of such minerals to the dissolver feed may allow sulfur removal requirements to be met with shorter reaction times and consequent lower hydrogen consumption.

The role of mineral additives in coal liquefaction processing is to increase desulfurization with minimal but sufficient hydrogenation. Selectivity is a measure used to rate the effectiveness of the different mineral additives studied. By definition, selectivity is the ratio of the amount of sulfur removal to the amount of hydrogen consumed for a given reaction time.

In previous studies, the effects of relatively large amounts of mineral additives on reaction rates have been examined (3) in order to clearly delineate the effects of the additives. However, in actual application, such large amounts would be prohibitive due to the associated material handling difficulties. Therefore, one of the major objectives of this work is to demonstrate that only small, easily processed, amounts of mineral additives are required for effective sulfur scavenging, provided that the iron contained in the additives is in a form available for reaction and is present in stoichiometric amounts.

EXPERIMENTAL

Reagents and Materials

Light recycle oil (LRO) and Western Kentucky 9/14 coal were obtained from the Wilsonville SRC Pilot Plant, operated by Southern Services, Inc. The LRO contains

0.2 % sulfur and the Western Kentucky coal is analyzed to be 67.8% C, 4.9% H, 3.10% S and 12% mineral matter. The coal was dried overnight at 100°C and 25 inches Hg vacuum before use.

Coal minerals, SRC residue ash; magnetite; pyrite; hematite; reagent grade Fe_2O_3 ; commercial Fe_2O_3 catalyst; and reagent-grade reduced iron, were used as mineral additives for hydrogenation and hydrodesulfurization reactions. Commercial grade Fe_2O_3 (Fe-0301T, 20% Fe_2O_3 mounted on activated alumina) was obtained from the Harshaw Chemical Company. This catalyst was ground to various particle sizes to study the effect of mass transfer on the reactions. Hematite was obtained from Cities Services and magnetite, from Chemalloy Chemical Company. SRC residue obtained from the Wilsonville SRC Pilot Plant was oxidized before use. Hydrogen gas of 99.995% purity was obtained from Union Carbide. All other chemicals were reagent grade.

Equipment

A small tubing bomb reactor and a commercial 300 cc magnedrive autoclave (Autoclave Engineers) were used for all reaction studies and have been previously described (2-4). Varian gas chromatographs (Models 1800 and 920) were used for analysis of liquid and gas liquefaction products. The sulfur content of coal and liquefaction products was determined by using a Leco Sulfur Analyzer (Model 532). Elemental analyses of various mineral additives were determined by energy dispersive X-ray fluorescence analysis (EDXRF). The surface area of the mineral additives was determined by the nitrogen adsorption technique.

Reaction Conditions:

Coal liquefaction reactions were performed for time periods ranging from 15 to 120 minutes, at 410°C and with stirring rates of 1000 rpm except during mass transfer studies when the reactions were stirred at different rates ranging from 600 to 1400 rpm. The autoclaves were charged with 40g of coal, 80g of LRO, and 10g of additive. Benzothiophene desulfurization was studied in a small tubing bomb reactor (12ml capacity). The benzothiophene reaction, 10% benzothiophene in dodecane with appropriate amounts of mineral additives, was performed at 1250 psi hydrogen pressure (at room temperature) and 410°C for 30 minutes.

RESULTS AND DISCUSSION

Effect of the Amount of Additive

Elemental iron has been shown to act as an effective *in situ* sulfur scavenger (2-4). The effect of different amounts of iron on the sulfur content of the total liquid products from coal liquefaction reactions is shown in Figure 1 where the ratio S/S_B is plotted versus Fe/Fe_S . These ratio terms are defined as: S is the weight percent of the residual sulfur; S_B , residual sulfur for the baseline case, i.e. no iron present for the same reaction conditions; Fe, the weight percent of iron added; Fe_S , the stoichiometric amount of iron required to react with the sulfur to be removed. Fe_S is computed on the following basis: 1) the organic sulfur content of the coal is 1.23%; 2) pyritic sulfur of the coal, 0.79%, is reduced to the FeS form; and 3) the sulfur content of the solvent is 0.27%. The residual sulfur (S/S_B) decreased significantly (from 0.79 to 0.53) with increasing amounts of iron ($\text{Fe}/\text{Fe}_S = 1.3$ to 20). The decrease in residual sulfur content is most significant when Fe/Fe_S is less than 10. When Fe/Fe_S is increased from 10 to 20, a decrease of only 0.07 occurred in S/S_B which is just slightly more than the standard deviation of S/S_B (± 0.02). Therefore, in this range, additional amounts of iron appear to have little effect on sulfur removal.

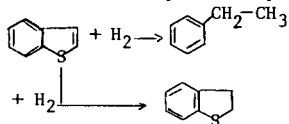
The effect of different amounts of Fe_2O_3 on residual sulfur is also shown in Figure 1. No significant decrease in residual sulfur occurs, when 71% of the stoichiometric required amount of iron is present as Fe_2O_3 (i.e. $\text{Fe}/\text{Fe}_S = 0.71$).

It should be noted that the surface area of the Fe_2O_3 used in this study is $8.9 \text{ m}^2/\text{gm}$. (Table I) Apparently, since no hydrogen sulfide (H_2S) is present in the product gases when stoichiometric amounts of iron are present, all of the iron present in the form of relatively high surface Fe_2O_3 reacts with any H_2S formed. Furthermore, essentially the same degree of desulfurization occurs with a stoichiometric excess of Harshaw iron catalyst, which has a surface area of $60 \text{ m}^2/\text{gm}$, as that obtained with an equivalent amount of Fe_2O_3 . Therefore, the greater surface area of the Harshaw catalyst does not appear to have any significant effect on desulfurization, because equivalent amounts of iron are available in both cases to react with the H_2S produced in the reactor.

The effect of different amounts of iron and Fe_2O_3 on the final hydrogen partial pressure and, consequently, on total hydrogen consumption is shown in Figure 2. The same amount of hydrogen is consumed in either the presence or absence of iron: $H_f/H_o = 0.58 \pm 0.02$, where H_f and H_o are the final and initial hydrogen partial pressures, respectively. Under the same reaction conditions, more hydrogen is consumed when Fe_2O_3 is present: $H_f/H_o = 0.45 \pm 0.01$; however, approximately the same amount of hydrogen is consumed irrespective of the amount of Fe_2O_3 present. Since hydrogen consumption does not depend on the quantity of Fe_2O_3 present, Fe_2O_3 is not significantly reduced at the reaction conditions used. Since more hydrogen is consumed with Fe_2O_3 , the selectivity of iron (sulfur removal per hydrogen consumption) is higher than that of Fe_2O_3 , provided that sufficient iron, i.e. $\text{Fe}/\text{Fe}_S=10$, is present (Fig. 3).

Model Compound Studies

The hydrogenation of benzothiophene under different reaction conditions and with different catalysts produces a variety of products including ethylbenzene, dihydrobenzothiophene, styrene and phenylethanethiols (5,6). Using the iron additives listed in Table I and the reaction conditions stated, the major products observed in this study are ethylbenzene and dihydrobenzothiophene.



The conversion of benzothiophene to these reaction products as catalyzed by the different mineral additives is given in Table I. The mineral additives, Fe_2O_3 and Co-Mo-Al, promoted complete conversion of benzothiophene to ethylbenzene. However, complete conversion to ethylbenzene does not result when iron is the mineral additive; in fact, only 45% of the benzothiophene is converted to ethylbenzene with no significant dihydrobenzothiophene formation. In the benzothiophene reaction, the amount of iron used is considerably less than the amount found necessary for maximum desulfurization of coal/oil reaction mixtures. The Fe/Fe_S for the benzothiophene reaction is 2.7 compared to the optimum Fe/Fe_S of 10 observed for the coal/oil slurries. While in the range of $\text{Fe}/\text{Fe}_S < 10$, desulfurization has been shown in the coal/oil reactions to depend on the amount of iron present. This result is verified in the benzothiophene reaction as given in Table II, where the conversion of benzothiophene is shown to vary significantly with the amount of iron present during the reaction. The conversion of the benzothiophene increases from 23% to 54% with a corresponding increase of Fe/Fe_S from 0.72 to 2.7. Furthermore, when a Harshaw catalyst is used and iron is present in the amount of $\text{Fe}/\text{Fe}_S = 0.37$, a low conversion of benzothiophene is observed; whereas, complete conversion to ethylbenzene occurs when approximately twice the required stoichiometric amount, $\text{Fe}/\text{Fe}_S = 1.9$, is used. As observed in the coal/oil reactions discussed previously, the higher surface area Harshaw Fe_2O_3 catalyst does not result in any significant increases in the desulfurization of the benzothiophene system.

Iron sulfide additives, pyrite and FeS_{1+x} , do not react with the H_2S product, and, as previously reported (3,4), are not as effective in increasing desulfurization

rates as iron and Fe_2O_3 . The results given in Table II concur with these conclusions. In the presence of the iron sulfide additives, the benzothiophene is converted primarily to dihydrobenzothiophene -- a product of hydrogenation -- instead of ethylbenzene -- a product of hydrodesulfurization. In contrast, when iron or Fe_2O_3 is present during reaction, the primary product is ethylbenzene.

Effect of Reaction Time

The rate of hydrodesulfurization of coal liquids is generally consistent with that of petroleum feedstocks: both substances are considered mixtures of sulfur-containing compounds, each of which reacts at a rate proportional to its concentration. The rate of the total sulfur removal can be approximated as if there are only two reactive components.

$$r_{\text{HDS}} = \alpha_1 K_1 C_S + \alpha_2 K_2 C_S$$

where C_S is the total concentration of the sulfur-containing compounds; α_1 and α_2 are the fractions of reactive and unreactive components, respectively; K_1 and K_2 are the rate constants of the reactive and unreactive components (7).

The parameters, α_1 , α_2 and K_1 , K_2 , vary according to the additive present during reaction as shown in Figure 4. When Fe_2O_3 is added, more sulfur is removed in the first 15 minutes of reaction than in two hours when no additive is present. In addition, considerably less hydrogen is consumed when Fe_2O_3 is present in a 15 minute reaction than after two hours without any additives (See Figure 5). The hydrogen consumption with Fe_2O_3 is 20% as opposed to 44% for no additive. The use of mineral additives such as Fe_2O_3 is beneficial, in that shorter reaction times are needed for desulfurization with less total hydrogen consumption. Furthermore, these minerals can be added without any sacrifice in coal conversion as shown in Figure 6.

Influence of Mass Transfer

The three phase reaction system present in coal liquefaction may be influenced by mass transfer effects. To determine whether mass transfer regulation is occurring, experiments were performed using different stirring rates and different particle sizes.

A direct test to determine the importance of gas/liquid transport was performed by varying the stirring rates while holding all other variables constant. As can be seen in Table 5, for stirring rates between 600 and 1400 rpm, neither the rate of desulfurization nor hydrogen consumption is very sensitive to and, consequently, is not affected by agitation rate. Therefore, gas/liquid mass transport has no apparent influence on either hydrogenation or desulfurization.

Generally, decreasing the catalyst particle size increases the effectiveness factor and the liquid/solid mass transfer coefficient. Reducing the particle size will increase the observed reaction rate when the reaction is controlled either by liquid/solid mass transport or by pore diffusion. However, reducing the particle size is not a definitive test for pore diffusion. Although the behavior of Fe_2O_3 is more like a reactant than a catalyst, the absence of particle size effects should be indicative of the absence of liquid/solid mass transfer control.

A series of experiments were performed with different Fe_2O_3 particle sizes to determine the effect of particle size on desulfurization. The rate of desulfurization is observed to be essentially independent of particle size as shown in Table IV. The rate of hydrogen consumption does vary slightly with different particle sizes.

Since the observed desulfurization rate is independent of both the Fe_2O_3 particle size and the stirring rate (within experimental error), it appears that

desulfurization is neither pore diffusion nor liquid/solid mass transfer controlled, implying then that the reaction is kinetically controlled. The rate of hydrogen consumption may be somewhat limited by mass transfer since it is influenced by particle size. An indication of the importance of particle size on hydrogen consumption rate is demonstrated in Table V. The rate of hydrogenation increases with decreasing particle size.

Comparison of Activities of Different Coal Mineral Additives

Coal mineral residues from the SRC process and ashes from the residues and Western Kentucky 9/14 coal were added to the coal liquefaction reactions to determine their effect on desulfurization and hydrogen consumption. An elemental analysis of the additives is given in Table VI. The iron content of these additives ranges from a low of 3.37% in SRC residue to a high of 26.92% in Western Kentucky ash while the sulfur content ranges from 0.47% in SRC ash to 3.81% in Kerr-McGee residue. The apparent differences in the elemental composition of SRC residue and Kerr-McGee residue observed in Table VI may be accounted for when the source of each is considered: SRC residue is obtained from filtration and Kerr-McGee residue is obtained through solvent deashing. In both cases, the residues were ashed to eliminate the carbonaceous coating and to convert the minerals to an oxide form for sulfur scavenging.

A comparison of the activity of different coal mineral additives is given in Table VII. In the cases of no additive, SRC residue, and Kerr-McGee residue, the organic sulfur removed from the system is essentially identical. The same is true for hydrogen consumption. After ashing, both the Kerr-McGee and SRC residue ashes show increased activity for sulfur removal; from ~ 23% for the residue to 43% for the ashes. Two possible reasons for these differences are: 1) the carbonaceous coating may not completely dissolve under reaction conditions, in effect, inhibiting sulfur scavenging or 2) the change in mineral form upon oxidation may provide the correct form for sulfur scavenging. Although the iron concentration in the Kerr-McGee residue ash is approximately three times higher than that of the SRC residue ash, the sulfur removal is essentially the same. This fact may be due to the difference in coal type, the mineral forms in the coal feedstock and the mineral forms present after processing and ashing. Mineral inhibitors may also be present in the Kerr-McGee residue ash that limit sulfur removal. Another possible reason for the same sulfur removal even with different iron contents for the two ashes is that the sulfur content of the Kerr-McGee residue ash is greater than that of the SRC residue ash.

The activity of iron, magnetite (Fe_3O_4) and Fe_2O_3 is compared in Table VIII. Fe_2O_3 and Fe show essentially the same amount of sulfur removal although their surface areas differ by more than an order of magnitude. In contrast, magnetite has a surface area between that of Fe and Fe_2O_3 but does not have the ability to remove sulfur like Fe_2O_3 . It appears from Table VIII that magnetite is not as effective as a sulfur scavenger as Fe; however, since equivalent amounts of iron, Fe/Fe_S , are not used and sulfur removal is sensitive to the amount of iron present when $\text{Fe}/\text{Fe}_S < 10$, more experimental data is needed to compare their relative activities. Both magnetite and Fe have a low surface area and low hydrogen consumption while Fe_2O_3 has a relatively high surface area and a much higher hydrogen consumption. Since hydrogenation appears to be somewhat limited by mass transfer, the differences in selectivity among Fe, magnetite and Fe_2O_3 may be due to the effects of mass transfer.

ACKNOWLEDGMENTS

This work was supported by the Department of Energy. The authors wish to acknowledge the technical assistances of Don Colgrove and David Watson of the Auburn University Chemical Engineering Department.

REFERENCES

1. Lebowitz, H.E., and Kulik, C.J., "Improved Coal Liquefaction Technology" EPRI Contractor's Meeting, May 1979.
2. J.A. Guin, A.R. Tarrer, J.W. Prather, J.R. Johnson and J.M. Lee, I & EC, Process Des. Dev., 17 (2), 118 (1978).
3. J.M. Lee, A.R. Tarrer, J.A. Guin and J.W. Prather, ACS Div. Fuel Chem, Preprints, 22 (6), 120 (1977).
4. J.M. Lee, H.F. Vanbrackle, Y.L. Lo, A.R. Tarrer and J.A. Guin, Symposium of the 84th National AIChE Meeting; Atlanta, Ga., Feb. 26-March 1, 1978 (51b).
5. Daly, F.P., Journal of Catalysis, 51, 221-228 (1978).
6. Furmisky, E. and Amberg, C.H., Can. J. Chem., 54, 1507 (1976).
7. Schuit, G.C.A., and Gates, B.C., AIChE Journal, 19, 3, 417, May, 1973.

Table I: EFFECT OF MINERAL ADDITIVES ON THE HYDRODESULFURIZATION OF BENZOTHIOPHENE

ADDITIVE	Fe/Fe _s	BENZOTHIOPHENE CONVERSION,%	PRODUCT DISTRIBUTION OF CONVERTED BENZOTHIOPHENE,%		
			DIHYDROBEN- ZOTHIOPHENE	ETHYL- BENZENE	HYDRODESULFUR- IZATION,%
NONE	-	0.0	0.0	0.0	0.0
CO-MO-AL	-	100.0	0.0	100.0	100.0
Fe ₂ O ₃ (Reagent grade)	1.9	100.0	0.0	100.0	100.0
Fe	2.7	45.0	5.0	95.0	43.0
Reduced Pyrite,	-	42.0	65.0	35.0	15.0
FeS _{1+X} Pyrite, FeS ₂	1.2	40.0	90.0	10.0	8.0

Benzothiophene: 0.45g
Additive: 0.5g

Table II: EFFECT OF Fe AND Fe₂O₃ ON HYDRODESULFURIZATION OF BENZOTHIOPHENE

ADDITIVE	Fe/Fe _s	BENZOTHIOPHENE CONVERSION,%	PRODUCT DISTRIBUTION OF CONVERTED BENZOTHIOPHENE,%		
			DIHYDROBEN- ZOTHIOPHENE	ETHYL- BENZENE	HYDRODESULFUR- IZATION,%
NONE	-	0.0	0.0	0.0	0.0
Fe(3%)	0.72	23.0	39.0	61.0	14.0
Fe(6%)	1.4	35.0	26.0	74.0	26.0
Fe(10%)	2.7	54±2.0	0.0	100.0	54±2.0
HARSHAW Fe ₂ O ₃ (10%)	0.37	24.0	40.0	60.0	13.0
POWDER Fe ₂ O ₃ (10%)	1.9	100.0	0.0	100.0	100.0

Benzothiophene: 0.45g
Additive: 0.5g

Table III: EFFECT OF AGITATION RATE ON COAL LIQUEFACTION USING A HARSHAW IRON CATALYST

RPM	H ₂ S PARTIAL PRESSURE, psig	SULFUR DISTRIBUTION, %		YIELD ^b H _f /H _o %	HYDROGEN ^c CONSUMPTION, %	SULFUR ^d REMOVAL, %	DESULFURIZATION RATE, %	HYDROGEN CONSUMPTION RATE, %	HYDROGEN CONSUMPTION RATE, %
		LIQUID	SRC						
600 ^e	0.0	0.26	0.58	87.0	0.38	56.0	0.467	0.517	0.517
800	0.0	0.25	0.56	87.0	0.37	58.7	0.489	0.525	0.525
1000	0.0	0.29	0.65	90.0	0.34	51.7	0.431	0.55	0.55
1400	0.0	0.28	0.57	90.0	0.42	53.3	0.444	0.483	0.483

Reaction Time: 120 minutes Initial Hydrogen Pressure: 2000 psi Additive: 10g

^aSo = 0.60% Organic Sulfur Content of the Coal Oil Slurry $\text{byield, \%} = \frac{\text{Ash}_f - \text{Ash}_i}{\text{Ash}_f(1 - \text{Ash}_i)} \times 100$

^cHYDROGEN CONSUMPTION, % = $1 - \frac{H_f}{H_o} \times 100$ (This is % of hydrogen charged initially into the reactor.)

^dSULFUR REMOVAL, % = $\frac{\text{So} - \text{Total Liquid Sulfur}}{\text{So}} \times 100$ ^eStirring rates below 600 are impractical due to solid settling problems.

Table IV: EFFECT OF Fe₂O₃ PARTICLE SIZE ON COAL LIQUEFACTION

PARTICLE SIZE, MESH	H ₂ S PARTIAL PRESSURE, psig	SULFUR DISTRIBUTION, %		YIELD, H _f /H _o %	HYDROGEN CONSUMPTION, %	SULFUR REMOVAL, %	DESULFURIZATION RATE, %	HYDROGEN CONSUMPTION RATE, %	HYDROGEN CONSUMPTION RATE, %
		LIQUID	SRC						
-35+ 60	0.0	0.26	0.56	73.0	0.53	56.7	0.472	0.392*	0.392*
-60+ 80	0.0	0.30	0.64	90.0	0.43	50.0	0.417	0.475	0.475
-80+150	0.0	0.26	0.54	89.0	0.50	56.7	0.472	0.617	0.617
-80+150	0.0	0.26	0.59	90.0	0.46	56.7	0.472	0.45	0.45
-200	0.0	0.29	0.65	90.0	0.34	51.7	0.431	0.55	0.55

*Lower hydrogen consumption because of incomplete coal dissolution (73.0% as opposed to 90.0%).

Reaction Time: 120 minutes
Fe₂O₃: 10g

Table V: PORE-DIFFUSION STUDY

PARTICLE SIZE, MESH	AVERAGE SIZE, mm.	HYDROGEN CONSUMPTION RATE, %/MIN.
-35+ 60	0.335	0.392
-60+ 80	0.214	0.475
-80+150	0.141	0.417
-80+150	0.141	0.45
-200	0.0895	0.55

Table VI: X-RAY ANALYSES OF DIFFERENT COAL LIQUEFACTION RESIDUES AND THEIR ASHES

ELEMENT	SRC RESIDUE (KY 9/14 COAL)	SRC ASH (KY 9/14 COAL)	WEIGHT		KY 9/14 COAL ASH
			K-M RESIDUE (KY 6 COAL)	K-M-ASH (KY 6 COAL)	
Si	13.54	27.86	6.97	23.86	18.02
Fe	3.37	6.80	5.66	18.49	26.92
Ca	1.30	3.03	0.31	1.16	1.55
K	0.43	1.01	0.67	2.02	1.75
Cl	0.22	0.37	0.62	0.26	0.46
Ti	0.14	0.34	0.19	0.61	0.66
Mn	0.02	0.05	0.03	0.09	0.09
Sr	0.04	0.09	-	-	0.07
Zn	-	0.02	0.02	0.06	0.03
V	-	0.04	0.02	-	0.09
Cu	-	0.02	0.02	0.14	0.10
Br	-	-	-	-	-
Rb	-	-	-	-	0.01
Pb	-	-	-	-	-
Al	3.86	9.20	3.29	10.51	11.11
Mg	-	2.10	2.20	-	-
S	2.14	0.47	3.81	0.58	0.86
C	54.02	-	59.33	-	-
H	2.67	-	3.44	-	-
N	1.35	-	1.56	-	-
O(by difference)	16.90	51.40	11.86	42.22	38.28
	100.00	100.00	100.00	100.00	100.00
Surface Area m ² /gm.	-	4.78±0.03	-	8.8±0.14	4.6±0.045

Table VII: COMPARISON OF ACTIVITY OF DIFFERENT COAL MINERAL ADDITIVES

ADDITIVE	PARTIAL PRESSURE OF H ₂ S, ps±g	HYDROGEN CONSUMPTION, %	TOTAL LIQUID SULFUR, %	ORGANIC SULFUR REMOVAL %	Fe/Fe _s	Se	SURFACE AREA m ² /g
None	16.0	41.0	0.46	23	-	0.57	
SRC Residue	58.0	42.0	0.46	23	0.56	0.56	
SRC Ash	3.0	51.0	0.34	43	0.81	0.85	0.85
Kerr McGee Residue	14.0	46.3	0.47	22	0.98	0.47	
Kee McGee Ash	1.0	49.0	0.35	42	2.25	0.85	0.85
Western Ken. 9/14 Coal Ash	1.8	52.0	0.34	43	3.21	0.83	0.83

Average Coal Dissolution is 90.0% in all cases.

Reaction Time: 120 minutes

Additive: 10g

Table VIII: COMPARISON OF ACTIVITY OF Fe, MAGNETITE AND Fe₂O₃ (REAGENT GRADE)

ADDITIVE	PARTIAL PRESSURE OF H ₂ S, ps±g	HYDROGEN CONSUMPTION, %	TOTAL LIQUID SULFUR, %	ORGANIC SULFUR REMOVAL, %	Fe/Fe _s	Se	SURFACE AREA m ² /gm.
Fe ₂ O ₃ (Reagent Grade)	0.0	55.0	0.25	55	6.86	8.9±0.04	1.0
Magnetite	0.0	43.6	0.35	41	8.83	0.75±0.02	0.94
Fe	0.0	41.5	0.28	53	10.42	0.25±0.01	1.3

Figure 1
 THE EFFECT OF Fe AND Fe₂O₃ ON THE
 SULFUR CONTENT OF THE
 TOTAL LIQUID PRODUCTS

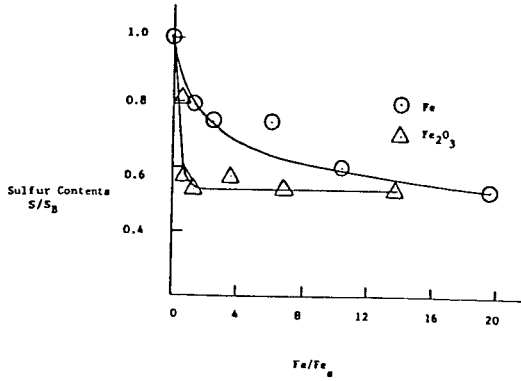


Figure 2
 THE SELECTIVITY OF Fe AND Fe₂O₃
 FOR SULFUR REMOVAL ON THE BASIS OF EQUIVALENT AMOUNTS OF Fe

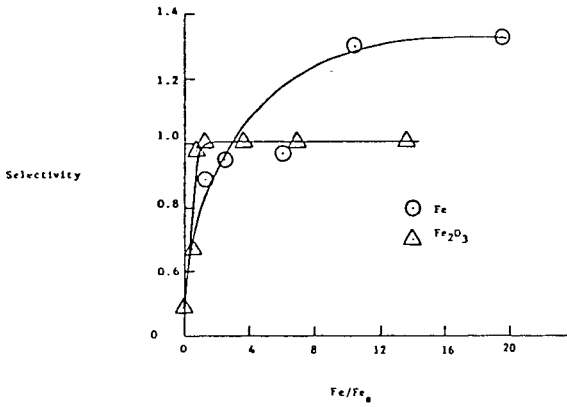


Figure 3
 THE EFFECT OF Fe AND Fe₂O₃ ON HYDROGEN
 CONSUMPTION AS A FUNCTION OF Fe CONCENTRATION

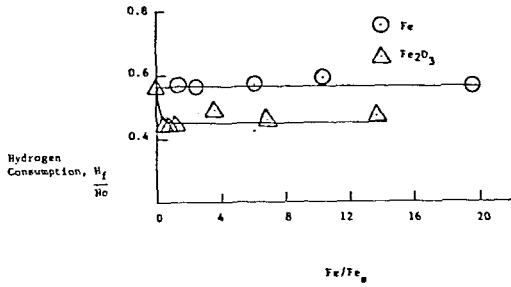


Figure 4
 THE EFFECT OF ADDITIVE TYPE
 ON SULFUR REMOVAL

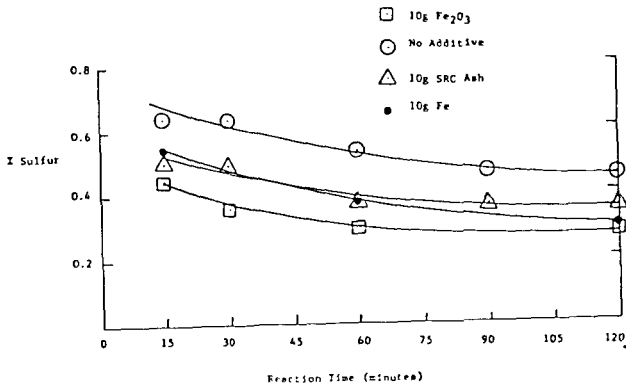


Figure 5
THE EFFECT OF ADDITIVE TYPE
ON HYDROGEN CONSUMPTION

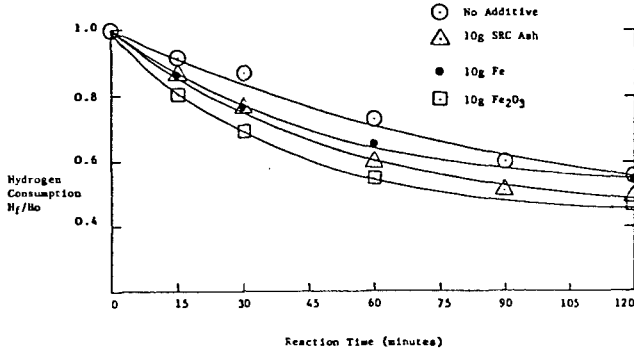
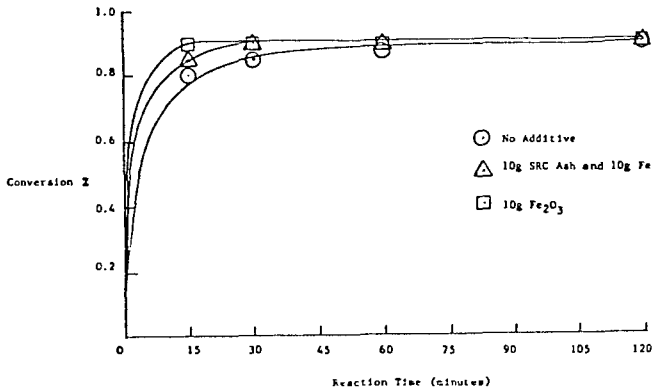


Figure 6
THE EFFECT OF ADDITIVE TYPE
ON COAL CONVERSION



CHEMICAL CHARACTERIZATION OF A hvb COAL

Kwang E. Chung, Larry L. Anderson and Wendell H. Wiser

Department of Mining and Fuels Engineering
University of Utah
Salt Lake City, Utah 84112

Introduction

Numerous physical and chemical means are employed to elucidate the general properties and nature of coal (1,2,3). Coal has been examined directly as a solid and indirectly in liquefied form. Nevertheless, our present understanding of coal is surprisingly limited, preventing us from more efficient utilization of coal for energy and chemicals.

Ultimate and proximate analyses are routinely performed on coals, but most other information is general or descriptive. Direct examination of coal by various spectroscopic means have resulted in useful, but usually qualitative information. Solvent extraction has not been too successful due to poor solubility of coal in known solvents. Information from coal-derived liquids (CDL) has been related to the structure of coal only superficially. The complexity and insolubility of coal have defied many ingenious approaches and modern analytical means as far as the exact chemical nature of coal is concerned.

Here we report the development of a suitable scheme for characterizing CDL, which identified and quantified major structural units in a high volatile bituminous coal. We will describe how this characterization scheme for CDL was formulated, and discuss the preparation and characterization of three CDL's. Our findings will then be related to the chemical structure of the particular coal we examined.

Characterization Scheme for CDL

Since a complete analysis of CDL is impractical, if not impossible, due to the complexity in composition, "characterization" is performed, meaning determination of the quantitative distribution of compound types and the functional groups present. Although it is practical to do so, the nature of the characterization work needs to be carefully examined in terms of purpose, the material to be characterized, and the procedure.

The purpose of characterization in petroleum research has been mainly to obtain necessary information for further processing of petroleum or its fractions. In coal research, elucidation of the chemical structure of the CDL precursor (coal) is of much interest. Improvements in understanding of coal structure is essential in devising a better characterization scheme for CDL, which in turn will improve our understanding of coal structure.

Available information on coal and CDL (1-4) was carefully evaluated and incorporated into a new characterization scheme. Coal was considered as a composite of polymer-like materials. It may consist of numerous constituents having different types of structural units and linkages. Accordingly, the liquefaction of coal was assumed as basically a depolymerization process.

In preparing CDL, the following has been taken into consideration: (1) a CDL should represent the coal under investigation, (2) the degree of depolymerization needs to be carefully chosen, and (3) the liquids must be accessible by analytical means possibly at the molecular level. Based upon these considerations, CDL were prepared in high conversion processes (with a relatively high degree of depolymerization).

Considering the nature of the depolymerization process, the molecular size was chosen as a separation criterion for the fractionation of CDL, and vacuum distillation

was employed. For non-distillable CDL solvent extraction was used for separation. Each fraction from the separation was analyzed by elemental analysis, molecular weight determination and NMR spectroscopy. This scheme is different from others(5) previously employed, especially in the preparation of CDL and the methods used for the separations.

Experimental

A hvb coal (Clear Creek, Utah) was liquefied in a dry coiled-tube reactor(6). The coal had 39.1% of volatile matter, and its elemental composition (wt. percent) was: C, 76.1; H, 5.6; N, 1.4; and O, 17.9. Reaction conditions used in the liquefaction process were: T = 500°C; P_{H2} = 1800 psig; catalyst = 5% ZnCl₂; and residence time, several seconds. Product yields were: gases, 10%; light liquid, 5%; heavy liquid, 55%; char, 15%; and H₂O, 15% (based on MAF coal).

The heavy liquid had a boiling range from 250°C to more than 500°C, and accounted for more than 70% of the condensed-phase products which included light and heavy liquids, and char. The condensed-phase products were assumed to retain the skeletal structure of coal. This assumption was supported by C¹³ NMR analysis of starting coal and liquid products (7). Thus the heavy liquid was examined further in the subsequent investigation. Paraffinic material in the liquid was removed by solvent extraction. The liquid material remaining after this extraction was designated as HVL-P. HVL-P was distilled at temperatures below 260°C at a pressure of 3 Torr. The distillate was divided into three fractions, Light, Middle and Heavy according to their physical appearance with the non-distillable fraction termed Resid. Light and Middle were fluid at room temperature, but a phase separation appeared between them. Heavy and Resid were solids.

In another preparation of CDL's, the same coal was solubilized by reacting with sodium hydroxide and ethanol at 300°C and 320°C for 100 minutes in an autoclave using a procedure similar to that of Makabe (8). The products were named SP-300 and SP-320, the former being from 300°C runs and the latter being from 320°C runs. Each product was divided into four fractions. Two of them (Fractions I and J in SP 300, and Fractions I' and J' in SP-320) were soluble or floating in a strong basic solution, but precipitated in different fashion upon neutralization. The rest of the products were extracted with pyridine at room temperature to obtain Fractions K and K' (pyridine soluble) and pyridine insoluble portions.

Elemental composition was determined with a Perkin-Elmer Model 240 Analyzer. Oxygen was determined separately. NMR spectra were obtained with an EM-390 spectrometer (Varian). Pyridine-D₅ and CDCl₃ were used as solvent. Molecular weights were determined by vapor phase osmoemtry using a Corona Model 117 apparatus (Wescan Instruments, Inc.). The experimental procedure and conditions were carefully chosen to ensure the correct determination of molecular weight (9).

Results and Discussion

Structural parameters of average molecules in the CDL fractions were calculated from the elemental composition, molecular weight and proton NMR spectra. Their definitions and formulae (10) are:

Number of aromatic carbons

$$C_A = C - \frac{1}{2} (H_{2\alpha} + H_B) - \frac{1}{3} (H_{3\alpha} + H_Y) \quad (1)$$

Fraction of aromatic carbons (=aromaticity)

$$f_A = \frac{C_A}{C} \quad (2)$$

Total number of rings

$$R = \frac{2C - H + 2}{2} - \frac{1}{2} C_A \quad (3)$$

Number of aromatic clusters

$$C_{AP} = H_A + \frac{1}{2} H_{2\alpha} + \frac{1}{3} H_{3\alpha} \quad (4)$$

$$n = \#cl = \frac{1}{3} (C_{AP} - \frac{1}{2} C_A) \quad (5)$$

Number of aromatic rings

$$R_A = \frac{1}{4} (C_A - 2n) \quad (6)$$

Number of naphthenic rings

$$R_N = R - R_A \quad (7)$$

Values of C and H were from the empirical formula of each fraction. Hydrogen (H) was divided into four types based on NMR spectra: H_A , 5 - 9 ppm; $H_{2\alpha}$, 2.2 - 5 ppm; $H_{3\alpha}$, 2.0-2.2 ppm; H_β , 1.1-2.0 ppm; and H_γ , 0.3-1.1 ppm.

Table 1 summarizes yields from the distillation along with structural parameters of HVL-P fractions. All data are experimental values except for those in parentheses. Values in parentheses were calculated from those of the four fractions. The yields show that Light, Middle and Heavy fractions are a major portion of HVL-P.

Structural parameters change significantly from one fraction to another. For example, number of total rings, R, of HVL-P is 3.2, but it varies from 1.8 to 5.6 in its fractions. The number of total rings decreased by 1.9 from Resid to Heavy, 1.4 from Heavy to Middle, and 0.5 from Middle to Light. The number of aromatic rings, R_A , and molecular weight decreased in a similar fashion.

These differences are so large that the fractions were grouped into three, A, B, and C (Light and Middle, Heavy, and Resid respectively). The number of aromatic clusters ($\#C1$) reveals that most molecules in the first two groups (A and B) have one aromatic cluster, while about 30% of molecules in C have, on the average, two clusters. Overall, molecules in HVL-P have almost one aromatic cluster, indicating that HVL-P was essentially completely depolymerized.

Structural parameters were used to sketch possible structures of the four fractions. The structures in Fig. 1 contain the appropriate numbers of aromatic rings, aromatic clusters and naphthenic rings. The presence of functional groups or side chains on the structures are qualitative.

If one assumes that the aromatic double bonds were neither produced nor broken during the liquefaction process (in the production of HVL-P), the components in Group C were not converted to substantially smaller molecules (like A or B). Also Group B molecules were not converted to Group A. This non-convertibility indicates that the three groups were produced from three different structural units of the feed coal.

The assumption was drawn from the following consideration: (1) the liquefaction conditions were unfavorable for hydrogenation or dehydrogenation of aromatic structure in coal: most notably the residence time was too short, and (2) the large differences in molecular size among the three groups would have not resulted from the conversion of a large component group to a smaller one. Examination of the solubilization products, SP-300 and SP-320, provides further supporting information for this assumption as well as other interesting features of coal structure.

Table 2 contains yields and structural parameters of the solubilization products. As expected from the experimental conditions, the yields and molecular size of the products are substantially larger than those of HVL-P. Yet comparison of the structural parameters of HVL-P and SP-300 reveals a remarkable resemblance in an important structural feature: the average aromatic cluster sizes, $R_A/\#cl$, are the same, 2.2, in both products. This agreement can be related to approximate size of the average aromatic cluster in coal.

Considering that 15% of the char yield and 5% of the light liquid yield in producing HVL-P, the average aromatic cluster size of the condensed-phase products (HVL-P, light liquid and char), which are supposed to retain the skeletal structure of coal, is expected to be larger than 2.2. On the other hand, SP-300 represents more than 97% of coal matrix (pyridine insoluble <2% of coal), but its average aromatic cluster size is supposed to have been reduced somewhat due to the nature of the reaction among coal, NaOH and ethanol. According to Makabe and Ouchi (8), the reaction slightly hydrogenates aromatic rings in coal under our experimental conditions. In any event, our observations on two separately prepared CDL's indicate that the size of the average aromatic cluster of the hvb coal is larger than 2.2, but not much different from 2.2.

The agreement in $R_A/\#cl$ between HVL-P and SP-300 suggest that large aromatic clusters like those ($R_A/\#cl = 3.4$) in Resid of HVL-P should exist in SP-300, i.e. most probably in Fraction K. Comparison of the structural parameters of SP-300 with those of SP-320 helps clarify this point. The large difference in $R_A/\#cl$ between SP-300 and SP-320 is directly related to the question of the large aromatic clusters.

The difference in $R_A/\#cl$ is due to the conversion of Fraction K to a portion of Fraction J' and Fraction K' as revealed by their $R_A/\#cl$'s and yields. Fraction J' consists of two large portions, one coming from Fraction J and the other from Fraction K. Still Fractions J' and J behaved similarly in a strong basic solution as described in their preparation, and they have similar $R_A/\#cl$ and molecular weight (based on an estimation of a separate conversion of J to a portion of J'). This indicates that there was a portion of K which was similar to Fraction J in chemical structure, and which was different from the rest of K: the two portions are termed Fractions K_J and K_K respectively. Thus it is most likely that J and K_J experienced a similar transformation to become part of J'. In the conversion to J', apparently $R_A/\#cl$ of J was not changed, and so' was not that of K_J . Then the large change of $R_A/\#cl$ between SP-300 and SP-320 is due to a large change of the same parameter between K_K and K'. $R_A/\#cl$ of K_K was large, but it reduced to that of K' upon the hydrogenation of NaOH/ethanol reaction.

Model compound studies by Ross and Blessing (11) support this interpretation. They observed that clusters consisting of single aromatic ring were not hydrogenated in a reaction with KOH/methanol at 400°C for 30 minutes, but a cluster containing three fused aromatic rings underwent hydrogenation. Estimation of $R_A/\#cl$ of K_K came out to be 3.4, which is the same as that of Resid in HVL-P. The large decrease in $R_A/\#cl$, from 3.4 (for K_K) to 1.4 (for K') upon hydrogenation suggests that the aromatic rings in the clusters of K_K were mostly cata-condensed. Thus considerable amounts of polynuclear aromatic clusters were observed in HVL-P and SP-300 which were supposed to retain most of skeletal structure of the hvb coal.

Recently Whitehurst (12) and Farcasiu (13) reported that there is no significant amount of large aromatic clusters in coal. Their coals and experimental method were different from ours, but most notably their determination of the size of aromatic clusters was semi-quantitative (13). Although their conclusion might hold with the particular coals they examined, our findings support the conventional view that most bituminous coals contain considerable amounts of polynuclear aromatic clusters.

These observations lead to the conclusion that there were originally three classes of average aromatic clusters in terms of their size in the hvb coal. Two of them have, on the average, 1.9 and 1.3 aromatic rings per cluster, and they were collected in Fractions I' and J'. The third class has, on the average, 3.4 or more aromatic rings per cluster, and was collected in Fraction K mixed with the precursor of J'. The average size of the third class of clusters is expected to be larger than 3.4 since hydrogenation of the aromatic clusters is suspected as discussed previously. Now we will examine how these three classes of aromatic clusters would be further depolymerized.

The findings with SP-300 and SP-320 substantiate the assumption made earlier, i.e. that the aromatic double bonds experienced little change, if any, in the liquefaction

process in producing HVL-P. In the process, non-aromatic bonds between aromatic clusters in the coal were broken almost completely. Considering the milder reaction conditions in producing SP-300 and the same $R_A/\#cl$ of HVL-P and SP-300, further treatment of SP-300 in the liquefaction process would result in a complete depolymerization of SP-300 yielding a product similar to HVL-P. There are a couple of non-aromatic bonds linking aromatic clusters in SP-300 as revealed by $\#cl$.

The comparison of structural parameters which are shown in Tables 1 and 2 provides detailed information on the conversion of SP-300 to completely depolymerized product. The three fractions of SP-300, however, were insufficiently depolymerized to draw useful information from their structural parameters. Instead the structural parameters of Fractions I' and J' were examined since Fractions I, J and K_J were converted to Fractions I' and J'. The numbers of aromatic rings, R_A 's, of I' and J' are already smaller than that of Resid in HVL-P. Thus upon further depolymerization, Fractions I' and J' could become Light, Middle or Heavy such as those in HVL-P. According to R_A and $\#cl$, 80% of J' will become Light or similar fraction in HVL-P (the predicted value is 17% of MAF coal, compared to 15% of Light plus light liquid). The rest of J' will become Heavy. Likewise, 70% of Fraction I' will become Middle/Heavy (the predicted value is 21%, compared to 17% of actual yield). The rest of I' will become Resid. Also the rest of SP-300, Fraction K_K, could become Resid/Char since both K_K and Resid have the same $R_A/\#cl$ (the predicted value came out to be the same as the actual yield, 35%). Taking account of the paraffinic material removed, 4%, and the loss, 5%, in preparing HVL-P, the predictions agree well with the actual yields.

The quantitative convertibility of SP-300 to HVL-P fractions further substantiates that the skeletal structures (or aromatic bonds) of coal were conserved during the liquefaction process as well as during the solubilization process at 300°C. Therefore the component groups A, B and C in HVL-P can be visualized as structural units of the coal. Almost all structural units were collected in SP-300 and they were grouped into three (Figure 2). The structural units in the first group, X, have one to two aromatic rings, and they are connected to each other by non-aromatic bonds. Although our data revealed that the linkages exist, their nature has not been studied yet. The structural units in the second group, Y, have two to three aromatic rings, and the third group consists of structural units having, on the average, four or more aromatic rings. Thus, the particular hvb coal has been characterized in terms of major structural units and their distribution. The same data analyzed so far provide valuable information also on the reduction of molecular size during the liquefaction, weak bonds, and the hydrogenation of aromatic clusters in coal, and this will be reported elsewhere.

Conclusion

A new characterization scheme for CDL has been devised based on the assumption that coal liquefaction is basically a depolymerization process. This scheme was instrumental in disclosing the following structural features of a hvb coal and its liquids:

- (1) A CDL (HVL-P), produced at 500°C with very short residence time, was almost completely depolymerized, i.e., essentially all linkages between aromatic clusters were broken, and consisted of three major component groups, A, B and C. The components in Group A had mostly one aromatic ring, those in Group B two to three fused aromatic rings and those in Group C four or more fused aromatic rings. The fused aromatic rings have attachments such as naphthenic rings and aliphatic side chains. The three groups apparently are not convertible to each other under the liquefaction conditions used, and therefore, must have been produced from three different structural units in coal.
- (2) A solubilization product (SP-300), obtained in a reaction with NaOH/ethanol at 300°C, revealed that it was less depolymerized than HVL-P, but the size of average aromatic cluster was the same, 2.2 aromatic rings per cluster, as that of HVL-P. SP-300 consisted of three classes of average aromatic clusters having 1.3, 1.9 and 3.4 aromatic rings per cluster. The distribution of the clusters was found by examining another solubilization product (SP-320)

prepared at 320°C. The aromatic rings of the large clusters appear to be cata-condensed.

- (3) The clusters containing 1.3 and 1.9 aromatic rings per cluster are convertible to smaller species like Groups A and B in HVL-P, while the larger clusters of 3.4 aromatic rings will become Group C in HVL-P.
- (4) The three groups of HVL-P were identified as the three major structural units of coal, and their distribution in the hvb coal was estimated from the examination of SP-300 and SP-320

These findings are unique to the characterization scheme for CDL. The results of this characterization of coal could be related to product potential in liquefaction, solvent refining and pyrolysis of coal. Taking into account the heterogeneity of coal and its inaccessibility by analytical means, the present approach appears to be a practical, useful way to characterize the chemical structure of coal. The same approach will be utilized with other coals which can be solubilized to further substantiate this method.

Acknowledgements

This work was supported by the U.S. Department of Energy, Office of Fossil Energy, and the University of Utah through contract E(49-18)-2006.

References

- (1) Lowry, H.H., Ed. Chemistry of coal Utilization, Supp. Vol., John Wiley and Sons, New York, 1963.
- (2) Van Krevelen, D.W., Coal, Elsevier Publishing Co., New York, 1961.
- (3) Friedel, R.A., Ed. Spectrometry of Fuels, Plenum Press, New York, 1970.
- (4) Larsen, J.W., Ed. Organic Chemistry of Coal, ACS Symposium Series 71, Am. Chem. Soc., Washington, D.C., 1978; Vahrman, M. Chem. Ber. 8, 16, 1972.; McIntosh, M.J., Fuel 55, 59, 1976.; Wiser, W.H., Anderson, L.L., Qader, S.A., and Hill, G.R., J. Appl. Chem. Biotech. 21, 82, 1971.; Gould, R.F., Ed. Coal Science, Adv. in Chem. Series 55, Am. Chem. Soc., 1966.; Neavel, R.C., Preprints, Div. of Fuel Chem., Am. Chem. Soc., 24 (1) 73, 1979.
- (5) Farcasiu, M., Fuel, 56 9, 1977.; Given, P.H., Cronauer, D.C., Spakman, W., Lovell, H.L., Davis, A., and Biswas, B. Fuel, 54, 40, 1975.; Schultz, H. and Mima, M.J., Preprints, Div. of Fuel Chem., Am. Chem. Soc., 23 (2) 76, 1978.
- (6) Wood, R.E., and Wiser, W.H., Ind. Eng. Chem., Process Res. Devel., 15, 144, 1976.
- (7) Zilm, K.W., Pugmire, R.J., Grant, D. M., Wood, R.E., and Wiser, W.H., Fuel, 58, 11, 1979.
- (8) Makabe, M., and Ouchi, K. Fuel Proc. Tech., 2 131, (1979).
- (9) Chung, K.E., Anderson, L.L., and Wiser, W.H., Fuel, accepted for publication.
- (10) Chapter XXII in Reference (2).; Clutter, D.R., Petrakis, L., Stenger, R.L., Jr., and Jensen, R.K., Anal. Chem. 44 (8) 1395, 1972.; Kanda, N., Itoh, H., Yokoyama, S., and Ouchi, K., Fuel, 57, 677, 1978.
- (11) Ross, D.S., and Blessing, J.E. Preprints, Div. of Fuel Chem., Am. Chem. Soc., 24 (2), 125 (1979).

- (12) Whitefurst D.D., Organic Chemistry of Coal, Ed. by Larson, J.W., ACS Symposium Series 71, Am. Chem. Soc., Washington, D.C. 1978, p. 1.
- (13) Farcasiu, M., Preprints, Div. Fuel Chem., Am. Chem. Soc., 24 (1) 121, 1979.

TABLE 1
Analytical Data on HVL-P and Its Fractions

	Yield, Wt%	Mol. Wt.	R _A	R _N	#c1	f _a
HVL-P	100 (92.5)*	258 (268)	2.4 (2.4)	0.8 (0.9)	1.1 (1.1)	0.63 (0.60)
Light	19.2	183	1.2	0.6	1.0	0.55
Middle	15.7	210	1.6	0.7	1.1	0.58
Heavy	17.6	272	2.4	1.3	1.0	0.59
Resid	40.0	396	4.4	1.2	1.3	0.68

*Calculated from those of the four fractions.

TABLE 2
Structural Parameters of the Solubilization Products

	Yield*	Mol. Wt.	R _A	R _N	#c1	f _A	R _A /#c1
SP-300**	85.7	843	5.6	3.9	2.6	0.52	2.2
Fraction I	23.9	777	5.0	3.3	2.7	0.52	1.9
J	9.1	643	3.4	3.4	2.5	0.53	1.4
K	52.7	930	6.6	4.4	2.6	0.51	2.5
SP-320**	76.5	520	3.2	2.4	2.1	0.52	1.5
Fraction I'	26.6	478	3.2	2.3	1.7	0.55	1.9
J'	23.8	444	2.4	2.0	1.8	0.50	1.3
K'	26.1	690	4.4	3.1	3.1	0.52	1.4

*Weight % of coal (MAF)

**The parameters were calculated from the three fractions.

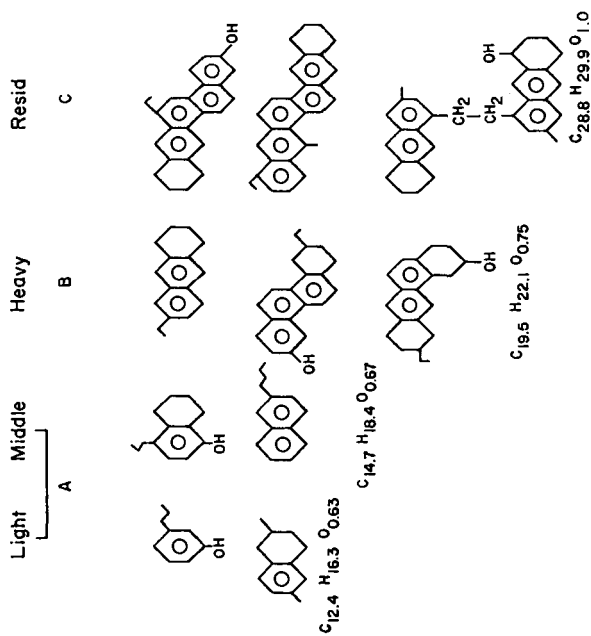


Figure 1. Sketches of Possible Structures of HVL-P Fractions.

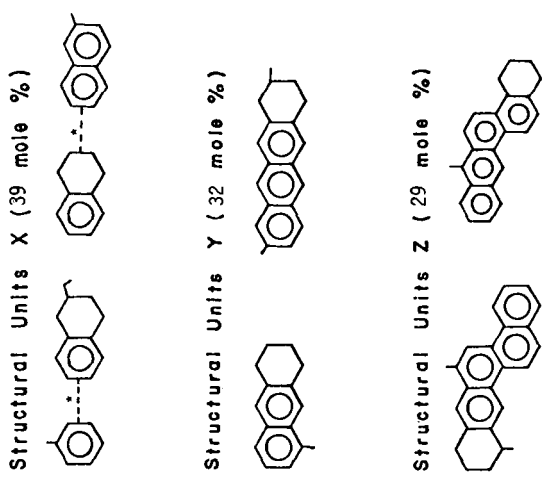


Figure 2. Structural Units Comprising A hvb Coal

*Linkages exist but were not identified.

STRUCTURAL CHARACTERISTICS OF VITRINITES

SWADESH RAJ

Ebasco Services Incorporated
Two Rector Street
New York, New York 10006

INTRODUCTION

It is generally accepted that the various petrographic constituents of coals are derived largely from partly decayed organs of the higher plants and the chemical substances in them. Lignin, in particular, is thought to be an important part of the input to coalification processes both in preserved woody tissue and after the microbial action. The nature of the substances from which coals are derived are fairly well known. However, the chemical structures that they give rise to in coals are poorly understood. It was thought worthwhile to undertake a structural study of a set of vitrinite-rich coals (ie, derived from woody tissue), using experimental approaches that would assist in evaluating the extent to which lignin structures are still recognizable after coalification. A reductive degradation method of Burges et al (1), which has previously revealed the presence of lignin-derived phenols in the humic acids of soils, was adopted. Since coals of higher rank than lignites do not contain humic acids, humic-acid-like materials were generated in high yields (80 - 110 percent) by a mild oxidation (2) using aqueous performic acid and the products subjected to the reductive degradation.

Paleobotanic studies show that the main types of plants that contributed to coal formation in the Carboniferous were primitive gymnosperm, tree ferns, seed ferns and club mosses. In the other main eras of coal formation, the Cretaceous and the Tertiary, the source plants were angiosperms of the modern type. It is observed that there is likely to be a significant spread in some structural features of the lignin and flavonoids in such a wide range of plant types. Therefore, geological history is also considered a potentially important factor in determining structural characteristics of vitrinites. Two peat samples, three lignites and thirty-eight subbituminous and bituminous coals were studied. The mixtures of phenols and phenolic acids obtained as trimethylsilyl ethers and escers were analyzed by gas chromatography/mass spectrometry.

EXPERIMENTAL INVESTIGATION

Selection of Coal Samples

For this study three sets of coals from different geological provinces were selected. These coals are rich in vitrinite plus pseudo-vitrinite (70 - 90 percent), and cover a wide range of rank. Ten coals each from Eastern and Interior provinces and fifteen coals from Rocky Mountain province were selected. Three lignites were selected from Texas and North Dakota. Two peat

samples were taken from the Southern Everglades of Florida. Details on the analysis of selected peat, lignitic, subbituminous and bituminous coal samples are given in Reference (3).

Experimental Method

The oxidation of coal by performic acid was carried out under controlled conditions and the temperature was maintained at 50 - 55°C. Humic acids were extracted from peats and lignites with 0.5 N NaOH and from oxidized coals with 1 N NaOH. The washed and dried humic acids were dissolved in NaOH, treated with 3 percent freshly prepared sodium amalgam, and the solution was heated in an oil bath to temperatures of 110 - 115°C for 4 - 5 hours. The resulting phenols and phenolic acids were precipitated and extracted by centrifugation with ether and methylene chloride. The solvents were removed and the residues were treated with sylvol HTP reagent under the specified conditions for converting phenols and phenolic carboxylic acids to their corresponding ethers and esters. The trimethyl ethers and esters were analyzed by gas chromatography with and without coinjection. A few of the identifications were made by Bimer et al (4) by gas chromatography with coinjection of standards. With the wider range of coals and with a wider set of standards more compounds were identified using GC/MS/Computer System. Experiments showed OV 101 Column Packing (3 percent on 80/100 mesh supelco port) to be the most effective for GC and GC/MS of the six packings tested. The GC/MS instrument was provided with a data system. The data system was used to subtract the mass spectrum at the foot of each peak just before it began to elute, or just after the elution, from the spectrum recorded as the maximum of the peak was eluted. The raw MS data, described above, were reported for standards and unknowns as printouts tabulating m/e values and relative intensities. The comparisons were made by visual inspection of the printed data and the retention times.

EXPERIMENTAL RESULTS

It is impracticable to reproduce here all the chromatograms and all the mass spectra obtained. Most of them are illustrated in Reference (3). It is observed that humic acids obtained both by the extractions of lignites and the oxidation of the insoluble residues, and the humic acids obtained from most (but not all) of the coals from the Rocky Mountain Province, gave poorly resolved chromatograms, while those from the Carboniferous coals of Interior and Eastern Provinces gave chromatograms where resolution ranged from reasonable to excellent. The products from the peat humic acids showed moderately good resolution. Taking an overview, 18 of 43 samples studied showed poor resolution.

There are a number of difficulties in discussing the compounds identified and assessing their significance. Humic acids are poorly defined substances of diverse origin, and their structures are unknown. In order to facilitate discussion of the distribution of compounds identified, all of the compounds partially or completely identified are listed in Table 1-3, where the coals from which they come are classified partly by rank and partly by the province. In each set of tables, the compounds are listed as far as possible in order of increasing complexity.

In Table 1 are presented the phenols and acids whose structures are simple or nonspecific about their origin. Table 2a contains compounds that appear to have been derived from the A ring of flavonoids. In Table 2b are compounds of more complex structure with a very clear relationship to the breakdown products of lignin and B ring of flavonoids. Table 3 lists relatively complex compounds which again may have had a biological origin, but this cannot be proved; for many of them the substitution pattern in the benzene ring has not been identified. What is shown in the tables is the frequency of occurrences of the various compounds. At the head of each column of the tables is shown the total number of samples of each class studied, and against the name of each compound is shown the number of reaction products in which it was identified.

Throughout the study, a number of relatively large peaks could not be matched with the Standards available, and no more than the general character of the Structure could be inferred from the mass spectra. These peaks were scanned for negative as well as positive information. The principle conclusions arising from the examination of unidentified peaks were as follows:

1. A majority of the large unidentified peaks represented phenols or phenolic acids.
2. Some evidence of the presence of biphenyl groups was seen.
3. In each chromatograms presence of hydroxy pyridines is seen.
4. No evidence of the presence of Sulfur compounds was seen.
5. Some mass spectra indicate the presence of either linkages (other than methoxyl) and of Carbonyl compounds.

DISCUSSION OF RESULTS

The most striking result of the whole study is the presence of cinnamic acid, which was found in 42 out of the 43 materials analyzed; the one product that did not contain cinnamic acid did contain the corresponding alcohol. The acid is found in a region of the chromatograms where the peaks rise directly from the baseline in almost all cases, and the peak corresponding to it was almost always sharp and intense. In addition, substances closely related to it were found in a few products, with the aliphatic side chain in a different state of oxidation, ie, not as $-\text{CH}=\text{CH}-\text{COOH}$ but as $-\text{CH}_2.\text{CO}.\text{COOH}$ or $-\text{CH}_2.\text{CH}_2.\text{COOH}$ or $-\text{CH}_2.\text{CO}.\text{CH}_2.\text{OH}$. However, cinnamic acid is of common occurrence in plants as a biosynthetic precursor to lignin, flavonoids and phenylalanine, so that it could have entered peats as such and be incorporated into peat humic acids.

There is also present in many samples a group of compounds related to *p.* hydroxycinnamic acid (or *p.* coumaric acid). Again the side chain is in various states of oxidation ($-\text{CH}=\text{CH}-\text{CH}_2.\text{OH}$, $-\text{CH}_2.\text{CO}.\text{COOH}$, $-\text{CH}_2.\text{CH}_2.\text{COOH}$). *p.* Coumaric acid itself is the most abundant of these, being found in about

half the products from subbituminous and bituminous coals, but only in one of the lower rank materials. On the other hand, p. hydroxybenzoic acid, which can be derived from coumaric acid and related compounds by oxidation of the side chain, was found in almost all of the low rank materials and in rather less than half of the products from the higher rank coals.

There are a large group of compounds related to 3-methoxy-4-hydroxy-cinnamic acid (ferulic acid). This substitution pattern is the most abundant in the lignin of Gymnosperms and in some less highly evolved plants such as the Lycopods, but is found also in Angiosperms. Vanillin (3-methoxy-4-hydroxy-benzaldehyde), formed in peats by microbial oxidation of ferulic acid was found in every one of the low rank materials studied, in 12 out of 15 samples from the Rocky Mountain Province, and in about one-half of those from the other provinces. In addition, the related compound, vanillic acid was found to be quite abundant. Ferulic acid itself, and caffeic acid (3,5-dihydroxy cinnamic acid) were each found in about 40 percent of the samples; a sample that contained one in general did not contain the other. Oddly enough, caffeic acid is the only substance in this group that has had the original 3-methoxy substituent demethylated to hydroxy. The other substances in this group contain the aliphatic side chain in various states of oxidation, of greater variety than was found with the compounds related to coumaric acid ($-\text{CH}_2\cdot\text{CO}\cdot\text{CH}_2\text{OH}$) $-\text{CH}_2\cdot\text{CO}\cdot\text{COOH}$, $-\text{CH}_2\cdot\text{CH}_2\cdot\text{CHO}$, $-\text{CH}_2\cdot\text{CH}_2\cdot\text{CH}_2\text{OH}$ and $-\text{CHOH}\cdot\text{CHOH}\cdot\text{COOH}$.

The final group of substances related to lignin have the 1, 3, 4 and 5 substitution pattern in the benzene ring. As with the groups already discussed, the side chain was found in a variety of oxidation states. Again only one demethylated derivative was found 3, 4, 5-trihydroxy cinnamic acid. What might be termed the parent compound, 3, 5-dimethoxy-4-hydroxy cinnamic acid, was found in 11 samples which was entirely restricted to the higher rank materials. Syringic acid and syringaldehyde, in which two of the carbon atoms in the aliphatic chain have been removed by oxidation, were the most frequently found members of this group (19 and 13 samples respectively), and their occurrences were fairly evenly distributed over all classes of coals, including the peats.

CONCLUSIONS

By no means all of the substances that gave peaks on the chromatograms were identified, but a careful scrutiny of the data showed that identifications made were reasonably certain. The products derived from the Carboniferous coals of the Interior and Eastern Provinces were markedly less complex mixtures, and the degree of resolution was considerably better. From the results there are a number of important implications for understanding the chemistry of vitrinites. These may be summarized as follows:

1. Many benzene rings in vitrinites bear not only an OH group but often one or two methoxy groups as well; occasionally a second OH group may be present instead of methoxy. This would explain, among other things, the difficulty of sulfonating or nitrating vitrinites without accompanying oxidation.

2. Methoxyl groups survive in vitrinites to a considerably higher level of rank than previously reported.
3. Bicyclic and polycyclic aromatic ring systems, other than biphenyl, appear to be less frequent. It is possible that most of the polycyclic structures from coals accumulated in the ether-insoluble material.
4. The structure of vitrinites, even of High Volatile A Bituminous rank, appears to be similar to that of lignin, in being based to an important extent on phenyl propane and phenyl methane skeletons.
5. Olefinic double bonds are abundant in vitrinite structures as such or they are generated by the degradation processes used, in a manner difficult to envisage at this time.

The conclusions are consistent with a feasible interpretation of the X-ray scattering data of Hirsch (5). Further, it is also consistent with the conclusions of Montgomery et al (6) and of Chakrabartty et al (7) on their studies of the products of severe oxidation of coals.

ACKNOWLEDGEMENTS

The author wishes to thank Professor Peter H. Given for his advice during the course of this investigation. Author is also thankful to Dr William Spackman for the PSOC coal samples and to Dr C. Exarchos for the peat samples. Valuable assistance given by Mr David Hindenlang and Dr Larry Hendry is also gratefully acknowledged for GC/MS data.

REFERENCES

1. Burges, M.A., Hurst, H.M. and Walkden, S.B., *Geochim et Cosmochim Acta* 28, 1547, (1964).
2. Given, P.H., Brown, J.K., Lupton, Vera and Wyss, W.F., *Proceedings of Institute of Fuel Conference, "Science in the Use of Coal,"* 38, 537 (1958).
3. Raj, S., Ph.D. Thesis, The Pennsylvania State University (1976).
4. Bimer, J., Given, P.H., and Raj, S., *ACS Symposium Series, No. 71, Organic Chemistry of Coal*, (1978).
5. Hirsh, P.B., *Phil. Trans Roy. Soc. (252A)*, 68 (1960).
6. Montgomery, R.S., Holly, E.D. and Gohlke, *Fuel* (35), 60 (1956).
7. Chakrabartty, S.K. and Berkowitz, N. *Nature (Lond.)*, (1976).

TABLE 1

Simple Phenols and Acids Identified

Compound	Direct Humic Acid		Humic Acid from Oxidized Coals		
	Peats	Lignites	15	10	10
			Rocky Mountain Province Coals	Interior Province Coals	Eastern Province Coals
Acetic Acid	2	3		1	1
Propionic Acid		1	2	1	1
Benzoic Acid	2	3		1	3
Phenol	2	1	3	5	4
p-Cresol	2	1	12	2	
o-Methoxy Phenol	2	2	3	2	
m-Methoxy Phenol	2	2	3		
Hydroquinone	1	1			
m-Hydroxy Benzoic Acid	1	1	3	1	1
Catechol	2	2	7	5	3

TABLE 2a

Phenols Identified Having Biological Associations
(A-ring of Flavonoids)

Compound	Direct Humic Acid		Humic Acid from Oxidized Coals		
	Peats	Lignites	15	10	10
			Rocky Mountain Province Coals	Interior Province Coals	Eastern Province Coals
Resorcinol	2	1	7	2	3
Phloroglucinol	2		2	1	1
2-Methyl Resorcinol		1	3	4	5
2,4-Dihydroxy Toluene	1	3	7	3	5
o-Hydroxy Benzoic Acid			5	2	1
2,4,6-Trihydroxy Benzoic Acid	1	1	1	1	1
2,4,6-Trihydroxy Toluene				1	5

TABLE 2b

Phenols Identified Having Biological Associations
(Lignin and its Precursors; A-ring of Flavonoids)

Compound	Direct Humic Acid		Humic Acid from Oxidized Coals			
	2 Peats	3 Lignites	3 Lignites	15 Rocky Mountain Province Coals	10 Interior Province Coals	10 Eastern Province Coals
Cinnamic Acid	2	3	3	14	10	10
Cinnamic Alcohol				1		
Phenyl, 3-Pyruvic Acid	1	1			2	2
Phenyl, 3-Propionic Acid				1	1	1
Phenyl, 3-Pyruvic Alcohol				2		
p-Hydroxy Benzoic Acid	2	3	3	5	4	3
p-Coumaric Acid			1	6	4	5
p-Coumaryl Alcohol	1			1		2
p-Hydroxy Phenyl, 3-Pyruvic Acid		1	1	2	3	2
p-Hydroxy Phenyl, 3-Propionic Acid			1	3	2	2
Pyrogallol	2	1		1	1	1
Gallic Acid				1		1
Vanillin	2	3	3	12	5	6
Vanillic Alcohol				2	1	
Vanillic Acid	2	2	1	5	5	3
Acetovanillone	1			4	1	1
Ferulic Acid	1	1	1	4	3	7
Caffeic Acid	1		1	6	4	6
3-Methoxy, 4-Hydroxy Phenyl, 3-Pyruvic Alcohol		2	1	3	2	4
3-Methoxy, 4-Hydroxy Phenyl, 3-Pyruvic Acid		1	2	3		4
3-Methoxy, 4-Hydroxy Phenyl, 3-Propion- Aldehyde		1		2	2	3

TABLE 2b (Cont'd)

Compound	Direct Humic Acid		Humic Acid from Oxidized Coals			
	Peats	Lignites	Lignites	15		Eastern Province Coals
				Rocky Mountain Province Coals	Interior Province Coals	
3-Methoxy, 4-Hydroxy Phenyl, 3-Propanol						
3-Methoxy, 4-Hydroxy Phenyl, 3-Glyceric Acid	1	1	1	3	1	
Dehydrovanillone				2	1	
Syringic Aldehyde	1	1	1	5	3	2
Syringic Alcohol				3	2	4
Syringic Acid	2	1	1	7	5	3
3, 5-Dimethoxy, 4-Hydroxy Phenyl, 3-Pyruvic Aldehyde		2	1		1	4
3, 5-Dimethoxy, 4-Hydroxy Phenyl, 3-Propionic Acid				1		
3, 5-Dimethoxy, 4-Hydroxy Phenyl 3-Glyceric Acid					1	
3, 5-Dimethoxy, 4-Hydroxy Phenyl 3-Pyruvic Acid	1	1		2		
3, 5-Dimethoxy, 4-Hydroxy Cinnamic Acid				3		
x, γ -Dimethoxy Cinnamic Alcohol					1	
x, γ -Dihydroxy Cinnamic Aldehyde					3	2

TABLE 3

Complex Phenols Identified of Unknown or Uncertain Biological Associations

Compound	Direct Humic Acid		Humic Acid from Oxidized Coals			
	2	3	15		10	
			Lignites	Rocky Province Coals	Interior Province Coals	Eastern Province Coals
2,6-Xylenol	2	3	2	9	4	5
3,5-Dihydroxy Toluene	1	1	1	1	1	1
Hydroquinone	1	1	1	1	2	1
x,y-Dimethoxy Phenol	1	1	1	2	2	1
x-Phenyl Phenol						
x,y-Dihydroxy Benzophenone			1			
x-Methoxy Phenyl,	2					
3-Propionic Acid				6	1	1
x-Methyl Benzoic Acid				1	1	1
x-Methoxy Benzoic Acid				1	1	1
2,5-Dihydroxy Benzoic Acid				2	2	3
x,y-Dimethoxy Phenyl,						
3-Propionic Acid				1		
x,y-Dimethoxy Cinnamic Alcohol					1	
x,y-Dihydroxy, Monomethyl Benzoic Acid					3	1
v,x-Dimethoxy, Y,Z-Dihydroxy Benzoic Acid				2	1	
v,x-Dimethyl, Y,Z-Dihydroxy Benzoic Acid				2	1	
1,2,4-Trihydroxy Benzoic Acid	2	2				
Benzoic Acid						
Saligerum				3		

Thermolysis and Oxidation of the Alberta Oil Sand Bitumen

K.N. Jha, D.S. Montgomery and O.P. Strausz

Hydrocarbon Research Centre
Department of Chemistry
University of Alberta
Edmonton, Alberta
Canada T6G 2G2

INTRODUCTION

The composition and the rates of evolution of light gases and volatile materials from Athabasca and Cold Lake oil sand bitumen and their separated fractions have been described as a function of temperature.¹⁻³ From the estimation of the Arrhenius parameters for product formation it was concluded that both these reservoirs are currently undergoing a slow but measurable thermal decomposition even at the formation temperature. The activation energies for the formation of products for the whole oil sand system were low, ranging between 6 and 26 kcal/mol, indicating the catalytic effects of mineral matter present in the oil sand. Previous work suggests a common origin for these oils, and our own results¹⁻³ suggested similar thermal diagenetic histories for the Athabasca and Cold Lake oil sand deposits. Similar studies have now been conducted on the Peace River oil sand to gain deeper insight into the relationships between this oil and the other two oil sands.

Preliminary results on the kinetics of consumption of molecular oxygen in the thermolysis of the Athabasca oil sand, extracted bitumen, asphaltene and maltene have shown that the rate of thermolysis of each product was substantially increased in the presence of molecular oxygen and that the rate of depletion of oxygen followed first order reaction kinetics.^{3,4} Exposure of the oil sand to oxygen resulted in a substantial increase in the asphaltene content of the sample.

These studies have been extended to include the effects of oxygen pressure and heating time on the yields of the products from the whole oil sand as a function of temperature in order to clarify geological processes such as the introduction of molecular oxygen into the bitumen via oxidizing ground water and weathering processes occurring at the oil sand outcrops or in piles of mined bituminous sand.

EXPERIMENTAL

The experimental details for the collection and analysis of gases and the volatile materials have been described previously.¹⁻³ The Peace River oil sand was received from Shell Canada Ltd., labeled OBS-5 Shell Cadotte OV, 4-21-85-18 W5 from a depth of 563-573 m. These samples were contained in split cores which had been exposed to air at some stage. The oil sands were manually homogenized before use for most of the experiments in order to obtain reproducible results.

The bituminous sands from the Saline Creek tunnel area of the Athabasca reservoir were used for the oxidation experiments. Bitumen was extracted from this oil sand and separated into asphaltenes and maltenes using standard techniques.⁵ Trace amounts of clay and mineral matter present in these fractions were removed by centrifugation. Non-condensable gases at 77°K were analyzed by gc on a 2.4 m molecular sieve column and the gases volatile at 195°K but condensable at 77°K on a 4.6 m Porapak Q column. Since neopentane, acetone, propionaldehyde and carbon disulfide are unresolved on Porapak Q, this total fraction was trapped from the effluent and further analyzed on a 4.6 m tricresylphosphate column, on which excellent resolution was achieved.

RESULTS AND DISCUSSION

The composition and rates of the light gases evolved from the Peace River bituminous sand at 278, 298, 323, 343, 368, 388, 403 and 423°K are presented in Table I. The volatile material obtained up to 298°K, which is the formation

Table I. Composition of Gases Evolved from the Peace River oil sand as a Function of Temperature

Temperature (°K)	10 ⁻⁸ mol hr ⁻¹ kg ⁻¹ oil sand							
	278	298	323	343	365	388	403	423
Heating Time (hours)	5.5	5.5	5.5	5.2	3.0	2.0	2.0	1.0
Methane	0.62	0.85	1.4	7.6	20.7	80.1	165	577
Ethylene	n.o. ^a	0.10	10.2	12.7	7.9	24.3	35.8	43.4
Ethane	n.o.	0.03	0.58	6.1	3.2	8.9	20.1	50.5
Methanol	n.o.	n.o.	n.o.	0.11	4.3	11.7	11.6	16.1
Acetaldehyde	0.03	0.18	12.2	26.4	80.2	126	101	155
Propylene	0.10	0.11	10.9	11.6	15.6	37.2	62.6	156
Propane	n.o.	n.o.	1.8	4.2	22.2	12.6	34.7	357
i-Butane	n.o.	n.o.	0.09	0.9	11.6	7.9	20.8	151
i-Butene	n.o.	n.o.	6.3	6.2	8.7	27.5	50.3	124.5
n-Butane + Butenes	n.o.	0.13	0.78	3.0	7.4	17.0	21.8	86.7
Pentanes + Pentenes	17.7	26.4	6.7	13.0	65.8	112	170	609
C ₆	7.3	9.8	2.7	6.2	10.9	24.9	38.0	119
Carbon monoxide	0.24	0.54	14.4	20.3	483	261	548	2,050
Carbon dioxide	143	500	3,260	6,820	24,300	13,400	26,800	101,000
Carbonyl sulfide	0.03	0.04	0.59	1.30	11.5	20.3	31.8	105

^aNot observed.

temperature, are CH₄, C₂H₄, C₂H₆, CH₃CHO, C₃H₆, n-C₄H₁₀, 1- or 2-C₄H₈, C₅, C₆, CO, CO₂ and COS, and these are considered to be constituents present in the formation. Neopentane was not detected in these samples, in contrast to the Athabasca and Cold Lake bituminous sand.¹⁻³

It is observed that a considerable similarity exists in the gases found to be present in the Peace River, Cold Lake and Athabasca deposits with the notable exception of neopentane, which is absent in the Peace River reservoir.¹⁻³ The formation temperatures for the Athabasca, Cold Lake and Peace River reservoirs are 278, 293 and 300°K, respectively. The yields of hydrocarbon gases - with the exception of methane - from three reservoirs at 343°K increase with increasing formation temperature.³

The yields of all materials after a given time are enhanced with increasing temperature, indicating that both thermolysis and desorption processes may be involved in determining the yield. The amounts of volatile materials evolved at 278°K are less from the Peace River bituminous sand than those from the Athabasca and Cold Lake samples.¹⁻³ However, the rates of increase of most of the products with rising temperature are higher in the former than in the latter.

The yields of products as a function of reaction time of Peace River oil sand were studied in detail at 423°K using homogenized bituminous sand samples. The homogenization process was done quickly to minimize additional contact of the bituminous sand with air. The results show that although the product yields increase with increasing reaction time, however, the rates of formation of some of the products actually decreased. This is illustrated for the cases of CH₄, C₂H₄, i-C₄H₈, CO and COS in Figure 1 where rates of formation could be estimated from the slopes of the curves. From these plots it appears that CH₄, CO and COS are primary

products while the principal origins of C_2H_4 and $i-C_4H_8$ are secondary in nature.

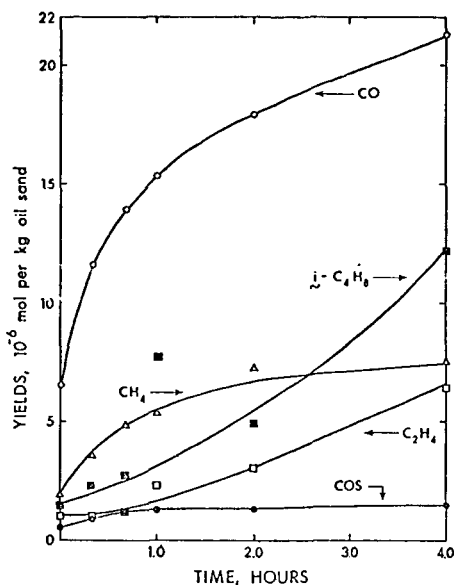


Figure 1. Yields of gases as a function of time in the Peace River oil sand at 423°K.

Kinetic treatment of some of the data in Table I, i.e., plots of the logarithms of rates versus reciprocal temperatures yielded Arrhenius parameters which are listed in Table II. The corresponding values estimated from the Cold Lake and Athabasca data are included in Table II for comparison. The activation energies for the most of the product formation from Peace River oil sand are higher than those from Athabasca or Cold Lake samples. This implies that the former reservoir is more mature than the latter two. It is interesting to note, however, that the activation energy of 4.1 kcal/mol for ethylene formation from Peace River oil sand is much lower than those for Athabasca or Cold Lake, which are 11.8 and 12.4 kcal/mol, respectively. It must be pointed out that all the activation energies measured are very low, indicating that catalytic processes are involved. The rates of product formation at 278°K, calculated by extrapolation of the Arrhenius parameters, are included in Table II. These rates, which are small but significant even at 278°K, indicate that all these oil sand reservoirs of Alberta are presently undergoing similar thermal maturation processes.

The distribution of the products and the values of the Arrhenius parameters for these oil sand formations support our earlier conclusion that these deposits have a common origin and a similar diagenetic history.^{1-3,6}

The yields of the volatile materials collected from Athabasca oil sand at 333°K in the absence and presence of oxygen are listed in Table III. In the absence of oxygen C_1-C_6 hydrocarbons, CH_3CHO , CO and CO_2 were detected. In the presence of oxygen acetone, propionaldehyde and carbon disulfide are produced in addition to the above compounds. It was observed that oxygen has an enhancing effect on the yields of every product except olefins. These results are in contrast to those

Table II. Arrhenius Parameters for the Thermolysis of Peace River (PR), Cold Lake (CL) and Athabasca (AT) Oil Sands

Product	A (mol hr ⁻¹ kg ⁻¹)			E _a (kcal/mol)			R _{278°K} (mol hr ⁻¹ kg ⁻¹)		
	PR	CL	AT	PR	CL	AT	PR	CL	AT
CH ₄	1.8 x 10 ³	3.1	6.5	16.6	12.8	13.6	1.7 x 10 ⁻¹⁰	3.1 x 10 ⁻¹⁰	1.4 x 10 ⁻¹⁰
C ₂ H ₄	5.5 x 10 ⁻⁵	3.8 x 10 ⁻¹	9.5 x 10 ⁻²	4.1	12.4	11.8	3.3 x 10 ⁻⁸	8.0 x 10 ⁻¹¹	5.1 x 10 ⁻¹¹
C ₂ H ₆	5.3 x 10 ¹		1.2 x 10 ⁻³	15.5		8.3	3.2 x 10 ⁻¹¹		3.5 x 10 ⁻¹⁰
C ₃ H ₆	7.1	9.6 x 10 ⁻²	1.4	12.9	11.2	13.8	4.7 x 10 ⁻¹⁰	1.7 x 10 ⁻¹⁰	2.2 x 10 ⁻¹¹
i-C ₄ H ₆	8.8 x 10 ²		2.9 x 10 ⁻⁵	17.3		6.8	2.2 x 10 ⁻¹¹		1.3 x 10 ⁻¹⁰
1-C ₄ H ₁₀	5.5 x 10 ¹	5.5 x 10 ⁻⁶	1.5 x 10 ⁻⁴	14.8	5.1	8.3	1.3 x 10 ⁻¹⁰	5.6 x 10 ⁻¹⁰	4.5 x 10 ⁻¹¹
CO	7.6 x 10 ³	1.4 x 10 ¹	2.0 x 10 ¹	16.7	9.4	8.8	5.5 x 10 ⁻¹⁰	6.5 x 10 ⁻⁹	2.4 x 10 ⁻⁸
CO ₂	1.1 x 10 ²			9.8			2.1 x 10 ⁻⁶		
COS	4.9 x 10 ¹	3.5 x 10 ⁻³	9.1 x 10 ⁻²	14.9	9.0	11.6	1.0 x 10 ⁻¹⁰	3.3 x 10 ⁻¹⁰	7.3 x 10 ⁻¹¹

Table III. Composition of Gases from the Oxidation of the Athabasca Oil Sand at 333°K^a

Product	O ₂		O ₂	
	Nil ^b	6.37 mmol ^c	Nil ^b	6.37 mmol ^c
	Rates, 10 ⁻⁸ mol hr ⁻¹ kg ⁻¹ oil sand		Rates, 10 ⁻⁸ mol hr ⁻¹ kg ⁻¹ oil sand	
Methane	0.18	0.26	Pentanes + Pentenes	0.55
Ethylene	0.41	0.12	C ₆	0.10
Ethane	0.05	0.06	Acetaldehyde	0.06 ^d
Propylene	0.39	0.14	Acetone	n.o.
Propane	0.01	0.04	Propionaldehyde	n.o.
i-Butane	0.01	0.03	Carbon monoxide	0.08
1-Butene	0.27	0.05	Carbon dioxide	38.8
n-Butane	0.03	0.04	Carbon disulfide	n.o.
Neopentane	0.12	0.32		

^a Each sample contained 200 g oil sand. ^b The sample was heated for 1846 hours. ^c The sample had an initial 411 torr pressure of oxygen and was heated for 1822 hours. ^d Not observed.

obtained at 403°K where oxygen has an enhancing effect on the yields of each product.⁴

The rates or ratios of rates of evolution of some of the gases at 403°K for 4 hrs heating time as a function of oxygen pressure are plotted in Figure 2. It is apparent from these plots that the rate of thermolysis increases with increasing pressure of oxygen; however, the rates of some products rise more rapidly than those of others.

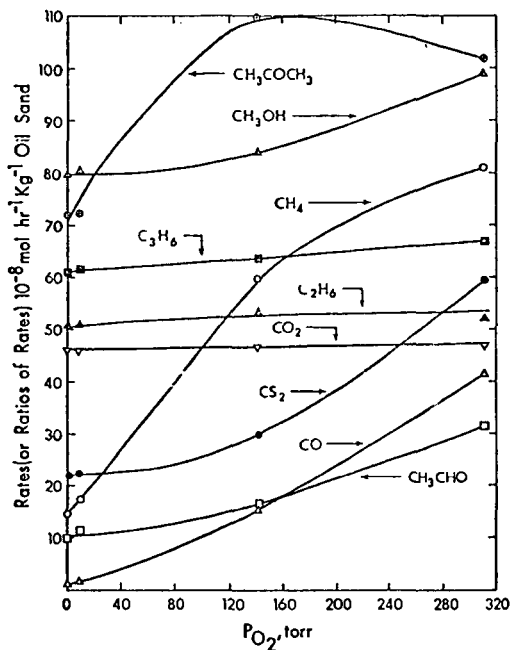


Figure 2. Rates or ratios of rates (based on the rate in the absence of $O_2 = 1.00$) in the thermolysis of Athabasca oil sands at 403°K as a function of oxygen pressure:

- , CH_4 (rates);
- △, CO (rate ratios);
- ▽, CO_2 (rate ratios + 45);
- , CH_3CHO (rate ratios + 10);
- , CS_2 (rates + 20);
- ▲, C_2H_6 (rates + 50);
- , C_3H_6 (rates + 60);
- ⊕, CH_3COCH_3 (rates + 70) and
- △, CH_3OH (rates + 80).

It has been observed that the rates of evolution of CH_4 and CO at 373°K are not appreciably affected in the presence of a few torr oxygen but are markedly enhanced at higher pressures. These results imply that either the product yields are insensitive to trace amounts of oxygen in the system or that the sample was already contaminated with oxygen during storage and handling.

The yields of a few typical products are plotted as a function of time in Figure 3. Those of CH_3CHO , CH_3COCH_3 , C_2H_5CHO and CS_2 initially increase with increasing conversion of the bitumen, then decline, as secondary reactions begin to predominate. The trend in the CO production is not as clearly defined but it is highly improbable that such a stable molecule would undergo secondary reactions; very likely, its yield becomes constant as the precursors become depleted.

CH_3CHO , CH_3COCH_3 and C_2H_5CHO are typical products observed in the thermolysis of hydrocarbons in the presence of molecular oxygen and also have been observed to pass through a maximum with increasing conversion.⁷⁻¹⁰ In these systems, however, CO is a minor product at low conversion and CO_2 is only detected at high conversions, of the order of 30%.¹⁰ In contrast, even at very low conversions, CO and CO_2 are the most abundant products formed upon oxidation of oil sands, and the CO_2 yields are much higher than those of CO . It is tempting to conjecture that these

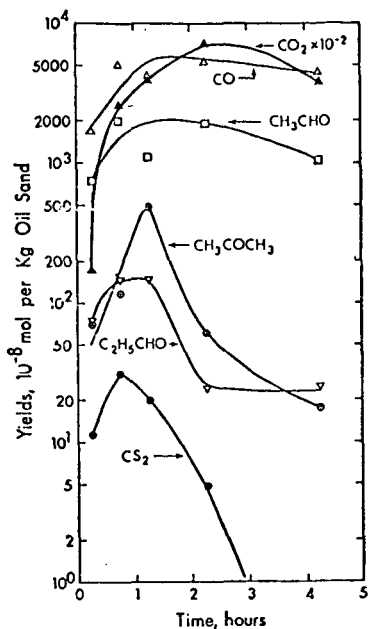


Figure 3. Yields of the thermolysis products of Athabasca oil sand in the presence of oxygen at 403°K as a function of time.

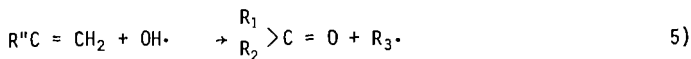
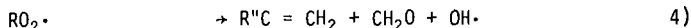
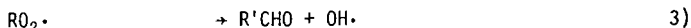
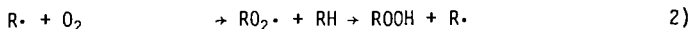
products are formed mainly, if not entirely, from carboxylic acids and aldehydes already present as constituents in the bitumen and that the other identified products are formed *via* oxidation of hydrocarbon precursors; however, we have observed that the CO and CO₂ yields depend to some extent on the nature of the sample and its previous history and therefore much more work is needed before the reaction channels can be elucidated.

The oxidation of hydrocarbons by molecular oxygen involves a complex reaction network; however, it is commonly accepted that a chain mechanism is operative and that one of the first products formed is a hydroperoxide which may be oxidized further or decompose thermally, initiating new chains.⁷⁻¹²

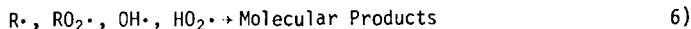
- initiation:



- chain propagation:



- chain termination:



Detailed discussions of this general mechanism have been presented in several publications.^{7,8,10-11} This type of mechanism applies to pure hydrocarbons and its application to a complex system such as Athabasca oil sand is of very limited scope; moreover, it does not account for most of the CO₂ and CO yields evolved in this low temperature region, 278 to 403°K.

It should be noted that the quantities of CO and CO₂ evolved are the most sensitive indicators of the degree of oxidation of the sample and therefore can shed light on its previous history. For example, CO was demonstrably absent among the products evolved upon thermolysis of a fresh oil sand sample from the Athabasca reservoir, strongly suggesting that this deposit has not been exposed to air in the recent past.

ACKNOWLEDGMENTS

This work was supported by the Alberta Oil Sands Technology and Research Authority. We wish to thank Dr. E.M. Lown for help in the preparation of this manuscript.

REFERENCES

1. Strausz, O.P., Jha, K.N. and Montgomery, D.S., *Fuel* (1977) 56, 114.
2. Jha, K.N. and Strausz, O.P., Preprints, Div. Fuel Chem., ACS, (1977) 22, 14.
3. Jha, K.N., Montgomery, D.S. and Strausz, O.P., "Oil Sand and Oil Shale Chemistry", Eds. Strausz, O.P. and Lown, E.M., Verlag Chemie Int., New York, (1978), 33.
4. Jha, K.N., Rao, P.M. and Strausz, O.P., Preprints, Div. Fuel Chem., ACS, (1978), 23, 91.
5. Selucky, M.L., Chu, Y., Ruo, T. and Strausz, O.P., *Fuel* (1977) 56, 369.
6. Jha, K.N., Gray, J. and Strausz, O.P., *Geochim. Cosmochim. Acta*, in press.
7. Sieg, L., "Low Temperature Oxidation", ed. Jost, W., Gordon and Breach Science Publishers, New York (1965), 191.
8. Drysdale, D.D. and Norrish, R.G.W., *Proc. Roy. Soc. A.*, (1969), 308, 305.
9. Kovalev, G.I. and Denisov, Y.T., *Neftekhimiya*, (1976), 16, 457.
10. Baker, R.R., Baldwin, R.R., Everett, C.J. and Walker, R.W., *Comb. and Flame*, (1975), 25, 285.
11. Allara, D.L., Mill, T., Hendry, D.G. and Mayo, F.R., "Oxidation of Organic Compounds, Vol. II", *Adv. Chem. Series*, (1968), 76, 40.
12. Boboleva, S.P., Bulygin, M.G. and Blyumberg, E.A., *Neftekhimiya*, (1974), 14, 730.

The Reactions of Coal with Transition Metal Halides

Herbert Beall

Department of Chemistry
Worcester Polytechnic Institute
Worcester, Massachusetts 01609

Introduction

Many studies(1) of the X-ray diffraction patterns of coal have yielded the result that increasing coal rank results in increasingly sharp diffraction patterns(2). Furthermore, as the rank limit is approached the very high rank metaanthracites give diffraction with essentially all of the features of a pattern obtained from graphite(3). These results have led to the general acceptance of the model that coalification involves the growth of polynuclear condensed aromatic structures into graphite-like units(1,4). It is of interest to determine if chemical properties of graphite are manifested by coal. In particular, it is well-known that graphite will undergo reactions with a variety of reagents to form intercalation compounds where the graphite layers are separated to accommodate a variety of species between them(5,6). It is therefore of interest to establish if such intercalation compounds can be prepared from coal and, in fact, a recent report very strongly supports that such compounds can be prepared from coal and potassium(7). This paper describes attempts to prepare coal intercalation compounds with the chlorides of iron(III), chromium(III), and copper(II). Analysis of the results is by X-ray powder diffraction. The 002 line in the X-ray powder pattern of graphite is the strongest graphite line and represents the spacing between planar polyaromatic layers of carbon. Formation of intercalation compounds separates these carbon layers and affects this 002 line.

Results and Discussion

Initial experiments(8) were carried out in which anhydrous iron(III)chloride (FeCl_3) was reacted with four different coals. FeCl_3 was chosen for the initial studies because its intercalation compounds with graphite are among the best known and most easily prepared(5,6). The coals selected were the following: PSOC-379, Pennsylvania semi-anthracite (P&M'B'); PSOC-151, New Mexico high volatile bituminous C (Lower Split of Blue); PSOC-240, Washington sub-bituminous B (Big Dirty); and PSOC-247, North Dakota lignite (Noonan). These four coals were treated directly with FeCl_3 after pulverization and air drying at 120° and were also treated with FeCl_3 after a demineralization(9) which involved washing with 10% HCl at 50°C for 18-24 hours followed by air drying at 120° . X-ray diffraction patterns of the untreated and demineralized coals were essentially identical except that enhanced crystallinity of the demineralized samples was evidenced by the shorter diffraction times needed to obtain equivalent diffraction patterns. PSOC-151, PSOC-247, and PSOC-240 showed principally the 002 graphite line whereas PSOC-379 gave this line strongly as well as other lines from crystalline matter.

In each of these six reactions with FeCl_3 approximately 1.0 g of coal and 0.6 g of FeCl_3 were mixed and then heated to 230° for ten minutes. No obvious evidence of reaction was observed and the final

products look similar to the coal starting material. Incorporation of the FeCl_3 into the coal is evidenced by the failure of the reaction products to react readily with water to form the yellow-brown hydrate which the unreacted FeCl_3 forms. The diffraction patterns of the coal- FeCl_3 products of PSOC-151 and PSOC-240 do not include the 002 graphite line which was prevalent in the coal starting material and this line is almost completely eliminated for PSOC-379. More rigorous conditions using 2 g of FeCl_3 per gram of coal and heating for 36 minutes at up to 250° were found to produce products where the 002 graphite line was eliminated for PSOC-379. The products under these more rigorous conditions were observed to be more gray and powdery than the starting coal. The more rigorous conditions required for PSOC-379 could be attributed to more extensive graphite-like structures in the semi-anthracite coal. Examination of the diffraction patterns of the PSOC-247(lignite)- FeCl_3 products gave ambiguous results with removal of the 002 graphite line evident only in the demineralized sample. However, the 002 line in the starting material is relatively weak.

A further observation is the appearance of diffraction lines attributable to $\text{FeCl}_2 \cdot 2\text{H}_2\text{O}$ in the patterns of some of the reacted samples. This evidence of reduction and hydration of the FeCl_3 was observed for the demineralized samples of PSOC-379, PSOC-151 and PSOC-247, and both dried and demineralized samples of PSOC-240. The nature of the material in the coal which was oxidized was not determined. The H_2O of hydration may have come from moisture still adsorbed on the hydrophilic surface of the coal which may have been rendered more hydrophilic by the demineralization process. Other sources of the H_2O are possible and cannot be overruled.

The demineralized PSOC-379 and PSOC-247 products with FeCl_3 were then washed with 10% HCl at 50° for 18 hours and subsequently dried in air at 120° . The diffraction patterns obtained from the samples after washing were identical to those of the coal samples prior to reaction with FeCl_3 except that a longer time seemed to be needed to obtain the same intensity of diffraction possibly indicating some breakdown of the crystallinity. Thus the reaction with FeCl_3 is largely reversible in these cases. Testing of the wash liquid obtained from these experiments with $\text{K}_3\text{Fe}(\text{CN})_6$ solution gave a strong test for Fe^{++} in corroboration of the X-ray evidence above that $\text{FeCl}_2 \cdot 2\text{H}_2\text{O}$ is formed in the coal- FeCl_3 reaction.

Comparison experiments were run in which FeCl_3 was reacted with amorphous carbon powder (Acheson Graphite, Grade 38) which can be regarded as microcrystalline graphite. These experiments yielded observations which were parallel to those obtained with coal except that more FeCl_3 and more rigorous conditions were required to eliminate completely the 002 diffraction line of the amorphous carbon. The carbon would be expected to be able to intercalate more FeCl_3 than the much more heterogeneous coal structure. Diffraction lines for $\text{FeCl}_2 \cdot 2\text{H}_2\text{O}$ were faintly discernible in the diffraction patterns of the carbon- FeCl_3 product and a distinct Fe^{++} test was obtained in the 10% HCl wash liquid. Presumably this can be attributed to adsorbed moisture on the carbon surface and oxidation of some of the carbon.

These experiments were extended to anhydrous chromium(III)-chloride (CrCl_3) and anhydrous copper(II)chloride (CuCl_2). Each of

these salts was reacted with demineralized PSOC-240 and dried PSOC-379 in an approximate ratio of 1.8:1 (g coal: g salt) at 250°. Acidic vapors were evolved in each reaction; the reaction with CuCl_2 resulted in removal of the 002 graphite line but the reaction with CrCl_3 did not. Examination of the coal- CuCl_2 product diffraction patterns did not yield perceptible lines for any material other than CuCl_2 . Washing of the PSOC-379 product with 10% HCl resulted in the return of the diffraction pattern of the starting coal. It was noted that the PSOC-379 had been converted to an extremely fine powder in the course of reaction with CuCl_2 and then washing with 10% HCl. This would seem to be indicative of very extensive penetration of the CuCl_2 into the coal structure.

Further investigations involved the reactions of coal with the corresponding hydrated salts, $\text{FeCl}_3 \cdot 6\text{H}_2\text{O}$, $\text{CrCl}_3 \cdot 6\text{H}_2\text{O}$, and $\text{CuCl}_2 \cdot 2\text{H}_2\text{O}$. Demineralized and untreated samples of PSOC-379, PSOC-151, and PSOC-240 were reacted with approximately equal weights of $\text{FeCl}_3 \cdot 6\text{H}_2\text{O}$ at 215° for 3 minutes. Each of these mixtures was observed immediately to become liquid and chemical reaction was evidenced by bubbling which occurred for about one minute. At that point the mixtures suddenly solidified and were noticeably more grey in color than the starting pulverized coal. Disappearance of the 002 graphite line was observed in the reactions of the PSOC-379 samples with $\text{FeCl}_3 \cdot 6\text{H}_2\text{O}$ and this line was almost completely removed in the PSOC-151 and PSOC-240 reactions. All diffraction patterns of the reacted products showed that $\text{FeCl}_2 \cdot 2\text{H}_2\text{O}$ had been produced. Washing the products of demineralized PSOC-379 and $\text{FeCl}_3 \cdot 6\text{H}_2\text{O}$ with 10% HCl at 50° brought back the original demineralized coal diffraction pattern although with lines slightly weaker and slightly more diffuse. The liquid remaining from this washing gave a strong test for Fe^{++} again corroborating the formation of $\text{FeCl}_2 \cdot 2\text{H}_2\text{O}$ in the reaction. Parallel experiments with amorphous carbon resulted in virtual removal of the 002 diffraction line when the ratio of $\text{FeCl}_3 \cdot 6\text{H}_2\text{O}$ to carbon was about 2.5:1 (g:g). No $\text{FeCl}_2 \cdot 2\text{H}_2\text{O}$ lines were observed in the patterns from the carbon- $\text{FeCl}_3 \cdot 6\text{H}_2\text{O}$ product and the original carbon diffraction pattern could be returned by washing this product with 10% HCl at 50°.

Reactions of demineralized samples of PSOC-379 and PSOC-151 with $\text{CrCl}_3 \cdot 6\text{H}_2\text{O}$ and $\text{CuCl}_2 \cdot 2\text{H}_2\text{O}$ both resulted in removal of the 002 graphite lines in the coals. The ratio of coal to salt was about 1.25:1 (g:g) and the reaction conditions were 250° for nine minutes. Dehydration and evolution of acid vapors were evident with both salts; diffraction lines for anhydrous CuCl_2 were evident in the coal- $\text{CuCl}_2 \cdot 2\text{H}_2\text{O}$ product patterns. No diffraction lines for crystalline salts were evident in the products of the reactions of coal and $\text{CrCl}_3 \cdot 6\text{H}_2\text{O}$. The PSOC-379 diffraction pattern was returned when the products of each of the salts and this coal were treated with 10% HCl at 50°. This washing of the PSOC-379- $\text{CuCl}_2 \cdot 2\text{H}_2\text{O}$ product again gave back the coal in an extremely finely divided state as was the case in the reaction with anhydrous CuCl_2 (above). Comparison reactions in which $\text{CrCl}_3 \cdot 6\text{H}_2\text{O}$ and $\text{CuCl}_2 \cdot 2\text{H}_2\text{O}$ were reacted with amorphous carbon gave results which were generally parallel to the results of the reactions of these salts with coal except that more salt was needed to effect removal of the 002 line with $\text{CuCl}_2 \cdot 2\text{H}_2\text{O}$ and complete removal of this line was not achieved with $\text{CrCl}_3 \cdot 6\text{H}_2\text{O}$.

Experimental

Reagents were obtained from standard commercial sources and coal samples were donated by Pennsylvania State University. Powder diffraction patterns were recorded on film using FeK α radiation.

Acknowledgment

The author is grateful to Dr. Alan Davis of the Coal Research Section of the Pennsylvania State University who supplied the coal samples.

References

1. D. W. van Krevelen, Coal, Elsevier, Amsterdam, 1961.
2. R. Westrik, unpublished results reported in (1).
3. M. Mentser, H. J. O'Donnell, and S. Ergun, Fuel, 41, 153(1962).
4. H. L. Retcofsky, in B. R. Cooper, Ed., Scientific Problems in Coal Utilization, p. 79-99, U. S. Department of Energy, 1978.
5. W. Rudorff, Advances in Inorganic Chemistry and Radiochemistry, 1, 223(1959).
6. G. R. Henning, Progress in Inorganic Chemistry, 1, 125(1959).
7. L. Lazarov, I. Roshkov, and S. Angelov, Fuel, 57, 637(1978).
8. H. Beall, Fuel, 58, 319(1979).
9. R. G. Jenkins, S. P. Nandi, and P. L. Walker, Jr., Fuel, 52, 288(1973).

Thermal Decomposition of Aromatic Substances

R. E. Miller and S. E. Stein

Department of Chemistry, West Virginia University, Morgantown, WV 26506

Introduction

Carefully designed experiments, allied with thermochemical kinetics analysis (1) of reaction mechanisms have led to useful working models of complex process such as hydrocarbon pyrolysis, atmospheric chemistry and combustion. A comparable understanding of even the basic chemical features of coal conversion has not yet been developed. Using a combined experimental and thermochemical kinetics approach, this work is intended to lead to effective, semiquantitative chemical models for aspects of coal pyrolysis, polymerization, hydrogenation and liquefaction.

The theoretical foundation for this research is the well-developed understanding (2) and predictive tools (1) for free radical kinetics and thermochemical estimation methods for aromatic substances (3, 4) and free radicals (5). Experiments determine rates of product evolution over as wide a range of conditions as possible with the aim of quantitative description using elementary kinetics models.

Numerous useful experiments using "model" compounds to simulate coal conversion reactions have been reported (6). The present program is not intended to simulate coal reactions, but to reveal characteristic reaction pathways in thermal aromatic chemistry and their kinetic properties, with the aim to eventually extrapolate the results to coal reactions. Two aspects of this program are reported here along with some speculations on coal chemistry.

Experimental

All liquid-phase reactions were carried out in a sealed, evacuated pyrex tube heated in an aluminum block oven. Temperature stability and accuracy were $\pm 1^\circ\text{C}$. Heat-up and cool-down times were generally negligible (< 2 min) relative to reaction duration (15 min - 48 hours). Solids were purified by recrystallization and sublimation and generally found to be 99.5+% pure by gas chromatography (gc). Tetralin was purified by distillation in a spinning band column. GC was the primary analytical tool with benzene and acetone used as solvents for reaction mixtures. Hydrogen, methane and benzene were determined via mass spectrometry. Identities of products with retention times up to that of phenanthrene were determined by coinjection on a WCOT SE-30 glass capillary column. Other products were determined on OV-101 and FFAP glass columns using temperative programming. Most kinetic analyses were carried out on packed OV-101 glass columns. A more complete account of these experiments is under preparation. The gas phase decomposition rate of 1,2 diphenylethane (12DPE) was determined using very low pressure pyrolysis methods (7).

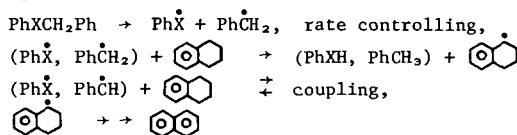
Homolytic Bond Cleavage ($\text{R-R}' \rightarrow \text{R}\cdot + \text{R}'\cdot$)

Simple cleavage of covalent bonds to generate two free radicals is commonly regarded as a major first step in coal liquefaction and pyrolysis. Therefore, it is clearly useful to be able to reliably estimate rates of bond cleavage for bonds likely to be present in coal conversion. It is possible at present to estimate rates of such cleavage in the gas-phase for a wide variety of chemical bonds using available thermodynamic and kinetic data (1, 8). While it is commonly assumed that such rate constants are roughly the same in condensed phases as in the gas-phase, this assumption has been well tested only for peroxide decomposition at $\lesssim 200^\circ$ (9).

To directly test the accuracy of the above assumption, rate constants, k_d , of bond scission for 12DPE, benzyl phenyl ether, benzyl phenyl amine and benzyl phenyl sulfide were determined in tetralin solution and compared to corresponding gas phase rate constants, k_g . As shown in Table I, the reliability of this assumption is good.

Gas phase rate constants were determined in the following manner. Very-low pressure pyrolysis was employed to find $k_g(12DPE)/s^{-1} = 2.9$ at $650^\circ C$. By assuming a central C-C bond strength of 61 kcal/mol in 12DPE (10), $\log k_g(12DPE)/s^{-1} = 14.9 - 61000/4.58 T$. For the remaining substances, k_g was estimated relative to $k_g(12DPE)$ using literature data for related compounds (11).

Liquid phase rate constants were determined in tetralin with the mole fraction of tetralin between 0.8 and 0.95. The dissociation of 12DPE was extensively studied from $325-425^\circ C$ (Figure 1), and $k_d(12DPE)/s^{-1} = 16-64800/4.58 T$. The mechanism of these reactions was consistent with the following (X = CH₂, O, NH, S):



In support of this mechanism, the disappearance of PhXCH₂Ph was first order with respect to time and independent of the initial concentration of PhXCH₂Ph. The coupling pathway was generally minor, and decreased with increasing temperature. 1,2 Dihydronaphthalene was always seen as a reaction intermediate, while 1,4-dihydronaphthalene could not be detected.

Rate constants, k , (or half-lives, $\tau_{1/2} = \ln 2/k$) for a wide variety of bond structural types can now be estimated with reasonable accuracy, and some selected examples are given in Table 3. Of special note is the prediction that under conditions where coal begins to decompose ($\sim 400^\circ C$) the only bonds to appreciably cleave are those that generate two resonance stabilized radicals.

1,2 Diphenylethane Pyrolysis

To develop an understanding of the chemistry of complex systems, it is first necessary to understand the chemistry of "simple" systems as completely and unambiguously as possible. The pyrolysis of 12DPE was chosen as a starting point for these studies since, on paper, it appeared to have a straightforward decomposition pathway, and several relevant rate constants have been measured in solution (2). A complete product analysis has been carried out at 25° intervals over the temperature range $325-450^\circ C$. Results at $375^\circ C$ for the selected products are given in Figure 2. Through analysis via thermochemical kinetics techniques and computer models the mechanism given in Figure 3 has been deduced. Some noteworthy features are:

- (1) All features of the reaction can be reasonably interpreted by a free radical scheme.
- (2) Combination of 12DPE radicals (step 3a) is favored by ≈ 3 over disproportionation (step 3b). This is similar to the behavior of the related 1-phenylethyl radical (2).
- (3) A major pathway for trans-1,2-diphenylethane (t-stilbene) production is via radical coupling (step 3a) followed by an H atom abstraction (step 4).
- (4) 1,1 diphenylethane results from an uphill ($\Delta G \sim 11$ kcal/mol) "neophyl" rearrangement (2) followed by an H-atom abstraction from 12DPE.
- (5) The formation of phenanthrene is hypothesized to occur through an unusual isomerization involving several H-atom shifts.

A set of rate constants consistent with literature values and thermochemical kinetics constraints have been deduced for this mechanism and has been found to adequately predict primary product formation rates up to $\sim 60\%$ decomposition. A

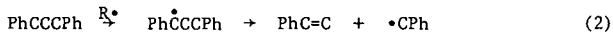
good mass balance has been achieved, and little effect on product formation upon increasing surface area has been found.

Implications for Coal Chemistry

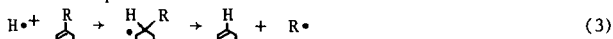
Based on experimental evidence in non-coal systems, and free radical thermochemical kinetics, certain specific features of coal conversion chemistry may be suggested.

(1) The first covalent bonds to homolytically cleave upon heating coal are those that generate two resonance stabilized radicals (e.g., benzyl radicals,  ...). In fact, under normal liquefaction conditions ($\approx 450^\circ\text{C}$) such bonds will be virtually the only bonds to break in this manner. Other reaction pathways may generate more reactive organic free radicals, however, these can be expected to abstract benzylic H-atoms, thereby producing resonance stabilized radicals. Hence, to a large extent, the free radical chemistry of coal is determined by the chemistry of resonance stabilized radicals.

(2) Modes of bond rupture other than simple bond cleavage may be very significant in coal reaction. Two well known free radical pathways, β -bond scission,



and free radical displacement



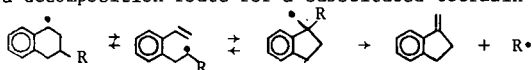
occur in 12DPE (and many other) pyrolyses. The thermal instability reported for the compounds PhCCCPH, PhCCCCPh, PhCOCC in tetralin (6b) are likely due to chain reactions involving sequence (2).

(3) In view of the relatively high temperatures and free radical concentrations (12) in coal conversion, it might be surmised that free radical isomerizations take place under coal conversion conditions which are not observed in conventional solution phase free radical experiments. In fact, the mechanism of Figure 3 contains two such reactions of the 12DPE radical in steps 5 and 6. Isomerization of tetralin and related structures has been reported by several workers. A likely path, for instance, for tetralin isomerization to 1-methyl indane (6f) is through the tetralyl radical:



Similar isomerizations can lead to structures which are thermally labile.

For instance, a decomposition route for a substituted tetralin structure in coal might be



Hence, hydroaromatic structures in coal not only act as H-donors, but may also lead to radical induced bond cleavage.

(4) The unique ability of tetralin and related compounds to act as effective donor solvents cannot be explained simply by its rate of reaction with free radicals (6d). Two other factors concerning high temperature, free radical reactions of tetralin may help explain its special solvent properties.

First, to irreversibly transfer H-atoms to radicals, the donor solvent must be transformed to a substance stable under coal conversion conditions. For instance, diphenyl methane and methyl naphthalene are effective low temperature free radical traps, however, at elevated temperatures the radicals formed upon loss of H-atoms from these molecules cannot be permanently terminated. These radicals will rapidly build up in concentration and act as H-atom acceptors from coal molecules. In support of this idea, we have found that 5:1 mixtures of diphenyl methane:12DPE at 400°C react virtually the same as does pure 12DPE at

this temperature. Despite the fact that PhCPh radicals are undoubtedly the predominant radicals in this system, these radicals will simply build up in concentration, and abstract H-atoms from 1,2-DPE. Substances such as ethyl naphthalene and indane are also not expected to be as effective as tetralin, since their dehydrogenated molecules contain reactive styrene-like structures which may be either reduced by coal back to the starting substance, or aid in the polymerization of coal.

A second, rather unique property of tetralin-like structure is the possible reactive intermediate , in which the weak C-H bond strength is only

26 kcal/mol (5). By comparison the weakest C-H bond in  is 48 kcal/mol.

This radical will lose an H-atom which can be quite effective in depolymerizing coal through displacement reactions (e.g., 8b in Figure 3).

Conclusion

For the liquid-phase thermal decompositions studied, free radical pathways appear capable of explaining even the finest details in at least a semiquantitative manner.

In our opinion, there is no convincing evidence indicating that homogeneous coal reactions are not primarily free radical in nature. In any case, further complete studies of coal-related pyrolytic systems will indicate not only likely modes of coal reaction via free radical kinetics, but will also reveal contributions from ionic, molecular or heterogeneous pathways.

Acknowledgement

The authors gratefully acknowledge support of this research by the Department of Energy, Fossil Energy Division (Grant EF-77-G-01-2751) and the West Virginia University Energy Research Committee.

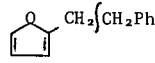
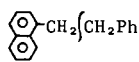
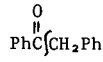
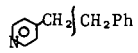
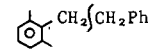
References

1. S. W. Benson, "Thermochemical Kinetics, Second Edition", Wiley and Sons, New York, 1975.
2. "Free Radicals, Vols. I, II", J. Kochi, ed., Wiley and Sons, New York, 1973.
3. S. E. Stein, D. M. Golden and S. W. Benson, *J. Phys. Chem.*, **81**, 314 (1977).
4. R. Shaw, D. M. Golden and S. W. Benson, *J. Phys. Chem.*, **81**, 1716 (1977).
5. S. E. Stein and D. M. Golden, *J. Org. Chem.*, **42**, 839 (1977).
6. (a) C. J. Collins, V. F. Raaen, B. M. Benjamin and G. W. Kabaika, *Fuel*, **56**, 107 (1977); (b) B. M. Benjamin et al., *ibid.*, **57**, 269 (1978); (c) Y. Kamilya, T. Yao, S. O. Kawa, Preprints Amer. Chem. Soc. Div. Fuel. Chem., **24** (2), 116 (1979); (d) D. S. Ross and J. E. Blessing, *ibid.*, p. 125; (e) L. W. Vernon, *ibid.*, p. 413; (f) P. S. Virk, et al., *ibid.*, p. 144.
7. D. M. Golden, G. N. Spokes and S. W. Benson, *Angew. Chemie, Int. Ed. Engl.*, **12**, 534 (1973).
8. See, for example, J. A. Kerr and A. F. Trotman-Dickinson, "Strengths of Chemical Bonds" in *CRC Handbook of Chemistry and Physics*, Chemical Rubber Co., Cleveland, OH, 1977.
9. "Organic Peroxides", D. Swern, ed., Wiley Interscience, New York, 1970.
10. M. Rossi and D. M. Golden, *J. Amer. Chem. Soc.*, **101**, 1230 (1979).
11. A. J. Colussi and S. W. Benson, *Int. J. Chem. Kinetics*, **10**, 1139 (1978); **9**, 295 (1977); A. J. Colussi, F. Zabel and S. W. Benson, *ibid.*, **9**, 161 (1977).
12. L. Petrakis and D. W. Grandy, *Analytical Chem.*, **50**, 303 (1978).

Table I. Comparison of Dissociation Rate Constants in Gas-Phase and Liquid (tetralin)-Phase

	$\log k_g$ (est'd)/s ⁻¹	k_l (exper)/s ⁻¹ at T	k_l/k_g at T
PHCH ₂ CH ₂ Ph	15.08-61000/4.58 T	1.02 x 10 ⁻⁵ at 400°C	0.54
PhOCH ₂ Ph	15.58-52800/4.58 T	3.0 x 10 ⁻⁵ at 300°C	1.08
PhNHCH ₂ Ph	15.28-57600/4.58 T	4.4 x 10 ⁻⁵ at 375°C	0.61
PhSCH ₂ Ph	15.58-52700/4.58 T	1.04 x 10 ⁻⁵ at 300°C	0.34

Table II. Liquid Phase Bond Dissociation Rate Constants, k_l , and Half-Lives $\tau_{1/2}$ ($\theta = 4.58$ T/1000)

	$\log k_l/s^{-1}^a$	$\tau_{1/2}$ (400°C)		$\log k_l/s^{-1}$	$\tau_{1/2}$ (400°C)
	16.7-54.2/ θ^b	5 sec		16.4-61.3/ θ^d	37 min
	16.3-60.6/ θ^b	20 min	PhO(CH ₂ Ph)	16.4-55.0/ θ^b	20 sec
PhCH ₂ {CH ₂ Ph	16.0-64.8/ θ^c	21 hr		16.0-63.3/ θ^d	69 hr
	16.0-62.2/ θ^b	3 hr		16.0-70.8/ θ^b	78 days
	16.8-57.6/ θ^d	1 min		16.0-65.8/ θ^d	44 hr
	16.0-60.8/ θ^d	1 hr			

^a Upon substitution of an alkyl group for Ph, k is reduced by $\sim 10^3$ at 400° and ~ 370 at 500°C; $k = Ae^{-E/RT}$, A is accurate to factor of 10, E is accurate ± 5 kcal/mol, k is accurate to factor of 5 (errors in A and E are correlated).

^b Derived from gas-phase data from literature (see text).

^c Derived from Figure 1. All other k values are derived from this value by correcting for differences in E and A (reference 1).

^d Derived from gas-phase data determined in our lab.

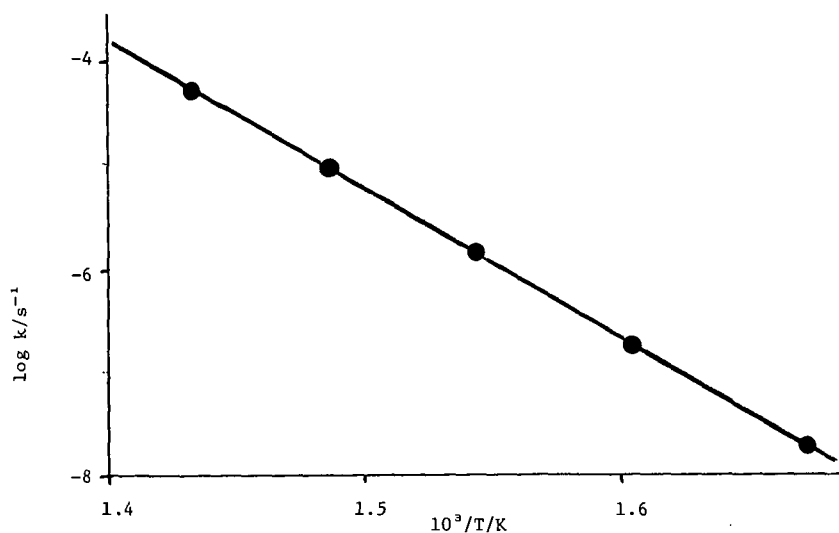


Figure 1. Arrhenius plot for 1,2 diphenylethane dissociation in tetralin

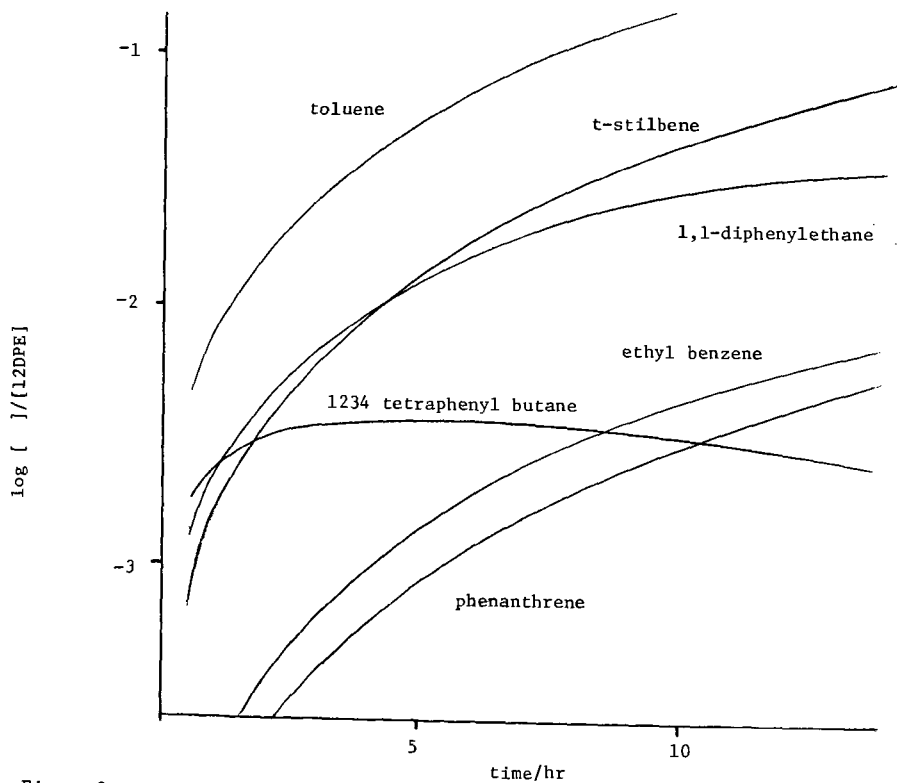


Figure 2. Product evolution in 1,2 diphenyl ethane pyrolysis at 375°C.

POLYMERIZATION OF PHENANTHRENE INDUCED BY 1-METHYLNAPHTHALENE AT HIGH TEMPERATURES AND PRESSURES. Curtis L. Knudson, Bruce W. Farnum and Eugene A. Kline. Grand Forks Energy Technology Center, US DOE, Box 8213 University Station, Grand Forks, ND 58202.

A study of the effects of tetralin and synthesis gas (CO-H_2) on the polymerization of phenanthrene induced by thermally cracked 1-methylnaphthalene at 4000 psi between 440^o and 500^o C was carried out. Five sets of reactants were studied: (a) phenanthrene and N_2 , (b) 1-methylnaphthalene and N_2 , (c) phenanthrene, 1-methylnaphthalene and N_2 , (d) tetralin, phenanthrene, 1-methylnaphthalene and N_2 , and (e) phenanthrene, 1-methylnaphthalene and CO-H_2 . The reactants were charged into a cold autoclave, heated to 450^o C, and held one hour at each 10^o temperature increment up to 500^o C. Reactor gas and liquid phases were sampled during the reactions. Gas samples were analyzed by on-line GC, and liquid samples were analyzed by gel permeation HPLC, LVMS and GC-MS to determine composition changes. Results indicated that CO-H_2 or tetralin present in the reactor greatly reduced the polymerization of phenanthrene.² Thermal cracking of 1-methylnaphthalene resulted in alkylation of phenanthrene in preference to 1-methylnaphthalene. Formation of biphenanthryl in preference to 1,2-dinaphthylethane or binaphthyl occurred in the mixed reactions. Synthesis of the various dimers was carried out to provide pure reference standards.

REGENERATION OF "SPENT" $ZnCl_2$ PRODUCT CATALYST
FROM HYDROCRACKING SUBBITUMINOUS COAL

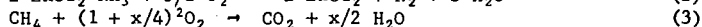
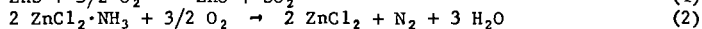
Clyde W. Zielke, William A. Rosenhoover and
Robert T. Struck

Conoco Coal Development Company
Research Division
Library, Pennsylvania 15129

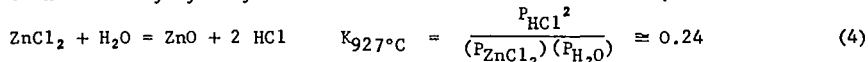
INTRODUCTION

It has been demonstrated in batch and continuous bench-scale units that molten zinc chloride is a superior catalyst for liquefaction of coal, coal extract or other heavy hydrocarbons. High quality gasoline of 90-92 Research Octane Number is produced in high yield in a single hydrocracking step (1,2,3,4,5). Large amounts of zinc chloride are used as the catalyst for high activity, i.e., usually 1 gm of $ZnCl_2$ per gm of coal or extract feed. From 1 to 2 parts by weight of product catalyst is generated during the hydrocracking process depending on the $ZnCl_2$ /feed ratio. This product catalyst is contaminated with zinc sulfide, ammonia or ammonium chloride complexed with zinc chloride (formed by the catalyst partially reacting with the sulfur and nitrogen in the feed during the hydrocracking step), carbonaceous residue that cannot be distilled out of the melt, and coal ash, when coal is the feed to the hydrocracking process. To keep the catalyst active, these impurities must be removed in a regeneration process in which the catalyst is converted back to essentially pure zinc chloride. The impurities do not settle out of the molten product catalyst; hence, the whole product catalyst must be subjected to the regeneration process. Thus, regeneration is a key step in the $ZnCl_2$ coal liquefaction process in development at Conoco Coal Development Company.

The regeneration is accomplished by burning out the impurities in a combustor containing a fluidized bed of "inert" silica sand:



Hydrogen chloride gas is added to the feed air to convert ZnO to $ZnCl_2$ and to prevent formation of ZnO by hydrolysis of zinc chloride in the combustor:



A previous paper described regeneration of essentially coal-ash-free spent melt produced by hydrocracking coal extract (6,7). However, there appear to be economic advantages to a process employing direct coal hydrocracking over a two-step process consisting of coal extraction followed by hydrocracking of the SRC therefrom. Therefore, demonstration of regeneration with low zinc losses of the ash-contaminated spent melt produced by direct hydrocracking of coal is of high importance in the process development. The first work in this regard was done using synthetic spent melt which simulated that produced by hydrocracking subbituminous coal. This work has been published previously (5). Simulated spent melt was used because natural spent melt was not available. Subsequent to that work, successful direct hydrocracking with $ZnCl_2$ catalyst of Colstrip subbituminous coal in a continuous bench-scale hydrocracker furnished feedstock for further development of the regeneration process. Continuous regeneration of this coal-ash-contaminated spent melt from direct hydrocracking of coal and efficient zinc recovery therefrom has now been demonstrated for the first time. In this work zinc recovery was enhanced by introducing a secondary zinc recovery step in which zinc, retained in the coal ash rejected in the primary regeneration step, is largely recovered. This paper presents some of the results of this regeneration work with natural spent melt from direct coal hydrocracking.

EXPERIMENTAL

Feedstocks

Spent Melt

The two feedstocks for the primary regeneration work were low-carbon spent melts produced by direct hydrocracking of Colstrip coal in a 3 lb/h continuous bench-scale hydrocracking unit. Hydrocracking conditions were: 413°C, 24.13 MPa (3500 psig), ZnCl₂/MF solvent-free Colstrip coal ratio of 1.5 and residence times ranging from 74 to 95 min. Normally a ZnCl₂/coal ratio of 1.0 is used; the higher ratio of 1.5 was used to speed up production of spent melt. It gave a yield of about 1.75 gm of spent melt per gm of MF coal feed vs. about 1.25 which is produced at a ZnCl₂/coal ratio of 1.0. The carbon content of the two spent melt feedstocks used were 6.65 and 6.31%, slightly more than required to furnish the heat when burned for carrying out the regeneration adiabatically. The total ash content of the feed melt is based on the sum of the eight most prevalent coal ash elements (Na, K, Ca, Mg, Fe, Ti, Si, Al) expressed as oxides, since the coal ash is mixed with non-combustible materials and, therefore, cannot be determined directly. The total ash determined in this manner is lower than the ash determined in coals or chars in the conventional manner, where sulfates and carbonates may be present, that are not taken into account here. Also, traces of minor elements are not considered here. Analyses of the spent melt are given in Table I.

Colstrip Coal

Minus 100 mesh Colstrip subbituminous coal (Rosebud Seam, Montana) was used as the feedstock for testing, in a 3 lb/h continuous hydrocracker. The activity of regenerated spent melt was compared with virgin zinc chloride. Analyses of this coal are given in Table I.

Cyclone Underflow Ash

This material, which is generated in the primary regeneration step, contains the coal ash and generally less than 2% of the zinc in the spent melt feed to the primary regeneration. It is fed to a secondary zinc recovery step wherein the majority of this "lost" zinc is recovered. Analyses of this material are given under the heading "Composite" in Table VI.

Equipment and Procedure

Primary Regeneration

Figure 1 is a diagram of the continuous 2-7/8" I.D. fluidized bed combustion unit in the configuration used for primary regeneration. The molten "spent" catalyst is fed via a Fluid Metering, Inc. Lab Pump and is dropped from a remote drip tip into a batch bed of fluidized silica sand. The feed gas consists of a mixture of air and anhydrous hydrogen chloride which enters at the apex of the reactor cone. In the fluidized bed, the zinc chloride is vaporized, the carbon, nitrogen and sulfur impurities are burned out and any zinc oxide is largely converted to zinc chloride by the HCl in the feed gas. The gas and zinc chloride vapor entrain the coal ash, leave the reactor and pass through the cyclone where the solids are collected. The cyclone underflow solids derive solely from the melt since the sizing of the silica sand bed solids is such that there is essentially no elutriation of this material. The solids collected at the cyclone then consist largely of coal ash contaminated by small amounts of zinc in the form of zinc chloride and zinc oxide or other compounds, and any unburned carbon or zinc sulfide. The gas then passes to the condenser where zinc chloride is condensed, then to the electrostatic precipitator to remove zinc chloride fog, and then to sampling and metering. The analytical methods and calculational procedures are substantially the same as those previously described (7).

Hydrocracking

The hydrocracker and its operating procedure have been described previously (9).

Secondary Regeneration

The apparatus used to conduct the secondary recovery studies was the same unit used for the primary regeneration studies with some modifications made to accommodate the use of a solid feed. The modifications consisted of replacing the melt feed system with a metering powder feeder for feeding the cyclone underflow solids to the unit. The drip tip was plugged off since it was not used.

The cyclone underflow ash is fed at a metered rate into the air feed gas line that transports the ash into the bottom of the batch fluidized bed of silica sand. Anhydrous HCl is injected into the air stream just upstream from the reactor. Some of the ash is temporarily trapped in the fluidized bed of silica sand, building up to a steady-state concentration. The remainder of the ash is carried out of the bed by the gas stream. At steady state, the amount of ash fed per minute equals the amount of ash per minute that is transported by the gas stream out of the bed. The average ash residence time in the reactor in minutes is then "grams of ash inventory in the bed divided by the ash feed rate in grams per minute."

The gas, ZnCl₂ vapors, and entrained ash leave the reactor and follow the same course described above for primary regeneration.

The feed gas is electrically preheated to 316°C (600°F) before it enters the reactor. The remaining heat required is put in through the reactor walls by electrical heaters.

The run was started when the cyclone underflow ash feed to the reactor started. The product cyclone underflow was collected in 5 to 10 min, increments as a function of running time. The run was ended when the ash feed stopped.

The ash inventory in the bed was measured to enable precise calculation of the average residence time in the bed.

Run duration was about 40 minutes, which required about 200 grams of ash per run. This was low enough that the relatively limited ash supply was sufficient to conduct a reasonably complete program. Thus, in runs of 10-12 minutes residence time, the longest times investigated, there were at least three changes of ash inventory.

The reaction was followed by analyzing the product ash increments for total and water-soluble zinc, chlorine and iron. Steady state was indicated by constant concentrations of zinc in the increments.

In general, complete material and elemental balances were not made because the small amount of material collected in the labyrinthine collection equipment downstream from the cyclone made accurate collection of small amounts of product very difficult. Instead the yield of effluent ash was determined by a silica balance around the ash in and the ash out. This, together with metals analyses of the feed and product ash, provided the data for calculation of metals removal.

RESULTS AND DISCUSSION

Primary Regeneration

The variables and the levels at which they were investigated are:

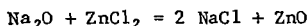
Temperature, °C	871, 927, 954, 982
Pressure, kPa (psig)	119 (3)
% of Stoichiometric Air (nominal)	115
Mol % of Anhydrous HCl in Feed Air	5.5, 8.5, 11.5
Fluidized Bed Solids	297 x 595 μm Silica Sand
Fluidized Bed Depth, meters	0.305
Superficial Linear Velocity, meters/sec	0.305

Operability

The criterion for operability is that the coal ash leaves the bed by elutriation and that it is not retained in the bed due to size growth by sintering or clinker formation. Based on this criterion operability was as follows:

1. With 5.5% HCl in the inlet air:
 - a. 927°C (1700°F) is an operable condition, at least for short period.
 - b. 954°C (1750°F) is a marginally operable condition because of some sintering of ash in the bed.
 - c. 982°C (1800°F) is an inoperable condition because of severe ash sintering in the bed leading to clinker formation.
2. With 8.5 or 11.5% HCl in the inlet air:
 - a. 927°C is an operable condition.
 - b. 954°C is an operable condition.
 - c. 982°C probably is a marginally operable condition with some minor size growth in the ash grain size to be expected. This may be desirable from the standpoint of preventing ash buildup in the regenerated melt.

Some slight sintering may be desirable to give more efficient cyclonic removal of the ash from the gas stream. The sintering that restricts operability is likely promoted by the fluxing action of ash metal chlorides (NaCl, KCl, CaCl₂, MgCl₂) that can be formed in the hydrocracker by reactions such as



In general, 927°C was found to be the preferred temperature in that the temperature was low enough for good operability but high enough for good reaction kinetics, yielding efficient burnout of the impurities.

Results

The results presented will be confined to work done at 927°C and the effect of HCl concentration in the air on these results. Table II shows conditions and material balances for runs at 927°C with 5.5, 8.5 and 11.5 mol % HCl in the feed gas. Table II shows that good material balances were obtained. Products derived from four sources: the product melt, cyclone underflow solids, bed solids, and gas which includes water. The bed solids yield per unit of feed decreases as run duration, and hence the total amount of melt fed, increases, since a batch bed of silica was used.

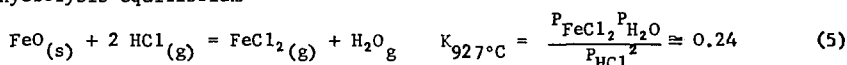
Table III shows the efficiency of regeneration for the three runs whose material balances have been given. Zinc recovery with 5.5% HCl in the feed air was 97.9% and it increased to 99.1% with 11.5% HCl in the feed air. Higher recovery is achieved with higher HCl concentration because the ZnCl₂ hydrolysis equilibrium is shifted farther to the ZnCl₂ side.

Recoveries of chlorine (Table III) greater than 100% of the chlorine in the feed melt reflect conversion of ZnO and ZnS in the feed to ZnCl₂ by interaction with the HCl in the gas.

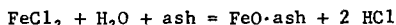
The small amounts of nitrogen, carbon and sulfur in the product melts (Table III) reflect the high efficiency of burnout of the NH₃, ZnS and carbonaceous residue, since essentially all of the remaining carbon, nitrogen and sulfur are in the unit offgases as combustion products: SO₂, CO, CO₂, N₂ and H₂O. Nitrogen and sulfur burnout were generally greater than 97% and carbon burnout was greater than 99%.

The low percentage of the feed ash in the product melt (Table III) shows that ash rejection at the cyclone was very efficient. Rejection of the individual metals of which the ash is comprised, was also efficient except for sodium and potassium, most of which appear in the melt. This is undoubtedly due to the formation of the highly-stable NaCl and KCl which are slightly volatile at regeneration

conditions (~ 3 and 5 torr vapor pressure at 927°C, respectively). A substantial fraction of the iron, most likely as FeCl₂ also appears in the melt. Over many cycles of hydrocracking and regeneration, vapor-liquid equilibria with respect to NaCl and KCl at a regeneration temperature of 927°C will limit the buildup of the sum of their concentrations in the ZnCl₂ catalyst to about 1.0 to 1.5 mol % when the regeneration is conducted at 3 atm pressure or even less at higher pressures. The hydrolysis equilibrium



or reactions such as



will restrict the FeCl₂ concentration in the regenerated ZnCl₂ catalyst to less than 10 mol %. A run in which the melt to regeneration was spiked with FeCl₂ tends to confirm this. Batch hydrocracking data indicate that, at these levels, these ash metal chlorides present essentially no problem regarding catalyst activity.

Table IV shows analyses of the product regenerated melts. The melts obviously are close to pure ZnCl₂ since the Zn:Cl atomic ratios are 1.95, 1.97 and 2.02.

After separating out the trapped ash and sampling, the used 28 x 48 mesh silica sand bed solids were employed in consecutive runs. The silica bed is almost inert to interaction with zinc and chlorine as shown by their extremely small contents in the silica sand bed after 54 hours of use in spent melt regeneration (Table V). There is some reaction of calcium and magnesium with the silica sand bed as indicated by an increase with time up to the concentrations of 1.49 and 0.44% of CaO and MgO after 54 hours.

Table VI gives analyses of the coal ash rejected by the cyclone during primary regeneration. The yields of these ashes were about 5.8% per 100 grams of feed melt exclusive of the steady-state concentration of ash trapped in the bed when the run was terminated. These ashes contain essentially all of the feed zinc not found in the product melt. The zinc retained in the ashes represent 1 to 2% of the feed zinc to regeneration, the retained zinc being lower when the HCl concentration in the air increases. It is in two forms: 1) zinc in the form of zinc chloride (water-soluble zinc) which is adsorbed on, entrained by, or diffuses to the cyclone underflow ash during the regeneration process, and 2) zinc in the form of ZnO, ZnO·SiO₂ and ZnO·Al₂O₃ (water-insoluble zinc) which is not completely converted to the ZnCl₂ because of equilibrium restrictions in reaction (4) and reactions of the type



Accordingly, the concentration of the water-insoluble zinc decreases as the HCl concentration in the feed air increases, whereas the water-soluble ash concentration remains more or less constant.

Since 1% zinc "loss" represents about 4¢ per gallon gasoline, recovery of the zinc in the ash is worthwhile from the economic aspect as well as from the environmental and conservation aspects. Therefore, investigations of "Secondary Zinc Recovery," that is, recovery of the zinc retained in the cyclone ash were made.

Secondary Zinc Recovery

Secondary recovery consisted of treatment of the cyclone underflow ash from the primary regeneration with ZnCl₂-free air plus HCl. The principle of this treatment is to reverse equilibria such as in reactions (4), (6) and (7) so that the water-insoluble zinc values are converted to ZnCl₂ which is evaporated from the ash substrate and recovered.

The cyclone ash used as feed in this work was a composite from a number of primary regeneration runs. Analysis of this feedstock is given in Table VI.

The levels of the variables studied in secondary zinc recovery are tabulated below:

Temperature, °C	816, 927, 1038
°F	1500, 1700, 1900
Pressure, kPa	119, 195, 271
psig	3, 14, 25
Mol % Anhydrous HCl in Feed Air	0 to 60
Feed Ash Residence Time, min	1.5 to 12.7
Fluidized Bed Solids	297 x 595 μ m Silica Sand
Fluidized Bed Depth, meters	0.013, 0.062, 0.124
Superficial Linear Velocity, meters/sec	0.18, 0.24, 0.30

Operability

Runs at all conditions tested gave excellent operability. No sintering of ash was found in any of the runs, even those at 1038°C.

Results

Figures 2, 3 and 4 summarize the results.

Figure 2 shows the breakdown of the recovery of water-soluble and water-insoluble zinc as functions of time and temperature, with a feed gas consisting of 20 mol % HCl in air. Essentially 100% of the water-soluble zinc in the cyclone ash was recovered in as little as one minute residence time at all the conditions tested. This is not surprising since no reaction is required, only volatilization of the ZnCl₂ that the water-soluble zinc represents. It has been shown that HCl is not required for this H₂O-soluble zinc recovery, that essentially 100% recovery can be obtained using HCl-free air or nitrogen. Figure 2 shows that the extent of secondary recovery of zinc is limited by the rate of reaction of the water-insoluble zinc to form volatile zinc chloride. The rate of recovery of the water-insoluble zinc is very fast initially but slows down markedly after the first minute of reaction time. Recovery is better the higher the temperature in the range of 816 to 1038°C.

Figure 3 is a plot similar to Figure 2 but it shows the total combined recovery of water-soluble and water-insoluble zinc. It is apparent from this plot that as high as 70% of the total zinc in the cyclone solids was recovered in as little as one minute residence time.

Greater than 73% of the chlorine in the cyclone underflow ash was volatilized and removed from the feed ash at all conditions tested.

Figure 4 shows that the water-insoluble zinc recovery increases moderately with increasing HCl partial pressure. The increase is unaffected by the HCl/air ratio. Hence, at a given HCl concentration in the feed air, the zinc recovery can be enhanced by increasing the total pressure and thereby the HCl partial pressure. Therefore, at the projected commercial operating pressure of 5 atm, 4 mol % HCl in the feed air should give results equivalent to the use of 20% HCl at 1 atm.

Thus, it has been shown that 70% or more of the zinc in the ash retained in the cyclone solids can be recovered in a relatively simple step added to the primary regeneration system. With secondary recovery of 70%, overall zinc recovery of 99.6 to 99.7% has been demonstrated. The secondary zinc recovery gives a savings in zinc makeup costs of about 3.5¢ per gallon of gasoline produced from coal via the ZnCl₂ process (8).

Hydrocracking Activity of Regenerated Melt

A run was made in the continuous bench-scale 3 lb/h hydrocracker in which the product ZnCl₂ catalyst from regeneration Run 19 was tested in hydrocracking Colstrip coal. As shown in Table VII, the regenerated catalyst was somewhat more reactive

than virgin zinc chloride. This is likely due to the fact that the regenerated catalyst contained less ZnO, which depresses ZnCl₂ activity, than the virgin zinc chloride.

References

1. Consolidation Coal Co., R&D Report No. 39, Office of Coal Research, U. S. Dept. of the Interior. Interim Report No. 2, "Research on Zinc Chloride Catalyst for Converting Coal to Gasoline--Phase I--Hydrocracking of Coal and Extract with Zinc Chloride," Vol. III, Book 1, March, 1968.
2. Zielke, C.W., Struck, R.T., Evans, J.M., Costanza, C.P., Gorin, E., "Process Design Develop.," Ind. Eng. Chem. (1966) 5, 151.
3. Ibid., 158.
4. Struck, R.T., Clark, W.E., Dudd, P.J., Rosenhoover, W.A., Zielke, C.W., Gorin, E., Ind. Eng. Chem. (1969) 8, 546.
5. Zielke, C.W., Rosenhoover, W.A., Gorin, E. -- Shale Oil, Tar Sands, and Related Fuel Sources (T. F. Yen, ed.) Advances in Chemistry Series No. 151, 153 (1976).
6. Zielke, C.W., Struck, R.T., Gorin, E., Ind. Eng. Chem. (1969) 8, 552.
7. Consolidation Coal Co., R&D Report No. 39, Office of Coal Research, U. S. Dept. of the Interior. Interim Report No. 2, "Pre-Pilot Plant Research on the CSF Process--Phase I--Regeneration of Zinc Chloride Catalyst," Vol. III, Book 2, March 1968.
8. Parker, W.A., et al., Conoco Coal Development Co. Report No. FE-1743-45 to DOE, Nov. 20, 1977.
9. Zielke, C.W., Klunder, E.B., Maskew, J.T. and Struck, R.T., "Continuous Hydroliquefaction of Subbituminous Coal in Molten Zinc Chloride," presented at the 85th National Meeting, A.I.Ch.E., Philadelphia, Pa., June 1978. Submitted for publication in I&EC, Proc. Des. Dev.

Acknowledgment

Appreciation is expressed for support of this work by the United States Department of Energy, Shell Development Company and Conoco Coal Development Company under DOE Contract EX-76-C-01-1743.

TABLE II

Primary Regeneration
Conditions and Material Balances

Run Number	16	22	19
Reactor Temperature, °C		927	119
% Stoichiometric Air	115	125	119
Pressure, psig		3	
Superficial Linear Velocity, m/sec		0.305	
Fluidized Bed Depth, m		0.305	
Inlet Gas Composition, Mol %			
Air	94.5	91.5	88.5
Anhydrous HCl	5.5	8.5	11.5
Melt Feed Rate, kg/h/m ²	305	299	294
Run Time, h	4.0	10.9	22.1
Feedstock Used	F-6	F-7	F-6
In, gm/100 gm Feed Melt			
Feed Melt	100.00	100.00	100.00
Air (ex argon)	126.52	129.16	131.17
Anhydrous HCl	9.39	15.25	21.78
Bed Solids	26.66	10.04	4.99
Total	262.57	254.45	257.94
Out, gm/100 gm Feed Melt			
Product Melt	83.73	85.39	85.57
Cyclone Solids	3.86	5.79	4.92
Bed Solids	28.93	10.62	5.46
HCl	8.80	17.47	22.02
H ₂ O	7.48	6.30	6.72
CO ₂	20.96	22.36	25.78
CO	1.90	1.86	1.60
SO ₂	1.01	0.81	0.40
N ₂	102.00	96.65	95.04
O ₂	6.65	7.15	6.33
Total	266.30	254.37	253.84
(out/in) (100)	101.4	100.0	98.4

TABLE I

Analysis of Feedstocks for
Primary Regeneration and
Coal Hydrocracking

	"Spent" ZnCl ₂ Melt, Feed to Primary Regeneration		-100 Mesh Colstrip Coal, Feed to Hydro- cracking
	F-6	F-7	
Volatile Matter	4.82	5.51	41.73
Ash (SO ₃ -free)	0.77	0.69	12.53
Organic Hydrogen	6.65	6.31	4.03
Carbon	0.22	0.05	66.53
Organic Nitrogen	0.03	0.00	1.00
Oxygen (by diff.)	0.02	0.00	14.72
Organic Sulfur	0.02	0.00	0.92
Pyritic Sulfur	0.02	0.00	0.27
Sulfate Sulfur	80.28	77.36	0.05
ZnCl ₂	0.91	1.28	
ZnS	2.71	3.31	
ZnO	0.56	0.72	
NH ₃	3.03	4.72	
Unidentified			
Ash Composition, Wt. %			
Na ₂ O	1.02	0.53	0.31
K ₂ O	0.40	0.27	0.31
CaO	13.43	13.58	12.72
MgO	5.09	5.36	5.59
Fe ₂ O ₃	9.37	8.93	7.55
TiO ₂	1.90	1.48	1.07
SiO ₂	49.46	52.34	51.33
Al ₂ O ₃	19.33	17.51	21.45

TABLE III

Efficiency of Primary Regeneration

Run No.	16	22	19
Mol % HCl in Air	5.5	8.5	11.5
	% of Feed Melt Component in Regenerated Melt		
Zn	97.9	98.8	99.1
Cl	102.0	107.3	106.2
C	0.6	0.7	0.9
S	9.7	2.0	2.4
N	0.0	2.7	2.5
Total Coal Ash	6.4	3.2	4.4
Na	63	92	75
K	80	122	66
Ca	1.9	1.7	2.6
Mg	1.7	1.4	2.6
Fe	33	12	20
Si	1.6	1.2	1.7
Al	2.1	1.7	0.2

TABLE IV

Primary Regeneration
Analysis of Product Melts

Run No.	16	22	19
<u>Anal. of Melt, Wt. %</u>			
H	0.15	0.13	0.17
C	0.05	0.05	0.07
N	0.00	0.02	0.02
O (by diff.)	1.49	1.63	0.40
Organic S	0.00	0.00	0.00
Sulfide S	0.04	0.01	0.01
Sulfate S	0.00	0.00	0.00
Zn	47.61	47.40	47.32
Cl	50.30	50.59	51.83
Ash	0.36	0.17	0.18
<u>Anal. of Ash, Wt. %</u>			
Na ₂ O	10.22	19.00	24.98
K ₂ O	5.23	12.55	8.71
CaO	4.03	9.20	11.29
MgO	1.43	3.01	4.36
Fe ₂ O ₃	49.21	19.55	20.11
TiO ₂	11.06	1.73	1.46
SiO ₂	12.41	23.68	27.72
Al ₂ O ₃	6.41	11.28	1.37

TABLE V

Primary Regeneration
Analysis of Effluent
Bed Solids

Run No.	19	22
Hours Used	32	54
	Weight %	
H	0.06	0.03
C	0.34	0.06
N	0.00	0.00
S	0.01	0.02
Zn	0.05	0.15
Cl	0.00	0.00
Na ₂ O	0.02	0.01
K ₂ O	0.05	0.04
CaO	0.78	1.49
MgO	0.30	0.44
Fe ₂ O ₃	0.20	0.19
TiO ₂	0.04	0.00
SiO ₂	97.35	96.23
Al ₂ O ₃	0.79	1.30

TABLE VI
 Primary Regeneration
Analysis of Cyclone Underflow Solids

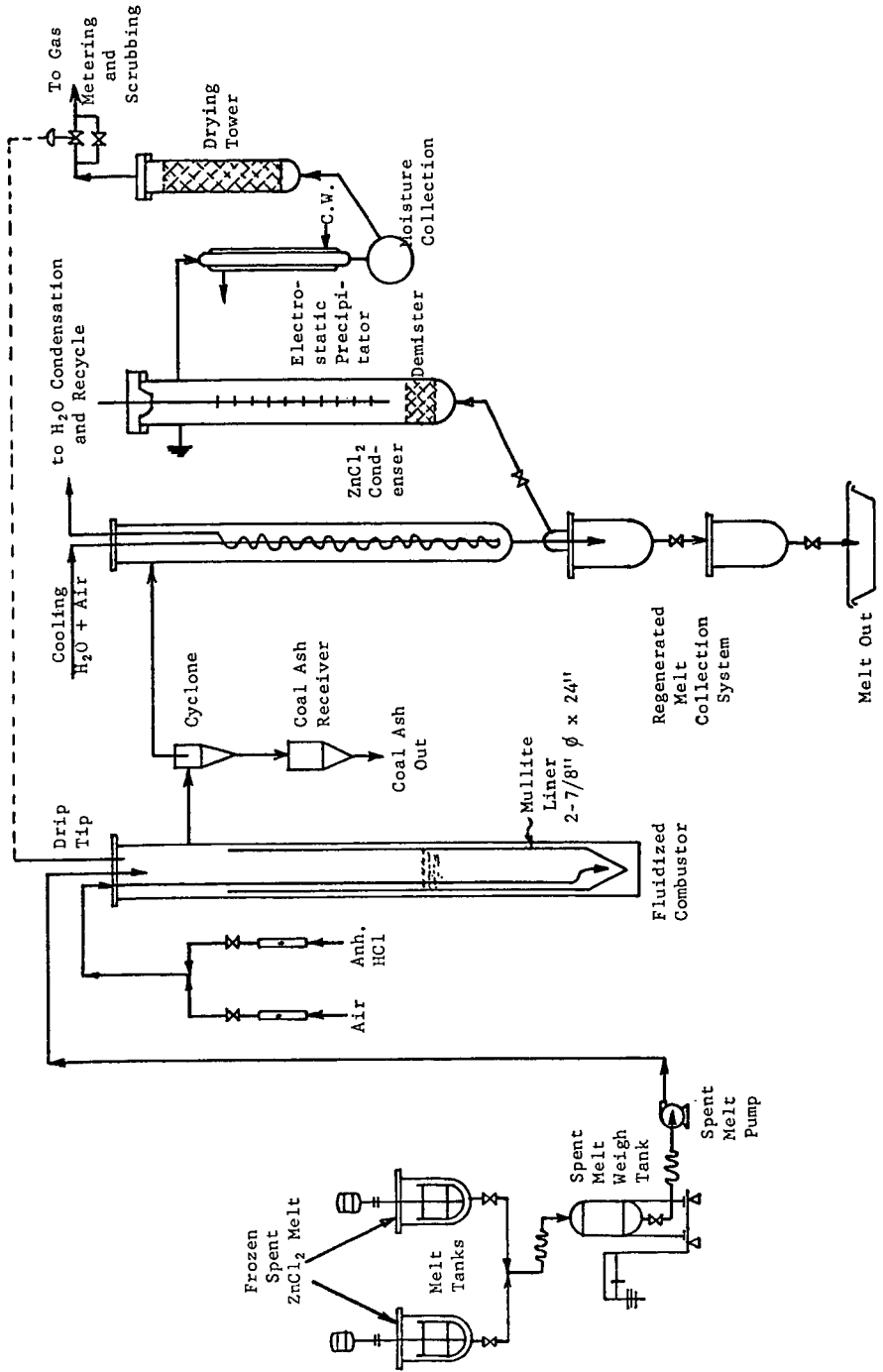
Run No.	16	22	19	<u>Composite</u>
% HCl in Feed Air	5.5	8.5	11.5	
<u>Analysis, Wt. %</u>				
Zn in ZnCl ₂ *	4.73	3.57	4.10	2.94
Zn in ZnO, ZnO·SiO ₂ , ZnO·Al ₂ O ₃ **	11.08	4.07	3.33	4.54
Cl	5.30	4.80	5.54	4.92
H	0.11	0.12	0.13	0.08
C	0.35	0.14	0.35	0.09
S (sulfate)	0.34	0.30	0.23	0.37
Na ₂ O	0.17	0.08	0.12	0.10
K ₂ O	0.04	0.02	0.02	0.03
CaO	9.65	11.87	9.48	11.40
MgO	4.04	4.41	4.14	4.45
Fe ₂ O ₃	3.67	4.06	2.98	3.90
TiO ₂	0.67	0.00	0.84	0.94
SiO ₂	33.36	44.75	43.21	42.86
Al ₂ O ₃	14.20	18.19	19.48	18.41

* Water-soluble zinc
 ** Water-insoluble zinc

TABLE VII
 Comparison of Hydrocracking
 Results With New and Regenerated
ZnCl₂ Catalyst

<u>Conditions</u>			
Feedstock		-100 Mesh Colstrip Coal	
Temperature, °C		399	
Total Pressure, psig		3500	
Melt Residence Time, h		1.29	
ZnCl ₂ /MF Coal, Wt. Ratio		1.0	
		Regenerated	New
<u>Yields, Wt. % MAF Coal</u>		<u>ZnCl₂</u>	<u>Catalyst</u>
C ₁ -C ₃		1.2	2.1
C ₄		4.2	2.7
C ₅ x 200°C Distillate		41.5	33.5
200 x 475°C Distillate		16.2	20.9
+475°C Distillate		6.0	6.1
MEK-Soluble Residue		17.7	15.8
MEK-Insoluble Residue		2.5	4.9
H Consumed		6.4	6.8
Conversion to Distillate		79.8	79.3

FIGURE 1
SIMPLIFIED FLOW DIAGRAM OF BENCH-SCALE (4 LB/HR) REGENERATOR



SECONDARY ZINC RECOVERY GRAPHS

FIGURE 2

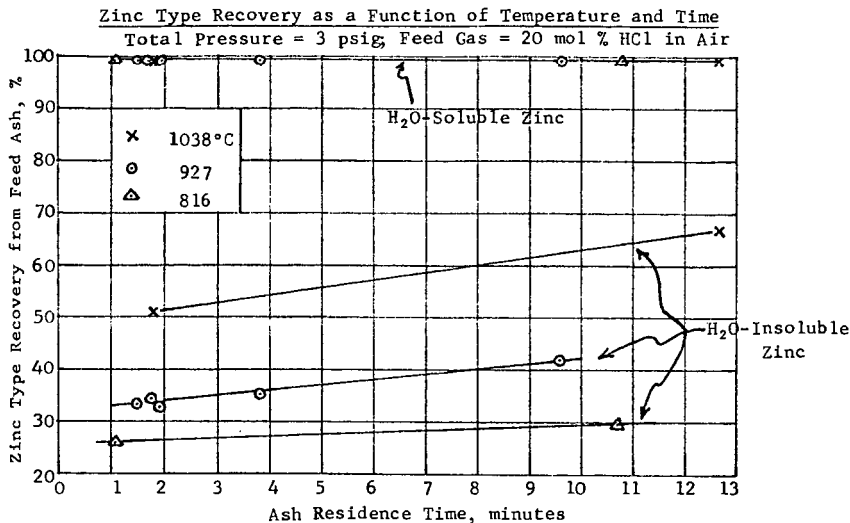


FIGURE 3

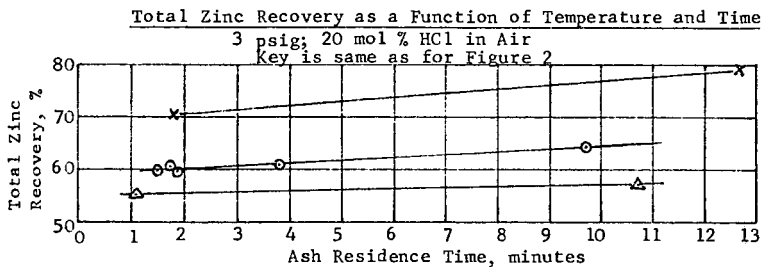


FIGURE 4

